# A non-conventional nuclear import pathway for circadian clock proteins

Inaugural-Dissertation

to obtain the academic degree
Doctor rerum naturalium (Dr. rer. nat.)

Submitted to the
Department of Biology, Chemistry and Pharmacy
of the Freie Universität Berlin

by Dipl. Biochem. SANDRA KORGE

born in Schkeuditz

2016

This thesis was conducted from 2012 to 2016,
supervised by Prof. Dr. rer. nat. Achim Kramer,
at the Laboratory of Chronobiology,
Institute for Medical Immunology, Charité, Berlin

1st Reviewer: Prof. Dr. rer. nat. Achim Kramer, Charité Berlin

2nd Reviewer: Prof. Dr. rer. nat. Florian Heyd, Freie Universität Berlin

Date of thesis defense: 18th of November 2016

# Contents

# List of Figures

# List of Tables

# List of Appendices

# Summary

In almost all vertebrate species, the adaptation to daily environmental changes is enabled by intrinsic clock mechanisms, which are constituted of cell-autonomous transcriptional-translational feedback loops (TTFLs). In mammals, those molecular clocks are composed of the heterodimeric transcriptional activators CLOCK and BMAL1, which bind to enhancer-elements in the promoter region of their target genes such as *cryptochrome* (*cry1-2*) and *period* (*per1-3*). CRY and PER undergo post-translational modifications in the cytoplasm prior to inhibition of CLOCK/BMAL1 in the nucleus. To repress transcription, PER and CRY proteins need to translocate back into the nucleus. Although, it is known that phosphorylation and ubiquitination control the fate of CRYs and PERs, triggering either their degradation or nuclear translocation, our understanding of the actual nuclear entry process through nuclear pores is limited. Proteins lager than 40 kDa such as PERs and CRYs depend on active nucleocytoplasmic translocation. The predominant, "classical" nuclear import is executed by Importin α and β, which recognize so-called classical nuclear localization signals (cNLS). Site-directed mutagenesis of circadian clock-derived cNLSs as well as RNAi-mediated perturbation of the classical nuclear import carriers decrease nuclear accumulation of circadian clock proteins. In addition, the reduction of *importin β* transcript levels lengthens the circadian period. Yet, up to now studies focused only on the classical nuclear import of circadian clock proteins, whereas more than 60 different proteins comprise the nucleo-cytoplasmic translocation machinery, suggesting a much more complex regulatory system.

Until now, no systematic approach was executed to investigate the impact of the nucleo-cytoplasmic translocation machinery on circadian rhythm dynamics. Therefore, we first examined the influence of nuclear import and export on the circadian clock upon application of broad pharmacological nuclear import or export inhibitors and obtained dose-dependent severe lengthening of the circadian period in U-2 OS reporter cells. As both nucleo-cytoplasmic pathways (import and export) are crucial for circadian rhythm generation, we systematically tested the necessity of individual components of the nucleo-cytoplasmic translocation machinery for normal near-24-hour rhythm generation. To this end, we performed RNAi-mediated knockdowns of 62 localization genes. Out of these, the expression of 14 is essential for normal circadian dynamics. Among the three components, whose knockdown led to period shortening, we identified Transportin 1 (TNPO1), a non-classical nuclear import carrier.

Until now, no data on TNPO1-mediated nucleo-cytoplasmic transport of circadian clock proteins is available. Therefore, we investigated a potential function of TNPO1 in nuclear import of circadian clock proteins. We show that the alternative nuclear import carrier TNPO1 is crucial for normal circadian rhythm generation as well as for normal nuclear PER1 accumulation. Upon knockdown of *tnpo1* expression, nuclear accumulation of PER1 but not PER2, is reduced and its import is decelerated as determined by fluorescence recovery after photobleaching. Furthermore, these effects are likely due to a direct interaction between TNPO1 and PER1.

Interestingly, we observed an increased binding between TNPO1 and PER1 under oxidative stress conditions, indicating TNPO1-dependent redox sensitivity of PER1 localization. To test this, we investigated nuclear import rates and subcellular distribution upon hydrogen peroxide treatment, which resulted in reduced as well as decelerated nuclear accumulation of PER1. Further, impaired nuclear PER1 import likely depends on TNPO1 as the oxidative stress in *tnpo1*-depleted cells did neither result in a stronger decrease of PER1 nuclear accumulation than the single treatments nor was the nuclear import further decelerated.

With this study, we present evidence for an alternative nuclear import pathway for circadian clock proteins, which is essential for normal near-24-hour rhythm generation. Upon perturbation of this TNPO1-mediated nuclear entry, nuclear accumulation of PER1 (but not PER2) is decreased, indicating a specific nuclear translocation pathway for distinct circadian clock proteins. Furthermore, the alternative nuclear import carrier TNPO1 might be an additional component of the mutual regulation between redox conditions and the circadian clock.

# Zusammenfassung

In fast allen Organismen ermöglichen intrinsische circadiane Uhrmechanismen, durch zellautonome Transkriptions-Translations-Rückkopplungsschleifen, die Anpassung an tageszeitabhängige Veränderungen. In Säugetieren bilden CLOCK und BMAL1-Heterodimere die transkriptionellen Aktivatoren der molekularen Uhr, welche spezifisch an Enhancer-Elemente in der Promoterregion ihrer Zielgene binden. Dadurch aktivieren sie u.a. die Expression von *Cryptochrom* (*Cry1/2*) und *Period* (*Per1-3*), welche im Zytoplasma translatiert und modifiziert werden. Um CLOCK/BMAL1 im Nukleus zu inhibieren, müssen PER und CRY zurück in den Kern translozieren. Während eine Stabilisierung von PER- und CRY-Proteinen deren Kernimport ermöglicht, führt die Destabilisierung der transkriptionellen Repressoren zu deren Abbau. Obwohl bekannt ist, dass die PER- und CRY-Stabilität durch Phosphorylierung und Ubiquitinierung reguliert wird, ist unser Wissen über den genauen Translokationsmechanismus durch die Kernpore sehr begrenzt. Proteine mit einem Molekulargewicht größer als 40 kDa, so auch PER und CRY, müssen aktiv in den Kern transportiert werden. Die meisten Proteine werden dabei durch die sogenannten „klassischen" nukleären Importine (nukleäre Import-Transporter), Importin *α* und *β*, in den Kern translociert. Dazu erkennen und binden die Transporter spezifische (klassische) Kernlokalisationssignale (cNLS) in ihren Cargos.

Zielgerichtete Mutagenese von Uhrprotein-spezifischen cNLS, sowie die RNA-Interferenz (RNAi)-basierende Störung des klassischen nukleären Importwegs verringert die nukleäre Anreicherung von Uhrproteinen. Darüber hinaus führt eine verminderte Importin *β*-Expression zu einer Verlängerung der circadianen Periode. Bis jetzt fokussierten sich Untersuchungen des Kernimports von Uhrproteinen ausschließlich auf den klassischen nukleären Importweg, obwohl mehr als 60 verschiedene Proteine am gesamten nukleo-zytoplasmatischen Translokationsapparat beteiligt sind. Der Umfang dieses Multiproteinnetzwerkes weist auf ein weitaus komplexeres Regulationssystem des nukleo-zytoplasmatischen Transports von Uhrproteinen hin.

Bis heute gibt es keinen systematischen Ansatz, um den Einfluss des nukleo-zytoplasmatischen Transportapparates auf die Generierung von circadianer Rhythmen zu untersuchen. Aus diesem Grund haben wir zunächst die Wirkung von pharmakologischen Kernimport- und -exportinhibitoren untersucht und eine dosisabhängige Verlängerung der circadianen Periode in U-2 OS Reporterzellen beobachten. Daraus schlussfolgern wir, dass

sowohl nukleärer Import als auch Export für die Generierung normaler circadianer Rhythmen essentiell sind.

Um die Notwendigkeit einzelner Komponenten des nukleo-zytoplasmatischen Transportapparates für die Generierung einer normale ~24-Stunden-Periode zu untersuchen, haben wir einzeln die Transkripte von 62 Komponenten des Kern-Translokationsapparates durch RNAi-depletiert. Dadurch konnten wir 14 Transkripte identifizieren, die notwendig für eine normale circadiane Periode sind. Unter den drei Komponenten, deren Knockdown zu einer Verkürzung der circadianen Periode führte, befand sich auch *Transportin 1* (*Tnpo1*), ein nicht-klassisches Importin.

Derzeit gibt es keine Informationen zu einem TNPO1-basierenden nukleären Import von Uhrproteinen. Deshalb haben wir den potentiell TNPO1-abängigen Kernimport von Uhrproteinen untersucht. Unsere Daten weisen darauf hin, dass TNPO1 als alternatives Importin sowohl für die Generierung normaler circadianer Rhythmen als auch für eine normale nukleäre PER1-Lokalisation notwendig ist. Der Knockdown von *Tnpo1*-Transkripten führt dabei sowohl zur Reduktion nukleärer PER1-Level, als auch zu einem verzögerten Kernimport von PER1. Zusätzliche Bindungsstudien zeigen, dass diese Effekte wahrscheinlich auf eine direkte Interaktion der beiden Proteine zurückzuführen sind. Im Gegensatz zu PER1, führte ein Knockdown der *Tnpo1*-Level zu keiner Veränderung der subzelluläre PER2-Verteilung und -Kernimportrate.

Interessanterweise haben wir eine verstärkte Bindung von TNPO1 und PER1 unter oxidativen Stressbedingungen festgestellt, was auf eine TNPO1-abhängige Redox-Sensitivität der PER1-Lokalisation hinweisen könnte. Die Induktion von oxidativem Stress führte zu einer reduzierten und verzögerten nukleären Akkumulation von PER1. Zusätzlich weisen unsere Daten darauf hin, dass dieser Mechanismus TNPO1-abhängig ist, da die Reduktion der nukleären PER1-Level durch Induktion von oxidativer Stress in *Tnpo1*-herunterregulierten Zellen nicht stärker ist als die der separaten Behandlungen.

Mit dieser Studie wurden erstmals Hinweise auf einen alternativen nukleären Import von Uhrproteine gewonnen, welcher essentiell für die Generierung normaler circadianer Rhythmen ist. Durch den Knockdown dieses TNPO1-basierenden Kernimports wird die nukleäre Akkumulation von PER1, jedoch nicht von PER2 verringert. Dies deutet auf einen spezifischen nukleären Importprozess für ausgewählte Uhrproteine hin. Darüber hinaus könnte TNPO1 eine zusätzliche Komponente für die gegenseitige Regulation der Redox-Homöostase und der circadianen Uhr sein.

# 1 Introduction

## 1.1 Circadian rhythms

Life has found a niche in virtually every place on earth. The existence of life under widely varying conditions is enabled by the ability to adapt to external influences. All organisms, from protozoa to multicellular organisms, adjust to their environment, such as food availability, coexistence with predators or daily changes in light and dark. Most of these external conditions are recurring, e.g. the annual rotation of the earth around the sun resulting in summer and winter or the daily earth's rotation leading to night and day.

Adaptation to daily changes is facilitated by an intrinsic near-24-hour rhythms, synchronizing the organism to external time cues. In diverse species, such as cyanobacteria, fungi, plants, flies and mammals, these circadian (lat. circa dies, "about a day") rhythms are generated by an organism specific clockwork [1-8].

In cyanobacteria, the molecular clock is basically composed of only three proteins (KaiA, B and C) [1]. *In vitro,* the purified Kai proteins are sufficient to generate a circadian rhythm under the hydrolysis of adenosine triphosphate [9]. However, the intracellular generation of a stable circadian rhythm is more complex. To investigate rhythm formation, a synthetic oscillator comprised of three independent transcriptional repressor systems, unknown to be part of a biological clock, was constructed in *Escherichia coli*. Although the repressor network, termed the "repressilator", was able to generate rhythmic transcription, it was cycling in a frequency of around three hours. The authors proposed that negative-feedback is insufficient to explain the circadian time-keeping. Cooperative positive and negative feedback mechanisms must interact to generate stable near-24-hour rhythms [10].

### 1.1.1 Short introduction to the history of Chronobiology

The first reported studies on daily cycles date back to the 18$^{th}$ century, when a time-of-day-dependent leave movement and blossoming of flowers was reported by de Mairan and Linnaeus. Further, they observed the persistence of these rhythmic events even in constant darkness. An intrinsic clock was also predicted by Darwin. However, neither de Mairain, Linnaeus nor Darwin was able to study the underlying molecular mechanism of daily time-keeping [11, 12]. Over the next 200 years biological rhythms

were mainly investigated in plants. At the end of the 19th century, Kiesel was the first to report time-of-day-dependent changes in retinal pigmentation of moths [13].

As the interest in circadian clocks increased in the 20th century, two pioneers of chronobiology, Aschoff and Pittendrigh, were the first to investigate the effect of light entrainment on endogenous clocks [14]. Until today, knowledge on circadian clocks increases continuously (see 1.1.3, 1.1.4, 1.1.5, 1.2.5, 1.3.4).

### 1.1.2 Properties of circadian rhythms

Intrinsic circadian rhythms are adapted to environmental stimuli, which are called "Zeitgeber". The process of "entrainment" describes the rhythm synchronization of internal oscillators to superior pacemakers or external time cues. Unsynchronized circadian clocks are "free-running", maintaining their endogenous rhythms with its intrinsic features (period, phase, amplitude, figure 1.1).

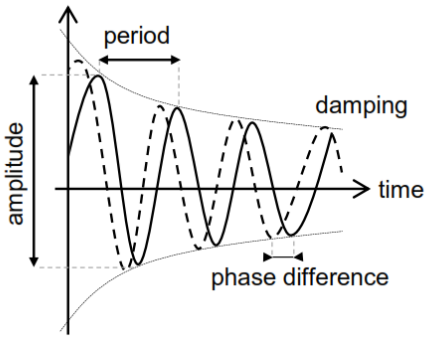


**Figure 1.1: Schematic oscillations of damped sinusoid-wave functions.** The two rhythms cycle with the same period as the time passed between two subsequent peaks is identical. The phase of the solid line oscillation is delayed compared to the dashed line oscillation, which is advanced, reaching a set reference point earlier. Both oscillations dampen, as their amplitudes decrease over time (modified from Vitaterna et al., 2001 [17]).

Single cells are the smallest living entity generating a near-24-hour rhythm. Although those cell-autonomous rhythms persist even in an unsynchronized environment, the time interval to complete a whole cycle vary, leading to Gaussian distribution of around 24 hours. On an intercellular levels the endogenous cycling of each cell leads to "asynchrony" within the cell population due to the lack of coupling [15].

By definition, a rhythm is a "strong, regular, repeated pattern of movement or sound" [16]. In contrast, oscillations do not necessarily repeat a pattern, thus every rhythm is an oscillation but not every oscillation is a rhythm. To characterize circadian rhythms several parameters will be defined: The time it takes to perform one rhythmic cycle is called "period" (e.g. peak to peak or trough to trough). Although different oscillations can cycle with the same period, they do not necessarily have to have their peak at the same time point. The time passed between a set reference point and an arbitrary point within the cycle is determined as "phase". Besides the period of a completed cycle and its phase, the "amplitude" represents another feature of an oscillation, indicating the distance of

peak to trough at a set reference point. Furthermore, the decrease in amplitude over time is referred to as "damping", which is observed in unsynchronized, non-self-sustained oscillators (figure 1.1) [17].

### 1.1.3 The mammalian timing system

To adapt to external conditions, environmental stimuli, such as light, entrain the master pacemaker, the suprachiasmatic nucleus (SCN), which in turn synchronizes cell-autonomous rhythm generation (figure 1.2). As an exception, no circadian rhythms were found in the testis, in which circadian clock genes are expressed at a constant level rather than rhythmically [18].

**Entrainment of mammalian peripheral tissues by external stimuli**

To entrain the master pacemaker, light is perceived by the eye and conveyed to the hypothalamus, where 20,000 neurons comprise the SCN [19]. In particular, retinal, visual as well as non-visual photoreceptors detect light and promote transmission of the photic information to the SCN via the retinohypathalamic tract (RHT) [20, 21]. Besides the RHT, two non-photic pathways, the geniculohypothalamic as well as the serotonergic hypothalamic tract, project to the SCN, the latter showing a time-of-day-dependent responsiveness to all three pathways [22]. Within the SCN, the conveyed signal synchronizes the cell-autonomous rhythm generation of the 20,000 SCN neurons.

In turn, the synchronized SCN neurons transmit the Zeitgeber signals by yet unidentified systemic factors to other brain areas as well as peripheral organs, leading to synchronization of behavior and cellular clocks (figure 1.2) [23].

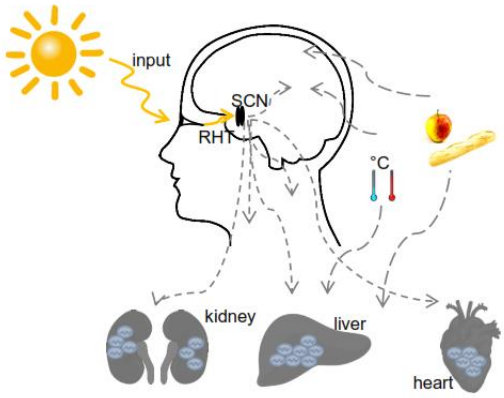


**Figure 1.2: Simplified model of mammalian entrainment to external Zeitgeber**. Environmental stimuli, here light, penetrates the eye, where specific retinal receptors receive the external signal (input). The retinohypothalamic tract (RHT) conveys the photic information to the suprachiasmatic nucleus (SCN). The entrained master pacemaker transmits the input signal to other brain regions as well as peripheral organs, including kidney, liver or heart, synchronizing the cell-autonomous clocks within the peripheral organs. Besides light, intrinsic clocks are also entraining to other Zeitgebers such as temperature cycles and feeding.

Interestingly, evidence was found that the presence of an intact SCN is not necessary for circadian oscillations of about 24 hours in peripheral tissues. Tahara *et al.*,

observed behavioral arrhythmicity in SCN lesioned mice, whereas the free-running periods of peripheral clocks (e.g. kidney, liver) were not altered when compared to pre-lesioned oscillations [24]. In line with those findings are several studies, which showed other Zeitgeber than light (e.g. food and temperature) to be sufficient for entrainment of peripheral organs [25, 26][26].

**The molecular clock in mammals**

Peripheral cells contain an intrinsic and cell-autonomous clock, constituted of a transcriptional-translational feedback loop (TTFL): The transcriptional activators Circadian Locomotor Output Cycles protein Kaput (CLOCK) and Brain and Muscle-Aryl hydrocarbon receptor nuclear translocator-Like protein 1 (BMAL1) form a complex and bind to enhancer elements (E-boxes) in the promoter sequence of their target genes [27, 28]. Promoting transcription, CLOCK/BMAL1 heterodimers induce expression of *cryptochrome 1* and *2* (*cry1*, *cry2*) as well as *period 1*, *2* and *3* (*per1-3*). After post-translational modification of CRYs and PERs, they translocate back into the nucleus, where they represses DNA binding of CLOCK/BMAL and thereby their own transcription [29-31].

Upon accumulation of cytoplasmic PER and CRY, they form multiprotein complexes of more than 1 MDa [32]. Additionally, post-translational modifications, such as phosphorylation and ubiquitination, prime PER and CRY proteins for future processes, including nucleo-cytoplasmic translocation or degradation [33, 34]. In the cytoplasm, Casein Kinase $\delta$ and $\varepsilon$ (CK1$\delta/\varepsilon$) are necessary for homeostasis of nuclear PER entry and degradation [35]. In turn, cytoplasmic CRY levels are regulated by an E3 ligase, the F-box and leucine-rich repeat protein 21 (FBXL21), which is directly involved in phosphorylation-dependent degradation. Interestingly, nuclear FBXL21 protects nuclear CRY from FBXL3-mediated destabilization (FBXL3 is a paralogue of FBXL21) [36, 37]. Several studies have illustrated the essential role of FBXL3 in normal circadian rhythm generation and even single base mutations (overtime mutant: I364T [38], afterhour mutant: C358S [39]) lead to long-period rhythms. Besides phosphorylation, also ubiquitination mediates the proteasomal degradation of circadian clock proteins, such as of PER2. Upon binding to nuclear CRY1, PER2 retains in the nucleus, thereby decreasing PER2 degradation (figure 1.3) [40]. As nuclear levels of PER/CRY decrease, CLOCK and BMAL1 are able to activate transcription again. A new cycle begins.

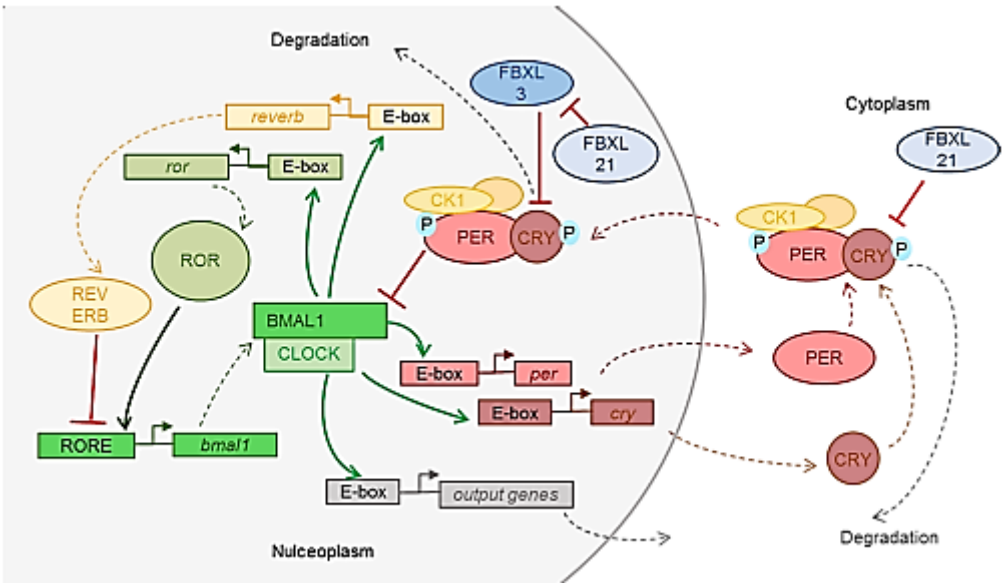


**Figure1.3: Simplified current view of the transcriptional-translational feedback loop in mammals**. In general: The transcriptional activators BMAL and CLOCK (green) bind to specific enhancer regions (E-boxes) in the promoter of their target genes, such as *per* and *cry* (green continuous arrows). PER and CRY (red) proteins accumulate in the cytoplasm, forming complexes with each other as well as with other proteins, such as kinases. Casein kinase $\delta/\varepsilon$ (CK1; among others) phosphorylate (P) PER and CRY, thereby determining the fate of the two proteins either to degradation or stabilization and nuclear entry. In contrast, cytosolic FBXL21 mediates ubiquitination of CRY, leading to CRY degradation. After translocation, the PER/CRY complexes inhibit (inhibition is depicted as continuous red lines) CLOCK/BMAL1 transactivation of E-box-driven genes. The repressor complex is stabilized by nuclear FBXL21, which protects CRY from FBXL3 mediated proteasomal degradation. As the levels of PER/CRY decrease, transcriptional activation of CLOCK/BMAL increases again. A second feedback loop regulates the transcription of *bmal1*, thereby stabilizing circadian rhythm generation. The expression of the E-box output genes *ror* and *reverb* lead to a competition of ROR and REVERB binding to the ROR-element (RORE) in the *bmal1* promoter region.

Another regulatory loop stabilizes the mammalian, molecular clock. Upon transcriptional activation of E-box-driven genes by CLOCK/BMAL1, retinoic acid-related orphan receptors (*ror* and *reverb*) are expressed. The two proteins compete for binding to ROR-responsive elements (RORE), which are present in the *bmal1* promoter, thereby regulating cyclic *bmal1* expression (figure 1.3) [41].

### Multiple homologs of *per* and *cry* genes are necessary for normal circadian rhythm generation

Most components of the molecular, circadian clock have several paralogues: e.g. *per1-3*, *cry1/2*, *bmal1/2*, *clock* and *neuronal PAS domain-containing protein 2* (*npas2*), *rora/β/γ* as well as *reverbα/β*. Until today, the individual functions of these related proteins are still not completely understood. However, evidence of distinct regulatory mechanisms of the individual PER and CRY proteins will be summarized in the next paragraphs:

Single gene disruption of either of the *per* or *cry* genes results in altered circadian rhythms. Mice, which lack expression of either the *cry1*, *per1* or *per2* gene show short period rhythms in wheel running activity, whereas knockout of the cry2 gene leads to long period behavior and molecular rhythms. *per3* null mice do not show altered rhythmicity [42]. The different orthologues are neither able to completely rescue a single gene disruption of another nor to maintain normal circadian rhythmicity. Furthermore, knockouts of both *per1* and *per2* genes lead to arrhythmicity in behavior and on the transcriptional level [43]. The same holds true for knockouts of both *cry1* and *cry2* [44].

Further evidence of distinct roles of PER1, PER2 and PER3 was demonstrated by Akashi *et al.* (2014), who suggested an inhibitory role for PERs on CRY-dependent transcriptional repression. Although both, PER1 and PER2, inhibited CRY1 (or CRY2) repression of CLOCK/BMAL1 transcriptional activation, PER2 seemed to be more effective than PER1. PER3 was not sufficient to inhibit the transcriptional repression by CRY [45]. The authors proposed a minor function of PER3 for rhythm generation, whereas PER1 and PER2 are essential components of the circadian core clock.

As for the three different PER proteins, indications on distinct roles of CRY1 and CRY2 have been predicted by opposing period alterations in $cry1^{-/-}$ and $cry2^{-/-}$ single knockout mice. Different DNA binding profiles of CRY1 and CRY2 (identified in a transcriptome-wide screen) strengthen these evidence for different regulatory functions of the two CRY proteins. Whereas the mean circular phase of peak binding to DNA of CRY1 is at circadian time 0.4 (CT0.4), the phase of peak binding of CRY2 is CT 15.4 [46].

Thus even though convincing evidence was reported for distinct roles of PER1, PER2 and PER3 as well as of CRY1 and CRY2, precise mechanisms are still missing.

### 1.1.4 The molecular clock in non-mammalian species

The timing system in mammals is evolutionary unique, however homologues of multiple circadian core clock components are also present in non-mammalian organisms. Yet, not all molecular timing mechanisms share similarities but two global principles:

- Delayed negative feedback to generate a near-24-hour rhythm
- A regulatory cascade of input effecting the oscillator and the latter effecting further intracellular components (output) [47].

### Circadian timing in *Drosophila melanogaster*

Similar to the mammalian system, a transcriptional activator complex of CLOCK and CYCLE binds to E-boxes in promoter regions of the negative regulators *per* and *timeless* (*tim*) [48]. After translation, several phosphorylation steps of PER and TIM by kinases, such as Doubletime (DBT) [49], Casein Kinase 2 (CK2) [50] and Shaggy [51] as well as dephosphorylation via phosphatases, such as Protein Phosphatase 1 (PP1) [52] and Protein Phosphatase 2a (PP2a) [53] alter the protein stabilization of the cytosolic circadian core clock proteins. In addition, studies on the phosphorylation state of PER2 propose a strictly determined order of PER2 phosphorylation events (figure 1.4) [54].

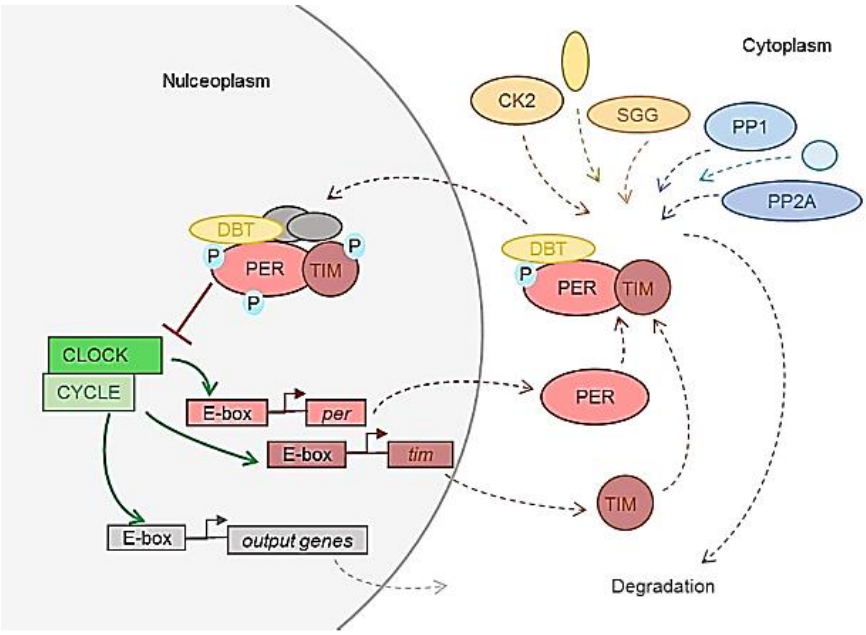


**Figure 1.4: Basic scheme of the molecular clock in *D. melanogaster*.** CLOCK and CYCLE form a transcriptional activating heterodimer (green) and promote the expression of E-box driven genes, such as *per* and *tim*. PER and TIM form complexes in the cytoplasm and post-translational modifications including phosphorylation (orange) via Doubletime (DBT), Shaggy (SGG) and Casein Kinase 2 (CK2) but also dephosphorylation (blue) via Protein Phosphatase 1 (PP1) and 2A (PP2A) alter stability and fate of the inhibitory complex to either proteasomal degradation or nuclear translocation. After nuclear entry, PER and TIM repress their own transcription by inhibiting CLOCK/CYCLE complexes.

The binding of TIM stabilizes the complex of PER and DBT, leading to accumulation within the cytoplasm and translocation back into the nucleus [55]. In the nucleus, PER/TIM complexes function as transcriptional repressors by inhibiting the CLOCK/CYCLE transcriptional activation (figure 1.4) [56].

### The molecular clock of *Neurospora crassa*

The circadian core clock of the fungus *N. crassa*, is comprised of two positive regulators, White Collar 1 and 2 (WC1 and 2), which form a complex (WCC), bind to

specific promoter regions (clock elements, cbox), thereby also activating transcription of the *frequency* (*frq*) gene [57]. In the cytosol, FRQ forms homodimers prior to binding the FRQ interacting RNA helicase (FRH), which is in turn stabilizing the whole complex [58]. Stabilization is also enhanced by the Protein Kinase A (PKA)-mediated phosphorylation of FRQ. In contrast to PKA, casein kinases phosphorylate FRQ thereby promoting its degradation [59, 60]. Although casein kinases facilitate FRQ degradation, the FRQ complex also promotes casein kinase-dependent phosphorylation of WCC, thereby inhibiting WCC transcriptional activity and in consequence lead to repression of *frq* expression (figure 1.5) [61, 62].

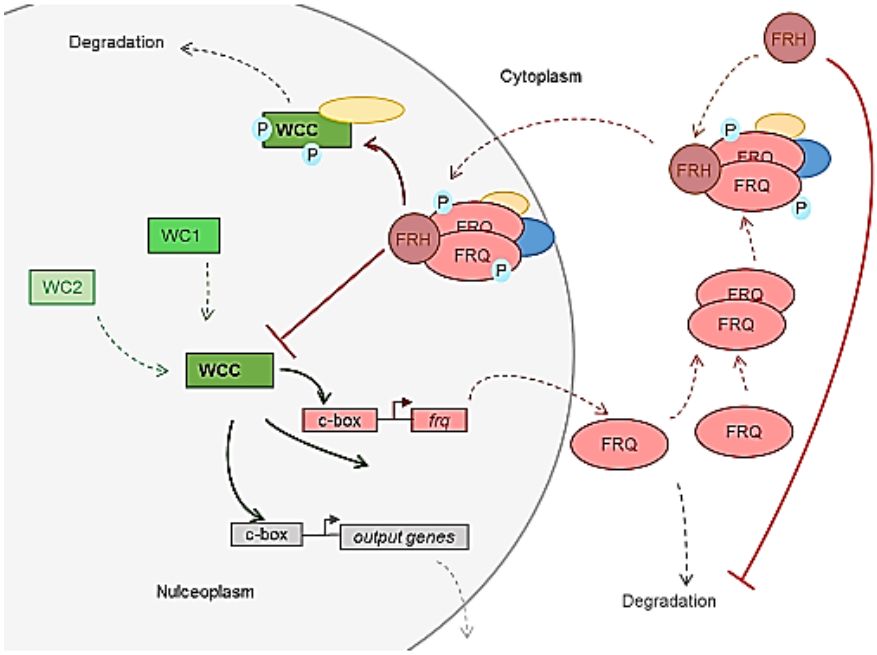


**Figure 1.5: Simplified model of the molecular cock in *N. crassa*.** White Collar 1 and 2 (WC1 and 2) form a transcriptional activator complex (white collar complex; WCC), which binds to specific promoter regions (clock elements; cboxes), thereby activating the expression of *frequency* (*frq*).The transcriptional repressor, FRQ (red), homodimerizes prior to binding FRQ interacting RNA helicase (FRH), which in turn stabilizes the whole complex. Additionally, post-translational events, such as phosphorylation and dephosphorylation, alter complex stability, leading either to nuclear translocation or degradation. After nuclear entry, the inhibitory complex promotes phosphorylation of WCC, which leads to degradation of the transcriptional activators thereby repressing the expression of cbox-driven genes (including the *frq* gene itself).

The complexity of rhythm generation is illustrated once again, in strains lacking *frq* expression. In contrast to the wild type *N. crassa* strain, which entrains to temperature as well as to light-dark cycles, *frq* null strains cannot synchronize to light and dark anymore. However, *frq* mutants still show rhythmic spore formation (asexual reproduction) upon temperature cycles, suggesting a non-circadian clock [63].

**The three-protein-oscillator in cyanobacteria**

Molecular clocks are not only found in eukaryotes. A clock mechanism constituted of three genes, *kaiA*, *B* and *C*, was identified in the prokaryotic cyanobacteria *Synechococcus elongatus* [64].

Cyanobacterial, circadian rhythms are generated by auto-phosphorylation of KaiC, which is promoted by direct interaction with KaiA [65, 66]. In contrast, KaiB binding promotes dephosphorylation of KaiC, thereby opposing the effects of KaiA [67]. Rhythmic auto-phosphorylation of KaiC is due to time-of-day-dependent variations of the cytosolic KaiB level. Whereas KaiA and KaiC are solely accumulated in the cytoplasm, KaiB is distributed in the cytoplasm or bound to the membrane. Due to time-of-day-dependent shifts of membrane-bound KaiB into the cytoplasm, the dephosphorylation of KaiC is regulated in a near-24-hour rhythm.

Dephosphorylated KaiC leads to dissociation of the KaiA/C complex, which effects transcription of the dicistronic *kaiBC* operon (*kaiA* is transcribed independently). Furthermore, KaiA is only able to activate transcription of *kaiBC* in the presence of phosphorylated KaiC. Unphosphorylated KaiC represses the *kaiBC* expression (figure 1.6) [64, 68].

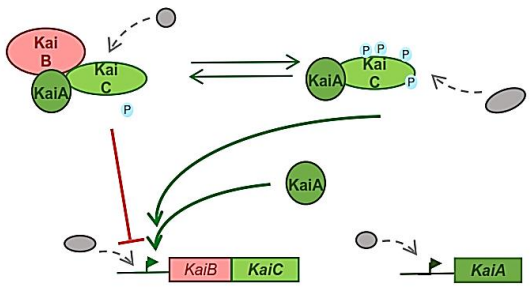


**Figure 1.6: Basic scheme of the cyanobacterial circadian clock.** Three proteins constitute the circadian core clock in cyanobacteria, KaiA,B and C. KaiA promotes auto-phosphorylation of KaiC. In contrast, KaiB suppresses the stabilization of KaiC, resulting in the dephosphorylation of KaiC. Besides stabilizing KaiC, KaiA activates the expression of the dicistronic *kaiBC* operon but only in the presence of phosphorylated KaiC. Dephosphorylated KaiC inhibits transcriptional activation of the *kaiBC* genes.

### 1.1.5 Cellular functions of the circadian clock

A functional circadian timing system is essential for normal cellular homeostasis due to the broad range of circadian clock-controlled intra- and intercellular events. Regulatory functions of the circadian clock have been identified at all mechanistic levels from gene expression to post-translational modifications of proteins. Furthermore, the circadian clock controls specific cellular functions including metabolism, defense mechanism and cell division [69, 70].

As a consequence of the wide-ranging regulatory functions of the circadian clock, it is not surprising that impairment of the circadian clock is linked to diseases.

However, only few clock gene disruptions are identified as a direct cause of distinct diseases. For example, mutations in the *per2* and in the *ck1* gene lead to familial advanced sleep phase syndrome (FASPS), which is associated with an extremely shifted sleep pattern (very early morning rise as well as early fatigue) [71, 72]. Besides FASPS, neurodegenerative disease, such as Parkinson's or Huntington's [73] or metabolic disorders (diabetes, obesity) [74], have been linked to the generation of perturbed circadian rhythms.

Interestingly, evidence of a link between metabolic diseases (as well as cancer) and the circadian timing system, was also found in shift work and jetlag experiments. Disruption of normal sleep-wake cycles, such as exposed to in jetlag or shift work, altered circadian expression profiles [75]. Further, an increased number of circadian clock gene polymorphisms in shift workers have been reported [76]. In line, studies on altered melatonin levels correlate with an increased risk of cancer. Exogenous light during the night suppresses melatonin signaling, which normally conveys the signal for the resting phase (nighttime) to peripheral tissues [77].

## 1.2 Nucleo-cytoplasmic translocation

Cellular compartmentalization in eukaryotes optimizes spatio-temporal regulation of diverse processes, including transcription and translation, receptor signaling or oxidative stress responses [78, 79].

Several compartments, such as the nucleus, mitochondria, the Golgi apparatus or the endoplasmic reticulum (ER), are separated from the surrounding cytoplasm by at least one membrane. In fact, the nucleus is surrounded by a two-membrane system, the nuclear envelope, which is protecting the majority of genomic information from the rest of the cell (reviewed in Alberts *et al.*, 2002 [80]).

### 1.2.1 The nuclear envelope (NE)

The NE is composed of an outer (ONM) and an inner (INM) nuclear membrane enclosing the perinuclear space, which in turn is connected to the lumen of the ER (figure 1.7) [81, 82, 83].

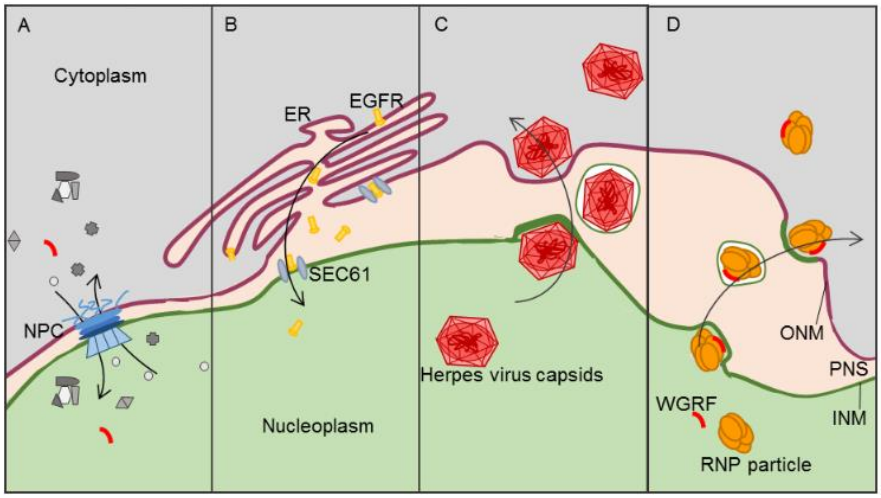


**Figure 1.7: Multiple pathways to cross the nuclear envelope (NE).** The NE is composed of an outer (ONM, purple) and an inner (INM; dark green) nuclear membrane, which enclose the perinuclear space (PNS). A) The nuclear pore complex (NPC; blue) permeates the NE, fusing to the ONM, PNS and INM, thereby facilitating nuclear import and export of small molecules (e.g. ions), RNA and proteins. B) The endoplasmic reticulum (ER) enables retrograde transport of receptors such as the epidermal growth factor receptor (EGFR). The receptors enter the ONM, pass through the PNS to the INM, where they are released into the nucleoplasm by the pore-forming protein SEC61. C and D) nuclear egress of either virus capsids (C; red) or ribonucleoprotein (RNP) particles (D; orange). The large herpes virus capsid developed the ability to pass the NE without translocating through the NPC but budding to the INM. Fusion of the vesicular-like coat of the capsid to the ONM releases the uncoated capsid into the cytoplasm. Likewise, the RNP particles, such as in the synaptic wnt signaling pathway, bud to the INM in association with wingless receptor fragments (WGFR) to exit the nucleoplasm.

To pass the NE, several nucleo-cytoplasmic translocation pathways have been identified:

- Nuclear pore complexes (NPCs) permeate the NE. Those multi-protein complexes facilitate nucleo-cytoplasmic translocation of RNA and proteins (see 1.2.2 and figure 1.8) [84, 85].
- The ER forms a NPC-independent retrograde translocation pathway to cross the ONM [86].
- Viruses such as the herpesvirus use an alternative, NPC-independent nuclear export pathway to replicate most efficiently. Rather than translocating through the NPC, the formed capsids bud to the inner and outer membrane of the NE to escape into the cytoplasm [87].
- In *D. melanogaster,* large ribonucleoprotein (RNP) particles are exported in a similar fashion than the nuclear export of viruses. The RNP particles bud directly to the NE to translocate into the cytoplasm [88].

- It is also hypothesized that nuclear export of insoluble protein aggregates, which cannot be degraded by proteasomes but rather by cytoplasmic autophagy is enabled by an endogenous egress pathway [89].

Despite those alternative translocation pathways, the majority of proteins and RNA molecules pass the nuclear pore to cross the NE barrier.

### 1.2.2 The global gate in and out of the nucleus

Over the past 65 years, NPCs have been characterized in multiple species. Interestingly, evidence was found that structural composition of eukaryotic NPCs is evolutionary conserved [90]. The number and size of NPCs (yeast size: about 66 MDa; mammals: about 125 MDa [91]) per cell vary depending on the cell size and the proliferation rate. The multiprotein complex is composed of about 30 proteins (nucleoporins; nups) in yeast as well as in mammals [92-95].

The structural composition of NPCs have been intensively studied by electron microscopy. Summarizing the structural findings, NPCs are organized as octagons and are composed of several rings. Filaments, which reach into the cytoplasm, are attached to the cytoplasmic ring, the latter being directly attached to the luminal spoke ring. The nuclear ring separates the luminal spokes ring from the nucleoplasm, where filaments are bridging the nuclear basket and the distal ring (figure 1.8) [99].

The outer and inner ring nups, composing the cytoplasmic and nuclear ring are scaffolding nups. The central tube nups function as barrier nups, which are enriched in phenylalanine-glycine (FG)-repeats, promoting translocation through the pore (see 1.2.3 and figure 1.8) [100, 101]. The approximately 30 nups are assembled in a multitude of eight (8 to 48 in yeast and mammals) due to the octagonal symmetry of the NPC [102, 103].

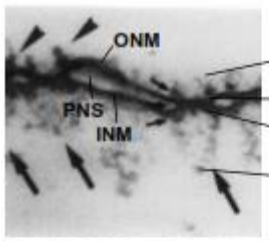


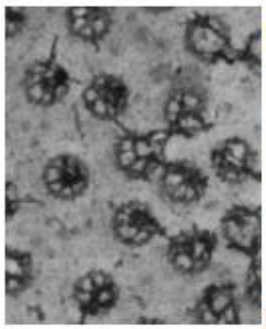

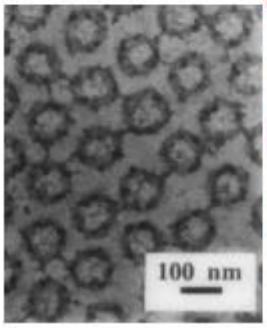


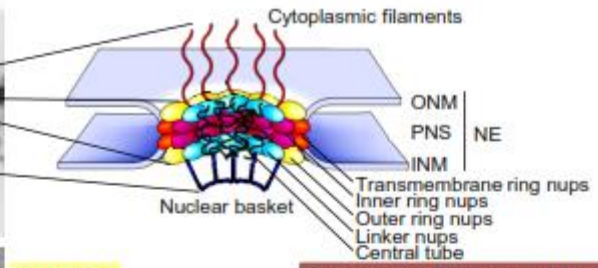


| Outer ring | |
|---|---|
| Vertebrate | Yeast |
| NUP133 | NUP133 |
| NUP160 | NUP120 |
| NUP96 | NUP145C |
| NUP75 | NUP85 |
| NUP107 | NUP84 |
| SEH1 | SEH1 |
| SEC13 | SEC13 |
| NUP43 | - |
| NUP37 | - |
| ALADIN* | - |

| Transmembrane ring | |
|---|---|
| Vertebrate | Yeast |
| GP210 | POM152 |
| - | POM34 |
| NDC1 | NDC1 |
| POM121 | - |

| Inner ring | |
|---|---|
| Vertebrate | Yeast |
| NUP205 | NUP192 |
| NUP188 | NUP188 |
| NUP155 | NUP170 |
| - | NUP157 |
| NUP35 | NUP53 |
| - | NUP59 |

| Cytoplasmic FG nups and filaments | |
|---|---|
| Vertebrate | Yeast |
| NUP358* | - |
| NUP214* | NUP159* |
| NUPL1* (CG1) | NUP42* |
| RAE1* | GLE2* |

| Nuclear FG nups and nuclear basket | |
|---|---|
| Vertebrate | Yeast |
| NUP153* | NUP1* (NUP60) |
| NUP50* | NUP2* |
| TPR* | MLP1* and MLP2* |

| Linker nups | |
|---|---|
| Vertebrate | Yeast |
| NUP93 | NUP93 |
| NUP88* | NUP82* |

| Central tube | |
|---|---|
| Vertebrate | Yeast |
| NUP98* | NUP145N* |
| - | NUP116* |
| - | NUP100 |
| NUP62 | NSP1 |
| NUP54 | NUP57 |
| NUP58 and NUP45 | NUP49 |

**Figure 1.8: Simplified structural composition of the nuclear pore complex (NPC).** Left: A Cross section (top), a nuclear (middle) and a cytoplasmic (bottom) top view of NPCs spanning isolated nuclear envelopes (NE) of *Xenopus laevis* oocytes (visualized in thin sectioned freeze-dried/rotary metal shadowed electron microscopy). The tripartite NE (ONM, PNS and INM) fuses to the NPC, which is likewise devided into the cytosolic, the spoke and the nuclear ring (small arrows). The cytoplasmic filaments (large arrow heads) as well as the nuclear basket (large arrows) associate to the respective ring structures, embedded in the NE (modified from Jarnik and Aebi, 1991 [96]). Right: Simplified schematic model of the octagonal, repetitive structure of NPCs (top), which are composed of symmetric as well as asymmetric (*) nucleoporins (nups). The homolog mammalian and yeast NUPs are listed on the bottom (modified from StrambioDeCastilla et al., 2010 [97] and Hölz et al., 2011 [98]).

Interestingly the existence of eight smaller channels, symmetrically positioned around the central tube have been reported. Passive translocation of small molecules, including ions and metabolites, through those channels, rather than by translocation through the central pore has been proposed (see 1.2.3 regarding active and passive nucleo-cytoplasmic translocation) [104, 105].

### 1.2.3 Passing through the nuclear pore

Besides the passive diffusion of small molecules through nuclear pores, the majority of proteins larger than 40 kDa are actively translocated via different localization signals, recognized by specific transport carriers (see 1.2.4) [106, 107]. Nevertheless, active

protein translocation is not necessarily depending on the protein weight and size. Several exceptions of small proteins (e.g. small G protein RhoA; 21kDa) which are actively shuttled in and out of the NPC are known [108].

The time to pass nuclear pores is predicted to be not rate-limiting within cellular processes, as one NPC has a transport capacity of up to 100 MDa per second and one mammalian cell comprises 1000-3000 NPCs [109]. Further, investigations support fast nuclear import rates within less than 10 milliseconds independent of the cargo size. However, a few exceptional translocation processes take longer than 100 milliseconds [110, 111]. Studies on mRNA translocation through the nuclear pore revealed a dwell time of 5 to 20 milliseconds for only less than 20 % of the investigated mRNAs. The majority of them needed about 180 milliseconds. Yet, the actual time within the central tube of the NPC was just 5 to 20 milliseconds, similar to the translocation time of fast moving mRNAs. Consequently, the nuclear docking and the cytoplasmic release takes most of the time (~80 milliseconds) [112].

The general mechanisms of active nucleo-cytoplasmic translocation through the NPC are well known. Surprisingly, the principles of nuclear import and export are similar in both directions [113]:

Cargos of active transport contain nuclear localization signals (NLSs) and/or nuclear export signals (NESs) as well as other localization signals (e.g. cytoplasmic localization signals) which are recognized by specific carriers of the karyopherin family (see 1.2.4).

To pass the central tube, the carrier (of the carrier-cargo complex) interacts with FG-repeats of several disordered nups [101, 114]. Note: only few exceptions bind to specific nups, see below.

After translocation, the release of the cargo and recycling of the carrier is mediated by the small GTPase Ran (see below).

The actual translocation process of the carrier-cargo complex through the central tube of the pore is controversially described. At least three different models have been proposed for FG-dependent nucleo-cytoplasmic translocation. One model predicts a hydrogel-like structure of FG nups, promoting the interaction between hydrophobic amino acids of the filamentous FG nups with the carrier-cargo complex [115]. On the other hand, the polymer-brush model focusses more on the entropic function of the extended FG nups and excludes a primary gating function of the hydrophobic amino acid

residuals [116]. Last, a bimodal structure in the FG nups might form a charge gradient, guiding the carrier-cargo complex through the NPC [117].

In contrast to the actual translocation process through the central tube, the cargo binding and release as well as the recycling of the carrier are consistently reported. All three processes dependent on Ran, which is present in the nucleus and in the cytoplasm [118]. However, Ran is either bound to guanosine triphosphate (GTP) or -diphosphate (GDP) in a GDP/GTP concentration-dependent manner, thereby mediating nuclear import in the GDP-bound and export in the GTP-bound state. Within the nucleus, RanGTP binds to the nucleo-cytoplasmic carrier, thereby altering the protein conformation of the carrier, which in turn promotes carrier-cargo dissociation of nuclear import complexes. In contrast, RanGTP binding to the nuclear export carriers facilitates also binding of export cargos to the carrier [119]. The ternary complex of RanGTP-carrier-export cargo dissociates in the cytoplasm, as the Ran GTPase activating protein (RanGAP) recycles Ran by hydrolysis of GTP [120]. Opposing RanGAP, nuclear Ran guanosine exchange factor (RanGEF) triggers the release of GDP, promoting Ran binding to GTP priming the GTPase for nuclear export [121].

### 1.2.4 Active nucleo-cytoplasmic translocation by karyopherins

Mainly two groups of karyopherins can be distinguished, the karyopherin alpha (kap*a*, KPNA) and karyopherin beta (kap*β*, KPNB) families.

The small family of kap*a* (KPNA1 to 6 in mammals, only one in yeast) is evolutionary evolved by gene duplication of *kapa1 [122]*. KPNA binds to classical NLSs, however it cannot individually promote translocation of the cargo. Besides a KPNA cargo recognition site, which is constituted of eight armadillo (ARM) repeats, structural analysis identified an N-terminal KAP*β*1-binding site (further referred to as Importin *β*, KPNB1), a member of the kap*β*-family [123, 124].

Members of the kap*β*-family (20 mammalian homologs, 14 in yeast, table 1.1) can only shuttle their cargos either in (importins; IPOs) or out (exportins; XPOs) of the nucleus. Two exceptions are known, which facilitate cargo translocation in both directions (mammalian Importin 13 [125] and yeast kap142 [126]).

**Table 1.1: Members of the kap*β*-family** (modified from O'Reilly *et al.*, 2011 [127], Mosammaparast and Pemberton, 2004 [128] and Quan *et al.*, 2008 [129]).

| mammalian kap | yeast homologue | shuttling process |
|---|---|---|
| Kap*β*1 (IMP*β*, KPNB1) | Kap95 | nuclear import |
| Kap*β*2 (TNPO1, KPNB2) | Kap104 | nuclear import |
| Kap*β*2*b* (TNPO2, KPNB2B) | | nuclear import |
| IPO4 (RanBP4) | Kap123 | nuclear import |
| IPO5 (RanBP5, Kap*β*3, KPNB3) | Kap121 (Pse1) | nuclear import |
| IPO7 (RanBP7) | Kap119 (Nmd5) | nuclear import |
| IPO8 (RanBP8) | Kap108 (Sxm1) | nuclear import |
| IPO9 (RanBP9) | Kap114 | nuclear import |
| IPO11 (RanBP11) | Kap120 | nuclear import |
| IPO12 (TNPO3) | Kap111 (Mtr10) | nuclear import |
| IPO 13 | | nuclear import and export |
| XPO1 (CRM1) | Xpo1 (Crm1) | nuclear export |
| XPO2 (CSE1L, CAS) | Cse1L | nuclear export |
| XPO4 | | nuclear export |
| XPO5 (RanBP21) | Kap142 (Msn5) | nuclear export (Kap142: nuclear import and export) |
| XPO6 (RanBP20) | | nuclear export |
| XPO7 (RanBP16) | | nuclear export |
| Xpot | Los1 | nuclear export |
| | Kap122 (Pdr6) | nuclear import |
| RanBP6 | | unknown |
| RanBP17 | | unknown |

Although, members of the kap*β*-family are similar in size (90 to 150 kDa) and are comparable in their isoelectric points (4.0-5.0), the conservation among the 20 mammalian KPNBs is only about 20 % [127, 128]. Interestingly, the interspecific conservation of the single members in yeast and mammals is high (table 1.1) [129] and cargo as well as Ran binding is similar in all members: an N-terminal binding site for

RanGTP as well as a C-terminal cargo binding domain are comprised of several HEAT repeats (named after the first four proteins, in which the structures have been identified: Huntingtin, Elongation factor 3, Protein Phosphatase 2A and TOR1 [130]). The HEAT structures are formed of two anti-parallel α-helices of about 40 to 45 amino acids, which are linked by small loops [129]. Phylogeny studies of KPNA and KPNB identified homologies in ARM and HEAT repeats, both forming two-helical secondary structures, predicted to enlarge the interaction interfaces [131]. Besides their main cellular function in nucleo-cytoplasmic translocation, several karyopherins as well as Ran contribute to spindle assembly during mitosis (e.g. XPO1, TNPO1) [133].

Interestingly, Chook and Süel predicted a multi-carrier characteristic for cargos with a less distinct NLS. Those carriers bind either to the same NLS or to distinctively different recognition sequences [132].

**Classical nucleo-cytoplasmic protein transport**

The nuclear import carrier, KPNB1, and its adaptor protein KPNA recognize so-called "classical" NLSs (cNLSs) [134]. The consensus sequences of these recognition motifs are either mono- or bipartite [135, 136]. Furthermore, six sub-classifications of cNLS have been proposed for KPNA1 binding, all of them are enriched in lysines and arginines (table 1.2) [137].

**Table 1.2: Sub-classifications of cNLS consensus sequences and the IBB domain of KPNA**. Basic amino acids are depicted in bold characters (* modified from Kosugi et al., 2009 [137], # modified from Lott and Cingulani, 2011 [138]).
Note: K/R (W/F/Y) - compatible amino acids at the indicated position; (-DE) - any amino acid except D or E; $X_b$ - any amino acid; b indicating the number of amino acids

| cNLS class | consensus sequence |
|---|---|
| 1-Monopartite* | K-R-K/R-R |
| | K-K/R-R-K |
| 2-Monopartite* | P/R-$X_2$-R-(-DE)-K/R |
| 3-Monopartite* | K-R-X-W/F/Y-$X_2$-A-F |
| 4-Monopartite* | R/P-$X_2$-K-R-K/R-(-DE) |
| 5-Monopartite* | L-G-K-R-K/R-W/F/Y |
| 6-Bipartite* | K-R-$X_{10-12}$-K-K/R-K/R |
| | K-R-$X_{10-12}$-K-K/R-X-K/R |
| IBB domain of KPNA# | AARLHRFKNKGKDSTEMRRRRIEVNVELRKAKKDDQMLKRRNVS |

Although KPNA acts as an adaptor protein for some cargos, KPNB1 is also able to bind directly to specific cargos [139]. Either the cargo or KPNA bind to the C-terminal HEAT repeats of KPNB1. Interestingly, KPNA adaptor proteins comprise a specialized NLS, which is enriched in basic amino acids, such as common in cNLSs. However, the importin $\beta$-binding domain (IBB) of KPNA is longer than the cNLSs of their cargos and solely present in the N-terminal region. Unlike cNLSs, the IBB domain forms a folded conformation in complex with KPNB, strengthening the binding to KPNB1 [140, 143]. Upon RanGTP binding to the N-terminal region of KPNB1, conformational changes of the carrier lead to dissociation of the translocation complex (figure 1.9 A).

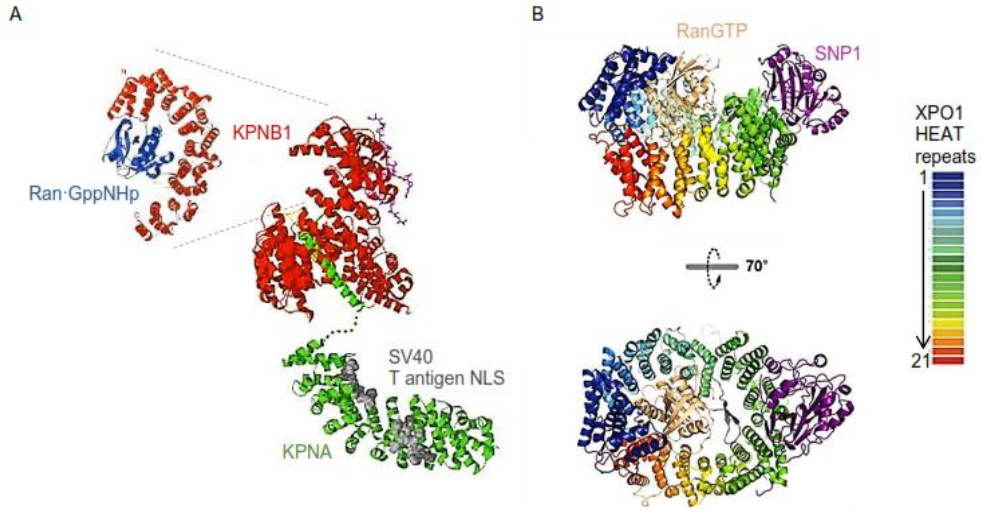


**Figure 1.9: Basic structures of karyopherin binding to either a cargo or to Ran.** A) Ribbon diagram of the KPNB-KPNA-cargo complex (top left: enlarged KPNB1-RanGTP complex). The C-terminal region of KPNB1 (red) interacts with the N-terminal KPNA domain (green). The C-terminal HEAT repeats of KPNA bind to cNLSs, exposed on the protein surface of the cargo (SV40 T antigen NLS; grey). Binding of RanGTP to the N-terminal region of KPNB1 lead to conformational changes of the carrier (here: Ran bound to a non-hydrolysable analogue of GTP). The carrier-cargo complex dissociates upon those steric rearrangements of KPNB1 (not shown). B) Model of the XPO1-SNP1RanGTP complex in two different rotations. XPO1 encloses RanGTP with β-sheets of the HEAT structures, whereas the α-helices are located at the XPO1 surface, interacting with the NES of the cargo, Snurprotein1 (SNP1; purple). [Modified from Chook and Blobel (2001) [141] and Monecke et al. (2009) [142].

In contrast to the classical nuclear import, nuclear export carriers such as Exportin 1 (XPO1; 115 kDa) bind directly to leucine-rich motifs (NES, table 1.3) without the help of an adaptor protein [144, 145]. In addition, binding of RanGTP to XPO1 is essential for nuclear export of the carrier-cargo complex. Structural analysis of XPO1 in complex with its cargo Snurprotein 1 (SNP1) and with RanGTP identified XPO1 as a ring-shaped protein constituted of 21 HEAT repeats. In order to form the ternary complex, XPO1 encloses the small GTPase, whereas the cargo, SNP1, binds to the XPO1 HEAT repeats on the outer surface (figure 1.9 B) [142, 146].

**Table 1.3 Sub-classification and consensus sequences of nuclear export signals** (modified from Kosugi et al., 2008 [145]).
Note: Φ - either L, I, V, M, F, C, W, A or T, where C, T, A and T are allowed only at one of the four positions; L/I/V/F/M (L/I) compatible amino acids at the indicated position; $X_b$ - any amino acid; b indicating the number of amino acids

| class of NES | consensus sequence |
|---|---|
| 1a | Φ-$X_3$-Φ-$X_2$-Φ-X-Φ |
| 1b | Φ-$X_2$-Φ-$X_2$-Φ-X-Φ |
| 1c | Φ-$X_3$-Φ-$X_3$-Φ-X-Φ |
| 1d | Φ-$X_2$-Φ-$X_3$-Φ-X-Φ |
| 2 | Φ-X-Φ-$X_3$-Φ-X-Φ |
| 3 | Φ-$X_2$-Φ-$X_3$-Φ-$X_2$-Φ |
| traditional | L-$X_{2-3}$-L/I/V/F/M-$X_{2-3}$-L-X-L/I |

**An alternative nuclear import carrier to pass the nuclear pore**

Besides the classical NPC-translocation pathways, alternative translocation carriers have been described. The kap*β*-family member kap*β*2*a* (further referred to as Transportin 1; TNPO1) binds directly to nuclear import cargos, such as the heterogeneous nuclear ribonucleoprotein A1; hnRNP A1 [147], however not through a cNLS. The consensus sequence of so-called M9-binding sites (recognized by TNPO1) is rather undetermined compared to cNLS which are essential for KPNA/KPNB1 binding. Structural analysis of non-classical NLS led to hydrophobic (M9) as well as basic-enriched consensus sequences as TNPO1-binding sites (figure 1.10) [148])

Furthermore, structural analysis of the S-shaped TNPO1 identified 20 HEAT repeats. Similar to KPNB1, the N-terminus of TNPO1 binds to Ran, whereas the C-terminal domain is interacting with its cargos. The cargo-recognition sites in TNPO1 are segmented into a high-affinity "A"-site and a lower affinity "B"-site.

After nuclear entry of the TNPO1-cargo complex, it dissociates upon TNPO1 binding to RanGTP. The interaction with RanGTP causes conformational changes of HEAT repeat 8, which sterically displaces the cargo (figure 1.11) [149].

A

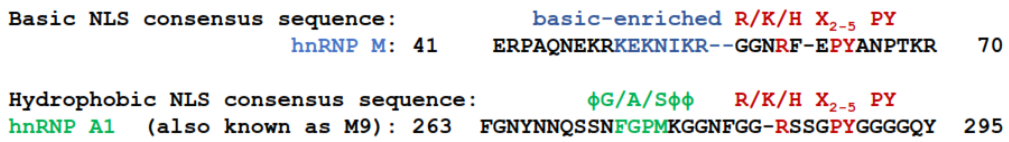


**Figure 1.10: Two consensus sequences of non-classical TNPO1-binding sites**. Both of the non-classical recognition sites in TNPO1 cargos, contain a proline-tyrosine (PY) motif as well as a basic amino acid (R/K/H) positioned two to five amino acids N-terminal to ($X_{2-5}$; X: any amino acid) the PY motif. In addition, either a basic (blue) or hydrophobic (green) motif is necessary for proper TNPO1 binding (Φ: any amino acid containing a hydrophobic residue; modified from Chook and Süel, 2011 [132]).

Interestingly, kap$\beta$2b (further referred to as Transportin2, TNPO2), which shares 84 % sequence similarities with TNPO1, can redundantly substitute TNPO1 for certain TNPO1 cargos, such as hnRNP A1 and HuR [150]. Further illustrating the "multiple carrier for one cargo" conclusion of Chook and Süel [132], TNPO1 as well as KPNB1 facilitate nuclear entry of the 350 kDa huntingtin protein. The protein, involved in the neurodegenerative disease Huntington, comprises a basic-rich non-classical NLS, recognized by the TNPO1 B-site and an arginine-proline-tyrosine motif, binding to the A-site of the alternative nuclear import carrier. Within the exceptional long linker region of the two TNPO1-binding sites, a cNLS is enclosed, which facilitates binding to KPNB1 [151].

Another feature of TNPO1 is exclusively reported for this non-classical nuclear import carrier. Besides M9 and M9-like NLS, TNPO1 is able to bind cargos in an M9-independent mechanism [152, 153]. Putker and colleagues identified TNPO1 as an interaction partner of Forkhead box O 4 (FOXO4) in a cysteine-disulfide-dependent screen. FOXO4 plays a role in redox signaling and in turn, it is regulated by reactive oxygen species (ROS) (see 1.3). TNPO1-FOXO4 binding was due to disulfide-bond formation and was only observed under oxidizing conditions [154]. Another TNPO1 cargo, the deglycase. DJ1 (mutations in the protein lead to a recessive form of Parkinson's disease [155]) binds to TNPO1 via a non-classical M9 motif under non-oxidizing conditions. However, an even stronger binding of TNPO1 to DJ1 was observed upon induction of oxidative stress, but no evidence of disulfide-bond formation between DJ1 and TNPO1 was found [156].

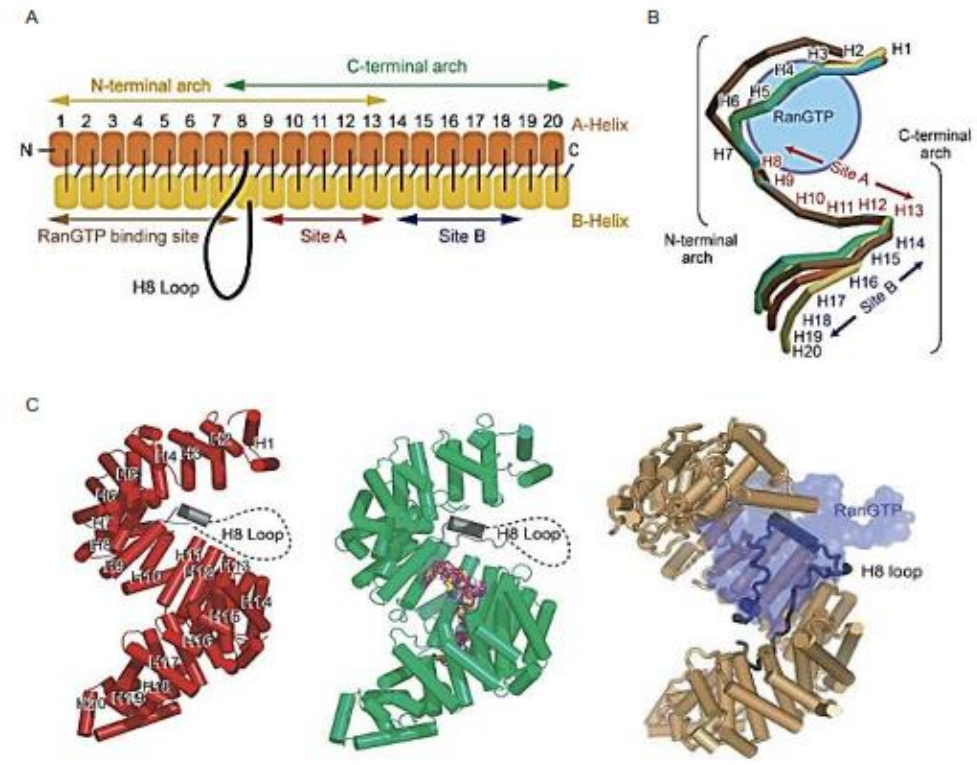


**Figure 1.11: Schematic structure of TNPO1 upon substrate binding**. A) Basic structure of TNPO1 domains. The antiparallel *a*-helices of the 20 HEAT repeats are depicted as A- (orange) and B-helix (yellow). Ran binds to the N-terminal region of TNPO1, whereas the cargos bind to the high (site A) and low (site B) affinity-binding sites in the C-terminal arch. The disordered region of HEAT repeat 8 (black line) is conformationally flexible. B) Overlay of the simplified structure of substrate-free TNPO1 (red) or upon binding to either hnRNP D NLS (green), TAP NLS (blue), JKTBP NLS (yellow) or RanGTP (brown). Illustrated are the conformational changes upon interaction with the different binding partners. C) Overall structure of TNPO1 alone (red) or bound to either hnRNP D NLS (green) or RanGTP (brown). During cargo binding and nuclear import, the disordered H8 loop is not interfering with the cargo-binding sites (dotted black line). However, upon interaction with RanGTP, conformational changes (solid black line) of the disordered H8 region initiate dissociation of the carrier-cargo complex (B to D: modified from Imasaki *et al.*, 2007 [149]).

### 1.2.5 Nucleo-cytoplasmic translocation of circadian clock proteins

Components of the basic molecular clock in mammals are widely identified. However, information on underlying mechanisms of near-24-hour rhythm generation are limited, such as for nucleo-cytoplasmic translocation, which will be summarized in this paragraph.

Several studies on CK1$\delta/\varepsilon$ and CK2, illustrate the regulatory function of phosphorylation on PER stability and the associated events of either nuclear entry or degradation [35, 157-159]. Besides PER, also CRY and BMAL1 are substrates of CK1$\varepsilon$ phosphorylation determining the fate of the two clock proteins [160]. Co-regulator of clock protein stability are protein phosphatases, which dephosphorylate their targets (e.g. inhibition of PP1 enhances degradation of PER2 [161]). Multiple phosphorylation and

dephosphorylation steps are necessary for normal circadian rhythm generation. However, the nexus of distinct amino acid (de-) phosphoylations to either nuclear import or degradation has to be elucidated.

Besides phosphorylation, the nuclear import is also regulated by mutual clock protein interaction. Evidence for normal CRY1 nuclear localization relying on the presence of PER2. Vice versa, the presence of CRY1 and CRY2 are essential for normal nuclear distribution of PER proteins [162, 163]. However, PER1 and PER2 are still localized in the nucleus in mice lacking functional *cry1* and *cry2* genes. To this end, PER3 was shown to act as dimerizing partner for PER1 and PER2 in the absence of CRY proteins, triggering their nuclear accumulation [164].

In regard to the facilitated nuclear entry upon clock protein interaction, our lab showed that the nuclear import of PER2 is decelerated upon impaired CRY1 binding to PER2 (nuclear export of PER2 was not affected) [165].

**Table 1.4: cNLSs and NESs in circadian clock proteins.** Amino acid (aa) positions are indicated in brackets.

| clock protein | NLS | NES |
|---|---|---|
| mBMAL1 | monopartite NLS (36-41 aa) | multiple (142-154 aa, 360-368 aa) |
| mCLOCK | bipartite NLS (32-47 aa) | unknown |
| mCRY1 | bipartite NLS (585-602 aa) | unknown |
| | monopartite NLS (274-278 aa) | |
| hCRY2 | bipartite NLS (550-597 aa) | unknown |
| mPER1 | monopartite NLS (83-5838 aa) | 486-498 aa |
| rPER2 | bipartite NLS (778-795 aa) | multiple (109118 aa, 460-469 aa, 963-990 aa) |
| hPER3 | monopartite NLS (744-752 aa) | 401-413 aa |
| mPER3 | monopartite NLS (726-734 aa) | 396-408 aa |
| hREV-ERBα | DBD domain (128-191 aa) | unknown |

Despite the beneficial effects of PER and CRY interaction (and their phosphorylation), clock proteins have to pass the NPC by interaction with a nuclear import carrier. Tamanini *et al.* (2005) summarizes cNLSs and NESs in clock proteins (table 1.4), reviewing the identification of different localization signals [166]. Recent

studies on nuclear import and export signals in clock proteins characterized additional cNLSs and NESs in BMAL1, CLOCK, PER1 and PER3 (table 1.4) [167-171].

Besides the identification of NLSs and NESs in circadian clock proteins, further studies showed supporting evidence that classical nuclear import and export are crucial for normal subcellular localization of clock proteins: Sakakida and colleagues showed that mutations of the bipartite cNLS in CRY2 lead to an impaired nuclear entry, subsequently preventing normal PER2 nuclear accumulation [172]. Umemura et al. (2014) reported an increase in cytoplasmic PER1 and PER2 upon misregulation (constitutive expression) of *kpna2* expression [173]. Additional evidence for essential classical nuclear import of clock proteins was demonstrated, using RNAi to reduce *kpnb1* expression. Depletion of the classical import carrier led to cytoplasmic retention of PER and CRY [174]. Similar findings were reported in *D. melanogaster*, where TIM binds to KPNA via a cNLS, thereby promoting nuclear accumulation of PER [175, 176].

Information on nucleo-cytoplasmic translocation mechanisms of circadian clock components in other species allow several hypotheses for temporal resolution on the nuclear entry of circadian clock proteins in mammals. One model of the *N. crassa* FRQ protein predicts a non-circadian, rather rapid translocation. Schafmeier *et. al.* (2008) presented evidence of nucleo-cytoplasmic FRQ shuttling within minutes [177]. Further, investigations on the transcriptional repressor led to the conclusion that a high nuclear distribution of FRQ is promoted by a reduced FRQ phosphorylation and rapid nuclear import rates, whereas phosphorylated FRQ is primarily distributed in the cytoplasm, unable to shuttle into the nucleus (figure 1.12 A) [178].

In contrast, the current model of PER and TIM nuclear entry in *D. melanogaster* implies a rather slow nuclear entry for the transcriptional repressors, which retain in the cytoplasm for up to six hours [179]. Additionally, the formation of PER/TIM cytoplasmic complexes is essential to enable the nuclear import of PER and TIM. However, evidence was found that the two proteins translocation separately into the nucleus (figure 1.12 B) [180].

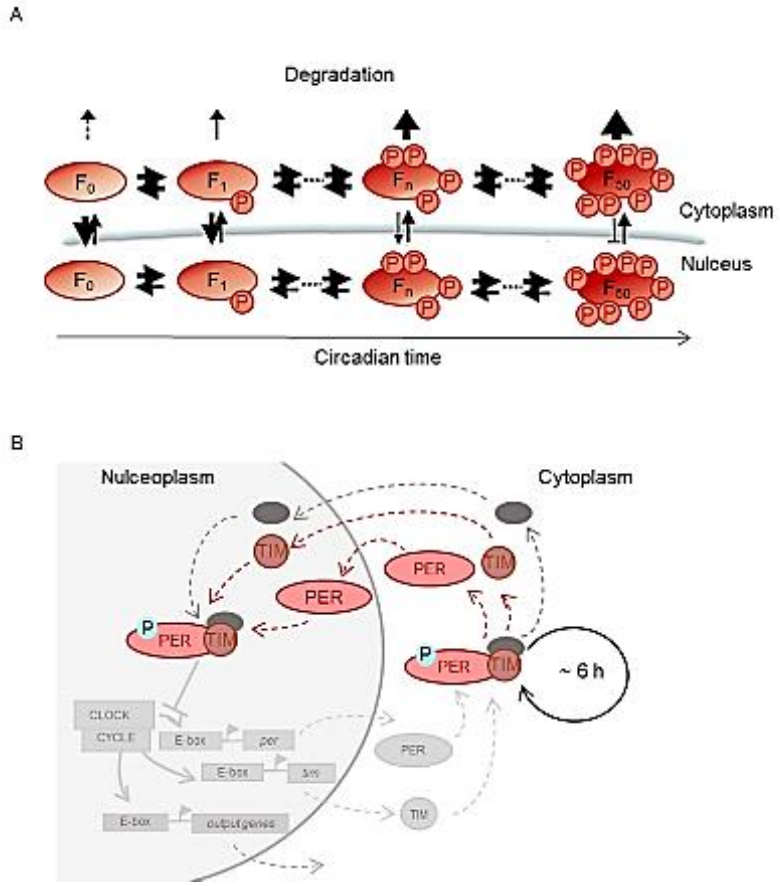


**Figure 1.12: Simplified model of nucleo-cytoplasmic shuttling in non-mammalian organisms**. A) Schematic illustration of phosphorylation, nucleo-cytoplasmic translocation and degradation of the *N. crassa* FRQ protein. Newly synthesized FRQ ($FRQ_0$) is unphosphorylated and shuttles rapidly in and out of the nucleus. Upon FRQ phosphorylation ($FRQ_1$, $FRQ_n$) nucleo-cytoplasmic translocation slows down and decreases, whereas the degradation rate increases. Upon final phosphorylation ($FRQ_{50}$), the nuclear import of FRQ is inhibited, promoting only its degradation (modified from Diernfellner et al., 2009 [178]). B) Nucleo-cytoplasmic translocation of the circadian, transcriptional repressors PER and TIM in *D. melanogaster*. PER and TIM form complexes in the cytoplasm and retain for about six hours until the two proteins enter the nucleus individually. Accumulating in the nucleus after translocation, PER and TIM reform complexes.

## 1.3 Redox homeostasis and oxidative stress

Cellular maintenance of redox (reduction and oxidation) homeostasis is essential for normal cellular functionality. Imbalance of highly reactive oxygen species (ROS) and ROS-scavenging antioxidants causes oxidative stress, which leads to an impairment of the cell vitality.

The property of molecular oxygen to form short-lived, highly reactive free radicals is due to two unpaired electrons in the outer electron shell of the molecule. Depending on the reaction, several reactive oxygen radicals are generated (figure 1.13) [181].

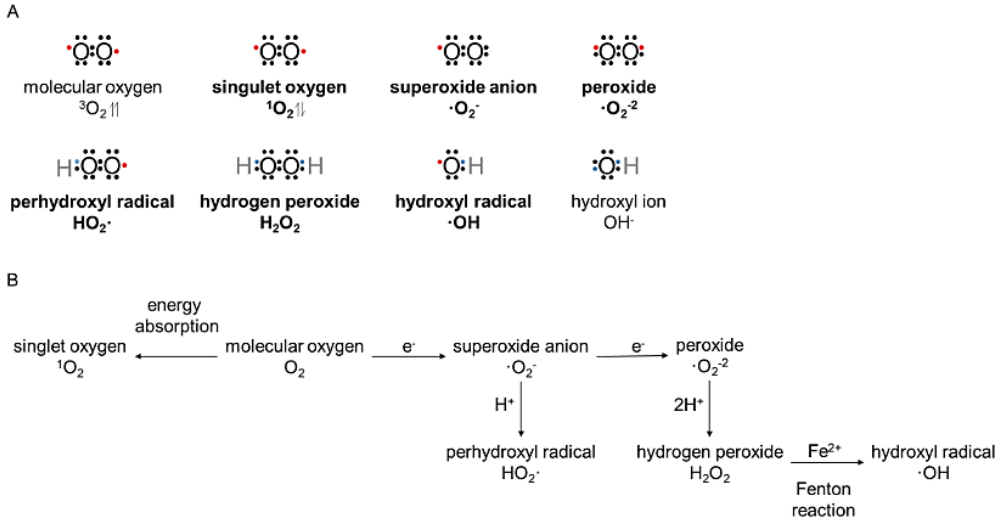


**Figure 1.13: Endogenously produced reactive oxygen species (ROS).** A) Two unpaired electrons in the outer electron shell of molecular oxygen enable the generation of highly reactive, short-lived oxygen radicals. In contrast, hydroxyl ions are not in a reactive state. B) Generation of ROS from molecular oxygen. A single electron reduction of molecular oxygen results in a highly reactive superoxide anion, which can either be reduced to peroxide anion or protonated to a perhydroxyl radical. Hydrogen peroxide derives from protonation of the peroxide anion. In the presence of distinct metal ions, exhibiting several oxidative states, such as iron or copper, hydrogen peroxide reacts to hydroxyl radicals. The highly reactive singlet oxygen is generated by energy absorption, altering the commonly parallel spin of the outer shell electrons into antiparallel spins (modified from Bhattacharya, 2015 [181]).

### 1.3.1 Endogenously generated ROS is essential for normal intracellular homeostasis

Under normal conditions most endogenous ROS are formed as by-products of specific reducing enzymes.

ROS-generating oxidases, including the NADPH oxidase, produce free radicals by accepting electrons from their substrates rather than transferring electrons to it [182]. In addition, ROS is produced by mono and dioxygenases, which belong to the family of oxidoreductases. In contrast to oxidases, they metabolize the molecular oxygen, thereby transferring one (or two) oxygen(s) to their substrates, simultaneously generating reactive oxygen as by-products [183, 184].

ROS are also generated in mitochondria upon production of ATP in the electron transport chain. This process involves four multi-protein complexes (complex I to IV). NADH Dehydrogenase involved in complex I and the Ubiquinone Cytochrome C Reductase of complex III generate superoxide radicals [185, 186]. Other organelles, contributing to the endogenous ROS production are peroxisomes [187]. They are involved in several catabolic processes such as the biosynthesis of bile acid, the

*β*-oxidation and the amino acid metabolism [188]. Upon peroxisomal *β*-oxidation, superoxide and hydrogen peroxide are formed as by-products, similar to mitochondrial *β*-oxidation [189]. As the different cellular compartments produce ROS or respond to ROS, it is not surprising that the cellular redox levels vary from compartment to compartment [190].

Although, mainly generated as by-products, ROS are involved in many cell signaling processes, interacting also with the second messenger $Ca^{2+}$. In contrast to other second messengers, hydrogen peroxide is not specifically binding to a receptor but oxidizes the reactive thiol residue of cysteines. Besides the ROS concentration, this process is also regulated by accessibility of cysteines, which are either freely accessible at the protein surface or sterically hindered [191]. Processes as diverse as cellular immune responses, transcriptional regulation or cell differentiation depend on endogenous ROS signaling [192].

### 1.3.2 Exogenous stimulation of ROS

Despite endogenous sources of ROS, external stimuli induce oxidative stress and ROS production. An unhealthy lifestyle, including smoking and drug abuse as well as environmental chemicals (e.g. heavy metal), reinforces the risk of intracellular, free radical generation [193]. Furthermore, ionizing radiation (UV-radiation, X-rays, *γ*-radiolysis) is a main source of ROS generation. It increases the intracellular ROS production, such as stimulating the mitochondrial electron transfer chain [194].

Immediate consequences of the exogenously induced ROS are alterations of transcriptional and translational processes, including the elevated gene expression of the tumor suppressor gene *p53* [195]. Further, unphysiological ROS levels increase the error rate of translational processes. For example: exogenous concentrations of ROS inhibit the threonyl-tRNA synthetase, which hydrolyses wrongly attached amino acids off the threonyl-tRNA [196].

Depending on the degree of oxidative stress, it can lead to cellular necrosis and apoptosis as well as severe diseases [197, 198]. Although an increased risk of skin cancer upon UV radiation (e.g. by excessive sun bathing) might not be surprising, a correlation of tumorgenesis and ionizing radiation was also shown in tissues, not directly exposed to UV light [199]. Elevated ROS levels can also lead to cataract, atherosclerosis, lung inflammation as well as many other tissue disorders (reviewed in Rani *et al.*, 2016 [200]).

Interestingly, upon ionizing radiation (such as *a*-radiation or x-rays) DNA damage was observed even in non-irradiated, neighboring cells [201]. This phenomenon of radiation-dependent impairments in non-irradiated, neighboring cells is called bystander-effect. Recently, evidence was found that this effect involves signaling of the Nuclear Factor-*κ*B (NF-*κ*B) and of Mitogen-Activated Protein Kinases (MAPKs) between the irradiated and non-irradiated cells. MAPK and NF-*κ*B are involved in inflammation, immune response and cell survival and might be stimulated in an autocrine/paracrine feedback loop [202, 203].

### 1.3.3 Antioxidants and cellular oxidative stress responses

To prevent radiation from penetrating the human body, the outer layer (stratum corneum) of the skin is the first protective barrier against solar UV radiation [204]. However, depending on the type of radiation as well as the dose, the barrier function of the skin is limited. Therefore, intracellular antioxidants, which neutralize ROS as well as adaptive repair mechanisms respond to oxidative stress.

At least seven classes of enzymatic antioxidants are described in literature. They belong to the family of oxidoreductases, except for the glutathione-S-transferase, which is a transferase (table 1.5). Functioning as ROS scavengers, each class of enzymes interacts with distinct ROS [205].

**Table 1.5: Enzymatic antioxidants and their radical substrates**

| | enzyme commission number (EC) | metabolized ROS | reference |
|---|---|---|---|
| thioredoxins | 1.8.4.10 | hydrogen peroxide | [206] |
| catalases | 1.11.1.6 | hydrogen peroxide | [207] |
| glutathione peroxidases | 1.11.1.9 | hydrogen peroxide | [208] |
| peroxiredoxins | 1.11.1.15 | hydrogen peroxide | [209] |
| heme oxygenase1 | 1.14.14.18 | superoxide | [210] |
| super oxide dismutases | 1.15.1.11 | superoxide | [211] |
| glutathione-S-transferases | 2.5.1.18 | epoxides, hydroperoxides | [212, 213] |

Besides enzymatic antioxidants a range of non-enzymatic molecules serve as ROS scavengers, including vitamins and *β*-carotene, which interact with peroxide, hydroxyl and superoxide radicals [214]. In addition, glutathione is a highly abundant, intracellular

soluble antioxidant, which protonates free radicals [215]. Studies on the combinatorial effects of exogenous non-enzymatic antioxidants under oxidative stress conditions showed evidence of beneficial antioxidants combinations, such as of Vitamin A, C and zinc [216].

At high dosages of oxidative stress, the numerous ROS-scavenging antioxidants are insufficient to prevent cellular damage. In consequence, intracellular adaptive responses and repair mechanisms are activated to counteract ROS-induced cell damage, including protein misfolding and aggregation or DNA damage.

Correct protein folding (such as of secretory and membrane-bound proteins) takes place in the ER and is a chaperon-controlled mechanism. To reduce the number of misfolded proteins due to ER stress, an unfolded protein response (UPR) is initiated. Therefore, ER sensors indirectly detect increased levels of unfolded (or misfolded) proteins while the chaperones dissociate off the sensors to promote unfolded protein degradation [217]. Following dissociation, the ER sensors trigger reduction of protein synthesis, thereby decreasing the number of unfolded proteins [218]. Furthermore, the translation of proteins involved in ER-dependent protein folding as well as of antioxidants is increased. Elevated ER protein levels lead to an increased protein folding capacity, which additionally reduces the unfolded and misfolded proteins [219]. Increased protein degradation also reduces the level of misfolded or aggregated proteins [220]. If these responses are insufficient for cellular homeostasis, cell death is initiated [221].

Oxidative stress impairs protein folding but also induces DNA damage, such as lesions, spontaneous mutations or double strand breaks (DSB). Several mechanisms are necessary to repair the different damages:

Lesions of cyclobutane pyrimidine dimers or 6-4 photoproducts, such as produced by UV-radiation are repaired by nucleotide excision repair (NER). More than 15 proteins are involved in the detection, excision and refilling of the lesioned and distorted DNA region [222].

In contrast to NER, base excision repair (BER) is only initiated upon detection of spontaneous single base mutations, which do not distort the DNA helix [223]. Upon BER, the lesioned base is detected, removed and refilled.

The introduction of DSB causes mutations and can even lead to chromosomal rearrangements and transcriptional constraints [224]. To prevent loss of genetic information, either Non-Homologous End-Joining (NHEJ) or direct Homologous Recombination (HR) are induced. Whereas, several enzymes in NHEJ mainly anneal and

refill the DNA strands, thereby introducing short insertions or deletions (indels), HR is more complex, leading to chromosomal rearrangements. The latter process takes advantage of diploidy resulting in base pairing with the complementary strand of the homologous chromosome at the DSB (see 1.4.2, figure 1.14) [225].

### 1.3.4 Cross-talk of the circadian clock and the cellular redox system

Emerging evidence arises that the circadian clock and cellular redox processes regulate each other.

Indications for redox regulation of the molecular clock is given by impaired circadian oscillation upon hydrogen peroxide treatment in human cells [226]. In line with this evidence, mutations of the ROS-scavenging enzyme SOD 1 result in robust but period shortened rhythms in *N. crassa* [227].

Evidence such as the mentioned examples lead to the question, how redox states regulate the circadian clock? Although Period-Arnt-Sim (PAS) domains are one possibility for circadian clock proteins to sense redox levels, proteins without PAS sites are also able to detect changes in ROS levels (e.g. cyanobacterial circadian input kinase) [228]. In addition, indications on direct effects of oxidative stress on the clock are reported for the redox sensitive nicotinamide adenine dinucleotide ($NAD^+$), which inhibits CLOCK/BMAL1 binding to the DNA, whereas NAD(H)/NADP(H) enhance the binding [229]. Interestingly, Wagner *et al.* reported circadian rhythmicity in intracellular redox levels already in 1975. They gained evidence for a rhythmic adenylation as well as for time-of-day-dependent variations in the NADPH/NADP ratio in plants, while examining cellular metabolic states [230]. Furthermore, the circadian core clock gene *reverbα* was identified as an oxidative stress-sensitive gene, containing a NRF2-binding sequence in its promoter region. NRF2 itself induces antioxidant expression upon oxidative stress and is regulated by the circadian clock [231, 232]. Additional evidence of redox regulation of the clock was found in zebrafish, where *per* and *cry* expression is altered upon hydrogen peroxide signaling [233].

The discovery of rhythmic peroxiredoxin (PRX) oxidation states and the interspecies conservation of this PRX rhythmicity introduced a new link between circadian rhythms and redox regulation [234]. In line with those findings, Kil *et al.*, (2015) reported the time-of-day-dependent PRX-mediated mitochondrial release of hydrogen peroxide. PRX scavenges hydrogen peroxide simultaneously becoming hyperoxidized and inactive. Rhythmic mitochondrial abundance of sulforedoxin (SRX) reverses the

hyperoxidized state of PRX, and correlates with hydrogen peroxide scavenging and release levels [235]. The observation of persisting rhythms in a transcription-independent environment raises the possibility of an alternative, core clock-independent oscillator [236].

## 1.4 Clustered Regulatory Interspaced Short Palindromic Repeats (CRISPR)/CRISPR-associated (Cas9) genome engineering

Ectopic protein expression is a common tool to modulate or visualize cellular processes. However, the associated alteration of the protein concentration might lead to unphysiological protein interactions, which would never be observed at endogenous protein levels. Further, genetic approaches to repress gene expression (e.g. RNAi) lead only to a partial reduction of the transcript levels but unlikely to a complete knockout of the target. The residual transcript levels might still be sufficient for normal cellular homeostasis, which would restrict target characterization.

Within the last decades genome editing was discovered as a tool of defense in diverse species and translated into efficient and specific methods to permanently manipulate the genome in a site-directed and controllable manner. Genome editing techniques take advantage of the specific induction of DNA repair mechanisms found in nature (NHEJ and HR, see 1.3.4).

### 1.4.1 Summary of pioneering genome editing tools

The latest technique in genome engineering is CRISPR/Cas9 (see 1.4.2). However, other mechanisms have been used to alter specific genomic regions prior to the identification and utilization of CRISPR/Cas9.

#### Meganucleases

Early generation of knockout and mutant mice was a long and tedious process of screening embryonic stem cells for spontaneous HR [237]. As one of the first improvements, meganuclease were used to specifically generate DSB and increase the likelihood of NHEJ and HR [238, 239]. However, meganucleases comprise the DNA-binding and cleavage site within the same domain, which complicates the manipulation of the target specificity, leading to insufficient target recognition and lack of efficiency.

**Zinc-finger nucleases (ZFN)**

Upon optimization of genome engineering, ZFNs (partially) replaced meganucleases. In contrast to meganucleases, ZFNs comprise two distinct domains for DNA recognition (and binding) and DSB-introduction. Specific recognition of target sites is accomplished by combinations of usually three to six different ZFNs, which each bind three base pairs within the genome [240]. The Fok I nuclease of ZFNs dimerizes prior to introducing DSB at the predetermined target sites [241, 242].

**Transcription activator-like effector nucleases (TALEN)**

The TALE nuclease technology takes advantage of a bacterial nuclease, which specifically recognizes single base pairs (rather than triplets) within the DNA. These nucleases contain several sets of about 34 amino acid long repeats, which each binds to a single base pair [243, 244]. As an advantage of the TALE nuclease tool, only one protein harbors all the recognition repeats, whereas ZFN target recognition is a multinuclease process, which was reported to decrease efficiency. However, as a limitation of TALEN, the first base of the DNA-target site must be a thymidine in order to be recognized [245].

Besides the benefit of genome-wide targeting and specificity, the synthesis of custom-made ZFNs or TALENs is expensive and self-made assembly can be complex and time-consuming.

### 1.4.2 CRISPR/Cas9 genome engineering

In contrast to the genome editing tools described above (see 1.4.1), CRISPR/Cas9 targets the cleavage site by separately transcribed small RNA sequences. The editing system was adapted from a bacterial immune defense mechanism, which uses CRISPR/Cas9 against invading DNA [246].

The system is constituted of a guide RNA combined with a Cas9 endonuclease, the latter introduces DSB by consolidation of the guide RNA. The guide RNA is comprised of a target recognition CRISPR RNA (*crisp*RNA) as well as of a trans-activating *crisp*RNA (*tracr*RNA), directing the Cas9 to the target site. The specific cleavage site is determined by the consecutive Protospacer Adjacent Motif (PAM), which originally enabled the bacterial enzyme to distinguish intruder DNA from its own (figure 1.14) [247, 248].

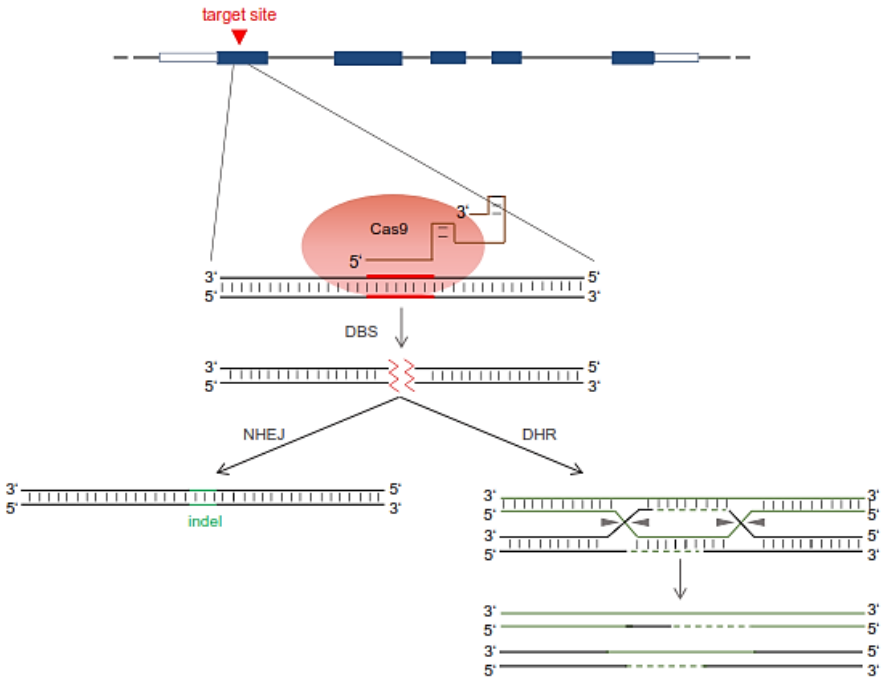


**Figure 1.14: Schematic image of the CRISPR/Cas9 mechanism**. The guide RNA (composed of the crisprRNA and tracrRNA) directs the Cas9 endonuclease directly to the specific target site in the presence of the protospacer adjacent motif (PAM). The Cas9 introduces double strand breaks (DSB), which in turn evokes either non-homologous end-joining (NHEJ) or homologous recombination (HR). Whereas NHEJ introduces short insertions or deletions (indels) in the DSB region, HR promotes an interaction with the complementary region of the homologous chromosome. In order to generate knockin genes, HR-mediated introduction of extracellular DNA is enabled by the fusion of homologous arms to both sides of the "knock-in DNA". These complementary arms, will lead to DNA annealing in the DSB region and in consequence to an increased likelihood of HR (modified from Korge et al., 2015 [255]).

Applications of CRISPR/Cas9 are diverse, such as deletions of whole genes or specific mutations introduced in cells, plants and animals [249, 250, 251]. Improvements of the CRISPR/Cas9 system are reported frequently, such as optimized target specificity due to altered nucleases. For example: nickases cut only single strands of DNA, therefore two guide RNAs have to direct two nickases to the target site, reducing off-target effects [252]. Furthermore, the Argonaut endonucleases were reported as alternative genome engineering tool. Although the function of Argonautes is similar to Cas9 playing a role in gene expression and host defense, PAM sequences become redundant using the Argonauts, which bind their guides via a less conserved consensus scaffold than CRISPR/Cas9 [253, 254].

## 1.5 Aim of this study

Transcriptional-translational feedback loops regulating circadian rhythm generation are comprised of a multi-layered regulatory system. Compartmentalization of transcriptional and translational processes is controlling circadian rhythm generation in a spatio-temporal manner. Whereas transcription takes place in the nucleus, the translation of mRNA is localized in the cytoplasm. To regulate transcriptional processes, circadian clock proteins have to be actively translocate back into the nucleus after maturation. Despite the critical importance of timely nuclear localization of the circadian repressor complex, its dynamics as well as involved carriers needed for active nuclear transport are largely unknown.

In this study, we aimed to gain more information on nucleo-cytoplasmic shuttling of circadian clock proteins. We first focused on the influence of classical nuclear import and export on circadian clock dynamics. To this end, the application of pharmacological inhibitors targeting the classical nuclear import and the main nuclear export pathway, should provide information on circadian rhythm alterations upon impaired classical nucleo-cytoplasmic shuttling.

In order to investigate nucleo-cytoplasmic translocation in a more comprehensive approach, we used RNA-interference to systematically knockdown components of the nuclear pore complex as well as translocation-associated carriers and co-factors. The obtained data should identify individual nucleo-cytoplasmic translocation-associated components essential for normal circadian rhythm generation. Additionally, the RNAi-screen should increase our general understanding of nucleo-cytoplasmic shuttling mechanisms, which regulate circadian dynamics.

In the second part of this study, we wanted to characterize the function of the identified alternative nuclear import carrier Transportin 1 (TNPO1) on the circadian clock. To do so, the CRISPR/Cas9 genome engineering technique was established to generate homozygous *tnpo1* knockout cells, which were used to validate the findings of the performed RNAi-screen. Furthermore, we raised the question which sites of circadian clock proteins interact with TNPO1 to enable nuclear localization. This was tested using subcellular distribution assays in steady state conditions. Besides these steady state investigations, we wanted to focus on nuclear import kinetics of TNPO1-interacting circadian clock proteins. Therefore, we used fluorescence recovery after photobleaching (FRAP) to investigate nuclear import of PERIOD 1 and PERIOD 2 upon perturbation of TNPO1-mediated nuclear shuttling.

In order to examine a potential role of TNPO1 in the oxidative stress-induced regulation of the circadian clock, we repeated the subcellular distribution and FRAP assays under hydrogen peroxide-induced oxidative stress conditions. The results of the subcellular distribution assay and of the determined nuclear import kinetics should reveal insights into an alternative nuclear import pathway for circadian clock proteins. In addition, the hydrogen peroxide treatments should validate TNPO1 as potential link between oxidative stress and the circadian clock.

# 2 Material and Methods

## 2.1 Materials

### 2.1.1 Bacterial strains

| bacterial strain | source |
|---|---|
| E.coli DH10β | Life Technologies |
| E.coli DH5α | Life Technologies |
| E.coli TOP10 | Life Technologies |
| E.coli XL1 blue | Agilent Technologies |

### 2.1.2 Human cell lines

| cells | source | article number | description |
|---|---|---|---|
| HEK293 | ATCC | CRL-1573 | human ebryonic kidney cell line |
| HEK293T | ATCC | CRL-11268 | human embryonic kidney cell line, high transfectability |
| U-2 OS | kind gift of the AG Hagemeier, Charité Berlin, Germany | | human osteosarcoma cell line |
| U-2 OS bmal1:luc | | | U-2 OS cells stably expressing luciferase driven by a 0.9 kb bmal1 promoter [159] |
| U-2 OS per2:luc | | | U-2 OS cells stably expressing luciferase driven by a 0.5 kb per2 promoter [256] |

### 2.1.3 Self-prepared buffers and media

| buffers and media | composition |
|---|---|
| PKB buffer | 50 mM Tris-HCl, pH 7.5<br>1 % Trtion-X-100<br>1.5 mM $MgCl_2$<br>5 mM ethylenediaminetetraacetic acid (EDTA)<br>100 mM NaCl |
| Bicinchonic acid assay (BCA) solution A | 2 % (w/v) $Na_2CO_3$<br>1 % (w/v) BCA-$Na_2$<br>0.95 % (w/v) $NaHCO_3$<br>0.4 % (w/v) NaOH<br>0.16 % (w/v) $Na_2$-tartrat<br>solved in aq. dest.; pH 11.25 |
| BCA solution B | 4 % (w/v) $CuSO_4$ x 5 $H_2O$ |
| blocking solution | 1 x TBS<br>0.05 % Tween® 20<br>5 % (w/v) skim milk |
| Co-immunoprecipitation (Co-IP) buffer | 20 mM tris-HCl, pH 8.0<br>140 mM NaCl<br>1.5 mM $MgCl_2$<br>1 mM TCEP<br>1 % Triton-X-100<br>10 % glycerine<br>solved in aq. dest.; sterile filtered<br>prior to use: addition of 1:100 protease inhibitor cocktail |
| Co-IP wash buffer | 20 mM tris-HCl, pH 8.0<br>150 mM NaCl<br>0.5 % Igepal CA-630<br>solved in aq. dest.; sterile filtered<br>prior to use: addition of 1:100 protease inhibitor cocktail |
| HEPES-buffer | 50 mM HEPES<br>140 mM NaCl<br>1 mM $Na_2HPO_4$<br>solved in aq. dest.; pH 7.0; sterile filtered |

| buffers and media | composition |
|---|---|
| LB-medium | 10 g NaCl<br>10 g Bactotrypton<br>5 g yeast extract<br>ad 1 l aq. Dest<br>agar plates are supplemented with 10-15 g agar<br>autoclave |
| phosphate buffered saline (PBS, 10 x) | 1.37 M NaCl<br>27 mM KCl<br>100 mM $Na_2HPO_4$<br>20 mM $NaH_2PO_4$<br>solved in aq. dest.; pH 7.2; autoclave; use 1 x PBS |
| radio-immunoprecipitation assay buffer (RIPA) | 1 % Igepal CA-630<br>0.5 % sodium deoxicholat<br>0.1 % sodium dodecyl sulfate (SDS)<br>solved in 1 x PBS; sterile filtered<br>prior to use: addition of 1:100 protease inhibitor cocktail |
| SDS tris-glycine running buffer | 0.25 M tris-base<br>1.92 M glycine<br>1 % (w/v) SDS<br>solved in aq. dest.; pH 8.5 |
| SDS transfer buffer | 1 x SDS tris-glycine running buffer<br>20 % methanol |
| separation gel buffer | 1.5 M tris-base<br>solved in aq. dest.; pH 8.8 |
| stacking gel buffer | 0.5 M Tris-HCl<br>solved in aq. dest.; pH 6.8 |
| tris-buffered saline (TBS, 10 x) | 1.37 M NaCl<br>100 mM tris-base<br>solved in aq. dest.; pH 7.3; autoclave<br>use: 1 x TBS supplemented with 0.05 % Tween®20 |
| tris-bor-EDTA buffer (TBE, 5 x) | 54 g tris-base<br>27.5 g boric acid<br>20 ml of 0.5 M EDTA (pH 8.0) ad 1 l |

| buffers and media | composition |
|---|---|
| | aq dest. |
| tris-acetate-EDTA buffer (TAE, 50 x) | 2 M tris-base<br>50 mM EDTA<br>1 M 100 % acetic acid<br>solved in aq. dest.; pH 8.5; use 1 x TAE |

### 2.1.4 Commercially available buffers

| buffer and media | supplier | order # |
|---|---|---|
| Direct PCR Lysis buffer | PeqLab | 31-301-C |
| Dulbecco's Modified Eagle Medium (DMEM, high Glucose) | Life technologies | 41965039 |
| DMEM, high Glucose, phenolred-free | Life technologies | 21063029 |
| HEPES Buffer Solution 1 M, liquid | Invitrogen | 15630056 |
| New England Biolabs buffer 1 to 4 | Invitrogen | B7001-B7004 |
| NuPAGE MES SDS running buffer, 20 x | Invitrogen | NP0002 |
| NuPAGE transfer buffer | Invitrogen | NP00061 |
| Opti-MEM | Life technologies | 31985047 |
| passive lysis buffer, 5 x | Promega | E1941 |
| TE Buffer, 1 x, Molecular Biology Grade | Promega | V6231 |

### 2.1.5 Composition of cell culture media

| media | composition |
|---|---|
| complete medium (CM) | DMEM<br>10 % fetal bovine serum (FBS)<br>1 % penecillin/streptomycin<br>25 mM HEPES-buffer |
| freezing medium | 90 % FBS<br>10 % dimethyl sulfoxide |
| measurement medium | DMEM, phenolred-free<br>10 % FBS<br>1 % penecillin/streptomycin<br>250 *µM* D-luciferin |

### 2.1.6 Antibiotics

| antibiotic | supplier | order # | final concentration |
|---|---|---|---|
| penicillin-streptomycin | ThermoFisher Scientific | 15140122 | 10000 U/ml |
| ampicilin | Carl Roth | K029.2 | 100 µg/ml |
| kanamycin | Carl Roth | T832.1 | 100 µg/ml |
| zeozin | Life technologies | 46-0509 | 25 µg/ml |
| puromycin | Sigma-Aldrich | P9620 | 10 µg/ml |
| blasticidin | Life technologies | R210-01 | 10 µg/ml |

### 2.1.7 Antibodies

| antibody | species | supplier | order # | final dilution western blot |
|---|---|---|---|---|

| | | | | |
|---|---|---|---|---|
| **primary antibodies** | | | | |
| anti-betaACTIN, clone AC-15 | monoclonal, mouse | Sigma-Aldrich | A5441 | 1:100000 |
| anti-CRY1 | polyclonal, rabbit | lab effort | | 1:100 |
| anti-CRY2 | polyclonal, rabbit | lab effort | | 1:100 |
| normal mouse IgG | mouse | Santa Cruz | sc-2025 | |
| anti-MYC-tag (9E10) | monoclonal, mouse | Santa Cruz | sc-40 | 1:1000 |
| anti-PER1 | polyclonal, rabbit | lab effort | | 1:100 |
| anti-PER2 | polyclonal, rabbit | lab effort | | 1:100 |
| anti-TNPO1 [D45] | monoclonal, mouse | Abcam | ab10303 | 1:1000 |
| anti-V5-tag | monoclonal, mouse | Life technologies | R96025 | 1:5000 |
| **secondary antibodies** | | | | |
| anti-mouse IgG-HRP | goat | Santa Cruz | sc-2005 | 1:1000 |
| anti-rabbit IgG-HRP | donkey | Santa Cruz | sc-2305 | 1:1000 |

### 2.1.8 Reagents

| reagent | supplier | order # |
|---|---|---|
| Arrest-In™ | Open Biosystems | EGN042808 |
| *β*-mercaptoethanol | Carl Roth | 4227.1 |
| bovine serum albumin (BSA) | Sigma-Aldrich | A7030 |

| reagent | supplier | order # |
|---|---|---|
| dexamethasone (stock 1 mM in EtOH) | Sigma-Aldrich | D4902 |
| dimethyl sulfoxide (DMSO) | AppliChem | A3672 |
| D-Luciferin (stock 0.1 mM in CM) | PJK | 102112 |
| dNTP Mix 10 mM | ThermoFisher Scientific | 611352 |
| ethidium bromide | Carl Roth | 2218.1 |
| fetal bovine serum (FBS) | Life Technologies | 10106-169 |
| random hexamers | Thermo Fisher Scientific | SO1492 |
| HPLC water | Carl Roth | A511.2 |
| hydrogen peroxide | Carl Roth | 8070.2 |
| luciferase assay reagent I (LARI) | Promega | E1500 |
| Lipofectamine2000® | Life technologies | 11668019 |
| NuPAGE 10-15 % SDS poly acrylamide gel | Life Technologies | NP0335PK2 |
| nitrocellulose membrane protan BA85, pore size 0.45 µM | Schleicher and Schuell | 10401196 |
| Oligo $(dT)_{12-16}$ | Thermo Fisher Scientific | 18418012 |
| peqFECT | Peclab | 13-8010 |
| resazurin | R & D systems | AR002 |
| protamine sulfate | Sigma-Aldrich | P3369 |
| protein $G^+$agarose beads | Santa Cruz | sc-2002 |
| SuperSignal West Pico | ThermoFisher Scientific | 34080 |
| SYBR green master mix | ThermoFisher Scientific | K0364 |
| trypan blue | Sigma-Aldrich | T8154 |

| reagent | supplier | order # |
|---|---|---|
| Trypsin/EDTA (1 x), 0.5 g/l trypsin | Lonza Biozym | 882040 |

### 2.1.9 DNA and protein standards; loading buffers

| reagent | supplier | order # |
|---|---|---|
| 100 bp DNA ladder | New England Biolabs | N3231 |
| 1 kb DNA ladder | New England Biolabs | N3232 |
| Magic Mark XP | Life technologies | LC5602 |
| NuPAGE sample buffer (4 x) | Life technologies | NP0007 |
| Orange Load. Dye (6 x) | ThermoFisher Scientific | R0631 |
| Spectra multi-color broad range | ThermoFisher Scientific | 26634 |

### 2.1.10 Enzymes

| enzyme | supplier | order # |
|---|---|---|
| Alkaline phosphatase, calf intestinal, 10 U/µl | New England Biolabs | M0290 |
| DNA polymerase I, large (Klenow) fragment | New England Biolabs | M0210 |
| LR-Clonase II enzyme mix | Life technologies | 11791020 |
| PureLink®DNase set | Life technologies | 12185010 |
| M-MLV Reverse Transcriptase, 200 U/µl | ThermoFisher Scientific | 28025021 |
| Pfu Turbo DNA polymerase, 2 U/µl | Agilent Technologies | 200523 |
| Platinum® Pfx DNA proymerase, 2.5 U/µl | Life technologies | 11708013 |
| Phusion® High-Fidelity DNA polymerase, 2 U/µl | Biozym Scientific GmbH | F-530S |
| Proteinase K | Carl Roth | 7528.1 |

| enzyme | supplier | order # |
|---|---|---|
| T4 ligase (Fast-Link™ set) | Biozym Scientific GmbH | LK6201 |
| T4 polynucleotide kinase, 10 U/µl | New England Biolabs | M0201 |
| T7 endonuclease I, 10 U/µl | New England Biolabs | M0302 |
| **restriction enzymes** | | |
| BglII, 10 U/µl | New England Biolabs | R0144 |
| BlpI, 10 U/µl | New England Biolabs | R0585 |
| BsmBI, 10 U/µl | New England Biolabs | R0580 |
| BsrgI, 10 U/µl | New England Biolabs | R0575 |
| DpnI, 20 U/µl | New England Biolabs | R0176 |
| MluI, 10 | New England Biolabs | R0198 |
| NotI (HF®), 20 U/µl | New England Biolabs | R0189 |
| SalI, 10 U/µl | Thermo Fisher Scientific | RE0645 |
| SmaI, 20 U/µl | New England Biolabs | R0141 |

### 2.1.11 Pharmacological inhibitors

| inhibitor | supplier | order number |
|---|---|---|
| ivermectin | Sigma-Aldrich | I8898 |
| leptomycin B | Biozol | CAY-10004976 |
| | AppliBiochem | A7780 |
| protease inhibitor cocktail | Sigma-Aldrich | P8340 |

### 2.1.12 Primer and oligonucleotides

**Random hexamers**

| oligonucleotides | Sequence (5' → 3') |
|---|---|

| | |
|---|---|
| Oligo (dT) | TTTTTTTTTTTTTTTT |
| random hexamers | NNNNNN |

**Quantitative real-time PCR (qRT-PCR) primer**

| target | Qiagen order # | sequence (5' → 3') |
|---|---|---|
| h*gapdh** forward | | TGCACCaCCAACTGCTTAGC |
| h*gapdh** reverse | | ACAGTCTTCTGGGTGGCAGTG |
| h*tnpo1* | QT00084490 | |
| h*per1* | QT00113337 | |

*h*gapdh* primer are ordered at Eurofins MWG Operon and are mixed and diluted in TE buffer such as the QuantiTect primer assays.

**Amplification primer**

Amplification primer were designed using GENtle and Primer-BLAST - NCBI. Melting temperatures ($T_M$) were calculated using the GENtle software. Note: The $T_M$ of the forward (fwd) TOPO® cloning primers (*) were calculated without the non-coding 5' - CACC - 3' recognition sequence. All primers were ordered at Eurofins MWG Operon.

| | internal labeling | sequence (5' → 3') | TM |
|---|---|---|---|
| hbmal1 (522-599 aa) forward | hBmal1PY1 _BglII f | TTGAGATCTTTGGTACCAACATGCAACG C | 54 °C |
| hbmal1 (522-599 aa) reverse | hBmal1PY1 _SalI rv | AATGTCGACTTACAATTCATCGTCTGAT AGAAAAGTTG | 53 °C |
| hbmal1 (522-599 aa) forward | hBmal1PY2 _BglII f | TATAGATCTTCTCCAGGAGGCAAGAAG | 53 °C |
| hbmal1 (522-599 aa) reverse | hBmal1PY2 _SalI rv | GTAGTCGACTTAGTCTATACCTATGTGG GGGTTCTC | 53 °C |
| hcry1 (227-269 aa) forward | hC1PY_BglI I_fwd | TATAGATCTAGAAAGGCCTGGGTGGCAA A | 54 °C |
| hcry1 (227-269 aa) reverse | hC1PY_SalI _rev | GTAGTCGACTTATAGTTTGAAATAAAAC AGCCGACATG | 53 °C |

| | internal labeling | sequence (5' → 3') | TM |
|---|---|---|---|
| hcry2 (246-289 aa) forward | hC2PY_BglII_fwd | CACAGATCTCGGAAGGCCTGGGTTGCCA | 56 °C |
| hcry2 (246-289 aa) reverse | hC2PY_SalI_rev | TTTGTCGACTTACCACAGGCGGTAGTAAGAGG | 55 °C |
| hper1 (293-337 aa) forward | hP1PY1_BglII_fwd | AATAGATCTGAGAAGTCCGTCTTCTGCCGTAT | 57 °C |
| hper1 (293-337 aa) reverse | hP1PY1_SalI_rev | AATGTCGACTTAGCAGCACGGCTGTGCAGGG | 59 °C |
| hper1 (857-900 aa) forward | hP1PY2_BglII_fwd | TAAAGATCTTCACACCCCTCACCCGTGCCAC | 59 °C |
| hper1 (857-900 aa) reverse | hP1PY2_SalI_rev | TAAGTCGACTTAAGGGGGAAGAGGCTGGGGGCC | 59 °C |
| hper1 (909-952 aa) forward | hP1PY3_BglII_fwd | TAAAGATCTGCTTTCCCCGCCCCTTTGGT | 59 °C |
| hper1 (909-952 aa) reverse | hP1PY3_SalI_rev | TAAGTCGACTTAGTGCGAGGCAGGAGTGGGAG | 59 °C |
| hper2 (219-262 aa) forward | hP2PY1_BglII_fwd | TAAAGATCTAGAGATGCCTTCAGCGATGCC | 57 °C |
| hper2 (219-262 aa) reverse | hP2PY1_SalI_rev | TAAGTCGACTTATTGAGTAAAAGAATCTGCTCCACTGC | 56 °C |
| hper2 (250-315 aa) forward | hP2PY2_BglII_fwd | AATAGATCTGAGAAATCTTTCTTTTGCCGTGTCAG | 56 °C |
| hper2 (250-315 aa) reverse | hP2PY2_SalI_rev | AATGTCGACTTAGCAGCAAAGVTGACTCTCAGC | 56 °C |
| hper2 (1196-1239 aa) forward | hP2PY3_BglII_fwd | AATAGATCTACGGGCGGCCTGCCCG | 55 °C |
| hper2 (1196-1239 aa) reverse | hP2PY3_SalI_rev | AATGTCGACTTATTTGGTGTCCGACACTTCGCTG | 56 °C |
| htnpo1 (full-length) forward | TNPO1-1 Fwd | CACCATGGTGTGGGACCGGCAAACCAAGATG | 61 °C |
| htnpo1 (full-length) reverse with stop | TNPO1 Rev w St | TTAAACACCATAAAAAGCTGCAAGACGCTCTTT | 63 °C |

| | internal labeling | sequence (5' → 3') | TM |
|---|---|---|---|
| htnpo1 (full-length) reverse without stop | TNPO1 Rev wo St | AACACCATAAAAAGCTGCAAGACGCTCTTTTAA | 63 °C |
| htnpo1 amplification CRISPR/Cas9 region forward | TNPO1-5' CRISPR | GGCTGCCAGGAGCAGTTCC | 54 °C |
| htnpo1 amplification CRISPR/Cas9 region forward | TNPO1-3' CRISPR | GATACTTGTTGCACGGTTCTCT | 52 °C |

**Sequencing primer**

| | internal labeling | sequence (5' → 3') | $T_M$ |
|---|---|---|---|
| tnpo1 amplification | TNPO1 Seq1 | AACCAGAGGTACGGAAAAATGT | 51 °C |
| tnpo1 amplification | TNPO1 Seq2 | ACCTGAAGCCATTAATGACAG | 49 °C |
| m13 fwd | M13-Fwd | GTAAAACGACGGCCAGT | 46 °C |
| m13rev | M13-Rev | CAGGAAACAGCTATGAC | 41 °C |
| sequencing PY peptides | FW pEGFP-C | CAAAGACCCCAACGAGAAG | 48 °C |

**Phosphorylated oligonucleotides**

| | internal labeling | sequences (5' → 3') |
|---|---|---|

| | | |
|---|---|---|
| h*cry2* N-NSLΔC forward with stop (phosphorylated) | C2 NSL fwd STOP | CACCAACTCCCTCCTGGCCAGCCCCA CAGGCCTCAGCCCCTACTAA |
| h*cry2* N-NSLΔC reverse with stop (phosphorylated) | C2 NSL rev STOP | TTAGTAGGGGCTGAGGCCTGTGGGGC TGGCCAGGAGGGAGTTGGTG |

**Mutation primer**

Mutagenesis oligonucleotides were designed as described in the manufacturer's protocol of the Pfu site-directed mutagenesis guidelines (# 200523, Agilent technologies).

| | internal labeling | sequences (5' → 3') | $T_M$ |
|---|---|---|---|
| *cry2* PY → PA forward | Cry2PY-PA fwd | GCCCCACAGGCCTCAGCCCCGCGCT GCGCTTTGGTTGTCTCTCC | 88 °C |
| *cry2* PY → PA reverse | Cry2PY-PA rev | GACAACCAAAGCGCAGCGCGGGGCT GAGGCCTGTGGGGC | 86 °C |
| *cry2* PY → AA forward | mCry2AA fwd | GCCCCACAGGCCTCAGCGCCGCGCT GCGCTTTGGATGCCTCTCC | 82 C° |
| *cry2* PY → AA reverse | mCry2AA rev | GGAGAGGCATCCAAAGCGCAGCGCG GCGCTGAGGCCTGTGGGGC | 79 °C |
| cry2 RK → AA forward | C2 RK->AA fwd | TACAAGTCCGGACTCAGATCTGCGG CGGCCTGGGTTGCCAACTAT | 81 °C |
| cry2 RK → AA reverse | C2 RK->AA rev | ATAGTTGGCAACCCAGGCCGCCGCA GATCTGAGTCCGGACTTGTA | 81 °C |
| cry2 RPR → APA forward | C2 RPR->APA fwd | TGGGTTGCCAACTATGAGGCACCCG CAATGAACGCCAACTCCCTC | 81 °C |
| cry2 RPR → APA reverse | C2 RPR->APA rev | GGGAGTTGGCGTTCATTGCGGGTGC CTCATAGTTGGCAACCCAGG | 82 °C |
| per2 PY → PA forward | Per2PY2-PA fwd | CACCCCTTCCGCATGACGCCCGCTG GTCAAGGTGCGGGAC | 86 °C |

| | internal labeling | sequences (5' → 3') | $T_M$ |
|---|---|---|---|
| per2 PY → PA reverse | Per2PY2-PA rev | CGCACCTTGACCAGCGCGGGCGTCA TGCGGAAGG | 82 ° C |

**guide RNAs (gRNA)**

gRNAs were designed using the Optimized CRISPR Design - MIT software. The oligonucleotides were designed with overhangs complementary to BsmB I restriction sites (sense oligo5' - CTTC - 3' and antisense oligo: 3' - CAAA - 5').

| | internal labeling | sequences (5' → 3') |
|---|---|---|
| gRNA1 targeting *tnpo1* exon2 forward | TNPO1 E2-1 fw | CACCGAGTGGAAACCTGACGAGCAA |
| gRNA1 targeting *tnpo1* exon2 reverse | TNPO1 E2-1 rv | AAACTTGCTCGTCAGGTTTCCACT |
| gRNA2 targeting *tnpo1* exon2 forward | TNPO1 E2-2 fw | CACCGTGCTGAAGCCCTTGCTCGTC |
| gRNA21 targeting *tnpo1* exon2 reverse | TNPO1 E2-2 rv | AAACGACGAGCAAGGGCTTCAGCA |

**Gen synthesis product**

Gen synthesis of thehuman hnRNP A1 M9 NLS was orderd at Eurofins MWG Operon and was provided in a pEX-A vector.

| | internal labeling | sequence (5' → 3') |
|---|---|---|
| M9 NLS | pEX-A M9 | AGATCTAATCAGTCTTCAAATTTTGGACCCATGAAGGGAGGAA ATTTTGGAGGCAGAAGCTCTGGCCCCTATGGCGGTGGAGGCCA ATACTTTGCAAAACCACGAAACCAAGGTGGCTATTAAGTCGAC |

### 2.1.13 Vector backbones

Vector maps can be found in the supplementary methods (see material A 2.1).

| vector backbone | supplier/source |
|---|---|

| | |
|---|---|
| pENTR/D-TOPO® | Life Technologies |
| pcdnaDEST 40 | Life Technologies |
| pEF Dest 51 | Life Technologies |
| pLenti6-Dest-V5 | Life Technologies |
| pLenti6-Dest-Venus | modified from pLenti6-V5 |
| lentiCRISPR v2 | addgene |
| pc-MYC-CMV-D12 | kind gift of the AG Wanker, MDC Berlin, Germany |
| pECFP-C1 | Clontech (not available anymore) |
| pGIPZ | GE Dharmacon |
| pMD2G | addgene |
| psPAX | addgene |
| pUC19 | New England Biolabs |
| pEX-A | Eurofins MWG Operon |

### 2.1.14 Protein and peptide coding sequences (CDS)

All coding sequences were verified by restriction enzyme digestion and sequencing. Peptide lengths are indicated in brackets.

| CDS | Entrez gene ID | origin |
|---|---|---|

| | | |
|---|---|---|
| hbmal1 (95-150 aa and 522-599 aa) | 406 | PCR-amplified cDNA library of U-2 OS cells |
| hcry1 (full-length) | 1407 | previously cloned within the laboratory |
| hcry1 (227-269 aa) | 1407 | PCR-amplified cDNA library of U-2 OS cells |
| hcry2 (full-length) | 1408 | previously cloned within the laboratory |
| hcry2 (246-289 aa) | 1408 | PCR-amplified cDNA library of U-2 OS cells |
| hhnrnpA1 (264-308 aa) | 3178 | gen synthesis (see 2.2.4) |
| mper1 (full-length) | 18626 | previously cloned within the laboratory |
| hper1 (293-337 aa, 857-900 aa and 909-952 aa) | 5187 | PCR-amplified cDNA library of U-2 OS cells |
| mper2 (full-length) | 18627 | previously cloned within the laboratory |
| hper2 (219-262 aa, 250-315 aa and 1196-1239 aa) | 8864 | PCR-amplified cDNA library of U-2 OS cells |
| htnpo1 (full-length) | 3842 | ordered by Thermo Scentific (Clone ID: 4178989) |
| lacz (full-length) | | previously clonedwithin the laboratory |
| firefly luciferase(full-length and LUC1: 1-407 aa, LUC2 : 408-560 aa) | | previously clonedwithin the laboratory |
| renilla luciferase (full-length) | | previously clonedwithin the laboratory |

### 2.1.15 RNA-interference (RNAi) constructs

We used shRNA for knockdown of gene expression. shRNA constructs targeting *tnpo1* and *per1* expression are listed below. All shRNA constructs used in the RNAi-screen,

in order to identify nucleo-cytoplasmic translocation-associated components essential for normal circadian dynamics, can be found in the supplements (table A 1.1)
Non-silencing shRNA and shRNA constructs targeting either *tnpo1* or *per1* expression are listed below.

| internal labeling shRNA | GE Dharmacon order number |
|---|---|
| non-silencing (ns) | RHS4346 |
| sh*tnpo1*_1 | V2LHS_133786 |
| sh*tnpo1*_2 | V2LHS_133788 |
| sh*tnpo1*-3 | V2LHS_133789 |
| sh*tnpo1*_4 | V3LHS_642145 |
| sh*tnpo1*_5 | V3LHS_642148 |
| sh*tnpo1*_6 | V3LHS_646032 |
| sh*per1*_1 | V2LHS_169842 |
| sh*per1*_2 | V2LHS_169845 |
| sh*per1*_3 | V2LHS_7714 |

### 2.1.16 Commercially available kits

| kit | supplier | order number |
|---|---|---|
| CalPhos™ Mammalian Transfection Kit | Clontech Laboratories | 631312 |
| Dual-Luciferase® Reporter Assay System | Promega | E1960 |
| Fast-Link™ DNA Ligation Kit | Biozym | 133625 |
| Gateway® LRClonase® II Enzyme mix | Life Technologies | 11791020 |
| Maxima™ SYBR Green qPCR Maser Mix | Thermo Fisher Scientific | K0223 |
| Melon™ gel IgG spin purification kit | Thermo Fisher Scientific | 45206 |

| kit | supplier | order number |
|---|---|---|
| QIAEX II® gel extraction kit | QIAGEN | 20021 |
| QuikChange Site - Directed Mutagenesis Kit | Agilent Technologies | 200518 |
| PureLink® HiPure Plasmid Filter Midiprep Kit | Life Technologies | K210015 |
| PureLink® Quick Mini Kit | Life Technologies | K210011 |
| PureLink® RNA Mini Kit | Life Technologies | 12183018A |
| SuperSignal West Pico Chemiluminescent Substrate | Thermo Fissher Scientific | 34080 |

### 2.1.17 Equipment and electronic devices

| Equipment | | supplier |
|---|---|---|
| agarose gel chamber | | Febikon |
| ALPS 50™ | manual heat sealer | Thermo Fisher Scientific |
| *β*-scout | luminometer | PerkinElmer |
| C1000 Touch™ | thermal Cycler | Bio-Rad Laboratories |
| CFX96 | quantitative real-time PCR cycler | Bio-Rad Laboratories |
| ChemoCam Imager 3.2 | imaging station | INTAS |
| centrifuges (5810R, 5424R and 5415D) | | Eppendorf |
| Consort E143 | electrophoresis power supply | Sigma-Aldrich |
| Filtropur S 0.45 | virus supernatant filtration | Sarstedt |
| GFL 3032 | shaking inkubator | GFL |
| Hera cell 150 | incubator | ThermoFisher Scientific |

| Equipment | | supplier |
|---|---|---|
| Hera cell 150i | incubator | ThermoFisher Scientific |
| Herasafe (S1) | biosafety cabinet | ThermoFisher Scientific |
| Herasafe KS class II (S2) | biosafety cabinet | ThermoFisher Scientific |
| HCX PL Fluotar, 40 x, NA:0.6 | lens | Leica |
| Inu stage top incubator | incubator for confocal microscope | Tokai Hit |
| L5 ET | filter, fluorescence microscope | Leica |
| Infinite F200 pro | microplate reader | Tecan |
| LumiCycle | luminometer | Antimetrics |
| Leica DMIL LED Fluo | fluorescence microscope | Leica |
| NanoDrop 2000c | determination of DNA and RNA concentration | ThermoFisher Scientific |
| Neubauer chamber | cell counting chamber | Karl Hecht GmbH & CoKG |
| Olympus IX81 | confocal microscope | Olympus |
| Orion II | microplate luminometer | Berthold Direction Systems |
| Lab pH meter inoLab®, pH7110 | pH meter | WTW |
| Liquidator™ 96 | Multipipette, 96 well format | Steinbrenner |
| MultiSCREEN® HTS | 96 well plates for lentiviral filtration | Merck |
| Nunc™ Lab-Tek™ chambered cover glass | 4-well chamber, confocal microscopy | Thermo Fisher Scientific |

| Equipment | | supplier |
|---|---|---|
| pipettes (1-1000 µl) | | Eppendorf or Gilson |
| Rainin AutoRep™ E | electronic multistep pipette | Rainin |
| rotating wheel | | Labor-Brand |
| standard power pack P25 | electrophoresis power supply | Biometra |
| Unitwist RT | rocking table shaker | UniEquip |
| tabletop centrifuge | | NeoLab |
| TC dish 35 x , Nunclon | cell culture dishes, LumiCycle | Thermo Fisher Scientific |
| Thriller® | thermal shaker | VWR |
| TopCount | luminometer | PerkinElmer |
| Uno thermal cycler | PCR machine | VWR |
| Upl Sapo 60 x, NA:1.2 | lens | Olympus |
| UV trans illuminator | | Konrad Benda |
| Vortex Genie 2 | | Scientific Industries, Inc. |
| Whatman gel blotting paper | | Schleicher and Schuell |
| White micro well 96F, Nunclon delta | white 96 well plates, TopCount luminometer assay | Thermo Fisher Scientific |
| XCell SureLock™ Mini-Cell | electrophoresis system | ThermoFisher Scientific |

### 2.1.18 Databases and online tools

| tool | URL |
|---|---|
| Ensemble genome browser | http://www.ensembl.org/index.html |

| | |
|---|---|
| Circa DB - circadian expression profiles data base | http://circadb.hogeneschlab.org/ |
| National Center for Biotechnology Information | http://www.ncbi.nlm.nih.gov/ |
| Optimized CRISPR Design - MIT | http://crispr.mit.edu/ |
| Primer3 V.0.4.0 | http://bioinfo.ut.ee/primer3-0.4.0/ |
| UniProt | http://www.uniprot.org/ |
| source bioscience | http://www.sourcebioscience.com/ |

### 2.1.19 Software

| software | supplier/source |
|---|---|
| CFX Manager | Bio-Rad Laboratories |
| ChronoStar 2.0 | in-house developed; S. Lorenzen, B. Maier |
| GENtle | open source (M. Mankske, University of Cologne) |
| GraphPad PRISM | GraphPad Software, Inc. |
| ImageJ 1.44p | open source (National Institute of Health) |
| LaTEX | open source (Leslie Lamport, LaTeX Project Team) |
| Leica Application Suite, V3.7 | Leica |
| LumiCycle, LabView vi | Actimetrics |
| LyX | open source (The Document Processor) |
| Matlab 7.0 | The MathWorks, Inc. |
| Microsoft office 2010 | Microsoft |
| OlympusFluoview software, V1.a | Olympus |

### 2.1.20 Company register

| company | location |
|---|---|
| Actimetrics | Wilmette, USA |
| addgene | Cambridge, USA |
| Agilent Technologies | Santa Clara, USA |
| Ansell | Iselin, USA |
| AppliChem GmbH | Darmstadt, Germany |
| Becton Dickinson (BD) | Franklin Lakes, USA |
| Berthold Detection Systems | Pforzheim, Germany |
| Biometra | Göttingen, Germany |
| Bio-Rad Laboratories | Hercules, USA |
| Biozym Scientific GmbH | Hessisch Olendorf, Germany |
| Carl Carl Roth | Karlsruhe, Germany |
| Clontech Laboratories | Mountain View, USA |
| Eppendorf | Enfield, USA |
| Eurofins MWG Operon | Ebersberg, Germany |
| Febikon | Wermelskirchen, Germany |
| Fermentas GmbH | Leon, USA |
| GE Healthcare Dharmacon Inc. | Lafayette, USA |
| GFL | Burgwedel, Germany |
| Intas | Ahmedabad, India |
| Karl Hecht GmbH & CoKG | Sondheim, Germany |
| Konrad Benda | Wiesloch, Germany |
| Labor Brand | Gießen, Germany |
| Life Technologies | Carlsbad, USA |

| company | location |
|---|---|
| Merck | Darmstadt, Germany |
| NeoLab | Heidelberg, Germany |
| New England Biolabs (NEB) | Ipswich, USA |
| Olympus | Hamburg, Germany |
| Open Biosystems | Huntsville, USA |
| P.J.K | Kleinblittersdorf, Germany |
| PAA Laboratories GmbH | Cölbe, Germany |
| Peqlab Biotechnologie GmbH | Erlangen, Germany |
| PerkinElmer | Rodgau, Germany |
| Promega | Madison, USA |
| Qiagen | Venlo, Netherlands |
| R & D systems | Wiesbaden, Germany |
| Roche | Mannheim, Germany |
| Carl Roth | Karlsruhe, Germany |
| SantaCruz Biotechnology | Dallas, USA |
| Sarstedt | Nümbrecht, Germany |
| Schleicher and Schuell | Munich, Germany |
| Scientific Industries, Inc. | Bohemia, USA |
| Sigma-Aldrich-Aldrich | St. Louis, USA |
| Serva | Heidelberg, Germany |

## 2.2 Methods

### 2.2.1 Cell culture assays

**Cultivation and passaging of human cells**

Cell lines, either HEK293 or U-2 OS, were cultured in complete medium (CM) (see 2.1.5) over a period of 8 weeks if not stated differently. Cells were passaged twice to thrice a week at a confluency of approximately 80 %. For splitting, the cells were washed once with pre-warmed 1 x phosphate buffered saline (PBS) prior to enzymatic detachment using trypsine for 5 minutes at 37 °C. The detached cells were dispersed in DMEM at an appropriate ratio and kept in an incubator at a constant temperature of 37 °C, 5 % carbon dioxide ($CO_2$) and a 100 % humidity.

**Cell counting**

If necessary, cells were counted using trypan blue and a Neubauer chamber. For cell counting, the cells were detached using trypsin (see above) and diluted 1:1 using trypan blue. The cell-trypan blue mix was applied to the Neubauer chamber and all cells in the four big squares (each composed of 4 x small squares) were counted. The cell concentration was calculated using equation 1:

$$\frac{\text{cells}}{\text{ml}} = \frac{\text{counted dilution} \times \text{dilution factor} \times 10000}{number\ of\ counted\ squares} \qquad (1)$$

**Cell vitality assay**

Cell vitality was determined using a Resazurin vitality assay. The procedure was carried out as stated in the manufacturer's protocol. Briefly: 10 % resazurin were added to the CM and incubated at a constant temperature of 37 °C for three to four hours. Afterwards, absorbance was measured using the Infinite F200 pro, TECAN fluorescence reader at an excitation of 535 nm and an emission of 590 nm. A normalized cell vitality of 0.75 was manually predetermined as cut off for vital cells

**Transient transfection of human cells**

Transient transfections were performed using either Arest-in™, pecFECT, Lipofectamine2000® or the CalPhos™ Mammalian Transfection Kit according to the respective manufacturer's recommendations. Briefly: cells were seeded at a confluency of approximately 80 % one day prior to the transfection. The DNA and transfection reagent were mixed and incubated prior to the cell treatment. On the next day, the medium was changed and follow-up assays could be performed.

Lentivirus production

Lentivirus production was performed as described in the standard operating procedure (suppl. material A2.2). Briefly: HEK293T cells were seeded one day prior to transient transfection. Transfection was performed using the CalPhos™ Mammalian Transfection Kit as described in the manufacturer's protocol. On the next day, the medium was changed. On day four and five virus particles were collected by decanting the supernatant into a falcon. The virus was stored at 4 °C until filtration. The filtered virus supernatant was ready to use and could alternatively be stored at -80 °C.

**Stable transduction**

The cells were detached using trypsine (see above) and diluted to a confluency of approximately 70-80 %. The viral supernatant was added to the cell suspension in a ratio of 1:1. The reaction mix was supplemented with a final concentration of 8 protamine sulfate. On the next day, the medium was changed. If necessary, an appropriate antibiotic (blasticidin or puromycin) was added at to the CM at a concentration of 10  to select for the transduction-positive cells. Note: For blasticidine selection cells were detached prior to addition of the selection medium.

**Pharmacological treatments**

Both pharmacological inhibitors, leptomycin B (LMB) and ivermectin (Iver), were solved in ethanol (EtOH) and stored at -20 °C. The U-2 OS cells were grown to confluency and prepared for bioluminescence recordings (see 2.2.2). After synchronization, the pharmacological inhibitors or solvent (EtOH) were added to the measurement.

**Hydrogen peroxide treatment**

Hydrogen peroxide was added at a final concentration of 200 µM to the adherent U-2 OS cells 30 minutes prior to either the cell harvest or imaging. To do so, the hydrogen peroxide was diluted 1:1000 in HPLC water and directly added to the CM. HPLC water was used as solvent control.

### 2.2.2 Imaging methods

**Bioluminescence recordings**

Bioluminescence recordings were performed as described in Maier *et al.* (2009) [159]. Briefly: U-2 OS cells expressing either harboring a *bmal1* or *per2* promoter-driven *luciferase* (see 2.1.2) were used for bioluminescence recordings. The cells were seeded in white 96 well plate or in 35 mm dishes and grown to 100 % confluency. Afterwards cells were synchronized adding 1 µM dexamethasone for 30 minutes at 37 °C. Post incubation, the cells were washed twice with 1 x PBS. Phenolred-free DMEM was supplemented with 250 µM D-luciferin. The 96 well plates or 35 mm dishes were sealed to prevent dehydration prior to placement in either the TopCount or LumiCycle luminometer device. Bioluminescence recordings were carried out over a period of four to seven days. Analysis were performed using the ChronoStar 2.0 software (see 2.2.9).

**Fluorescence microscopy**

Life cell imaging was performed using either the Leica DMIL LED Fluo fluorescence microscope or the Olympus IX81 confocal microscope. Images were recorded using either the Leica Application Suite software, V3.7 or the Olympus Fluoview software. Analysis were performed using ImageJ 1.44p (see 2.2.9).

**Fluorescence recovery after photobleaching (FRAP)**

For detailed description see Öllinger *et* al., 2014 [165]. The cells were seeded in 4-well glass-bottom-chambers to enable confocal microscopy. At 80-100 % confluency imaging was performed using an Olympus IX81 confocal microscope and the Olympus Fluoview software. Therefore, an attached climate chamber maintained optimal conditions at 5 % $CO_2$, a 100 % humidity and a constant temperature of 37 °C to prevent a decrease in cell vitality and to reduce cell movement. Fluorescence intensity was measured taking a stack of five pictures on the Z-axis. One image stack was captured prior

to bleaching as reference of the initial fluorescence intensity. Nuclei were separately bleached at a laser intensity of 100 % using the fast mode of the tornado-function in a time slot of 50 frames. Afterwards a post-bleach image stack was taken. Finally a time-series of fluorescence recovery was started at a period of 150 seconds for up to one hour. During measurement loss of focus was corrected manually. Analysis of the kinetics were executed using Olympus Fluoview software, V1.a and ImageJ 1.44p (see 2.2.9).

### 2.2.3 Protein assays

**Luciferase complementation assay**

The *firefly luciferase (luc)* gene was split in a C-termianl and N-terminal fragment (LUC1 amino acids (aa): 1-407, LUC2 aa: 408-560). Each one was fused to a protein of interest using the Gateway® cloning system (see 2.2.4). If the two proteins of interest will be in close proximity, the luciferase fragments will be enzymatically active, thereby metabolizing the supplemented substrate, luciferin. This process can be measured as luminescence. As a control for transfection full-length renilla luciferase was co-transfected.

For luciferase complementation assay, the Dual-Luciferase® Reporter Assay System was used according to the manufacturer's protocol. Briefly: one day prior to transfection, the HEK293 cells were seeded in a 24 well plate at a confluency of about 80 %. Cells were transiently transfected as described above (see 2.2.1). To harvest the cells after 48 hours, they were washed once with 1 x PBS and lysed in 1 x passive lysis buffer for at least 2 hours at -80 °C. The cell lysates were thawed, briefly vortexed, homogenized by pipetting up and down and transferred to a white 96 well plate. Luminescence was measured using the Orion II microplate luminometer. Each well was measured for 10 seconds with a pause of 2 seconds between firefly and renilla luciferase measurements.

**Whole cell lysate - protein extraction**

If not otherwise stated, cells were grown to confluency, washed once using 1 x PBS and lysed in either RIPA, Co-IP or PKB lysis buffer (for composition, see 2.1.3). CoIP and RIPA were supplemented with 1:100 protease inhibitor cocktail. The respective buffer was added to the cells and incubated for at least 30 minutes at 4 °C on a rocking shaker. Afterwards, cells were scraped off the dish and homogenized using a 20G x 1.5" syringe for 15 x times. Lysates were centrifuged for 30 minutes at 13200 rpm and 4 °C in

either a 5810R, a 5424R or a 5415D centrifuge. The supernatants, containing all soluble proteins, were transferred to new tubes and used in follow-up assays or stored at -20 °C.

**Determination of protein concentration**

Luciferase-based determination of the protein concentration

Protein input of the luciferase-fusion proteins, used in Co-immunoprecipitation assays (see below), was determined using the *β*-scout device. 25 µl Luciferase activity reagent (LARI) was added to 5 µl of the protein lysate and incubated for ten seconds prior to the first measurement. Luminescence was measured in different time intervals of 60 - 120 seconds over a period of up to ten minutes. The highest determined luminescence counts were used as protein input reference for Co-IP assays.

Bicinchoninic acid assay (BCA assay)

Bovine serum albumin (BSA) was used as standard and diluted in the appropriate lysis buffer depending on the sample lysis buffer. 5 µl of either the standard or the protein lysates were transferred into a 96 well plate. 200 µl of BCA solution was applied to each standard or protein sample. To prepare the BCA solution, solution A and B (see 2.1.3) were mixed in a ratio of 1:50. Afterwards, the protein-BCA-mix was incubated at 37 °C for 30 minutes. The protein concentration was determined using the Infinite F200 pro, TECAN to measure the optic density of the samples at 560 nm.

**Co-immunoprecipitation (Co-IP)**

The whole cell protein lysates (see above) were pre-cleared with 30 µl of agarose $G^+$ beads at 4 °C for one hour on a rotating wheel. If not otherwise stated, the lysates were centrifuged at 3500 rpm at 4 °C for 5 minutes and always kept at 4 °C. The supernatant was transferred to low-binding tubes. 2 µl of either anti-TNPO1, anti-MYC, anti-V5 or normal mouse IgG antibody were added and incubated for one hour on a rotating wheel. Note: A normal mouse IgG was used as negative control of unspecific binding to the antibody.

30 µl of agarose $G^+$ beads were added to the antibody-protein lysate mix and incubated for one hour on a rotating wheel. For determination of luciferase counts, the CoIPs were washed twice with ice cold 1 x PBS and dried with a 27G x 0.75" syringe. Repeated measurements using the *β*-scout device were performed as for the input determination (see above). The highest determined luminescence counts were used as an indication of the protein interaction and compared to the counts of the control.

**SDS-polyacrylamide gel electrophoresis (PAGE) and western blot**

The SDS-PAGE was either self-prepared (table 2.1) or ordered from Life Technologies. The whole cell protein lysates (see above) were supplemented with 4 x NuPage loading buffer and incubated at 95 °C for 10 minutes. Afterwards, protein lysates were loaded on the SDS-PAGE and run at either 120 V (self-prepared gels) or 200 V (commercial gels) for 60-180 minutes. Note: the commercial SDS-PAGEs are supplied with NuPAGE running and NuPAGE transfer buffer.

The proteins were blotted on nitrocellulose membranes using either a wet- or semidry blotting technique. For the performance of a wet blot, the membrane and the gel were sandwiched in a blotting cassette. Proteins were transferred for 90–360 minutes at 90 V. For semi-dry blotting, the Iblot2 was used as described in the manufacturer's protocol (25 mA, 10 min).

**Table 2.1: Composition of self-prepared SDS-PAGE**

composition of 1 x 1.5 mm gel

| stacking gel (6 %) | | separation gel (10 %) | |
|---|---|---|---|
| aq. dest. | 2.745 ml | aq. dest. | 14.4 ml |
| stacking gel buffer | 0.975 ml | separation gel buffer | 9 ml |
| acrylamide/bis-acrylamide 30 % | 0.6 ml | acrylamide/bis-acrylamide 30 % | 12 ml |
| 10 % SDS | 0.045 ml | 10 % SDS | 0.36 ml |
| 10 % APS | 0.0225 ml | 10 % APS | 0.18 ml |
| TEMED | 0.0045 ml | TEMED | 0.018 ml |

The membranes were blocked in 1 x tris buffered saline (TBS) supplemented with 0.05 % Tween®20 (TBS-T) and 5 % skim milk at room temperature for one hour on a rocking shaker. The primary antibodies were diluted 1:1000 to 1:5000 in TBS-T and incubated at 4 °C on a rocking shaker overnight. The blots were washed thrice in TBS-T prior to addition of the secondary antibodies. The appropriate secondary antibody was diluted 1:1000 in TBS-T prior to the incubation at room temperature on a rocking shaker for one hour. Afterwards, the blots were washed thrice with TBS-T prior to detection using Super Signal West Pico and the ChemoCam Imager 3.2.

**IgG spin purification**

In-house generated antibodies (see 2.1.7) were purified prior to their use in western blot application. To this end, unpurified antibody was Melon™ gel purified using the Melon™ gel IgG spin purification kit as described in the manufacturer's protocol. 500 *µl* of purified antibody were obtained and were either directly used in a dilution of 1:100 in TBS-T or stored at 4 °C.

### 2.2.4 RNA and DNA techniques

**RNA purification**

The cells were washed once with 1 x PBS and either frozen at -80 °C or directly processed using the column based PureLink® RNA Mini Kit. The extraction was performed as described in the manufacturer's protocol. The recommended, optional DNase treatment was performed to minimize DNA contaminations. The RNA was eluted in 30 µl RNase free water supplied with the kit prior to direct follow up assays or the RNA could be stored at -80 °C until further processed.

**Reverse transcription**

Reverse transcription was performed in a two-step-protocol. 0.5 to 2 µg RNA were used as starting material. Depending on the approach either random hexamers or Oligo (dT) was used for reverse transcription of total RNA to cDNA. To quantify gene expression levels random hexamers were added to the reaction. Oligo (dT) was used to generate cDNA as template for amplification of a specific regions of interest.

First, the RNA, water, hexamers and dNTPs were mixed and heat-inactivated to promote cleavage of long cDNA strand. Afterwards, M-MLV reverse transcription buffer, DTT, RNase inhibitor (Ribo block) and M-MLV reverse transcriptase were added to reversely transcribe the total RNA into cDNA (table 2.1).

**Table 2.2: Composition and protocol of cDNA synthesis**

| step | component | volume [µl] | PCR program |
|---|---|---|---|
| 1 | total RNA (0.5-2 *µg*) | variable | incubate reaction mix of first step at 65 °C for 5 min |
| | aq. dest. | ad 50µl final reaction volume | |
| | 10 mM dNTP mix | 1 | |
| | random hexamers (20 µM) or Oligo (dT) (100 pmol) | 5 or 1 respectively | |
| 2 | 5 x first strand buffer | 10 | incubation after addition of residual components:<br>10 min at 25 °C<br>50 min 37 °C<br>15 min at 70 °C<br>∞at 12 °C |
| | 0.1 M DTT | 5 | |
| | RNase inhibitor (40 U/µl) | 0.5 | |
| | M-MLV-reverse transcriptase | 0.25 | |

**Determination of the RNA and DNA concentration**

Concentrations of RNA and DNA were performed using the NanoDrop 2000c device as described in the manufacturer's protocol.

**DNA purification from bacterial cells**

DNA purifciation was performed using a PureLink® DNA extraction kit as described in the manufacturer's protocol. Depending on the size of bacterial culture either the mini, midi or maxi kit was used. DNA was eluted in an appropriate volume of HPLC water.

**Genomic DNA extraction**

The cells were grown to a 100 % confluency and detached using trypsin (see 2.1.1). 5 to 10 µl of the cell-trypsin-suspension were lysed in Direct PCR lysis buffer supplemented with 0.4 proteinase K. To do so, the reaction mix was incubated at 55 °C for 15 minutes prior to a second heating step at 85 °C for 45 minutes. The genomic DNA could either be used in follow up assays or stored at -20 °C.

**Restriction enzyme digest**

The DNA was complemented with an appropriate reaction buffer, depending on the used enzyme), BSA and the restriction enzyme. The reaction mix was briefly vortexed

and spun down. The reaction was incubated at an appropriate temperature, according to the manufacturer's protocol of the restriction enzyme, for at least one hour.

## PCR amplification

**Table 2.3: PCR composition and program using the Platinum® Pfx DNA polymerase**

| composition of reaction mix | V [µl] |
|---|---|
| genomic DNA | 4 |
| 10x Pfx reaction buffer | 5 |
| $MgSO_4$ | 1 |
| 10 mM dNTP mix | 1.5 |
| forward primer (10 µM) | 2 |
| reverse primer (10 µM) | 2 |
| Platinum® Pfx DNA polymerase | 0.5 |
| HPLC water | ad 50 |

| | PCR step | temp. | time |
|---|---|---|---|
| | initial denaturation | 95 °C | 5 min |
| 35 cycles | denaturation | 94 °C | 30 sec |
| | annealing | 56 °C | 30 sec |
| | extension | 72 °C | 40 sec |
| | final extension | 72 °C | 5 min |

**Table 2.4: PCR composition and program using the Phusion® High-Fidelity DNA polymerase**

| composition of reaction mi: | V [µl] |
|---|---|
| template (10-100 ng) | variable |
| 5 x high fidelity buffer | 10 |
| 10 mM dNTP mix | 1 |
| forward primer (10 µM) | 2 |
| reverse primer (10 µM) | 2 |
| Phusion®High-Fidelity DNA polymerase | 0.25 |
| HPLC water | ad 50 |

| | PCR step | temp. | time |
|---|---|---|---|
| | initial denaturation | 98 °C | 1 min |
| 30-35 cycles | denaturation | 98 °C | 10 sec |
| | annealing | depending on primer $T_M$ | 30 sec |
| | extension | 72 °C | 30 sec per kb |
| | final extension | 72 °C | 10 min |

### Oligonucleotide-annealing

Short oligonucleotide sequences such as of *cry2* N-NLS (see 2.1.12 and 3.4.3) are difficult to amplify using primers. Therefore, these sequence was ordered as phosphorylated oligonucleotides (up to 50 bp) and annealed prior to ligation. The composition of the reaction mix and the cycling program are listed in tables 2.5. 10 µl reaction mix was diluted 1:1000 using HPLC water and could either be used in follow up assays or was stored at -20 °C.

**Table 2.5: 1 x reaction mix and PCR program of primer annealing**

| composition of 1 x reaction mix | V [µl] | PCR step | temperature | time |
|---|---|---|---|---|
| forward primer (100 pmol/µl)] | 1 | | 37 °C | 30 min |
| reverse primer (10 0pmol/µl) | 1 | denaturation | 95 °C | 5 min |
| 10 x T4 ligation buffer | 1 | slow annealing | 95 °C to 25 °C | increment of 5 °C per min |
| HPLC water | ad 10 | | | |

### Phosphorylation of oligonucleotides

The purified PCR-product (see below) was incubate with the T4 polynucleotide kinase (for composition of the reaction mix table 2.6) at 37 °C for one hour prior to the addition of EDTA and an additional incubation at 65 °C for 20 minutes.

**Table 2.6: Composition of primer phosphorylation reaction mix**

| 1 x reaction mix | V [µl] |
|---|---|
| oligonucleotide (100 pmol/µl) | 7 |
| 10 x T4 ligase buffer | 4 |
| T4 polynucleotide kinase | 1 |
| HPLC water | ad 20 |
| EDTA, 100 mM | 3 |

### Quantitative real-time PCR

qRT-PCR was performed using the Maxima$^{TM}$SYBR Green qPCR Maser Mix and QuantiTect primer (primer list 12.1.12). cDNAs were diluted 1:2 to 1:10 depending on the reversely-transcribed amount of RNA prior to setup of the reaction mix (table 2.7).

The qRT-PCR cycling protocol was setup as advised in the manufacturer's protocol (table 2.7). An additional melting step was included to detect potential primer dimers.

**Table 2.7: Reaction mix and PCR program of qRT-PCR**

| reaction mix | V [µl] | | PCR step | temperature | time |
|---|---|---|---|---|---|
| Maxima™ SYBR green master mix | 10 | | | 50 °C | 2 min |
| commercially available primer mix | 2 | | initial denaturation | 95 °C | 10 min |
| pre-diluted cDNA | 8 | 40 cycles | denaturation | 95 °C | 15 sec |
| | | | combined annealing and extension | 60 °C | 690 sec |
| | | | melting curve | 95 °C | 10 sec |
| | | | | 65 °C to 95 °C | increment of 1 °C per sec |
| | | | | 95 °C | 0.5 sec |

**Site-directed mutagenesis**

Site-directed mutagenesis was performed using either the Pfu Turbo DNA polymerase or the Platinum® Pfx DNA polymerase. The mutagenesis primer (see 2.1.12) were designed using the QuikChange Site - Directed Mutagenesis protocol:

- primer length between 25-45 bp
- $T_M \geq 78$ °C
- calculation of $T_M$:

  $$T_M = 81.5 + 0.41 \times (\%GC) - 675 / N - \%\,mismatch \quad (2)$$

  Note: N indicates the number of bases without insertions or deletions.
- the desired mutation should be placed in the middle of the primer
- primers should have at least a minimum a 40 % GC content and end with G or C bases

Site-directed mutagenesis was performed as described in the manufacturer's protocol of the used polymerase. Reaction mix and cycling program are listed in tables 2.7. 50 ng template was used for Pfx-site-directed mutagenesis.

**Table 2.8: Mutagenesis 1 x reaction mix and PCR program**

| reaction mix | V [$\mu l$] | | step | temperature | time |
|---|---|---|---|---|---|
| template (5-50 ng) | variable | | initial denaturation | 95 °C | 30 sec |
| 10 x Pfu reaction buffer | 5 | | denaturation | 95 °C | 30 sec |
| 10 mM dNTP mix | 1 | 15-18 cycles | annealing | 55 °C | 1 in |
| forward primer (10 µM) | 1 | | extension | 68 °C | 1 min per kb |
| reverse primer (10 $\mu M$) | 1 | | | | |
| Pfu Turbo DNA polymerase | 1 | | | | |
| HPLC water | ad 50 | | | | |

The PCR-product was digested with DpnI prior to transformation into competent XL1blue bacteria (see below). Afterwards, DNA was extracted from liquid bacteria cultures and verified using restriction enzyme digest and sequencing.

### Agarose gel electrophoresis subsequent agarose-gel extraction

Size-dependent separation of DNA was performed using agarose gel electrophoresis. The DNA was supplemented with 6 x Orange loading dye and loaded onto an agarose gel. As a standard either a 100 bp or 1 kb DNA ladder was run with the samples. To purify the separated DNA, the QIAEX II® gel extraction kit was used as described in the manufacturer's protocol. The DNA or PCR-product was eluted in 20 µl HPLC water.

### Sequencing

Sequencing was outsourced to SourceBioscience. Sequencing requirements according to the SourceBioscience website:

- 5 µl of the extracted DNA, 100 ng/µl
- or 5 µl PCR-product, 1ng/µl per 100 bp
- 5 µl of the sequencing primer, 3.2 pmol/µl

**DNA ligation**

If necessary, linear plasmids were dephosphorylated to prevent recircularization prior to agarose gel electrophoresis and gel extraction. To do so, the linearized plasmids were incubated with calf intestinal alkaline phosphatase (CIP) at 37 °C for 30 minutes. Note: This step was repeated once.

The purified linearized DNA insert and plasmid backbone were ligated using the Fast-Link™ DNA Ligation Kit. The reaction mix (for composition table 2.9) was incubated at room temperature for 15 minutes. The ligation mix was transformed in competent bacterial cells (see below).

**Table 2.9: Composition of DNA ligation mix**

| reaction mix | V [*µl*] |
|---|---|
| linearized DNA insert | 3 |
| linearized plasmid backbone | 1 |
| 10 x Fast-Link™ ligation buffer | 1 |
| ATP (10 mM) | 1 |
| 10 x Fast-Link™ ligase | 0.5 |
| HPLC water | ad 10 |

**TOPO® clonning**

To shuttle the coding sequence of interest into pENTR/D plasmids, the region of interest was PCR-amplified from plasmids encoding the gene of interest or from cDNA (primer list2.1.12). For TOPO® cloning, 1 µl of the purified PCR-product (see above) was used in the reaction mix as described in the manufacturer's protocol. However, the reaction mix was incubated at room temperature for 30 minutes prior to transformation in competent TOP10 bacterial cells (see below).

**Gateway® cloning**

The Gateway® cloning system provides the insertion of coding sequences from entry clones, generated using the TOPO® cloning kit (see above), into a variety of destination vectors (vector list 2.1.13). The reaction was performed at room temperature for one hour (table 2.10 for composition of reaction mix) prior to a final protease K incubation step for at 37 °C for ten minutes.

**Table 2.10: Composition of Gateway® cloning reaction mix**

| reaction mix | V [µl ] | incubation step |
|---|---|---|
| pENTR/D_CDS (30 ng/µl) | 1 | |
| destination vector (30 ng/µl) | 1 | room temperature for 1 hour |
| LR Clonase® II | 0.5 | |
| Proteinase K 2 (µg/µl) | 0.25 | 37 °C for 10 min |

**Transformation of bacterial cells**

The plasmids were transformed into the competent bacterial strains (table 2.1.1) using a heat-shock-protocol. Briefly: the competent bacterial cells were thawed on ice. The TOPO®, Gateway® or ligation reaction mix (or 200 ng of plasmid DNA if re-transformed) was gently mixed with the competent bacteria prior to a 30 minutes incubation step on ice. Afterwards a heat-shock was performed at 42 °C for 60 seconds. The bacterial cells were briefly cooled down and incubated in 500 µl LB medium at 37 °C in a thermal shaker (750 rpm) for 30-45 minutes. The bacterial cells were plated on LB agar plates containing the appropriate antibiotics (depending on the transformed plasmid DNA) and incubated overnight.

**Cultivation and storage of bacterial cells**

Bacterial cells, were singularized on LB agar plates, supplemented with the appropriate antibiotic (depending on the carried plasmid), and incubated at 37 °C overnight. The singularized bacterial clones were transferred into liquid culture (supplemented with the respective antibiotic) and incubated for 14-18 hours on a horizontal shaker. For DNA purification (see above), the bacterial cells were spun down at 12000 x g for 30 seconds.

For long-time storage of the DNA, bacterial cells were grown in a liquid overnight culture. 700 µl of the overnight culture carrying the DNA of interest was supplemented with 500 µl of sterile glycerol. The mix was briefly vortex and incubated on ice for one hour prior to cryo-conservation at -80 °C.

**T7 endonuclease assay**

For a detailed description see Korge *et al.* (2015) [255]. Briefly: the region of interest was PCR-amplified from genomic DNA using appropriate primers (see above). The amplicon was denatured and slowly re-annealed to generate heteroduplex double-

stranded (ds) DNA if Cas9-mediated NHEJ introduced indels in the region of interest. The addition of the T7 endonuclease I, which cuts only single-stranded DNA, leads to smaller fragments of the genome-edited dsDNA but not of the homoduplex wild type dsDNA.

### 2.2.5 GFP-silencing

The pGIPZ vector encodes a *green fluorescent protein* (*gfp*) open-reading-frame (orf), which is interfering with the fluorescence of the ECFP-fusion proteins used in the subcellular distribution assay. To create a non-functional GFP an out-of-frame shift was induced in the *gfp* orf. To this end, the pGIPZ vector was restriction digested using BlpI, which cuts about 175 bp downstream of the *gfp* start codon. The sticky ends of the linearized pGIPZ vector were refilled using a Klenow polymerase (table 2.11 for composition of reaction mix). The reaction mix was incubated at 37 °C for one hour prior to a second incubation step at 70 °C for 15 minutes. Afterwards the plasmid was purified using the QIAEX II® gel extraction kit and re-ligated (see above). Verification was performed as restriction enzyme digest prior to lentivirus production.

**Table 2.11: Composition of Klenow reaction mix**

| reaction mix | V [µl] |
|---|---|
| BlpI-linearized DNA | 15 |
| 10 x NEB 2 buffer | 3 |
| 10 mM dNTP mix | 1 |
| Klenow polymerase | 2 |
| HPLC water | ad 20 |

### 2.2.6 RNAi-screen

pGIPZ plasmids were prepared in overnight bacterial cultures with ampicillin and zeozin resistance. On the next day, the DNA was purified (see 2.2.4) prior to lentivirus production in a 96 well format. To this end, the Liquidator™96 was used and virus supernatant was filtered in MultiSCREEN® HTS 96 well plates. Two different 96 well plate setups were used to produce virus particles of all 171 shRNA constructs, including the non-silencing control and three constructs of the positive control targeting *fbxl3* transcripts (suppl. material A2.3). Three repetitions of each plate were processed in

one experimental run. Two runs we were performed in total. Bioluminescence recordings were performed as described above (see 2.2.2). After termination of the bioluminescence recordings, cell vitality was determined using a resazurin assay (see 2.2.1).

### 2.2.7 Subcellular distribution assay

Circadian clock peptides were PCR amplified using the Phusion® High-Fidelity DNA polymerase (see 2.2.4). Amplification primer were ordered at Eurofins MWG Operons with a BglII restriction site at the 5'-end of the forward primer and a SalI-restriction site at the 5'-end of the reverse primer. PCR-products and the vector backbone either pECFP or pEYFP were restriction enzyme digested (see 2.2.4) using BglII and SalI. Prior to ligation (see 2.2.4), the linearized vector backbone and PCR-amplicons were purified using the QIAEX®II gel extraction kit (see 2.2.4). U-2 OS or HEK cells were transiently transfected (see 2.2.1) 24 to 48 hours prior to visualization and image analysis using a fluorescence microscope (see 2.2.1). Images were analyzed using the ImageJ 1.44p software (see 2.2.9).

### 2.2.8 CRISPR/Cas9 genome engineering

CRISPR/Cas9 genome engineering was performed as described in Korge *et al.*, 2015 [255]. Briefly: guide RNAs (gRNA) (see 2.1.12) were ordered at Eurofins MWG Operon including the essential BsmBI overhang to ligate the oligonucleotides into the BsmBI-linearized lentiCRISPv2 vector. Lentivirus of the verified (sequenced) lentiCRISPv2 encoding the gRNA prior to transduction of U-2 OS cells harboring a *bmal1* promoter-driven *luciferase*. After puromycin selection, the cell populations were prepared for bioluminescence recordings and placed in the LumiCycle (see 2.2.2). After termination of the bioluminescence recordings, mRNA and proteins were purified (see 2.2.3 and 2.2.4) and further processed to determine relative mRNA and protein level using reverse transcription, qRT-PCR (see 2.2.4), SDS-PAGE and western blot (see 2.2.3 ).

Genomic DNA of the cell populations was extracted (see 2.2.4) and amplified using the Platinum® Pfx DNA polymerase and the appropriate forward and reverse primer (see 2.1.12). The PCR-product were gel-purified and used in the T7 endonuclease assay (see 2.2.4).

The gRNA1 population was used for single cell dilution. To this end single cells were seeded in 96 well plates via limited dilution. At a confluency of about 80 % single cells were placed in the TopCount luminometer for bioluminescence recordings

(see 2.2.2). Additionally, genomic DNA was extracted (see 2.2.4) and the region of interest was PCR-amplified (for primers see 2.1.12). The PCR-product was phosphorylated and ligated into the SmaI-linearized and dephosphorylated pUC19 vector (see 2.2.4) prior to sequencing using the M13 forward primer (see 2.1.12 and2.2.4). Relative mRNA and protein levels were determined as described for the cell populations.

### 2.2.9 Bioinformatics and image analysis

**Bioluminescence time-series analysis**

Bioluminescence time-series were analyzed using the ChronoStar 2.0 software. The time series were trend-eliminated and fit to a sine-wave function. Detrending was automatically determined by division of individual data points to an average of 24-hours. The parameters were determined by a cosine-wave fit using equation 3.

$$y = amplitude \times e^{damping \times time} \times \cos 2 \times \pi \times time \times \frac{24}{period} + phase \qquad (3)$$

Additionally, an indication of the goodness of fit was determined by the correlation coefficient (CC).

**Image analysis**

All image analysis were performed using the ImageJ 1.44p software.

Subcellular distribution analysis

Images of the steady state, subcellular distribution of ECFP- or -Venus fusion proteins were manually analyzed. To this end, nuclei and whole cells were marked and the mean intensities as well as the respective mean areas (Ø area) were determined by the ImageJ 1.44p software. Additionally, a background intensity was determined and subtracted for each image. The cytoplasmic intensity was calculated using the mean intensities and whole areas of the regions of interest (equation 4).

$$mean_{cytoplasmic\ intensity} = \frac{mean_{cell\ intensity} \times \emptyset\ area_{cell} - mean_{nuc\ intensity} \times \emptyset\ area_{nuc}}{\emptyset\ area_{cell} \times \emptyset\ area_{nuc}} \qquad (4)$$

Afterwards the ratio of mean nuclear to mean cytoplasmic fluorescence intensity was determined.

FRAP assay

Analysis of the FRAP assays was performed as described in Öllinger *et al.*, 2014 [165]. However, after background subtraction the ratio of the mean nuclear to mean cytoplasmic intensity was determined for each individual image of each Z-stack.

Afterwards the mean of the three most focused images of each Z-stack (manually determined) was determined prior to normalization. To this end, the pre-bleached fluorescence intensity (t = -1 min) was set to 1. Fluorescence intensity at the time of bleaching (t = 0 min) was determined using a linear regression function (y = m x + n) of the first three data points after bleaching. The fluorescence intensity at the time of bleaching was set to 0 and all other values were adjusted.

To determine the recovery of 25 % of the initial fluorescence intensity a fit to a Michaelis-Menten-Equation (5) was used.

$$intensity = \frac{maximal\ intensity \times time}{K_m + time} \quad (5)$$

intensity - ratio of nuclear to cytoplasmic intensity (for calculation see image analysis subcellular distribution assay)
t - time
$K_m$ - Michaelis-Menten constant

**Statistical analysis**

All statistical analysis were performed using GraphPad PRISM. Steady state, subcellular distribution assays were statistically analyzed using One-way-ANOVA and either a Dunnett's or Tukey' multiple comparison test. FRAP assays (see above) were statistically analyzed using a Two-way-ANOVA and Sidac's multiple comparison test as post-test. Otherwise, a student's t-test was used for statistical analysis. For the RNAi-screen the determined p values were multiple-comparison corrected using a Bonferroni correction.

# 3 Results

Nuclear import of proteins is crucial to translocate them to their final compartment in a spatio-temporally controlled manner. Evidence was found that circadian core clock proteins of the mammalian circadian oscillator enter the nucleus by interaction with KPNB1 and its adaptor KPNA: Sakakida *et al.* (2005) reported KPNA-dependent classical nuclear import of CRY2. Different members of the kap*a*-family, KPNA1, KPNA3 and KPNA5 are able to bind to wild type CRY2 but not a cNLS mutant of the circadian clock protein [172]. In line with those findings, Umemura *et al.* (2014) reported altered PER1/PER2 localization upon misregulation of *kpna2* expression [173]. Lee and colleagues (2015) focused only on KPNB1. They showed impaired nuclear import of PERs and CRYs upon depletion of *kpnb1* expression using RNAi [174].

However, nucleo-cytoplasmic translocation processes are highly dynamic and multiple proteins are involved. Conclusions on nucleo-cytoplasmic translocation of mammalian clock proteins were mainly drawn from steady state, subcellular distribution assays or inhibition of single binding events. Up to date, systematic and dynamic investigations on nucleo-cytoplasmic translocation of circadian clock proteins are still missing.

## 3.1 Pharmacological perturbation of nucleo-cytoplasmic translocation alters circadian dynamics

The nucleo-cytoplasmic translocation system can be divided into different processes. The two main events are nuclear import and export. To test whether both mechanisms are essential for normal circadian rhythm generation pharmacological inhibitors were used to impair nuclear import as well as export. The nuclear import inhibitor ivermectin (Iver) was applied to inhibit classical nuclear entry via KPNA/KPNB1. Additionally, cells were treated with leptomycin B (LMB) to block XPO1-dependent nuclear export [165].

To this end, U-2 OS cells expressing either *per2* (*per2:luc*) or *bmal1* (*bmal1:luc*) promoter-driven *luciferase* were synchronized with 1 μM dexamethasone prior to addition of the inhibitors. LMB was applied at concentrations from 0 to 10 ng/ml, whereas Iver was added at concentrations of 0 to 10 μg/ml post synchronization. The cells were monitored over a period of up to six days using a TopCount luminometer (see 2.2.2). To

analyze the data, the time series were fitted to a sine wave (see 2.2.9) from twelve hours to five days (Iver) and twelve hours to four days (LMB) after synchronization. Cell vitality was verified using a resazurin assay (see 2.2.1).

**Table 3.1: Summary of significantly altered parameters upon application of 10 µg/ml Iver or 10 ng/ml LMB** (n.s. non-significantly different from solvent control).

| | period deviation [h] (mean ± SEM) | | phase deviation [h] (mean ± SEM) | | damping deviation [$h^{-1}$] (mean ± SEM) | | mean luciferase activity [cps] (mean ± SEM) | |
|---|---|---|---|---|---|---|---|---|
| | U-2 OS *per2:luc* | U-2 OS *bmal1:luc* | U-2 OS *per2:luc* | U-2 OS *bmal1:luc* | U-2 OS *per2:luc* | U-2 OS *bmal1:luc* | U-2 OS *per2:luc* | U-2 OS *bmal1:luc* |
| 10 µg/ml Iver | 3.6 ± 0.5 | 2.5 ± 0.3 | 2.1 ± 0.4 | -1.5 ± 0.4 | n.s. | n.s. | -28000 ± 7000 | -27000 ± 5000 |
| 10 ng/ml LMB | 2.7 ± 0.6 | 3.0 ± 0.2 | n.s. | n.s. | 0.7 ± 0.2 | 0.9 ± 0.2 | -11000 ± 2000 | -33000 ± 5000 |

Inhibition of classical nuclear import by 5 to 10 µg/ml Iver lengthened the circadian period in U-2 OS *per2:luc* as well as in U-2 OS *bmal1:luc* cells (figure 3.1 A and B, table 3.1 and suppl. figure A1.1). The highest concentration of Iver resulted in a period lengthening of more than three hours (table 3.1). This period phenotype was accompanied by a reduced mean luciferase activity (bioluminescence) and an earlier phase in both cell lines when treated with Iver (table 3.1, suppl. figure A1.1). The amplitude, the decrease in amplitude per 24 hours (damping) and the correlation coefficient (in regard to the sine wave fit; further referred to as CC) was not consistently altered upon Iver treatment (suppl. figure A1.1 C). The cells were vital throughout the measurements (suppl. figure A1.1 D).

Perturbed nuclear export also resulted in a period lengthening. The period was lengthened at concentrations as low as 2.5 ng/ml LMB in U-2 OS *per2:luc* cells. The circadian period of U-2 OS *bmal1:luc* cells was significantly lengthened at concentrations of 5 ng/ml LMB. At concentration of 10 ng/ml LMB period lengthening of more than two hours were observed in both cell lines (figure 3.1 C and D, table 3.1, suppl. figure A1.2 A). In addition, export inhibition decreased the mean luciferase activity and led to a stronger damping compared to the solvent control (table 3.1, suppl. figure A1.2 B). The phase, amplitude and goodness of fit to the sine wave (further referred to as correlation coefficient, CC) were not consistently altered upon increase of the LMB concentration (suppl. figure A1.2 C).

Cell vitality of cells treated with 1ng/ml LMB was comparable to cell vitality of control cells throughout the bioluminescence recordings. However, cell vitality strongly decreased with higher concentrations of LMB. Both cell lines, *per2:luc* cells and *bmal1:luc* cells, were vital within the first three days, but cell vitality from day six to seven was severely decreased at LMB concentrations of 2.5 ng/ml and higher. Therefore, we decided to analyze only data from day five to seven from the analysis (suppl. figure A1.2 D).

In conclusion, the disruption of nucleo-cytoplasmic transport by either Iver or LMB severely alters circadian rhythms at non-toxic concentrations. A functional translocation machinery is therefore essential for normal 24-hour rhythm generation. Iver inhibits classical nuclear import by KPNA and KPNB1, whereas LMB blocks XPO1-mediated nuclear export. However, the specific pathway, leading to pharmacological inhibitor-induced period lengthening in circadian rhythm generation is unknown.

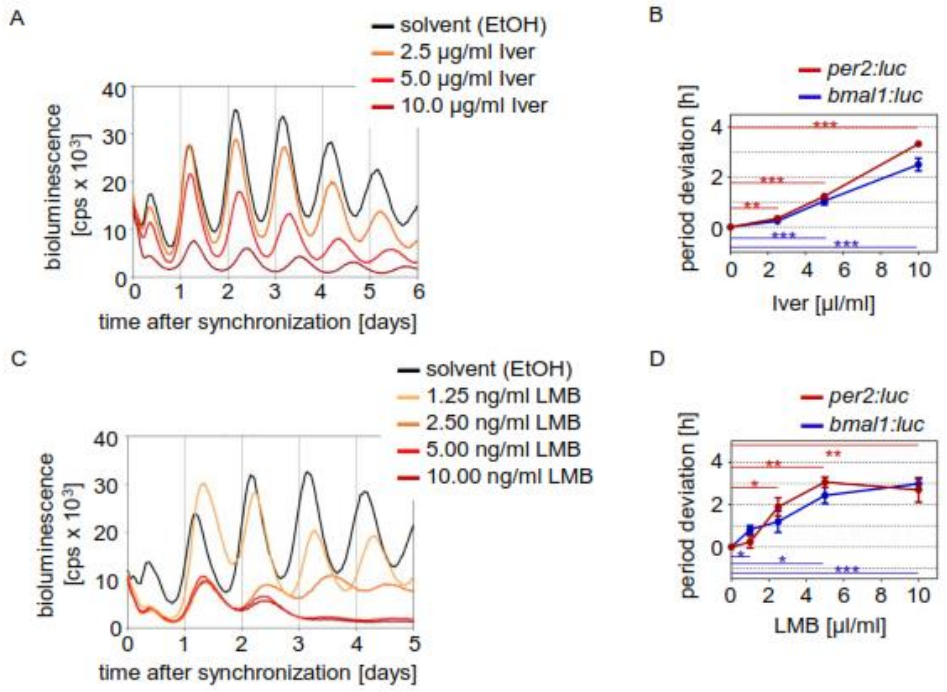


**Figure 3.1: Pharmacological inhibition of nuclear import and export lengthens the circadian period of human reporter cells**. U-2 OS cells, constitutively expressing either *per2* (*per2:luc*) or *bmal1* (*bmal1:luc*) promoter driven *luciferase*, were treated with solvent or pharmacological inhibitor after synchronization with 1 µM dexamethasone. A and C) Depicted are representative time series of U-2 OS *per2:luc* cells treated with solvent (black) and either the classical nuclear import inhibitor ivermectin (A; Iver, red) or nuclear export inhibitor leptomycin B (C; LMB, red). Treatments were applied at different concentrations of the pharmacological inhibitors and bioluminescence was recorded for six days. B and D) Quantification of the period deviation upon pharmacological treatment with either Iver (B) or LMB (D) of U-2 OS *per2:luc* (blue) or *bmal1:luc* (red) cells is shown (error bars = SEM, $n_{LMB}$ = 7 to 8, $n_{LMB}$ = 3 to 5 individual recordings; student's t-test: * $p < 0.05$, ** $p < 0.01$, *** $p < 0.001$).

## 3.2 Multiple components of the nucleo-cytoplasmic translocation machinery are required for normal circadian dynamics

The identification of classical nuclear import and export signals within circadian clock proteins [166-171] as well as evidence of KPNB1/KPNA-dependent nuclear accumulation of circadian clock proteins [172-174] let us assume that nucleo-cytoplasmic transport of circadian clock proteins involves multiple proteins. So far, genetic evidence for nucleo-cytoplasmic translocation-dependent circadian rhythm generation is missing.

### 3.2.1 Knockdown of nucleo-cytoplasmic translocation-associated genes leads to impaired circadian rhythm generation

To identify specific clock regulating genes of the nucleo-cytoplasmic translocation machinery, we systematically knocked down the expression of 62 genes (table 3.2) via RNA-interference (RNAi). We selected components of the nuclear pore complex, nuclear import and export carriers as well as associated proteins [97, 98, 257-260]. We tested up to three different RNAi constructs (GE Dharmacon) per gene and 167 shRNA constructs in total. A non-silencing (ns) short hairpin (sh) RNA (ns control) served as negative control. Three different constructs targeting *fbxl3* expression served as positive controls, as period lengthening and high damping upon *fbxl3* depletion was reported previously [261, 262]. Note: for a complete list of construct numbers suppl. table A1.1.

U-2 OS cells harboring a *bmal1:luc* reporter were lentivirally transduced with individual RNAi constructs and luciferase activity was measured for approximately six days (see 2.2.2). We performed these experiments six times independently. Time series were fit to a sine wave using the ChronoStar 2.0 software (see 2.2.9). Time series, with a correlation coefficient lower than 0.96 (0.97 in the second run) were excluded from further data processing.

In this study, we focused on the period deviation from the mean period of ns control cells (figure 3.2 and table 3.3). In addition, we also analyzed the phase, amplitude, damping of amplitude per 24 hours and mean luciferase activity (for a summary of all time series parameter see suppl. table A1.2).

**Table 3.2: Alphabetical list of RNAi-targeted transcripts**. The number of different tested shRNA constructs are indicated in brackets). * *ddx19* and *cas* were not tested.

| | | | | |
|---|---|---|---|---|
| *aladin* (3) | *nup35* (3) | *nup155* (3) | *ranbp4* (2) | *seh1* (3) |
| *cg1* (3) | *nup37* (3) | *nup160* (2) | *ranbp5* (3) | *tnpo1* (3) |
| *elys* (3) | *nup43* (3) | *nup188* (3) | *ranbp6* (3) | *tnpo2* (1) |
| *gle1* (3) | *nup50* (3) | *nup205* (3) | *ranbp7* (3) | *tnpo3* (2) |
| *kpna1* (1) | *nup54* (2) | *nup210* (3) | *ranbp8* (3) | *tpr* (3) |
| *kpna2* (3) | *nup62* (3) | *nup214* (2) | *ranbp9* (3) | *xpo1* (3) |
| *kpna3* (3) | *nup85* (3) | *nup L1* (3) | *ranbp10* (3) | *xpo4* (2) |
| *kpna4* (3) | *nup88* (1) | *pom121* (3) | *ranbp11* (3) | *xpo5* (1) |
| *kpna5* (3) | *nup93* (3) | *rae1* (3) | *ranbp13* (2) | *xpo6* (3) |
| *kpna6* (3) | *nup98* (3) | *ran* (3) | *ranbp16* (3) | *xpot* (1) |
| *kpna7* (3) | *nup107* (3) | *ranbp1* (3) | *ranbp17* (3) | |
| *kpnb1* (3) | *nup133* (3) | *ranbp2* (3) | *rangrf* (3) | |
| *ndc1* (3) | *nup153* (3) | *ranbp3* (1) | *sec13* (3) | |

The ns control shRNA had a period of 24.2 ± 0.1 hours (mean ± SEM). The knockdown of *fbxl3* transcripts as positive control, resulted in severe period lengthening (two constructs; max. period deviation 4.5 ± 0.1 hours; mean ± SEM) or low CC (figure 3.2, figure 3.3, table 3.3).

Interestingly, the depletion of several translocation-associated genes severely impaired the circadian oscillation of U-2 OS reporter cells. 51 of the 167 shRNA constructs resulted in a significant period deviation. Eleven additional constructs led to a low CC. Using those 62 RNAi constructs, we identified 14 components of the nucleo-cytoplasmic translocation machinery to be essential for normal circadian period generation. For those 14 transcripts at least two different shRNA constructs targeting the same transcript led to severe period alteration or low CC (figure 3.2 and table 3.3). Of note: transcripts with period lengthening and shortening upon knockdown using different constructs were neglected.

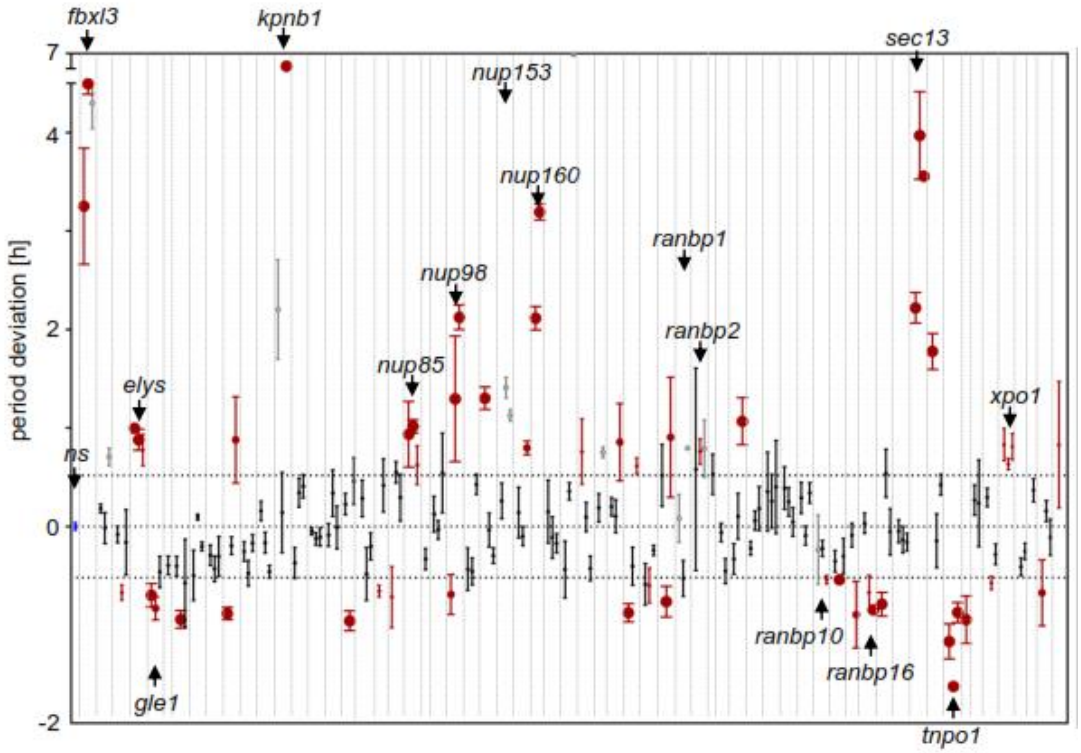


**Figure 3.2: Components of the nucleo-cytoplasmic translocation machinery are required for normal circadian periods**. U-2 OS *bmal1:luc* reporter cells were individually transduced with RNAi constructs and bioluminescence was recorded over approximately six days. Time series were fitted to a sine wave and period deviations quantified. Significance was determined performing a student's t-test against non-silencing control (ns, blue), followed by Bonferroni correction. Significant period deviations are depicted in red (q value < 0.05). The sizes of the red data points indicate the significance of period deviations (smallest: 0.05 < q value < 0.005, medium: 0.005 < q value < 0.001, largest: q value > 0.001). Non-significant period deviations are indicated in black. If constructs led to time series with low CC for at least four (of the six) independent experiments, the determined period deviations of the residual one or two time series are depicted in grey (error bars = SEM, grey: n = 1 to 2, black and red: n = 3 to 12). The dotted grey lines separate data points of different transcripts. The dotted black lines indicate 1.5 x standard deviations of the ns control period. Transcripts with at least two shRNA constructs promoting either low CC or a significantly and period deviation compared to time series of ns control cells are labeled within the diagram. Note: Knockdown of kpna5, pom121 and ran expression led to bidirectional period alterations upon perturbation with different shRNA constructs targeting the same transcript. Those two transcripts were not labeled within the diagram.

We quantified five different parameters for each time series: period, phase, amplitude, damping of amplitude per 24 hours, mean luciferase activity (recorded as bioluminescence). Selected time series of long and short period phenotypes upon knockdown of expression are exemplarily depicted in figure 3.3.

**Table 3.3: List of targeted transcripts with at least one RNAi construct significantly altering the circadian period compared to ns control**. Depicted are the q values, the mean period deviation and SEM of all tested constructs of the transcript. Transcripts are listed in descending order starting with the most significantly altering construct. Targets with two or three constructs leading to significant period deviations or low CC are depicted in bold characters (targets indicate targeted transcripts, * reduced cell vitality in run 1; # reduced vitality in both runs, note: no reduced cell vitality in run 2 only observed).

| | construct 1 | | | | construct 2 | | | | construct 3 | | | |
|---|---|---|---|---|---|---|---|---|---|---|---|---|
| targeted transcript | q value | period deviation [h] | SEM | | q value | period deviation [h] | SEM | | q value | period deviation [h] | SEM | |
| ns shRNA | | 0.00 | 0.04 | | | | | | | | | |
| fbxl3 (pos. ctrl) | 1.1E-34 | 4.5 | 0.1 | | 2.1E-24 | 3.3 | 0.6 | | low CC | | | |
| ***kpnb1*** | **1.3E-37** | **4.9** | **0.03** | **#** | **low CC** | | | **#** | | **0.1** | **0.4** | ***** |
| ***sec13*** | **5.7E-34** | **4.0** | **0.5** | **#** | **9.3E-28** | **3.6** | **0.1** | **#** | **1.2E-15** | **2.2** | **0.2** | **#** |
| ***nup160*** | **1.0E-24** | **3.2** | **0.1** | **#** | **8.0E-23** | **2.1** | **0.1** | ***** | | | | |
| *seh13* | 9.5E-18 | 1.8 | 0.2 | | | 0.4 | 0.1 | | | -0.2 | 0.3 | |
| ***nup98*** | **8.9E-15** | **2.1** | **0.1** | ***** | **5.8E-06** | **1.3** | **0.6** | **#** | **2.5E-03** | **-0.7** | **0.2** | |
| ***tnpo1*** | **9.90E-15** | **-1.6** | **0.03** | | **5.6E-06** | **-0.9** | **0.1** | | **2.2E-05** | **-1.2** | **0.2** | |
| *nup133* | 2.5E-10 | 1.3 | 0.1 | | | -0.04 | 0.2 | | | -0.3 | 0.1 | * |
| *kpna2* | 5.7E-07 | -0.9 | 0.1 | | | -0.4 | 0.1 | | | -0.6 | 0.6 | |
| ***nup85*** | **8.1E-07** | **1.0** | **0.1** | | **4.2E-04** | **0.9** | **0.3** | | **1.3E-02** | **0.6** | **0.2** | |
| *kpna5* | 3.0E-06 | -0.9 | 0.1 | | 1.2E-03 | 0.9 | 0.4 | * | | -0.2 | 0.1 | |
| *tnpo2* | 3.9E-06 | -1.0 | 0.2 | | | | | | | | | |
| *nup43* | 4.6E-06 | -1.0 | 0.1 | | | 0.2 | 0.1 | | | 0.5 | 0.2 | |
| *pom121* | 4.6E-06 | -0.9 | 0.1 | | 7.8E-03 | 0.6 | 0.1 | | | -0.4 | 0.2 | |
| ***elys*** | **4.9E-06** | **0.9** | **0.1** | | **6.0E-04** | **1.0** | **0.03** | | **4.2E-02** | **0.8** | **0.2** | ***** |
| ***ranbp16*** | **9.0E-06** | **-0.8** | **0.1** | | **1.1E-02** | **-0.8** | **0.1** | | | **-0.7** | **0.2** | |
| *ranbp17* | 8.0E-05 | -0.8 | 0.1 | | | 0.5 | 0.2 | | | -0.1 | 0.2 | |
| *ranbp11* | 1.2E-04 | -0.5 | 0.04 | | | -0.4 | 0.1 | | | -0.3 | 0.2 | |
| *ranbp5* | 2.0E-04 | 1.1 | 0.2 | | | -0. 3 | 0.2 | | | 0.1 | 0.2 | |
| *ran* | 2.2E-04 | -0.8 | 0.2 | | 7.3E-03 | 0.9 | 0.6 | | | 0.5 | 0.3 | |
| ***gle1*** | **9.7E-04** | **-0.7** | **0.1** | | **1.4E-03** | **-0.8** | **0.1** | | | **-0.5** | **0.2** | |
| *ranbp13* | 1.0E-04 | -0.9 | 0.3 | | | -0.1 | 0.1 | | | | | |

| | construct 1 | | | | construct 2 | | | | construct 3 | | | |
|---|---|---|---|---|---|---|---|---|---|---|---|---|
| targeted transcript | q value | period deviation [h] | SEM | | q value | period deviation [h] | SEM | | q value | period deviation [h] | SEM | |
| *nupl1* | 1.1E-03 | 0.9 | 0.4 | # | | 0.2 | 0.1 | * | | 0.1 | 0.2 | |
| *nup155* | 2.7E-03 | 0.8 | 0.1 | | | 0.1 | 0.3 | | | -0.1 | 0.1 | # |
| *nup62* | 7.8E-03 | -0.7 | 0.3 | | | 0.6 | 0.1 | | | 0.3 | 0.2 | * |
| *nup54* | 9.9E-03 | -0.7 | 0.1 | * | | 0.4 | 0.3 | * | | | | |
| ***xpo1*** | **1.6E-02** | **0.8** | **0.2** | **#** | **2.1E-02** | **0.8** | **0.1** | **#** | | **0.6** | **0.1** | |
| *nup210* | 1.6E-02 | 0.8 | 0.3 | | | 0.1 | 0.2 | | | -0.4 | 0.1 | # |
| *xpo6* | 1.6E-02 | -0.7 | 0.3 | | | 0.2 | 0.1 | | | -0.1 | 0.2 | |
| *rae* | 1.9E-02 | -0.6 | 0.2 | | | -0.1 | 0.2 | | | -0.2 | 0.1 | |
| ***ranbp10*** | **2.1E-02** | **-0.5** | **0.1** | | **low CC** | | | | | **-0.2** | **0.1** | |
| *tpr* | 2.1E-02 | -0.6 | 0.1 | * | | 0.3 | 0.1 | | | -0.3 | 0.1 | |
| *xpot* | 3.5E-02 | 0.8 | 0.6 | | | | | | | | | |
| *cg1* | 3.6E-02 | -0.7 | 0.1 | | | -0.1 | 0.1 | | | -0.2 | 0.3 | |
| ***ranbp2*** | **5.0E-02** | **0.8** | **0.1** | **#** | **low CC** | | | **#** | | **0.6** | **1.0** | |
| *nup153* | low CC | | | # | low CC | | | * | | 0.3 | 0.2 | * |
| *ranbp1* | low CC | | | | low CC | | | | | -0.7 | 0.2 | |
| *aladin* | low CC | | | | | 0.2 | 0.04 | | | -0.02 | 0.2 | |
| *nup205* | low CC | | | # | | -0.4 | 0.3 | | | 0.4 | 0.1 | |
| *nup214* | low CC | | | # | | 0.2 | 0.1 | # | | | | |

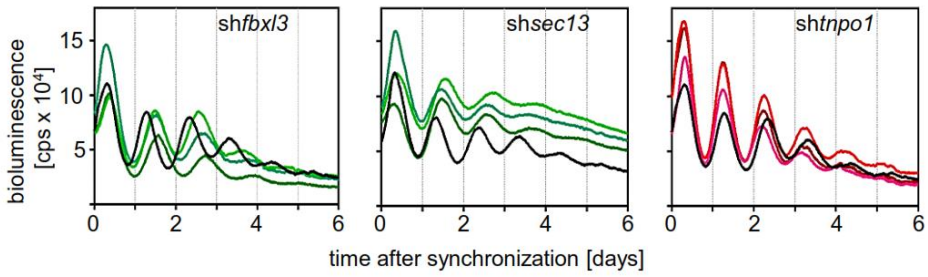


**Figure 3.3: Period alterations upon knockdown of specific nucleo-cytoplasmic translocation-associated transcripts**. U-2 OS cells, constitutively expressing *bmal1:luc*, were transduced with either ns control shRNA (black) or constructs targeting *fbxl3* (pos. ctrl), *sec13* or *tnpo1*. Targeting of *fbxl3* as well as of *sec13* results in significant period lengthening (green). Knockdown of *sec13* transcripts results in a reduced amplitude and higher damping as well as a higher mean bioluminescence. In contrast, knockdown of *tnpo1* expression leads to period shortening (red).

Additionally, we checked the cell vitality for all shRNA applications after termination of bioluminescence recordings (decreased cell vitality indicated in table 3.3). Knockdown of transcripts, which resulted in a time series with a low CC or severe period lengthening are often accompanied with reduced cell vitality. In contrast, cells oscillating with a shorter period upon shRNA treatment did not show reduced cell vitality (table 3.3 and figure 3.4). Therefore, we focused on transcripts with a severely shortened period upon RNAi application, which are *tnpo1*, *ranbp16* and *gle1*. The strongest period shortening with a maximum of -1.6 ± 0.0 hours period deviation was detected upon knockdown of *tnpo1* expression using construct V2LHS_133788 (sh*tnpo1*_2) . Additionally, *tnpo1* was the only target which resulted in a significantly shortened period upon knockdown of either of the three tested RNAi constructs (table 3.3).

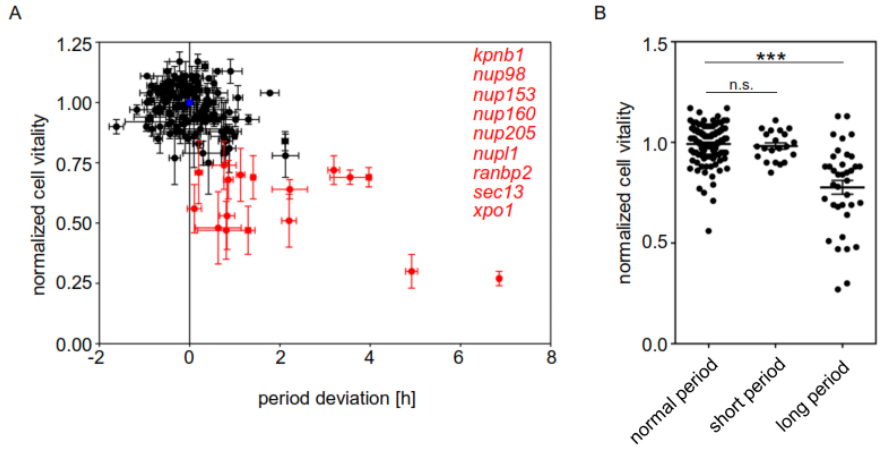


**Figure 3.4: Cells with a long period tend to have a reduced cell vitality**. A) U-2 OS reporter cells, harboring a *bmal1* promoter-driven luciferase, were lentivirally transduced with 167 individual RNAi constructs targeting components of nucleo-cytoplasmic translocation machinery. After bioluminescence recordings a resazurin cell vitality assay was performed. A normalized cell vitality of 0.75 was manually predetermined as cut off for vital cells. Means of normalized cell vitality were ploted against period deviation (cell vitality of ns control treated cells: blue; cell vitality > 0.75: black, cell vitality < 0.75: red, transcripts are indicated on the left; error bars = SEM; $n_{\text{cell vitality assay}}$ = 6 individual measurements, $n_{\text{period deviations}}$ = 3 to 6 individual measurements. Note: Constructs targeting *ranbp11* expression were transduced twice on each plate, therefore 12 time series of luciferase activity as well as 12 values of cell vitality were obtained for those cells. B) Dot plot of normalized cell vitality correlated to normal, short and long period phenotypes. For classification of normal, short and long periods time series were compared to non-silencing control cells and significances of period deviations determined using a student's t-test and Bonferroni correction (error bars = SEM; n = 21 - 109 (167 data points in total); One-way-ANOVA, post-test: Dunnett's multiple comparison: n.s. = non-significant, *** p value < 0.001).

Summarizing the RNAi approach to systematically knock down components of the nucleo-cytoplasmic translocation machinery, we identified 14 transcripts, which are essential for normal near-24-hour rhythm generation. Among the three transcripts, which resulted in period shortening upon perturbation of their expression, we identified TNPO1.

The non-classical nuclear import carrier, TNPO1, belongs to the kap$\beta$ family. It recognizes non-classical M9-NLSs and directly binds to its cargo prior to active nuclear translocation [132]. The alternative nuclear import carrier is constituted of 18 HEAT repeats and promotes nuclear entry in a Ran-GTP dependent manner. The GTPase binds to the N-terminus of the carrier, whereas the high and low affinity binding sites for cargo recognition are at the C-terminal arch. The distinct HEAT repeat 8 is located between the two arches. HEAT repeat 8 is comprised of an unstructured region, leading to conformational changes upon Ran-GTP binding, thereby initializing cargo dissociation (see 1.2.4) [263, 264].

### 3.2.2 RNAi-knockdown of *tnpo1* transcripts leads to period shortening of circadian oscillations

To validate the short period phenotype of *tnpo1* transcript depletion, nine different RNAi constructs were tested. To this end, U-2 OS *bmal1:luc* reporter cells were lentivirally transduced prior to luminescence recordings for approximately seven days.

Five of the nine RNAi constructs targeting *tnpo1* transcripts led to a period shortening of more than 30 minutes (max. period deviation: -1.4 ± 0.2 hours; figure 3.5 A and B). The three RNAi constructs, which did not consistently shorten the period more than 30 minutes, did at least show the same trend (figure 3.5 B). Furthermore, time series of U-2 OS cells showed a stronger damping upon knockdown of *tnpo1* expression than in ns control RNAi transduced cells (figure 3.5 A and C).

Efficient knockdown of the nine RNAi constructs targeting *tnpo1* expression was quantified on *tnpo1* mRNA levels. Further relative TNPO1 protein levels of five knockdown cells was determined (figure 3.5 D). All shRNA constructs reduced the relative *tnpo1* transcript levels. The minimal residual mRNA level was 0.10 ± 0.03 (construct # 3) whereas, the weakest knockdown of *tnpo1* expression resulted in 0.4 ± 0.2 % of residual *tnpo1* mRNA (construct # 9; figure 3.5 D). Surprisingly, there is no correlation of *tnpo1* knockdown efficiency and period deviation (or damping; suppl. figure A1.3 A and B). Nevertheless the likelihood of severe period shortening seems to be more frequent upon depletion of *tnpo1* expression to less than 0.2 % of relative mRNA.

Residual TNPO1 protein levels upon knockdown of *tnpo1* transcripts, correlated well with the relative *tnpo1* mRNA levels ($R^2 = 0.87$; suppl. figure A1.3 E). In line with those findings, neither the period deviation nor the deviation in damping correlated with the relative TNPO1 protein levels of the respective cells (suppl. figure A1.3 C and D).

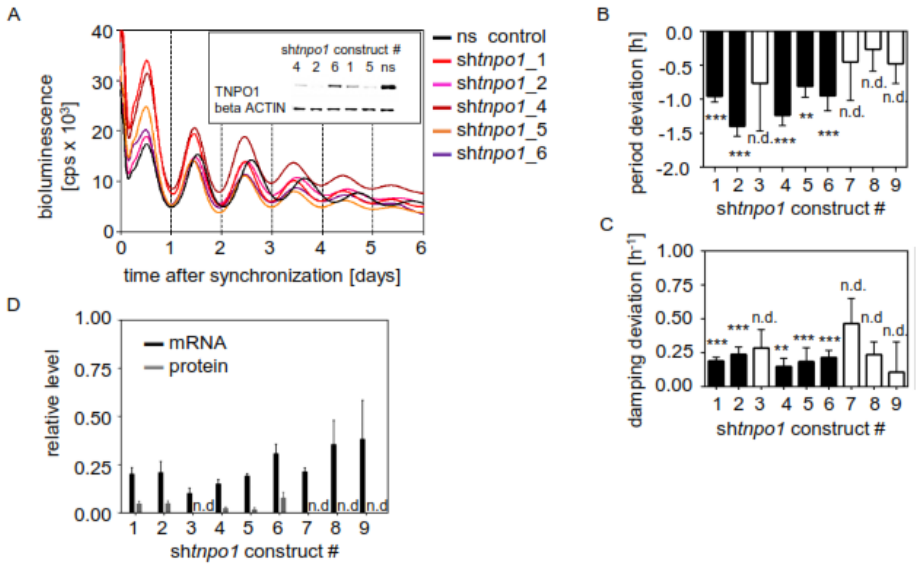


**Figure 3.5: *tnpo1* knockdown leads to period shortening and increased damping of circadian oscillations**. U-2 OS cells expressing a *bmal1* promoter-driven *luciferase* were individually transduced with nine different shRNA constructs and bioluminescence was monitored after synchronization with 1 µM dexamethasone. A) Raw data of representative time series for the application of five different sh*tnpo1* constructs (colored lines) and ns control shRNA (black). Inlet: Representative western blot of TNPO1 (betaACTIN) protein levels for the individual knockdown cells. Knockdown of *tnpo1* expression resulted in period shortening (B) and higher damping (C). Period and damping deviation of time series obtained from cells transduced with constructs, which were only tested twice are depicted as empty columns. Those constructs were not statistically tested (n.d.: not determined, error bars = SEM, n = 2 to 12 individual recordings, student's t-test: * $p < 0.05$, ** $p < 0.01$, *** $p < 0.001$). D) Relative *tnpo1* mRNA levels of all nine knockdown cells was determined and compared to the levels in ns control cells. In addition, protein levels of five knockdown cells as well as of ns control cells were quantified (n.d.: not determined; error bars = SEM, n = 2 to 12 individual recordings).

Taken together we found consistent evidence that the knockdown of *tnpo1* expression shortens the circadian period of *bmal1:luc* reporter cells to a maximum of -1.4 ± 0.2 hours (RNAi-screen: -1.62 ± 0.03 hours). However, application of RNAi reduces the *tnpo1* levels in knockdown cells just partially. In consequence, residual TNPO1 protein might be sufficient for nuclear entry of its cargos. For further investigation of a regulatory function of TNPO1 on circadian dynamics a complete *tnpo1* knockout would be of advantage.

### 3.2.3 CRISPR/Cas9 generated *tnpo1* knockout cells show a shortened circadian rhythm

To create gene specific knockouts we performed CRISPR/Cas9 genome engineering in U-2 OS *bmal1:luc* reporter cells. The genome editing using CRISPR/Cas9 is an easy, efficient and inexpensive method as demonstrated in various reports

(e.g. Ledford, 2015 [265]) and experienced by us (Korge *et al.*, 2015 [255]) as well as others (e.g. Sung *et al.*, 2014 [266], see also 1.4).

Cas9 endonuclease inserts DSB at a specific region of interest in the genome. In contrast to ZFN or TALEN, Cas9 is directed to the specific target locus by a individually transcribed guide RNA (gRNA). After introduction of DSB two intracellular repair mechanisms are possible. Whereas the HR is a rare event, DSB repair by NHEJ is observed more frequently (Maruyama *et al.*, 2015 [267]). NHEJ introduces either short insertions or deletions (indels), leading to in- or out-of-frame shifts. Out-of-frame shifts result in premature stop codons and thus shortened or misfolded proteins and degradation.

*tnpo1* has two transcript isoforms (NCBI reference: NM_002270.3 and NM_153188.2), with a start codon in exon 1 as well as an alternative start codon in exon 2 upon alternative splicing. Even though no functional differences have been described, we target a position of the *tnpo1* gene, which should lead to an out-of-frame shift in both transcript variants. To this end, we designed two different gRNAs (gRNA1 and gRNA2) using the free online tool: *crispr.mit.edu* provided as open source by the Zhang lab. The gRNAs target two positions in the second exon of the *tnpo1* gene, 22 bp and 31 bp downstream of the alternative *tnpo1* start codon (figure 3.6 A). They were cloned into the plenti6 CRISPRv2 vector prior to lentivirus transduction of U-2 OS reporter cells (see 2.2.8). Luciferase activity of the gRNA1 and gRNA2 derived cell populations as well as of control cells (wild type) was monitored over a period of six days post selection for positively transduced cells.

We analyzed the time series of the different cell populations (fitted to a sine-wave function by the ChronoStar 2.0 software, see 2.2.9) and determined a period shortening of -0.8 ± 0.1 hours for gRNA1 cells (p value = 0.001). In contrast, gRNA2 reporter cells did not generate significantly shorter rhythms (-0.2 ± 0.1 hours, p value = 0.11, figure 3.6 B and C). Furthermore, a significantly stronger damping of the amplitude per 24 hours was observed for time series of gRNA1 reporter cells and to a lesser extent also in gRNA2-derived oscillations (gRNA1cells: 0.3 ± 0.0 $hours^{-1}$, p value < 0.001; gRNA2 cells: 0.1 ± 0.0 $hours^{-1}$, p value = 0.023; figure 3.6 C).

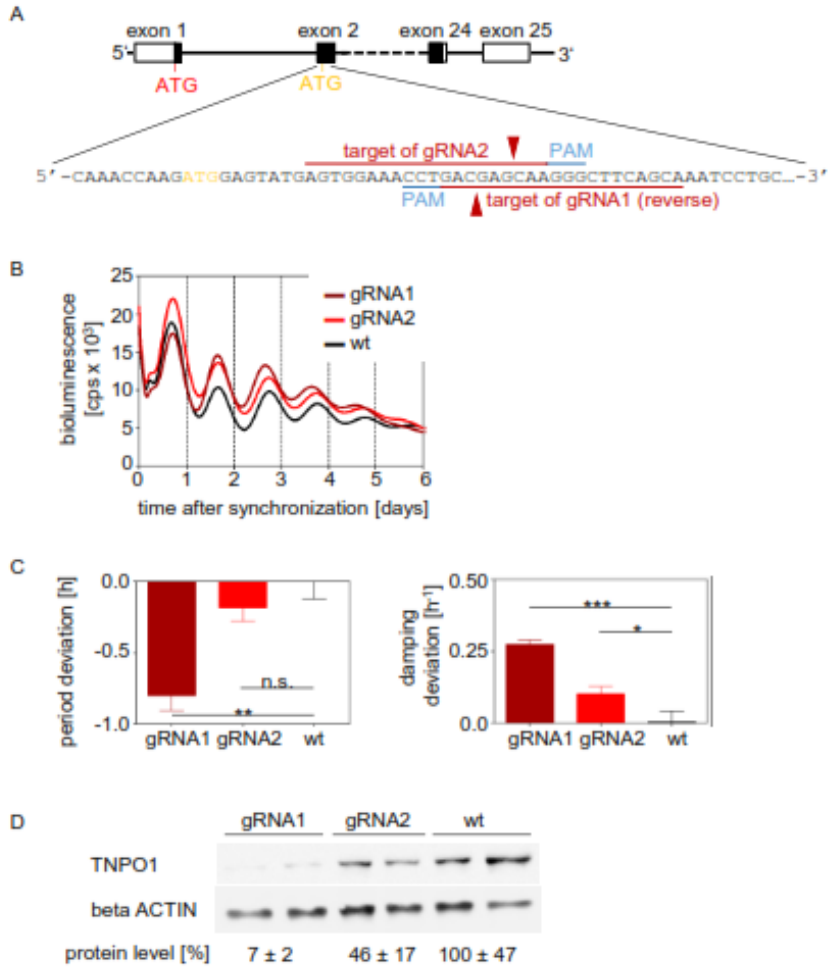


**Figure 3.6: Period shortening upon CRISPR/Cas9 genome editing of the *tnpo1* gene**. A) Schematic illustration of the *tnpo1* gene. The start codon (ATG) of isoform 1 (red, exon 1) and the alternative start codon (orange, exon 2) of transcript variant 2 are indicated. The guide RNAs 1 and 2 (gRNA1 and gRNA2) including the protospacer adjacent motifs (PAM; blue) direct the Cas9 endonuclease to their target sites. The predicted positions of the expected double strand breaks are indicated as dark red triangles. B to D) U-2 OS reporter cells expressing a *bmal1* promoter-driven *luciferase* were lentivirally transduced with pLenti6 CRISPR/Cas9v2 including either gRNA1 or gRNA2. B) Representative time series of three different cell populations after synchronization with 1 µM dexamethasone. Wild type (wt; black) and genome edited (gRNA1: dark red; gRNA2 red) cells were monitored over six days. C) Quantification of period (upper panel) and damping (lower panel) deviation (error bars = SD, n = 3, student's t-test: n.s.: non-significant, * $p < 0.05$, ** $p < 0.01$, *** $p < 0.001$). D) TNPO1 and betaACTIN protein levels of all three cell populations (wt, gRNA1 and gRNA2) were quantified after bioluminescence recording (mean % of protein levels ± SD, two dishes per cell population).

Even though the relative *tnpo1* mRNA levels of the genome edited cells were not altered (having a trend towards higher *tnpo1* mRNA levels; suppl. figure A1.4 A), the TNPO1 protein levels of gRNA1 and gRNA2 cells were both reduced. Relative TNPO1 protein levels of gRNA1 cells were decreased to 7 ± 2 %, whereas residual TNPO1 levels of 46 ± 17 % was detectable in gRNA2 cell lysates. The partial reduction of the TNPO1

protein levels in gRNA2 cells might be an explanation for the normal period length compared to control cells (figure 3.6 D).

The efficiency of CRISPR/Cas9 varies, depending on the target site (reviewed in Barrangou *et al.*, 2015 [268]) and neither Cas9 efficiency nor affected number of alleles in each cell can be bioinformatically predicted.

To quantify the CRISPR/Cas9 efficiency in the gRNA1 and gRNA2 cells, we performed a T7 endonuclease test. Briefly: the region of interest was PCR-amplified from genomic DNA prior to denaturation. Slowly re-annealing the different single stranded (ss) DNAs lead to the formation of heteroduplex dsDNA if NHEJ initially introduced indels. Finally T7 endonuclease I recognizes ssDNA (mismatches) digesting the heteroduplex dsDNA to shorter DNA fragments than wild type homoduplex dsDNA (see 2.2.4).

In contrast to our expectations based on the quantified residual TNPO1 protein levels, efficiency of CRISPR/Cas9 in gRNA1 cells was 81 % and 74 % in gRNA2 cells (suppl. figure A1.4 B). However, we determined a higher genome editing efficiency for gRNA1. In consequence, we chose the gRNA1 cell population, which showed a significantly shorter period and more efficient indel insertion, for further characterizations.

To identify homozygous knockouts in single cells, we performed limited dilutions and chose luciferase activity measurements as readout to identify short-period cell clones compared to periods of unedited cells. We assumed that the period distribution of the potential *tnpo1* knockout single cells will be shifted towards shorter periods. To control for normal period distribution of unedited cells, we additionally diluted wild type reporter cells.

We obtained 32 single wild type and 34 single gRNA1 cell clones and recorded time series of their *bmal1* promoter-driven *luciferase* activity. Unexpectedly, the period distributions of wild type and gRNA single cells were not different (mean period change of both cell lines: $0.1 \pm 0.1$ hours; suppl. figure A1.4 C). We quantified the residual TNPO1 protein levels of the five gRNA1 single cell clones, with a period shortening of more than -0.5 hours and compared them to two wild type cells oscillating with a shorter period than the mean of all single clone wild type cells. The relative TNPO1 protein levels in wild type cells varied strongly in the two examined cell lines either due to cellular conditions or further protein processing. However, the relative residual TNPO1 levels of the tested gRNA1 single cells was reduced down to 17 % or further (suppl. figure A1.4 D). Note: the monoclonal antibody detecting TNPO1 binds to the C-

terminus of TNPO1 and indels in the CRISPR/Cas9 targeted region of *tnpo1* do not directly affect the binding.

Subsequently, we expected at least a partial TNPO1 knockout in these gRNA1 single clones. To characterize the introduced indels and identify out-of-frame shifts within the *tnpo1* sequence of gRNA1 single cells, we sequenced six different cell clones of the genome edited single cells (figure 3.7 A).

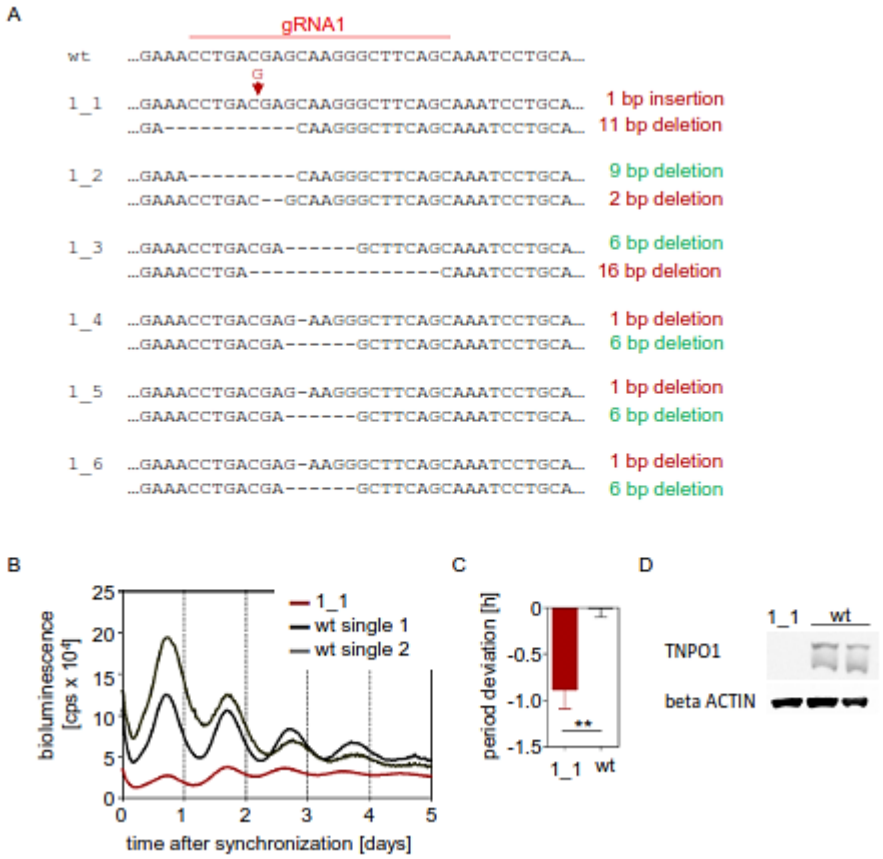


**Figure 3.7: Analysis of genome edited, potential *tnpo1* knockout single cells**. A) Sequences of single cell alleles derived from limited dilution of wild type (wt; top) and gRNA1 U-2 OS cell population harboring a *bmal1* promoter-driven *luciferase*. Efficient CRISPR/Cas9 genome engineering of the *tnpo1* gene leads to indels (insertions and deletions) and either in-frame (green) or out-of-frame (red) shifts. B) Representative time series of either wt (black and grey) or the gRNA1-derived *tnpo1* knockout (1_1, red) single clone. C) Quantification of the period shortening of the *tnpo1* knockout clone 1_1 and wt single cells (error bars = SEM, $n_{1\_1} = 4$, $n_{wt} = 18$; student's t-test: ** $p < 0.01$). D) Endogenous protein levels of TNPO1 and betaACTIN of genome edited (1_1) and wt single cells.

We identified indels in at least one of the two alleles in all of the eight tested gRNA1 single cells. However, just six of the eight cell clones resulted in a single allele out-of-frame shift (figure 3.7 A). Only one sequenced gRNA1 cell clone (gRNA1 1_1) contained indels on both alleles (an 11 bp deletion and a 1 bp insertion) that lead to out-of-frame shifts and hence premature stop codons (figure 3.7). We determined a period shortening of -0.8 ± 0.2 hours for this cell clone (figure 3.7 B and C) and a

reduction of TNPO1 protein levels to ~1 % (figure 3.7 D). One of the twelve sequencing results of cell clone gRNA1 1_1 showed a wild type sequence. This could either be due to a contamination during sample preparation or to a mixed cell population and needs further validation.

In summary, the CRISPR/Cas9 genome engineering was successfully used to edit the *tnpo1* gene of U-2 OS reporter cells. Oscillations of luciferase activity in the gRNA1 population were shorter than in control cells and TNPO1 protein levels were strongly reduced. The single clone 1_1 of the gRNA1 cell population resulted also in a short period and low TNPO1 protein levels. Furthermore, sequence analysis identified NHEJ-induced out-of-frame shifts on both alleles. However, the period shortening is comparable to the knockdown using RNAi and the sequencing results indicate a potential mixed cell population for the knockout cell line gRNA1 1_1.

Another disadvantage of total knockout cell lines are potential long-term compensatory alterations within those cells. In contrast, the use of RNAi is a rather short-term approach to reduce *tnpo1* expression and will therefore minimize compensatory effects. In conclusion, we will perform future investigations using RNAi rather than the total knockout cell line gRNA1 1_1, which needs further verification.

## 3.3 Bioinformatical identification of putative TNPO1-binding sites in circadian core clock proteins

The period shortening upon knockdown of *tnpo1* expression in U-2 OS reporter cells was found using RNAi and CRISPR/Cas9. However, no interactions between circadian clock proteins and TNPO1 are reported. If the nuclear import carrier binds directly to components of the core clock it is likely that these circadian clock proteins contain specific nuclear NLSs, recognized by TNPO1.

Most cargo proteins of TNPO1 contain so-called "M9" NLSs as TNPO1-binding site. These TNPO1-binding sites are less conserved than classical NLSs (see 1.2.4). Although M9 NLSs often contain hydrophobic or basic amino acids most amino acids of the non-classical NLS are not clearly defined. A comparison of M9 NLSs, belonging to different TNPO1 cargos (suppl. table A1.3), revealed a broad amino acid variation within different M9 sequences. The amino acids vary not only in position but can even be substituted by other amino acids with similar characteristics [132]. However, it seems that a PY motif is essential for most M9 containing cargos of TNPO1 as it is present in 23 of

the 24 M9 sequences. The only exception is a substitution from PY to PG in the amino acid sequence of heterogeneous nuclear ribonucleoprotein M (hnRNP M, suppl. table A1.3).

Thus, we bioinformatically analyzed the primary structure of six circadian clock proteins (CLOCK, BMAL1, CRY1/2 and PER1/2) looking for PY motifs to identify putative M9 sequences. We left out PER3, which was reported to play only a minor role in circadian rhythm generation [269].

To estimate the likelihood of putative M9 sequences and predict the number of PY motifs present in the circadian clock proteins we calculated the occupancy of PY within a protein of n amino acids (aa). In regard to the single occupancies of tyrosine and proline (proline: 4.6 %; tyrosine 3.5 % [270]), we expected two PY motifs in PER proteins (PER1 comprises 1290 aa, PER2: 1255 aa) and one in each of the other tested circadian clock proteins (BMAL1: 626 aa, CLOCK: 846 aa, CRY1: 586 aa, CRY2: 593 aa) using equation 6:

$$number\ of\ PY\ motifs\ = \ (n - 1) \times 0.00161 \qquad (6)$$

Inspection of the six circadian clock protein sequences identified a total of ten PY motifs within five of the six proteins (all except CLOCK, table 3.4). Each of the PER1 and PER2 sequences contain three PY motifs. We found two PY motifs in BMAL1 and one PY motif in each of the CRYs.

**Table 3.4: Amino acid position of PY motifs in human clock proteins**. Amino acid position of peptides used in the subcellular distribution assay are indicated in brackets.

| | uniprot accession number | position of 1st PY | position of 2nd PY | position of 3rd PY |
|---|---|---|---|---|
| BMAL1 | O00327 | 131/132 (95-150) | 565/566 (522-599) | - |
| CLOCK | 015516 | - | - | - |
| CRY1 | Q16526 | 253/254 (227-269) | - | - |
| CRY2 | Q49AN0 | 272/273 (246-289) | - | - |
| PER1 | O15534 | 320/321 (294-337) | 883/884 (857-900) | 935/936 (909-952) |
| PER2 | O15055 | 245/246 (219-262) | 293/294 (250-315) | 1222/1223 (1196-1239) |

As most functional domains seem to be conserved between different species [271], we aligned the human sequences of the five PY motifs to sequences of other

mammalian species (mouse, rat and if available monkey, cow). An interspecies conservation of the putative M9 sequence might indicate, a conserved functionality of those domains.

The full-length protein sequences of the five circadian clock proteins (BMAL1, CRY1, CRY2, PER1 and PER2) show high conservation in human, mouse and rat, having the lowest conservation of 76 % for PER2 and the highest of 97 % for BMAL1 (PER1, CLOCK, CRY1/2 90 to 92 %; alignments not shown). Further, analysis of the specific PY motifs resulted in an absolute conservation of the two neighboring amino acids in mammals. The peptide sequences 20 bp upstream of the PY motifs, belonging to the putative M9 NLS, did vary in conservation from 75 to 100 % (suppl. table A1.4). Whether the identified PY motifs are part of functional M9 NLSs, which promote nuclear entry of circadian clock proteins upon binding to TNPO1, will be investigated.

## 3.4 TNPO1-directed nuclear import is promoted by putative M9 NLSs of circadian clock peptides

### 3.4.1 Circadian clock protein-derived putative M9 peptides are sufficient for nuclear localization

To test, whether the identified PY motifs in circadian clock proteins are sufficient for nuclear distribution, we performed a subcellular distribution assay. For this purpose, we fused peptides containing a PY motif to ECFP. Due to the less distinct consensus sequence of the M9 NLS, we chose peptide lengths of 43 to 60 amino acids to cover the full length of putative M9 NLSs (for peptide coordinates and sequences table 3.4 and suppl. table A 1.5). The PCR-amplified DNA sequences, encoding the different clock peptides, were C-terminally ligated to ECFP prior to transient transfection into either U-2 OS or HEK293 cells (see 2.2.1 and 2.2.4). ECFP alone served as negative control, whereas the M9 NLS of heterogeneous nuclear ribonucleoprotein A1 (hnRNP A1) was used as positive control [272].

Proteins smaller than 40 kDa passively translocate through the nuclear pore without the need of an active carrier. As ECFP has a mass of approximately 27 kDa, it is able to pass the nuclear pore without a carrier. In consequence, we expected a diffuse subcellular distribution of ECFP alone. In contrast, the M9 NLS of hnRNP A1 was shown to promote distinct nuclear import by binding to TNPO1 [272].

If the circadian clock protein-derived peptides sufficiently function as M9 NLSs, we expect an increased nuclear distribution of ECFP-putative M9 fusion proteins. In turn cytoplasmic localization will be reduced as described for hnRNP A1-M9 [272].

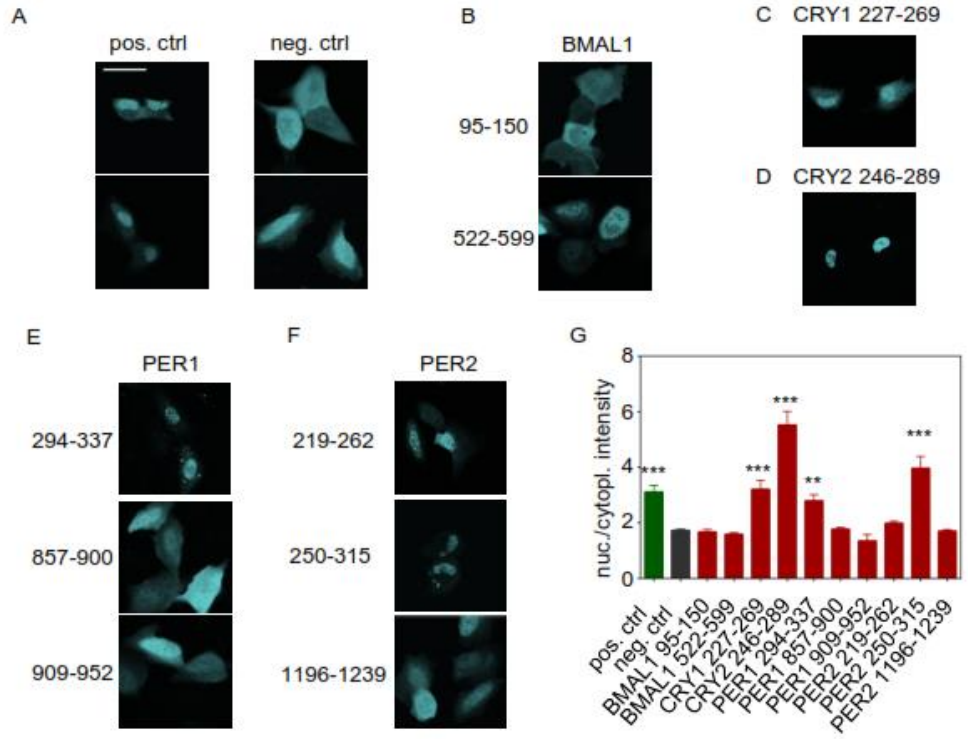


**Figure 3.8: Putative M9 clock peptides support nuclear accumulation**. Putative M9 clock peptides were C-terminally fused to ECFP prior to transient transfection of U-2 OS cells. Depicted are representative images of U-2 OS cells expressing ECFP alone (neg. ctrl; A) or fused to peptides of either the M9 NLS of hnRNP A1 (pos. ctrl; A) or to putative M9 NLSs of BMAL1 (B), CRY1 (C), CRY2 (D), PER1 (E) or PER2 (F). Images show ECFP fluorescence; scale bar = 50 µm. G) Quantification of mean nuclear to cytoplasmic fluorescence intensity of all analyzed cells. Depicted is the mean fluorescence (error bars = SEM, n = 51 to 164, One-way-ANOVA, post-test: Dunnett's multiple comparison test: ** $p < 0.05$, *** $p < 0.001$; all other peptides are non-significantly different from the neg. ctrl).

Analyzing the ECFP-clock peptide fusion proteins, the subcellular distribution of the observed fluorescence depends on the peptides fused to ECFP (figure 3.8). Both peptides of CRY1 and CRY2 (CRY1 227-269 and CRY2 246-289) led to an almost entirely nuclear accumulation of ECFP fluorescence (figure 3.8 C and D), whereas BMAL1 95-150 and BMAL1 522-590 did not alter the diffuse subcellular localization of ECFP compared to the negative control (figure 3.8 B). In each of the two PER proteins just one PY-motif promoted nuclear accumulation of ECFP (figure 3.8 E and F). The fusion proteins of PER1 294-337 and PER2 250-315 showed an increased nuclear and a decreased cytoplasmic localization. Neither PER1 857-900, PER1 909-952 nor PER2 219-262 or PER2 1196-1239 increased the nuclear ECFP distribution. In contrast,

PER1 909-952 fusion to ECFP resulted in a predominantly cytoplasmic accumulation of the fluorophore.

The positive (M9 of hnRNP A1) and negative (ECFP) controls showed the expected subcellular distributions. Fusion proteins of ECFP-M9 (hnRNP A1 264-308) were predominantly localized in the nucleus, whereas the nuclei of negative control cells were hard to distinguish from cytoplasm due to equal subcellular distribution of fluorescence intensity (figure 3.8 A). Those findings were observed in U-2 OS (figure 3.8) as well as in HEK293 (suppl. figure A1.5) cells.

In summary, the fusion of BMAL1 PY peptides did not lead to distinct nuclear localization of ECFP, we identified putative M9 sequences in PER and CRY proteins. Those putative M9 NLSs were sufficient to promote a predominantly nuclear localization of the ECFP fusion protein.

### 3.4.2 Nuclear localization of putative clock-derived M9 NLSs depends on the presence of TNPO1

If clock peptides fused to ECFP are functional M9 NLSs nuclear accumulation of the fusion protein should be due to TNPO1-mediated nuclear import. To test this, we depleted the expression of the non-classical nuclear import carrier TNPO1 using RNAi. Unfortunately, the pGIPZ vectors previously used for RNAi-mediated knockdown contain an open reading frame for GFP, leading to co-expression of the shRNA construct and GFP. The expressed GFP will interfere with ECFP fluorescence detected as readout in the subcellular distribution assay. To prevent an overlay of GFP and ECFP, we mutated the *gfp* sequence of pGIPZ vectors coding ns control RNAi and shRNAs targeting *tnpo1* mRNA (see 2.2.5). Upon transduction of those mutated pGIPZ vectors in U-2 OS cells, no residual GFP fluorescence was observed (data not shown).

To validate the shRNA efficiency of the mutated pGIPZ vectors (pGipz mut), we transduced U-2 OS reporter cells with lentivirus of either mutated or wild type pGIPZ (ns control shRNA, sh*tnpo*1_1 and sh*tnpo*1_4). The observed luciferase activity rhythms of control cells, transduced with either wild type or mutated pGIPZ coding for non-silencing shRNA, were comparable. Period shortenings as well as reduction of TNPO1 protein levels upon knockdown of *tnpo1* expression using RNAi constructs of either wild type or mutated pGIPZ were similar (suppl. figure A1.6). Note: Periods of all pGIPZ mut transduced U-2 OS cells were slightly longer (suppl. figure A1.4). Period deviation of *tnpo1*

expression targeted cells to ns control cells was comparable in wild type and pGIPZ mut cells.

To check whether the nuclear accumulation of the ECFP-putative M9 fusion protein is TNPO1-dependent, we transduced the mutated pGIPZ plasmids into U-2 OS (or HEK293) cells prior to individual transfection of the ECFP-putative M9 clock peptide fusion proteins (see 2.2.1).

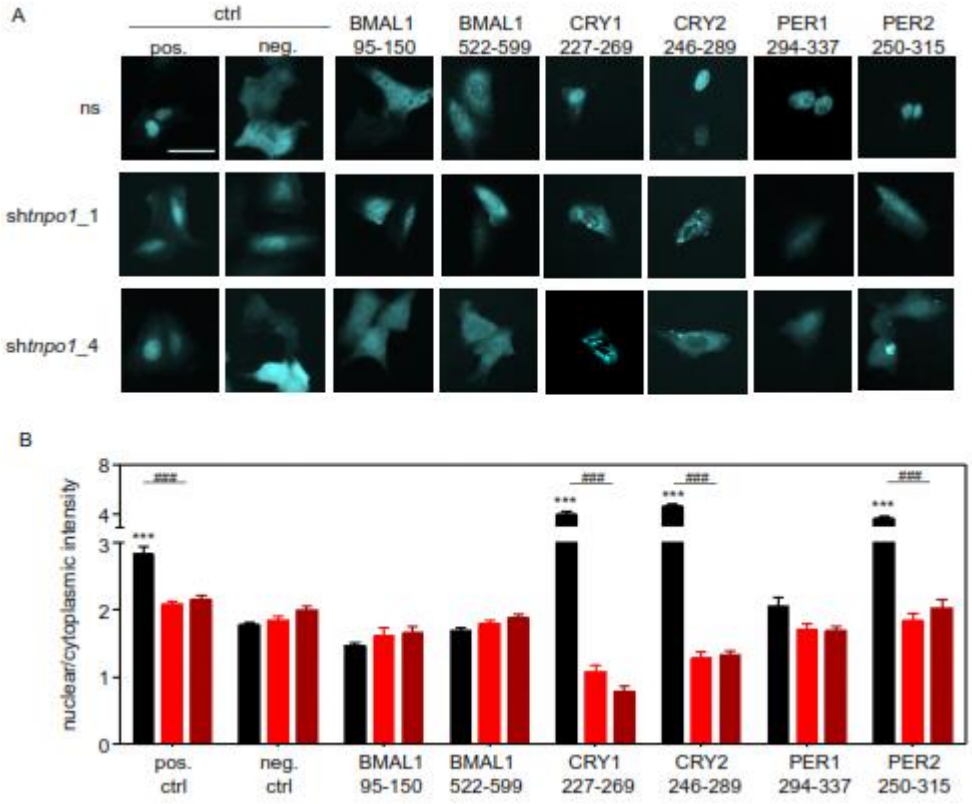


**Figure 3.9: Nuclear localization of specific circadian clock protein-derived putative M9 NLSs is TNPO1-dependent**. U-2 OS cells were lentivirally transduced with mutated pGIPZ vector coding either the ns control shRNA or shRNA targeting *tnpo1* expression (sh*tnpo1*_1 and sh*tnpo1*_4). Additionally, ECFP fused to putative M9 clock peptides was transiently transfected into the RNAi transduced U-2 OS cells. M9 of hnRNP A1 was used as positive control (pos. ctrl), whereas ECFP alone was transfected as negative control (neg. ctrl) for the subcellular distribution assay. Further, subcellular localization upon knockdown of *tnpo1* transcript levels was analyzed for putative M9 peptides of BMAL1, CRY1, CRY2, PER1 or PER2. A) Representative images of fluorescent cells: images in the in the top row show subcellular distribution in ns control cells. Nucleo-cytoplasmic distribution in *tnpo1* expression-depleted cells are depicted in the middle (sh*tnpo1*_1 transduced cells) and bottom (sh*tnpo1*_4 transduced cells) row. B) Mean ratio of nuclear to cytoplasmic ECFP-putative M9 fluorescence intensity upon knockdown of *tnpo1* transcripts (ns control: black, sh*tnpo1*_1: red and sh*tnpo1*_4: dark red; error bars = SEM, n = 8 to 130 cells, statistics: * indicates a significant difference of nuclear to cytoplasmic intensity ratios, when compared to the ratios of neg. ctrl (ECFP alone) in ns control cells; # indicates significant difference of nuclear to cytoplasmic intensity ratios of *tnpo1* expression-depleted cells compared to the ratios of ns control cells of the same ECFP fusion protein. Note: for statistical analysis, the ratios of both sh*tnpo1* targeted cell populations were combined prior to comparison to ratios of ns control cells. One way-ANOVA, post-test: Tukey's multiple comparison test: *** $p < 0.001$, ### $p < 0.001$).

At first we validated the assay using positive (M9 of hnRNP A1) and negative (ECFP alone) controls of the former subcellular distribution assay (see 3.4.1 and figure 3.9). As expected, the diffuse distribution of ECFP fluorescence in negative control cells (ECFP alone) was not altered upon knockdown of *tnpo1* expression. In contrast, the pronounced nuclear accumulation of ECFP fused to the hnRNP A1-derived M9 motif was decreased in cells with reduced *tnpo1* transcript levels (figure 3.9).

Upon depletion of *tnpo1* transcripts, the nuclear localization of ECFP fused to putative M9 NLSs of either CRY1 227-269, CRY2 246-289, PER1 294-337 or PER2 250-315 decreased (figure 3.9). Interestingly, ECFP fused to either of the CRY1 or CRY2 derived putative M9 peptides, showed a distinct cytoplasmic localization (less nuclear than the negative control) as well as cytoplasmic fluorescent aggregates. We did not observe any alterations in subcellular distribution of ECFP fused to BMAL1-derived putative M9 peptides upon repression of *tnpo1* transcription (figure 3.9). For statistical analysis we combined the nuclear to cytoplasmic intensity ratios of all *tnpo1* expression-depleted cells and compared them to ns control intensity ratios.

Additionally, we transfected plasmids encoding the ECFP fusion proteins into HEK293 cells expressing either non-silencing shRNA or RNAi constructs targeting *tnpo1* expression. Results of the subcellular distribution assay in HEK293 cells were similar to those obtained in U-2 OS cells, supporting a cell type-independent TNPO1-mediatd nuclear accumulation (suppl. figure A1.7).

Taken together, we identified putative M9 NLSs in CRY1 and CRY2 as well as PER1 and PER2 but not BMAL1 leading to a distinct nuclear accumulation of the ECFP fusion protein. Furthermore, we could show that this nuclear accumulation is TNPO1-dependent as all four putative M9 NLSs, which showed an increased nuclear localization in ns control cells, lost this phenotype upon knockdown of *tnpo1* expression. Note: the decrease in nuclear accumulation of the ECFP-PER1 294-337 fusion protein was only a trend and not statistically significant.

### 3.4.3 PY motifs of putative M9 NLSs in circadian clock proteins are necessary for nuclear accumulation

We identified putative M9 NLSs in CRY1, CRY2, PER1 and PER2, which promote nuclear accumulation in the presence of TNPO1. However, due to the lack of a well-defined M9 consensus sequence, we chose the peptide length of putative M9 NLSs to be longer than the reported M9 NLSs (see 1.2.4, table 3.4 and Chook and Süel,

2011 [132]). We showed TNPO1-dependent nuclear accumulation of those circadian clock protein-derived peptides. Yet, we did not investigate the particular need of amino acids within the circadian clock protein-derived putative M9 NLSs necessary for TNPO1-dependent nuclear accumulation.

**A single mutation in the PY motif does not alter subcellular distribution of circadian clock protein-derived putative M9 NLSs**

To test, whether the circadian clock protein-derived peptides are putative M9 NLSs, we focused on the PY motif as it was present in 23 out of 24 M9 NLSs of TNPO1 targets (suppl. table A1.4 and Chook and Süel, 2011 [132]).

We performed site-directed mutagenesis to exchange the tyrosine to a non-polar, non-aromatic alanine to yield CRY2 Y273A and PER2 Y294A. The mutated putative M9 peptides still showed a nuclear accumulation, when transfected in U-2 OS cells as ECFP fusion proteins. However, both mutated constructs did show the same trend of decrease in nuclear localization (suppl. figure A1.8 A).

As proof of concept, we perturbed *tnpo1* expression using RNAi prior to transfection of ECFP fused to the mutated version of putative M9 NLSs. The knockdown of *tnpo1* transcripts inhibited nuclear localization of the mutated CRY2 Y273A and PER2 Y294A as previously seen for wild type CRY2 246-289 and PER2 250 315 (see 3.4.2). The nuclear to cytoplasmic fluorescence intensity ratios of the ECFP-mutated M9 fusion proteins were similar to the ratios of negative control cells (ECFP alone). In cells with decreased *tnpo1* transcript levels no difference was observed upon ECFP fusion to the wild type or mutated putative M9 peptide (suppl. figure A1.8 B).

Concluding that a single exchange of tyrosine to alanine is insufficient to prevent nuclear accumulation of putative M9 clock peptides.

**Multiple site-directed mutations in the putative M9 NLS lead to decreased nuclear accumulation**

To identify essential amino acids in TNPO1-mediated nuclear import of clock-proteins, we systematically investigated the putative M9 NLSs in circadian clock proteins. In cooperation with a master student, Lea Ehrhardt, we examined the putative CRY2 M9 sequence more closely. Despite the PY motif within the M9 NLS, other amino acids are reported to be characteristic for the M9 consensus sequence (see 1.2.4 and Chook and Süel, 2011 [132]). We checked the necessity of several of these amino acids within the

peptide sequence of CRY2 by site-directed mutagenesis, exchanging them to alanine (figure 3.10). Four alterations of the putative CRY2 M9 NLS were analyzed:

- double mutation of the PY motif (PY272/273AA)
- double mutation in a potentially basic-enriched site (RK246/247AA)
- two mutations in a potentially basic-enriched site (RPR255-257APA)
- a 15 amino acids deletion of the N-terminus (Δ15N)

To investigate subcellular distribution upon alteration of CRY2 246-289, we optimized the subcellular distribution assay, exchanging the fluorophore from ECFP to EYFP, which resulted in a brighter fluorescent signal. Further, ECFP-BMAL1 540-588 was used as negative control rather than the fluorophore alone to reinforce comparability of the fusion proteins to negative control.

The optimized subcellular distribution assay revealed a reduced nuclear accumulation of EYFP fused to either of the four altered putative M9 peptides. None, of the mutated peptides led to a nuclear localization similar to the wild type peptide, CRY2 246-289. In contrast, all fusion proteins with either of the altered CRY2 putative M9 NLS were less nuclear than the negative control, EYFP-BMAL1 522-599 (figure 3.11).

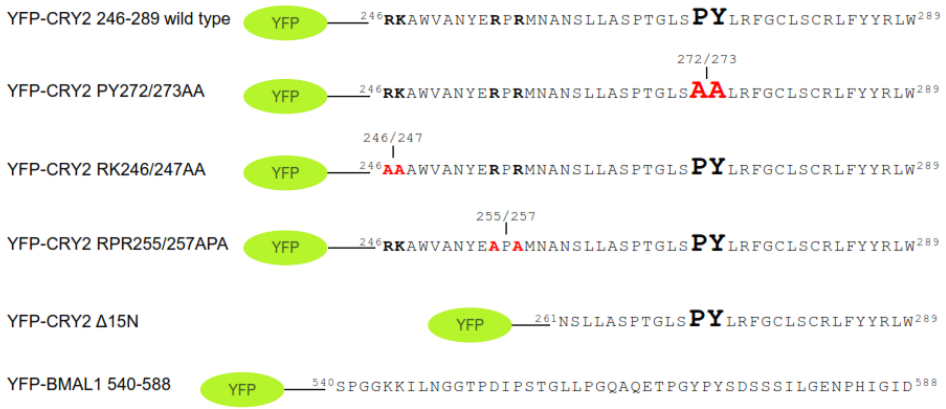


**Figure 3.10: Schematic illustration of altered YFP-CRY2 PY fusion peptides**. Three site-directed exchanges of the CRY2 peptide (PY272/273AA, RK246/247AA and RPR255/257APA; exchanges are indicated in red) as well as an N-terminally shortened peptide (Δ15N; CRY2 251 to 289) were created using the 44 amino acids long wild type peptide (CRY2 246-289) as template. The BMAL1 540-588 peptide is used as negative control. The peptides were C-terminally fused to EYFP prior to use in the subcellular distribution assay.

All tested amino acids of the putative CRY2-M9 peptide are necessary for nuclear localization. If these changes in subcellular distribution are due to loss of TNPO1 binding

to the putative M9 NLS, the absence of TNPO1 would not reduce nuclear localization of EYFP-putative M9 mutants any further.

To check whether depletion of *tnpo1* expression would even decrease nuclear localization of the mutated putative CRY2 M9 peptides, we used RNAi to knockdown *tnpo1* transcripts prior to expression of EYFP-putative M9 fusion proteins.

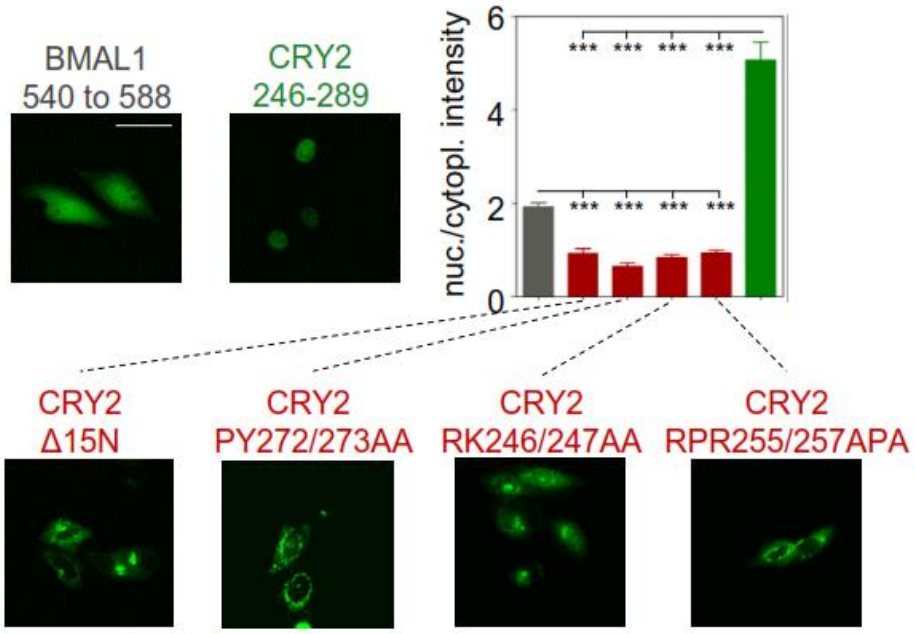


**Figure 3.11: Mutations of specific CRY2 M9 amino acids inhibit nuclear accumulation**. U-2 OS cells were transfected with YFP C-terminally fused to either wild type CRY2 246-289 (green; positive control) or mutated versions of it (red). The deletion of 15 amino acids at the N-terminus of CRY2 246-289 (Δ15N), the double mutant of PY (PY272/273AA), and two exchanges of basic-enriched sites (RK246/247AA and RPR255/257APA) lead to repression of nuclear accumulation. YFP-BMAL1 540-589 (grey) was used as negative control for the subcellular distribution assay (error bars = SEM, n = 54 to 71, One-way-ANOVA, post-test Tukey's multiple comparison test: *** $p < 0.001$).

In line with impaired TNPO1 interaction with putative M9 mutants, the reduced *tnpo1* transcript levels did not alter subcellular distribution of all four tested CRY2 M9 mutants. The putative CRY2 M9 wild type peptide, which had no introduced mutation showed a severely reduced nuclear accumulation upon knockdown of *tnpo1* transcription (data not shown).

Summarizing the bioanalytical approach to identify TNPO1-binding sites in circadian clock proteins, we identified one M9-like sequence in each of the CRY1, CRY2, PER1 and PER2 proteins. All of these putative M9 sequences were (at least as peptide fusion proteins) sufficient to promote nuclear accumulation of the fused fluorophores. Furthermore, we could show that TNPO1 as well as specific amino acids of circadian clock protein-derived putative M9 NLSs are necessary for nuclear localization of those

fusion proteins. Besides the PY motif (PY272/273), we identified three arginines (R246, R255, R257) and one lysine (K247) of the CRY2-M9-like sequence to be essential for normal TNPO1-dependent nuclear accumulation.

Putative non-classical NLSs in PER1/2 and CRY1/2 peptides are first indications of direct TNPO1 binding to circadian clock proteins. These clock-derived peptides represent a small part of full-length circadian clock proteins and it is unknown, whether the determined putative M9 NLSs are sufficient for nuclear accumulation of full-length circadian clock proteins.

## 3.5 TNPO1 interacts with full-length PER proteins

Performing the subcellular distribution assay using clock-derived peptides, we identified potential TNPO1 interacting domains in CRY1, CRY2, PER1 and PER2. To test whether the non-classical nuclear import carrier directly binds to full-length circadian clock proteins, we performed co-immunoprecipitation (CoIP) and luciferase complementation assays.

### 3.5.1 Establishment of the TNPO1 - circadian clock protein - CoIP assay

In order to investigate protein interaction in CoIP assays, several requirements have to be fulfilled. A working immunoprecipitation depends on:

1. expression of target proteins
2. binding strength of the proteins
3. antibodies, well-established for CoIP

Furthermore the detection of a possible interaction depends on the sensitivity of the readout.

Previous determination of endogenous TNPO1 protein levels in human cells (see 3.2.2 and 3.2.3) convincingly showed the efficacy of the anti-TNPO1 antibody (ab10303). In consequence, we tested the antibody in an IP to validate efficacy in IP assays. To this end, we prepared lysates of wild type U-2 OS cells. Additionally, we tested lysates of U-2 OS cells lentivirally transduced with either ns control RNAi or constructs targeting *tnpo1* expression (sh*tnpo1*_1 or sh*tnpo1*_4) to check for antibody specificity in IPs. Whole cell lysates were pre-incubated with agarose beads only to eliminate unspecific binding to the beads. Afterwards the pre-cleared lysate was incubated with antibody and

agarose beads prior to separation of supernatant and immunoprecipitate. SDS-PAGE and western blot were used to detect TNPO1 protein (see 2.2.3).

Using the lysates of wild type or ns control U-2 OS cells, we detected a clear TNPO1 signal in anti-TNPO1 IPs. In line with those findings, the supernatant of IPs using either wild type or ns control lysates showed a reduced TNPO1 protein levels compared to the input (suppl. figure A1.9 A). In contrast, the IPs using lysates of sh*tnpo1* targeted cells resulted only in faint input and IP signals (compared to ns control; suppl. figure A1.9).

Thus, besides western blot application, the tested anti-TNPO1 antibody against endogenous TNPO1 is also efficiently and specifically working in IP assays.

To investigate a potential interaction between TNPO1 and circadian clock proteins, we tried various CoIP approaches with either U-2 OS or HEK293 whole cell lysates. Using U-2 OS cells, we ectopically expressed PER1, PER2, CRY1, CRY2 fused to a fluorophore. In HEK293 cells, we transiently transfected those four circadian clock proteins tagged with a V5-tag as well as N-terminally MYC-tagged TNPO1. CoIPs were performed as described above (see above and 2.2.3). We used an additional idiotypic mouse antibody (further referred to as control IgG), to control for unspecific binding to the constant regions of the anti-TNPO1 and anti-MYC antibody.

We successfully immunoprecipitated TNPO1 in the IPs using an anti-TNPO1 or anti-MYC antibody but not in IPs using the control IgG. However, we only gained evidence for a potential TNPO1 binding to PER1 (but not the other tested circadian clock proteins). Unexpectedly, we detected a PER1-V5 signal in all CoIPs, including IPs using control IgG (suppl. figure A1.9 B). Additionally detecting the heavy chains of the precipitated antibodies illustrates a higher concentration of added unspecific control IgG compared to the applied anti-TNPO1 or anti-MYC antibodies (suppl. figure A1.9 B). This might be a reason, why we obtain a PER1-V5 signal in the lane of the control CoIP ($IP_C$), where we did not expect to detect PER1 as the unspecific normal IgG was used for immunoprecipitation in this sample. Taken the PER1-V5 signal and the higher concentrated control IgG together, we gained first indications of a possible PER1-TNPO1 interaction, although the evidence is weak.

Investigating a potential binding of TNPO1 to full-length circadian clock proteins in CoIP assays using western blot as readout illustrates the difficulties of the chosen approach. Appropriate controls must be considered and applied. We included a preincubation step of the protein lysates with agarose beads only prior to CoIP.

Furthermore, we used a control antibody to detect non-specific binding. A positive control for TNPO1 interaction would be beneficial; however a CoIP approach of TNPO1 and hnRNP A1 did not show a signal of the cargo in an IP using anti-TNPO1 directed against endogenous TNPO1 (data not shown). We hypothesize that binding of TNPO1 to its cargos might be weak. CoIP and subsequent western blot might not be sensitive enough to detect an interaction. Consequently, we optimized the CoIP assay once more, using a luciferase-based readout. This will not only be more sensitive in signal detection but requires less handling of the samples from IP to the final detection.

### 3.5.2 TNPO1 interacts with PER-LUC fusion proteins

To increase the signal to noise ratio of the readout, we fused the co-immunoprecipitated target protein to luciferase (LUC) facilitating the measurement of enzyme activity via luminescence recording after IP.

Performing the previous CoIP assays of TNPO1 and circadian clock proteins in various approaches (see 3.5.1) resulted only in evidence for a TNPO1-PER1 interaction using HEK293 cells and tagged proteins. Therefore, we will focus on this setup using whole cell lysates of transiently transfected HEK293 cells, investigating a potential TNPO1 interaction with PER proteins.

To test TNPO1 and PER1 (or PER2) in CoIP assays using luciferase as readout, we fused both of the PER proteins to full-length luciferase prior to co-transfection together with MYC-TNPO1 in HEK293 cells. The CoIPs were performed as in previous experiments (see 2.2.3 and 3.5.1). Immunoprecipitation of MYC-TNPO1 was performed using the anti-MYC antibody or the control IgG as control for non-specific binding. To measure luciferase signal of the co-immunoprecipitated PER-LUC fusion protein, D-luciferin was added to the pelleted IP prior to luminescence measurement. To control for equal application of antibodies and efficient immunoprecipitation of MYC-TNPO1, we loaded the luciferase activity measured CoIPs on a SDS-PAGE and performed western blots to detect the immunoprecipitated protein (MYC-TNPO1) as well as the antibody chains of anti-MYC or control IgG.

We consistently detected an enriched luminescence signal of PER1-LUC after CoIP using anti-MYC antibody compared to control IgG IPs (figure 3.12 A and C). Similar results were observed for PER2-LUC (figure 3.12 B and C).

To validate these findings, we inverted the approach and immunoprecipitated the circadian clock protein, while measuring luciferase activity of TNPO1-LUC in the

co-immunoprecipitated proteins. To this end, lysates of co-transfected HEK293 cells, expressing TNPO1-LUC and either PER1-V5 or PER2-V5 were used as input for anti-V5 or control IgG IPs. TNPO1-LUC signals were detected upon addition of D-luciferin. SDS-PAGE and western blot of the CoIPs were performed to control for equal application of precipitated antibody and specificity of binding.

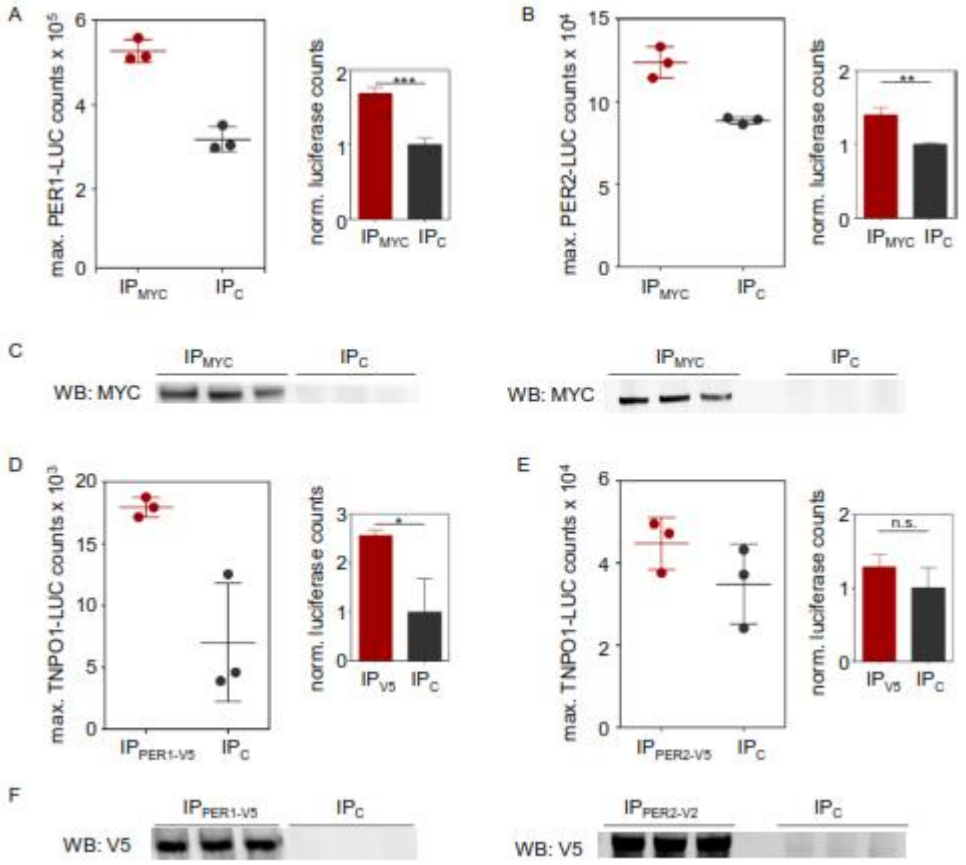


**Figure 3.12: Evidence of a potential interaction between TNPO1 and PER proteins**. Whole cell lysates of transiently transfected HEK293 cells transiently transfected with TNPO1 and either PER1 or PER2 were used in CoIPs using luciferase activity as readout. A and B) MYC-TNPO1 was immunoprecipitated using either a specific anti-MYC ($IP_{MYC}$; red) or control IgG ($IP_C$; grey). PER1-LUC (A) or PER2-LUC (B) activity was measured after CoIP. D and E) CoIP of PER1-V5 (D) or PER2-V5 (E) and TNPO1-LUC using either a specific anti-V5 ($IP_{PER-V5}$; red) antibody or unspecific control IgG. Depicted are maximum luciferase counts ± SD of one representative experiment (left) as well as the mean counts ± SD normalized to $IP_C$ of the representative CoIPs (right, student's t-test: n.s. = non-significant; * $p < 0.05$ ; ** $p < 0.01$; *** $p < 0.001$). To control for efficient immunoprecipitation, western blots of either MYC-TNPO (C) or PER1/2-V5 (F) were performed using the specific anti-MYC or anti-V5 IPs as well as the unspecific control IgG IPs. Experiments were repeated two to seven times.

Specific precipitation of PER1-V5 was detected in anti-V5 IPs but not control IPs. An enhanced luminescence signal of TNPO1-LUC activity in the specific anti-V5 IP was detected compared to control IP (figure 3.12 D and F). Although, we detected a

specific PER2-V5 signal only in anti-V5 IPs, the luciferase activity of TNPO1-LUC was not significantly increased compared to the signal in control IPs (figure 3.12 E and F).

Summarizing the results of the CoIP assays, we consistently showed that the IP of TNPO1 or PER1 resulted in an enriched luminescence signal of the respective, co-immunoprecipitated luciferase fusion protein (MYC-TNPO1 and PER1-LUC or PER1-V5 and TNPO1-LUC). Evidence of TNPO1-binding to PER2 is less consistent, as we observed only an enriched luciferase activity signal, when co-expressing MYC-TNPO1 and PER2-LUC but not PER2-V5 and TNPO1-LUC.

### 3.5.3 Evidence of TNPO1 binding to PER1 and PER2 performing luciferase complementation assays

To validate the results of the CoIP assays, we investigated a potential TNPO1 interaction with PER1 or PER2 performing luciferase complementation assays in HEK293 cell lysates. To do so, firefly luciferase was split in two parts (LUC1 or LUC2), which are only enzymatically active when they reach close proximity to each other, which is only enabled if the proteins of interest interact with each other.

We fused one luciferase part to either PER1 or PER2 and the second part to TNPO1 in various combinations. Hypothetically, the distance of both LUC fragments will be minimal if one of the PER proteins and TNPO1 directly interact. Subsequently, the enzymatically active firefly luciferase is able to metabolize its substrate luciferin, detectable as luminescence. Luminescence counts of firefly luciferase were normalized to co-transfected, full-length renilla luciferase to control for unequal transfection efficiencies.

The assay depends mostly on steric conditions of the potential binding partners as well as the fused luciferase fragments. Besides the possibility that both luciferase fragments might still be too far apart from each other to become enzymatically active, the LUC fragments might interfere with TNPO1 binding to PER, if miss-located at the interaction interface. Therefore, we tested all combinations of TNPO1 fused either N- or C-terminally to LUC1 or LUC2. The complementing second LUC fragments were fused to PER1 or PER2 (also N- or C-terminally).

Preliminary luciferase complementation results indicated a higher potential of binding between N-terminally fused LUC1-TNPO1 or LUC2-TNPO1 to circadian clock proteins rather than C-terminally (data not shown), which correlates with the identified cargo recognition sites at the C-terminus of TNPO1 [263]. In consequence we performed

the assay with N-terminally fused LUC-TNPO1 and all combinations of PER1- and PER2-LUC fusion proteins. In addition we used LUC1-PER1 or PER2-LUC1 together with CRY1-LUC2 as positive controls and combinations of LUC1-TNPO1 or LUC1-PER1 together with LUC2-$\beta$GAL as negative controls for the assay. Further, we transfected either TNPO1-LUC1 or TNPO1-LUC2 alone as another indication of the background luminescence. The highest background signal was observed in lysates of HEK293 cells transfected with LUC1-TNPO1 and LUC2-$\beta$GAL, which will be used as negative control for the TNPO1-PER-interaction signals. Overall the different background measurements had a mean ratio of firefly to renilla luciferase of $0.4 \times 10^{-3} \pm 0.2 \times 10^{-3}$ (mean ± SD, suppl. figure A1.10).

One constellation of N-terminally fused LUC1 to TNPO1 and C-terminally fused LUC2 to either PER1 or PER2 resulted in an enriched luminescence signal compared to the negative controls, indicating an interaction between TNPO1 and PER1 (or PER2) (figure 3.13). No other combinations led to an increased luciferase activity compared to the negative controls (suppl. figure A1.10).

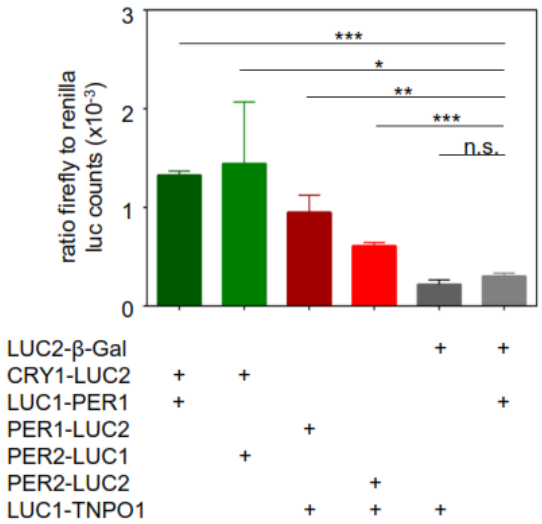


**Figure 3.13: Enriched firefly luciferase signal in TNPO1 and PER1 or PER2 luciferase complementation experiments**. HEK293 cells were co transfected with renilla luciferase and split firefly luciferase (LUC1 or LUC2) fusion proteins. LUC1 was N-terminally fused to TNPO1 (LUC1-TNPO1), whereas LUC2 was C-terminally fused to either PER1 (dark red, PER1-LUC2) or PER2 (red, PER2-LUC2). The assay was controlled by LUC1/2 fusion proteins of PER1 or PER2 and CRY1 (green) as positive controls. As negative control LUC1-TNPO1 or LUC1PER1 fusion proteins were co transfected with LUC2-$\beta$ Galactosidase (LUC2-$\beta$GAL, grey). Firefly luciferase activity was normalized on full length renilla luciferase activity. Depicted is on eof three representative experiment (error bars = SD, n = 3, student's t-test: n.s. = non-significant, * $p < 0.05$, ** $p < 0.01$, *** $p < 0.001$).

In previous investigations, we identified clock-derived peptides to be sufficient for TNPO1-dependent nuclear import (see 3.4). Questioning the relevance of these findings for full-length clock proteins, we used two luciferase-based interaction studies (CoIP and luciferase complementation) and obtained further evidence of a potential TNPO1 interaction with full-length PER1 (and less consistent of TNPO1 and PER2). Both assays indicate a specific interaction between the nuclear import carrier and the

transcriptional repressors, however it is unknown, whether the observed interactions effect nuclear localization of the putative TNPO1 cargos.

## 3.6 TNPO1-dependent nuclear accumulation of PER1

Is TNPO1 necessary for normal subcellular distribution of PER1 (or PER2)? Although, we gathered evidence for an interaction between TNPO1 with PER1 and PER2 performing CoIP and luciferase complementation assays, until now we only gained indications that TNPO1 is essential for normal nuclear accumulation of PER1 and PER2 using PER-derived peptides in the subcellular localization assay.

### 3.6.1 Altered PER1 subcellular distribution upon knockdown of *tnpo1* expression

To test whether normal nuclear localization of full-length PER depends on the presence of TNPO1, we performed subcellular distribution assays. To investigate a TNPO1-dependent subcellular distribution, we used RNAi (sh*tnpo1*_4) to reduce *tnpo1* transcript levels in U-2 OS cells ectopically expressing either PER1- or PER2-Venus.

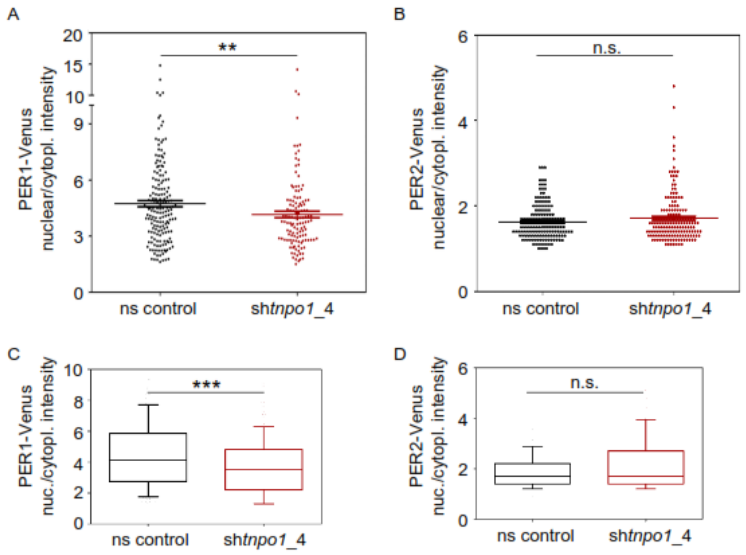


**Figure 3.14: Altered nuclear distribution of PER1 but not PER2 upon depletion of *tnpo1* transcripts.** U-2 OS cells ectopically expressing PER1- or PER2-Venus were lentivirally transduced with RNAi targeting *tnpo1* expression (sh*tnpo1*_4, red) or ns control shRNA (grey). A and B) Depicted are single cell ratios of nuclear to cytoplasmic fluorescence intensity of a representative experiment of either PER1- (A) or PER2-Venus (B) transduced cells (error bars = SEM, n = 124 to 173) C and D) Summary of all three experiments of either PER1 (C) or PER2 (D) (whiskers indicate the 10$^{th}$ to 90$^{th}$ percentile and boxes indicate the 25$^{th}$ to 75$^{th}$ percentile; n = 274 to 652 cells, One-way-ANOVA, post-test: Tukey's multiple comparison test: n.s. = non-significant, ** $p < 0.01$, *** $p < 0.001$)

Whereas previous investigations (the peptide-based subcellular distribution assay as well as the interaction studies) indicated a TNPO1-mediated nuclear import of both PER1 and PER2, the subcellular distribution assay of full-length PER proteins showed no reduction in nuclear PER2 levels. We even gained indications of a slight increase of nuclear PER2 accumulation upon depletion of *tnpo1* expression (figure 3.14 B and C). In contrast to PER2 subcellular distribution, PER1-Venus was less nuclear in cells with decreased *tnpo1* transcript levels (sh*tnpo1*_4) compared to ns control cells (figure 3.14 A and C). Efficient knockdown of *tnpo1* expression, was quantified on mRNA level (suppl. figure A1.11).

Interestingly, the subcellular localization assay of full-length proteins shows only TNPO1-dependent nuclear accumulation of PER1 but not PER2, although we previously found evidence for TNPO1 interaction with both circadian clock proteins.

### 3.6.2 Nuclear import of PER1 is decelerated upon knockdown of *tnpo1* expression

If the alternative nuclear import carrier, TNPO1, is necessary for normal PER1 nuclear accumulation, nuclear import dynamics of the circadian core clock protein might be also altered upon decreased *tnpo1* expression.

To determine the TNPO1-dependet nuclear import rate of PER1 (and PER2), we used fluorescence recovery after photobleaching (FRAP). The assay does not only provide insights in import kinetics of PER1 and PER2 but might also give further information on the function of TNPO1 in the nuclear entry process of PER2, which did not show TNPO1-dependent nuclear accumulation in the steady state subcellular distribution assay (see 3.6.1).

We lentivirally transduced U-2 OS cells, ectopically expressing PER1- or PER2-Venus, with either ns control shRNA or two RNAi constructs targeting *tnpo1* expression (sh*tnpo1*_1, sh*tnpo1*_4) prior to the FRAP assay, which was performed in three steps (see 2.2.2):

1. a picture of the unbleached cells was taken to record the pre-bleaching fluorescence intensity

2. the nuclei were bleached at a 100 % laser power

3. the recovery of nuclear fluorescence intensity was monitored every 2.5 minutes for up to one hour (figure 3.15)

We examined the nuclear import rate of PER1 first. To this end, we recorded time series of the recovery of fluorescence intensity in nuclei of ns control cells and quantitatively determined a mean recovery time of 13 ± 2 min (mean ± SEM) to regain 25 % of the pre-bleached fluorescence intensity. In contrast, the recovery time in *tnpo1* expression targeted cells was decelerated. We determined a mean fluorescence recovery time of 18 ± 3 min (mean ± SEM) for 25 % of initial nuclear fluorescence in cells, which were transduced with sh*tnpo1*_1. The second RNAi construct tested, sh*tnpo1*_4, prolonged the nuclear import even more and increased the mean recovery time of fluorescence intensity to 24 ± 5 min (mean ± SEM) to regain 25 % of the initial fluorescence intensity (figure 3.15 A and B). We verified an efficient knockdown of *tnpo1* expression on relative mRNA and protein level (suppl. figure A1.11). The intermediate nuclear import rate might be due to a less-efficient depletion of *tnpo1* expression using sh*tnpo1*_1, which left the relative mRNA levels twice as high as transduction of sh*tnpo1*_4.

In contrast to PER1, we did not determine a TNPO1-dependent nuclear accumulation of PER2 performing steady state subcellular distribution assay. It is possible that the TNPO1 dependency of PER2 is less severe than of PER1, therefore we determined PER2 nuclear import rates using only sh*tnpo1*_4, which led to a stronger decrease in *tnpo1* mRNA levels as well as to an increased deceleration of PER1 nuclear entry compared to application of sh*tnpo1*_1. However, no change of PER2 nuclear import kinetics was observed compared to ns control cells. The mean time to recover 25 % of initial nuclear fluorescence intensity was 16 ± 3 minutes (mean ± SEM) in ns control cells and 21 ± 5 minutes (mean ± SEM) in sh*tnpo1*_4 cells (figure 3.15 C).

To exclude insufficient knockdown of *tnpo1* expression, we also checked relative mRNA and protein levels of *tnpo1* in these cells (suppl. figure A1.11). The residual relative *tnpo1* mRNA levels in cells transduced with sh*tnpo1*_4 was less than 0.1 when normalized to ns control cells.

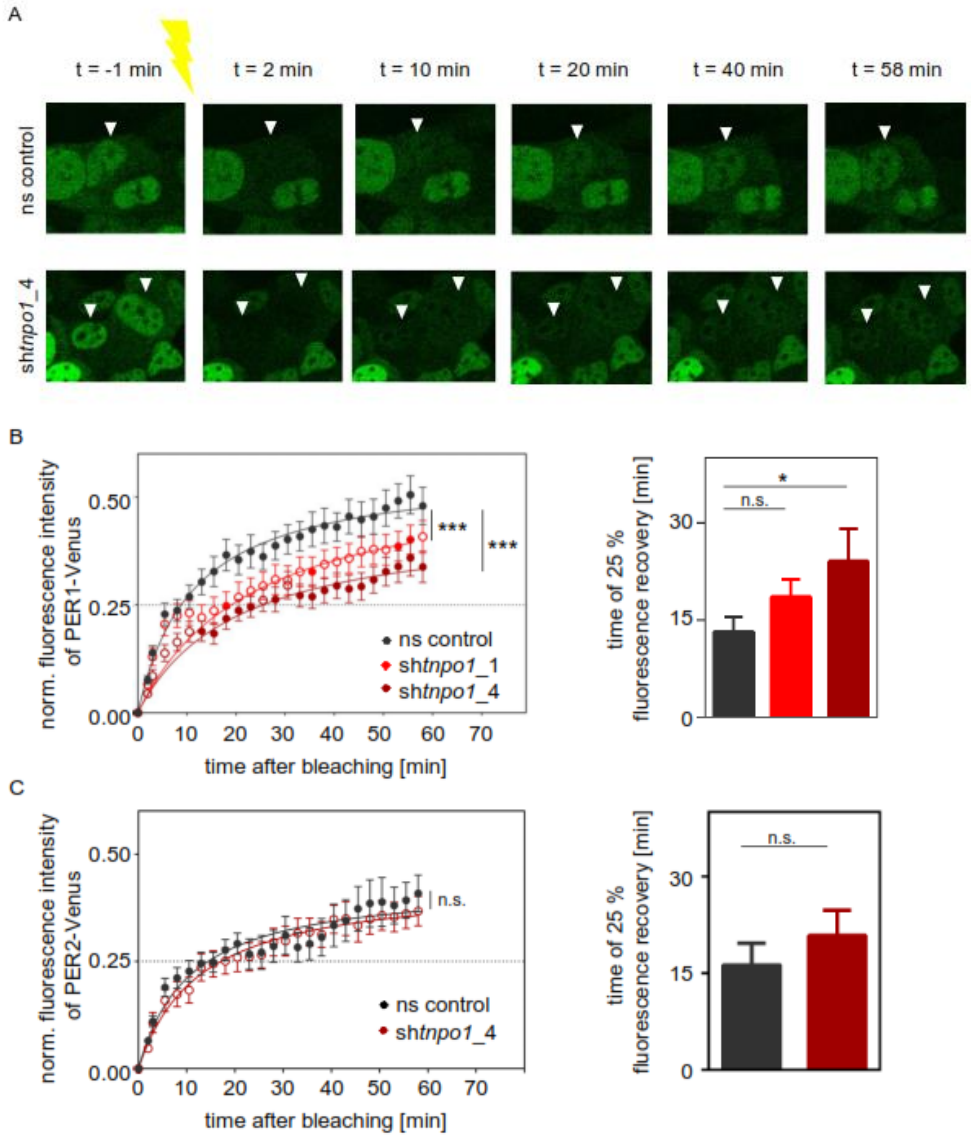


**Figure 3.15: Decelerated nuclear import rate of PER1 but not PER2 in *tnpo1*-depleted cells.** U-2 OS cells, ectopically expressing either PER1- (A and B) or PER2-Venus (C), were lentivirally transduced with ns control RNAi (grey) or constructs targeting *tnpo1* expression (red). Fluorescence recovery after photobleaching (FRAP) was performed in three steps. First, an image was taken to capture the pre-bleach fluorescence intensity (t = -1 min). Second, bleaching was performed at a 100 % laser power and third, images were taken every 2.5 min post-bleaching, for a total of ~1 h. A). Representative example of FRAP assay. Either ns control cells or *tnpo1* expression targeted cells, expressing PER1-Venus were monitored prior (t = -1 min) or post-bleaching (t = 2 to 58 min). Arrow heads indicate the bleached nuclei. B and C) Quantification of FRAP assay in ns control or *tnpo1* expression-depleted (sh*tnpo1*_1, red and sh*tnpo1*_4, dark red) U-2 OS cells. Post measurement, intensities of nuclei and respective whole cells were determined using the ImageJ software. Briefly: background intensities of each image was subtracted and nuclear intensity normalized to the cytoplasmic fluorescence. Initial (pre-bleaching; t = -1 min) fluorescence intensity was set to 1, whereas residual fluorescence intensity at the time of bleaching was calculated using a linear function of the first three time points after bleaching and set to 0. Left: kinetics of recovery over a period of ~60 min. Right: Mean time of 25 % recovery of the initial fluorescence intensity using a Michaelis-Menten equation of each individual recorded recovery curve (error bars = SEM, n = 8 to 18; statistics on import kinetics (left): Two-way-ANOVA, post-test: Sidak's multiple comparison test, note: significantly different single time points indicated as filled circles $p < 0.05$, empty circles indicate time points which are non-significantly different from ns control data points; statistics on recovery time to regain 25 % of initial fluorescence (right): student's t-test; * $p < 0.05$; *** $p < 0.001$)

Summarizing all data obtained in the subcellular distribution assays of peptide and full-length PER proteins as well as in the interaction studies, we found indications of a TNPO1-dependent nuclear import of PER1.

We identified putative M9 peptides in both PER proteins, which were sufficient for TNPO1-mediated nuclear import. In fact, PER2 250-315 showed a stronger nuclear accumulation upon presence of TNPO1 than PER1 294-337. Additionally, the knockdown of *tnpo1* expression resulted in a more severe cytoplasmic accumulation for PER2 250-315 compared to PER1 294-337. Unexpectedly, nucleo-cytoplasmic translocation of full-length PER2 seems to be independent of TNPO1, whereas PER1 showed stronger and accelerated nuclear import in the presence of the alternative nuclear import carrier. In line with those findings, our interaction assays consistently show a PER1-TNPO1 binding, whereas data for PER2 and TNPO1 are less coherent.

Reports on TNPO1 cargo binding focus mainly on non-classical M9 NLSs recognition but not all cargos interact via a M9 recognition motif. Studies on FOXO4 identified TNPO1 as an interacting protein, forming disulfide-bonds under oxidizing conditions [154]. Furthermore, investigations on the Parkinson disease-related protein DJ1 showed M9 NLS binding to TNPO1 in normal redox conditions and an increased binding of TNPO1 to DJ1 upon induction of oxidative stress [156]. Whether the cellular redox conditions influence interaction between TNPO1 and circadian clock proteins, in particular PER1 and PER2, is unknown.

## 3.7 Nuclear accumulation of PER1 is TNPO1-dependent under oxidizing conditions

In the previous investigations we ignored the fact that TNPO1 binds specific cargos only or stronger under oxidizing conditions. To test whether cellular oxidative stress alters the interaction between the non-classical nuclear import carrier and PER1 (or PER2), we repeated the full-length protein assays and applied 200 μM hydrogen peroxide to increase the intracellular oxidative stress levels.

### 3.7.1 Increased binding between TNPO1 and PER1 upon oxidative stress

To compare the binding strength of TNPO1 and PER1 (or PER2) under oxidizing and non-oxidizing conditions, we repeated the CoIP assays for PER1 and PER2 (see 2.2.3 and 3.5.2), applying hydrogen peroxide to the transfected HEK293 cells

30 minutes prior to lysis and approximately once every hour while performing the CoIP assay.

CoIPs were performed with either anti-MYC, anti-TNPO1 or the unspecific control IgG for lysates of MYC-TNPO1 and PER1-LUC. As expected, both specific CoIPs showed an enriched luminescence signal of PER1-LUC activity compared to control IPs in normal redox conditions. Under oxidizing conditions, the luminescence signal in the specific CoIPs was even higher than in non-oxidizing conditions (figure 3.16 A, B and D). The signal in CoIPs using the non-specific control IgG was similar in both redox conditions.

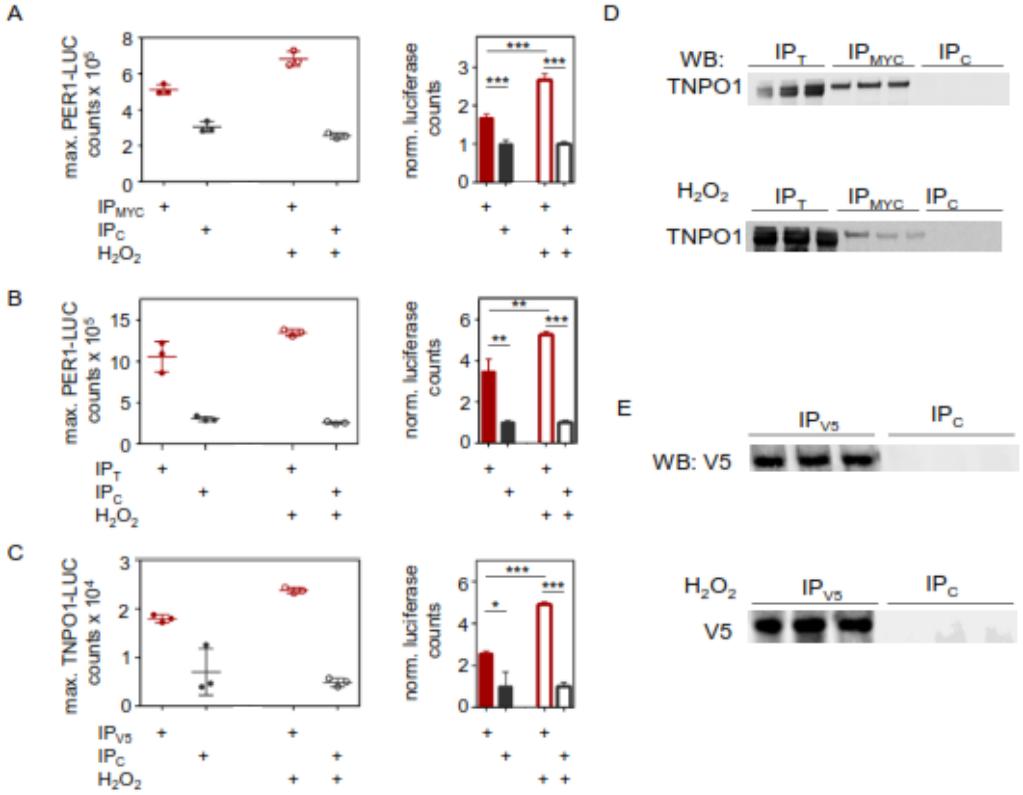


**Figure 3.16: Increased interaction between TNPO1 and PER1 upon induced oxidative stress**. Whole cell lysates of HEK293 cells ectopically expressing TNPO1 and PER1 were used for CoIP assays without (filled circles/bars) or upon (empty circles/bars) treatment with 200 µM hydrogen peroxide. MYC-TNPO1 was immunoprecipitated using either anti-MYC ($IP_{MYC}$; red; A) or anti-TNPO1 antibodies ($IP_T$; red; B) prior to detection of the PER1-LUC signal. anti-V5 CoIPs (C) were performed in assays co-transfecting PER1-V5 and TNPO1-LUC ($IP_{V5}$; red). All assays were controlled by the IP using an unspecific control IgG (IPC, grey). Depicted are representative experiments. A to C) Left: Total luciferase activity counts after CoIP. Right: Mean fold changes of the representative CoIPs normalized to the unspecific IgG IP under oxidative stress and native conditions. D and E) Western blot detection of the immunoprecipitated tagged proteins; either MYC-TNPO1 (C) or PER1-V5 (E) (error bars = SD, n = 3, student's t-test: * $p < 0.05$; ** $p < 0.01$; *** $p < 0.001$).

Validating the results, we switched the immunoprecipitated target and luciferase fusion protein. Therefore, we performed CoIP assays using anti-V5 and the unspecific

control IgG for lysates of cells transiently expressing TNPO1-LUC and PER1-V5. As in the MYC-TNPO1 approach, we obtained an enriched luciferase activity signal upon treatment with 200 μM hydrogen peroxide (figure 3.16 C and E). The IP of the tagged protein (either MYC-TNPO1 or PER1-V5) was verified in western blot (figure 3.16 D and E). Note: We did not observer any increased luciferase activity signal in the IP input, rather a trend towards decreased luciferase signal under oxidizing conditions (data not shown).

Performing the CoIP assays with TNPO1 and PER2 (in both variations either MYC-TNPO1 and PER2-LUC or TNPO1-LUC and PER2-V5), did not result in an enriched luminescence signal under oxidizing conditions. Using MYC-TNPO1 and PER2-LUC, we detected an increased luciferase activity signal in the specific anti-MYC IPs compared to IPs applying non-specific control IgG. These results were similar under normal and oxidizing conditions (see also 3.5.2). However, PER2-V5 IPs resulted in no consistent data. Upon treatment with hydrogen peroxide, the TNPO1-LUC derived luminescence signals were either similar or less intense than under normal conditions (suppl. figure A1.12).

In conclusion, we gained evidence for an increased TNPO1 binding to PER1 but not PER2 performing CoIP assays under oxidative stress conditions.

### 3.7.2 Decreased PER1 nuclear accumulation under oxidizing conditions

To evaluate the role of oxidative stress on subcellular distribution of PER1 (or PER2), we analyzed PER1- or PER2-Venus nuclear and cytoplasmic accumulation in hydrogen peroxide treated U-2 OS cells. PER localization was imaged prior to application of 200 μM hydrogen peroxide as well as 30 minutes and 2 hours after treatment.

Fluorescence intensity of PER1-Venus showed a reduced nuclear localization under oxidative stress conditions (figure 3.17, grey), which is already visible after 30 minutes of hydrogen peroxide incubation. After 2 hours the ratio of nuclear to cytoplasmic fluorescence intensity was not decreased any further. In contrast, PER2-Venus did not result in an altered subcellular distribution upon hydrogen peroxide treatment (having a trend to an increased nuclear accumulation in individual experiments, suppl. figure A1.13 A, grey). Concluding these findings, only nuclear accumulation of PER1 but not PER2 is decreased under oxidative stress conditions.

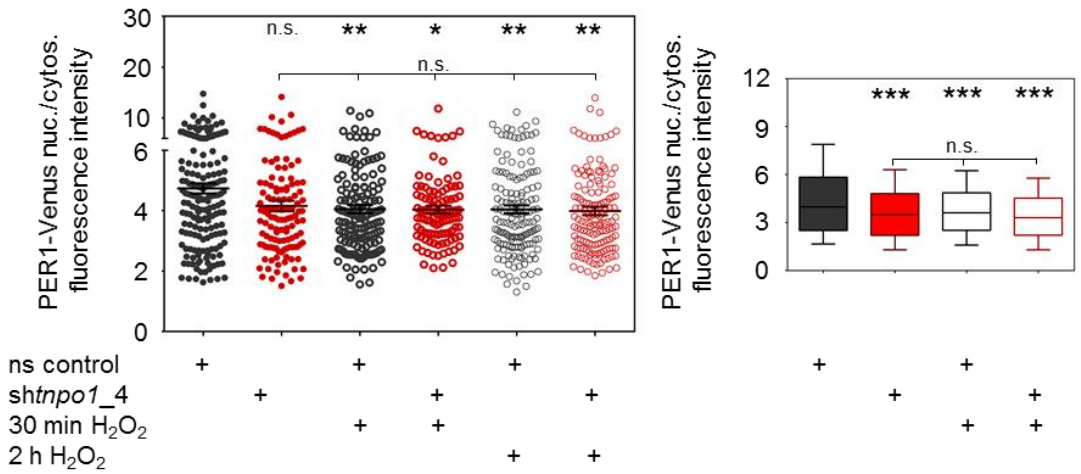


**Figure 3.17: Reduced nuclear accumulation of PER1 upon oxidative stress.** U-2 OS cells, ectopically expressing PER1-Venus, were lentivirally transduced with either ns control shRNA (grey) or sh*tnpo1*_4 (red). Subcellular distribution of PER1-VENUS was imaged prior (filled circles) to treatment with 200 µM hydrogen peroxide as well as 30 min (thick outlined circles) and 2 h (thin outlined circles) post-incubation. Depicted are nuclear to cytoplasmic fluorescence intensity ratio of single cells within a representative experiment (left) or the sum of all measured ratios determined in four individually performed experiments (right). Statistics are performed in comparison to untreated ns control cells if not otherwise indicated (error bars = SEM, $n_{epresentative}$ = 106 to 173 cells, $n_{all}$ = 326 to 686, One-way-ANOVA, post-test: Tukey's multiple comparison test: n.s. = non-significant, * $p < 0.05$, ** $p < 0.01$, *** $p < 0.001$).

If those oxidative stress-induced alterations of PER1 subcellular distribution are TNPO1-mediated and oxidative stress would reduce nuclear import via TNPO1, reduced levels of *tnpo1* expression should not decrease nuclear PER1-accumulation under oxidizing conditions any further. To test this, we depleted *tnpo1* transcription using sh*tnpo1*_4 and additionally treated the cells with 200 µM hydrogen peroxide.

As observed in previous experiments (see 3.6.2 and figure 3.17), the individual knockdown of *tnpo1* expression or treatment with hydrogen peroxide, resulted both in a reduced nuclear accumulation of PER1. Applying hydrogen peroxide to the sh*tnpo1*_4 treated cells did not lead to a further reduction of nuclear accumulation of PER1 (figure 3.17 A). We imaged the cells again 30 minutes and 2 hours after treatment with hydrogen peroxide but could not observe any differences within those two time points. PER2-Venus subcellular distribution was not altered using the same setup as for PER1. Neither depletion of *tnpo1* transcripts nor oxidative stress nor both applications together reduced the nuclear PER2-Venus levels (suppl. figure A1.13 A). Efficient knockdown of *tnpo1* expression was verified on mRNA levels (suppl. figure A1.11).

In summary, we obtained further evidence of a TNPO1-dependent, non-classical PER1 subcellular distribution under oxidizing conditions. Nuclear accumulation of PER1 was reduced upon hydrogen peroxide treatment, which was similar to the depletion of

*tnpo1* expression. Further, nuclear PER1 levels were not further decreased upon knockdown of *tnpo1* transcription prior to induction of oxidative stress.

### 3.7.3 Decelerated nuclear import of PER1 under oxidative stress conditions

Evidence of a TNPO1-dependent nuclear translocation of PER1 in normal redox as well as oxidative stress conditions were obtained performing steady state subcellular distribution assays. To test whether oxidative stress alters also PER1 nuclear import rate, we repeated the FRAP experiments (see 2.2.2 and 3.6.2) applying 200µM hydrogen peroxide to the U-2 OS cells 30 minutes prior to the FRAP assay.

The induction of hydrogen peroxide in wild type U-2 OS cells ectopically expressing PER1-Venus resulted in a reduced nuclear import rate upon oxidative stress compared to normal conditions (suppl. figure A1.14).

This preliminary data indicates a decelerated nuclear import of PER1 under oxidizing conditions. However, we were interested in the effect of oxidative stress on TNPO1-mediated PER1 nuclear import. Therefore, we depleted *tnpo1* expression using RNAi prior to oxidative stress treatment and FRAP.

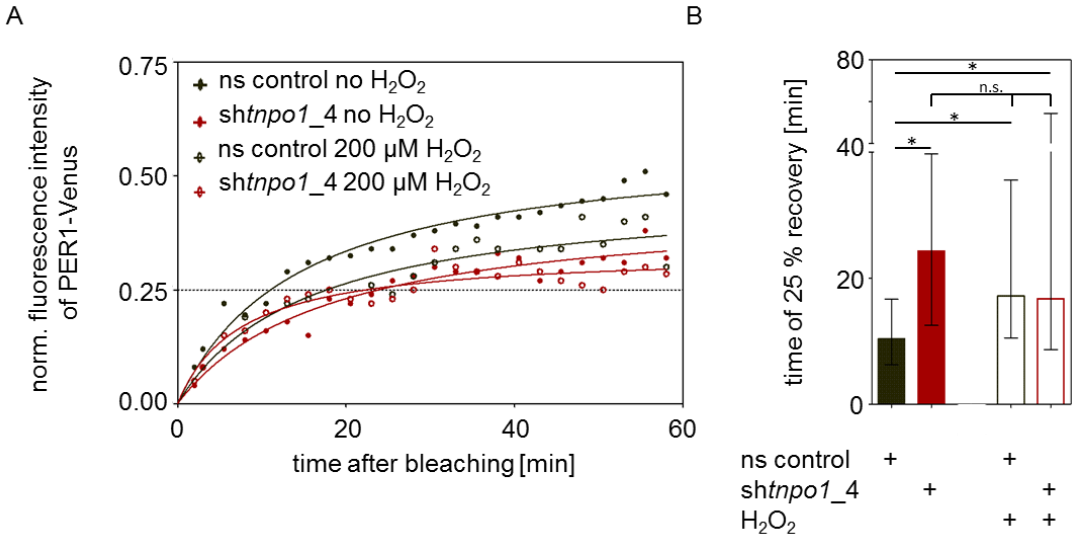


**Figure 3.18: TNPO1-dependent oxidative stress regulation of the PER1 nuclear import rate**. U-2 OS cells, ectopically expressing PER1-Venus, were lentivirally transduced with RNAi targeting *tnpo1* expression (sh*tnpo1*_4, red) or ns control RNAi (ns control, grey). A) Cells were imaged 30 min after treatment with 200 µM hydrogen peroxide (empty circles) or solvent control (water, filled circles). An image of pre-bleaching fluorescence was taken prior to bleaching the nuclei with 100 % laser intensity. Afterwards images were taken every 2.5 min for up to ~1 h. Depicted are medians of all acquired data. B) Median of the recovery time needed to regain 25 % of initial fluorescence intensity either with (empty bars) or without (filled bars) hydrogen peroxide treatment (error bars = interquartile range, representing the range between 25-75 % of all values, n = 11-18 cells for each condition, right: student's t-test: n.s. = non-significant, * $p < 0.05$)

We transduced U-2 OS cells using either ns control RNAi or sh*tnpo1*_4. FRAP analyses were performed as described for wild type U-2 OS cells under oxidative stress condition. To do so, we incubated the cells with 200 µM hydrogen peroxide for 30 minutes prior to the FRAP analysis. FRAP measurements were performed as described in 2.2.2 and 3.6.2. We analyzed 15 cells of each transduction (ns control or sh*tnpo1*_4) and determined the mean recovery curve as well as the mean recovery time of all cells to regain 25 % of the initial fluorescence (suppl. figure A1.15). In contrast to the FRAP analysis under normal redox conditions, the distribution of the recovery curves were not as evenly distributed. In conclusion, the very fast (and really slow) recovering cells distort the mean values of the overall recovery. To prevent this, we used the median rather than the mean to determine the average recovery curves as well as recovery times to regain 25 % of the initial fluorescence (figure 3.18; for images of single cell recovery data see suppl. figure A1.16).

Under oxidizing conditions, the median recovery time to regain 25 % of the initial nuclear fluorescence is similar in *tnpo1*-depleted and ns control U-2 OS cells (17 minutes). However, the interquartile range, indicating the range of 25-75 % of all included data is wide (ranging from three minutes to more than one hour). Comparing the determined recovery time for 25 % of initial fluorescence to the median recovery curve over a period of about one hour, the values for ns control cells under oxidizing conditions fit together. The determined 25 % recovery time for cells with impaired expression of *tnpo1* under oxidizing conditions and the corresponding median recovery curve are not as consistent. Examining the single cell recovery curves of *tnpo1*-depleted cells under oxidizing conditions in more detail, two populations of cells are present (suppl. figure A1.16). Whereas seven of the 15 cells need more than 30 minutes to recover 25 % of their initial nuclear fluorescence, six cells regained 25 % after 10 minutes. Note: At this point of our investigations, we cannot rule out multiple oxidative stress-induced regulatory pathways for PER1 nuclear import. A TNPO1-mediated deceleration PER1 nuclear import seems conceivable as the induction of oxidative stress in *tnpo1*-depleted cells is not further decelerating the individually induced reduction of nuclear fluorescence recovery time.

The ns control cells do not show a pattern as distinct as sh*tnpo1*_4 transduced cells under oxidizing conditions, but five of the 15 cells take more than 30 minutes to recover 25 % of initial nuclear fluorescence. Only three cells recover 25 % of initial fluorescence after 10 minutes and seven cells recover 25 % of initial nuclear fluorescence within 11 to 29 minutes.

Under normal conditions, the mean and median recovery curves of *tnpo1*-depleted cells were similar in regard to the recovery curve and the recovery time of 25 % of the initial nuclear fluorescence (mean: 24 ± 5 minutes, median: 24 minutes). The median recovery time of ns control cells was 10 minutes under normal conditions (mean recovery time: 13 ± 2 minutes).

Comparing the median recovery time to regain 25 % of initial nuclear fluorescence of cells with and without knockdown *tnpo1* expression under normal and oxidizing conditions, the recovery time of ns control cells under normal conditions is significantly lower than of all other approaches.

In conclusion of the FRAP assays, we found indications of a TNPO1-mediated nuclear import of PER1, which is decelerated upon depletion of *tnpo1* expression. Furthermore, nuclear import of PER1 is slowed down upon oxidative stress, but only in the presence of TNPO1. Oxidizing conditions do not further decrease the nuclear import rate in *tnpo1* expression-depleted cells.

Even under the same conditions, the variability of fluorescence recovery between single cells is high. Statistical significance and biological relevance of these results must be carefully related and further investigations might be necessary.

## 3.8 Preliminary indications of PER1-dependent period shorting upon depletion of *tnpo1* expression

At last, we were interested to translate the previous findings to the short-period phenotype upon depletion of *tnpo1* transcripts. To test whether the observed period shortening in circadian dynamics of *tnpo1* expression targeted reporter cells is due to TNPO1-mediated nuclear import of PER1, we simultaneously knocked down *tnpo1* (sh*tnpo1*_1) and *per1* (sh*per1*_1, sh*per1*_2, sh*per1*_3) transcription using RNAi. As a control, we additionally performed single transcript depletion of *tnpo1* or *per1*. As expected, the knockdown of *tnpo1* expression resulted in a one hour period shortening (-1.0 ± 0.1 hours; mean ± SD). In contrast, the depletion of *per1* transcript levels lengthened the period (maximum +0.5 ± 0.4 hours; mean ± SD). The sh*per1* derived period lengthening impedes a simple comparison of the period deviations upon knockdown of *tnpo1* expression only and of the double knockdown of *tnpo1* and *per1* expression (suppl. figure A1.17). Focusing on the sh*per1* construct, which led to the

mildest period lengthening of only +0.2 ± 0.1 hours (mean ± SD; sh*per1*_3). The corresponding double knockdown of *per1* and *tnpo1* expression resulted in a period deviation of -0.6 ± 0.1 hours (mean ± SD). Although, the period deviation of the double knockdown and single *tnpo1* transcript depletion is larger than 0.2 hours (observed in single RNAi targeting of *per1* expression), this is only a slight indication of a PER1-dependent period alteration upon knockdown of *tnpo1* transcription (suppl. figure A1.17).

# 4 Discussion

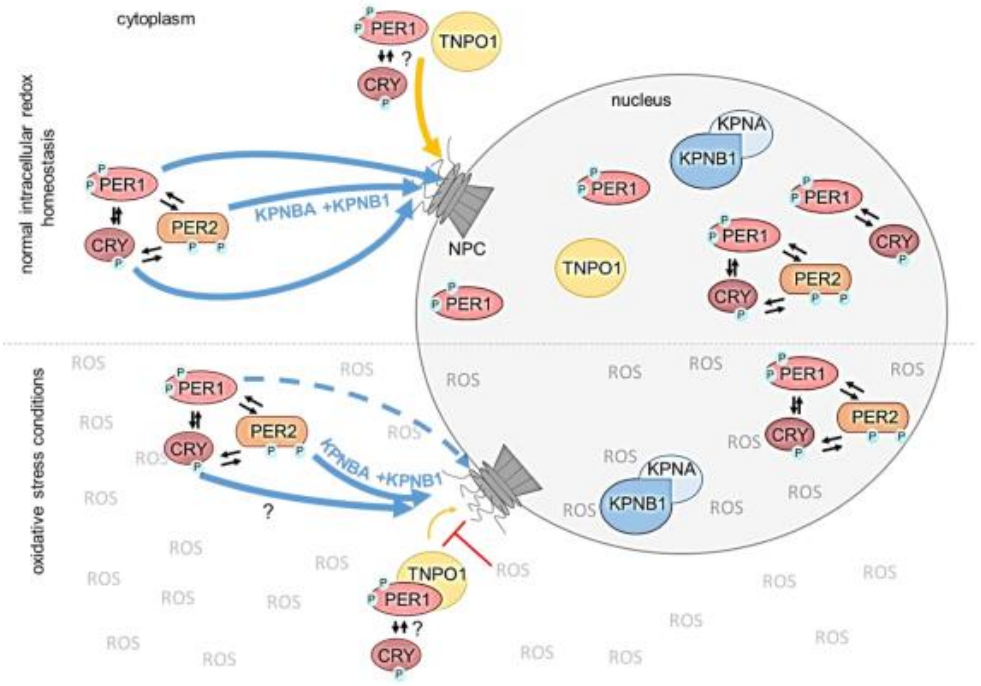


**Figure 4.1: Final predictive model of TNPO1-mediated nuclear import of circadian clock proteins**. Top: The non-classical nuclear import carrier TNPO1 (orange) binds to PER1 (red) under normal intracellular redox conditions thereby shuttling the circadian clock protein into the nucleus. Besides the alternative nuclear import pathway, clock proteins are also shuttled via the classical carriers KPNA and KPNB1 (blue). Bottom: Oxidative stress induction (depicted as ROS, grey) increases TNPO1 binding to PER1. However, PER1 nuclear accumulation is decelerated and decreased. In contrast to PER1, PER2 (brown) is only shuttled via the classical nuclear import pathway, which is not affected by exogenous ROS-level. Whether or not CRY proteins are directly or indirectly interacting with TNPO1 has to be elucidated.

Circadian rhythms are generated by TTFLs. The circadian core clock proteins CLOCK/BMAL1 promote expression of *per* and *cry* genes, which in turn inhibit the transcriptional activators. Even though the fundamental steps of circadian rhythm generation in mammals are known (see 1.1), not all specific mechanisms of the TTFL are understood. Cytoplasmic modifications of proteins including CRYs and PERs are essential for functionality. However, these proteins need to translocate back into the nucleus to actually inhibit CLOCK/BMAL1 transcriptional activation. Knowledge on this nucleo-cytoplasmic translocation process of circadian clock proteins is limited, although in general nuclear import and export through nuclear pores are well studied (see 1.2.5).

Proteins larger than 40 kDa are unable to passively diffuse through nuclear pores. Consequently, it is most likely that circadian clock proteins are actively shuttled into the nucleus. Evidence for classical nuclear import by KPNB1/KPNA was shown by Sakakida

*et al.* (2005) [172], Umemura *et al.* (2014) [173], Lee *et al.* (2015) [174] among others. However, nucleo-cytoplasmic shuttling involves more than 60 proteins and it is unlikely that only KPNB1 and KPNA play a role for circadian rhythm generation. Currently, our understanding of the nuclear import of circadian clock proteins is limited as no comprehensive studies of nucleo-cytoplasmic shuttling in regard to circadian clock control exist.

Therefore, we systematically investigated the necessity of nuclear pore complex components as well as other proteins involved in nucleo-cytoplasmic translocation for normal circadian dynamics. We used RNAi to knockdown expression of 62 targets and identified several components involved in nucleo-cytoplasmic translocation to be crucial for normal near-24-hour rhythm generation. Depletion of eleven transcripts resulted in severe period lengthening or low CC. In addition, application of several constructs targeting those transcripts led to reduced cell vitality (see 3.2.1). We identified only three transcripts leading to period shortening upon knockdown of their expression, which was never accompanied by loss of cell vitality. We hence found that these three transcripts, *tnpo1*, *ranbp16* and *gle1*, are essential for normal circadian rhythm generation. Depletion of their expression shortens the period by more than -0.5 hours. Note: knockdown of *tnpo1* transcript shortened the period by more than one hour (table 3.2).

RANBP16 (XPO7) and GLE1 are nuclear export carriers, whereas TNPO1 is a nuclear import carrier. Interestingly, knockdown of *tnpo1* expression shortens the circadian period while depletion of *kpnb1* transcription (coding for the classical nuclear import carrier) results in a period lengthening compared to time series of ns control cells.

Focusing on TNPO1, we identified putative TNPO1-recognition sites in multiple clock peptides, such as in CRY1, CRY2, PER1 and PER2, being sufficient for TNPO1-dependent nuclear accumulation of an ECFP fusion protein (see 3.4.1). Furthermore, we could show that TNPO1 interacts with full-length PER1 and that nuclear import of PER1 depends on the presence of TNPO1 (see 3.5 and 3.6). Additionally, we found evidence of a decelerated nuclear import of PER1 upon knockdown of *tnpo1* expression.

Altogether, we found evidence that the non-classical nuclear import carrier TNPO1, besides the classical transporter KPNB1 and KPNA, is essential for nuclear shuttling of circadian clock proteins. At least PER1 needs the presence of TNPO1 for normal nuclear distribution (figure 3.6.1). Therefore we hypothesize that the short period phenotype upon depletion of *tnpo1* transcripts might be due to perturbation of the TNPO1-mediated nuclear import of PER1. We tested this by double knockdown of *tnpo1*

and *per1* expression. As a result of the double knockdown we could only obtain preliminary indications that an impaired TNPO1-mediated nuclear import of PER1 is (at least) partially the reason of period shortening upon depletion of *tnpo1* expression. However, the slight period lengthening upon single knockdown of *per1* expression makes an interpretation of the partial rescue of the TNPO1-mediated period shortening in double knockdown cells complicated (see 4.1.3 for further discussion). To validate our hypothesis further, homozygous gene knockouts of *tnpo1* or *per1* would be an advantage. Although the circadian rhythm in those cells would be altered compared to wild type cells, an additional knockdown of the second target would show whether TNPO1 acts on the circadian clock via PER1 or not.

Our studies emphasize the complexity of nuclear import but also of nucleo-cytoplasmic translocation overall. Thereby, the RNAi-screen showed that more than one nuclear import carrier is essential for normal near-24-hour rhythm generation and further components involved in the translocation process are necessary for normal nucleo-cytoplasmic localization.

## 4.1 Circadian clock protein interaction with the non-classical nuclear import carrier TNPO1

### 4.1.1 Several conditions promote nuclear entry of circadian clock proteins

Nucleo-cytoplasmic shuttling of circadian clock proteins needs several post-translational modifications to take place (see 1.1). To translocate back into the nucleus, circadian clock proteins need stabilization and interaction with each other in order to promote the actual translocation process [35, 40, 157]. For PERs and CRYs but also for other circadian clock proteins, including CLOCK and BMAL1, several phosphorylation sites and interacting kinases are reported [34, 35, 273, 274]. However, it is unclear why so many phosphorylation processes take place to prime the protein either for nuclear entry or proteasomal degradation. Furthermore, several investigations on ubiquitination-mediated degradation of circadian clock proteins are reported and this pathway clearly promotes the decrease of PER and CRY levels and inhibits nuclear translocation [33, 36, 38, 39]. Until now our knowledge of the fate of the proteins is only limited. We know that interaction with other PER and CRY proteins stabilizes the repressor complex [40, 162, 164] but triggers for priming proteins to degradation or translocation are unknown.

In particular for PER1, it was shown that CK1$\delta/\varepsilon$ phosphorylates multiple sites and Ser661 and Ser663 seem to be of special interest for nuclear import [157]. Other kinases, including GRK2, also play a role for nuclear localization of PER1 (and PER2) [275]. Additionally, de-ubiquitination of PER1 by USP2 was shown to have no function in protein stability but rather in nuclear localization of PER1 [231, 276]. Besides these post-translational modifications it was reported that interaction with other circadian clock proteins, such as CRY1 and CRY2 are beneficial for nuclear import of PER1 [163]. However, in CRY1/2-deficient mice PER3 interaction with PER1 sufficiently promotes nuclear entry of PER1 [164].

Besides post-translational modification and circadian clock protein interaction with each other, they need active carriers to translocate in and out of the nucleus. In most circadian core clock proteins, such as PER and CRY, cNLSs were identified [166-171]. Perturbation studies of the classical nuclear entry which impair nuclear accumulation of circadian clock proteins and alter circadian dynamics, are in line with these findings [172, 173, 174]. Unfortunately, the majority of these investigations are steady state observations of the nucleo-cytoplasmic subcellular localization of circadian clock protein and only few results on dynamic alterations are reported. Until now, only one study by Lee and colleagues (2015) investigated the influence of RNAi-depleted classical nuclear import on circadian rhythm generation [174]. In addition, we studied PER2 nuclear import rates and gained evidence that the PER-CRY interaction is essential for normal nuclear import of PER2. Further, we showed that pharmacological inhibition of the classical import and export pathway prolonged the period [165].

Nevertheless, our understanding of the actual nuclear import mechanism by passing through the nuclear pore is very limited with no indications on the temporal resolution of PER1 being reported. We determined a recovery rate of PER2 fluorescence intensity of about 30 minutes to regain 50 % of the initial intensity, being the only indication of a time frame for nuclear import of mammalian clock proteins [165]. In non-mammalian species, two different timing mechanisms are reported for clock components. Saez and colleagues (1996) investigated nuclear shuttling of *Drosophila* PER and TIM. They reported a six hour delay of the PER/TIM complex in the cytoplasm. After cytoplasmic retention PER and TIM separate prior to individual translocation into the nucleus [179, 180]. In contrast to the relatively slow and delayed nucleo-cytoplasmic translocation in *Drosophila*, indications on a faster shuttling of circadian clock proteins were found in *Neurospora*. Schaffmeier *et al.* (2008) reported evidence of nucleo-

cytoplasmic FRQ translocation within minutes [177]. Furthermore, increased FRQ phosphorylation shifts the subcellular distribution towards the cytoplasm. Final phosphorylation of FRQ completely inhibits its nuclear entry [178].

Investigating nuclear import dynamics of PER1 and PER2 using FRAP experiments, we determined a recovery rate similar to previous findings [165] of about 15 minutes to recover 25 % of the initial fluorescence intensity. However, it is difficult to compare these results with the observations of *Drosophila* PER/TIM or *Neurospora* FRQ [177-180], as we neither determined the time of a potential cytoplasmic delay of PER proteins prior to nuclear entry, nor controlled the phosphorylation status of the transcriptional repressors. The nuclear recovery within minutes suggests a rather fast nuclear import of mammalian PER compared to *Drosophila* PER and TIM proteins.

### 4.1.2 TNPO1 is an alternative nuclear import carrier of PER1

In this study, we found indications that the interaction between TNPO1 and PER1 is essential for maintenance of normal nuclear PER1 accumulation, providing evidence of an alternative nuclear import pathway for circadian clock proteins. Expression of *tnpo1* is essential for normal nuclear localization of PER1, including nuclear import rates of PER1. We also gained evidence for a direct protein-protein interaction between TNPO1 and PER1 by performing CoIPs and a luciferase complementation assay. Indirect effects of TNPO1 cargos could also influence circadian dynamics as TNPO1 promotes nuclear import of mRNA-processing proteins, such as hnRNPs. In fact, one of those hnRNPs, hnRNPQ, was reported to mediate rhythmic translation of *per1* mRNA [277]. Nevertheless, two luciferase-based assays provide data which support a direct interaction between TNPO1 and PER1. This interaction might even be increased under oxidative stress conditions (see 4.2 for further discussion).

In addition, the peptide-based subcellular distribution assay identified a potential TNPO1 binding site in PER1 (PER1 294-337), which contains a putative M9 NLS recognized by TNPO1. We identified PY motifs in peptides of CRY1 and CRY2 as well as PER1 and PER2. Exchanging both amino acids of the PY motif in CRY2 to non-polar, non-aromatic alanines resulted in a strong decrease of nuclear accumulated CRY2 peptide. Site-directed mutagenesis to exchange several basic amino acids in the CRY2 peptide resulted in the same decrease of nuclear CRY2 peptide. Additionally, the depletion of *tnpo1* expression decreased nuclear localization of the identified clock peptides, indicating a TNPO1-dependent nuclear import of those peptides. Translating these peptide-based

data to full-length proteins, we examined the nucleo-cytoplasmic distribution of full-length PER1 and PER2 in presence and absence of normal TNPO1 levels. In line with the peptide-based assay, we found evidence for reduced nuclear PER1 accumulation but not for PER2. In conclusion, not all clock-derived, putative M9 NLSs are biologically relevant for nuclear import of full-length circadian clock proteins. Furthermore, we did not investigate whether the potential PY motif is necessary for nuclear import of full-length PER1. Yet, the subcellular distribution assay and the interaction studies of PER1 indicate direct binding of TNPO1 to PER1.

Different cargos of TNPO1 contain variable binding sites for interaction with the non-classical nuclear import carrier. Chook and Süel (2011) summarized some cargos in PY-containing NLSs and non-classical NLSs without a PY motif [132]. Besides those two groups of TNPO1 recognition signals, disulfide bonds can be formed between cysteines of the carrier and specific cargos as reported for FOXO4 [154]. Human FOXO4 consists of 505 amino acids (uniprot: P98177), including five cysteines. Nuclear magnetic resonance (NMR) spectroscopy was used to identify FOXO4 Cys239 which is essential for FXO4-TNPO1 disulfide-bond formation. Only Cys355 was also interacting with TNPO1, whereas all other three identified cysteines did not. The authors did not determine specific cysteines in the TNPO1 sequence, which interact with FOXO4. In contrast, the M9 NLS binding sites in TNPO1 are identified as strong affinity (A-site) and weak affinity (B-site) domains in the C-terminal region of the S-shaped TNPO1 structure (see 1.2.4) [148, 278].

To identify specific binding sites of PER1 and TNPO1, one could either focus on the circadian clock protein or the carrier, but the diversity of possible interaction sites exacerbates the identification of the actual binding site: PER1 is a large protein of 1290 amino acids (uniprot: O15534) and besides putative PY or non-PY containing M9 NLSs, it contains 27 cysteines. An estimation which of them might be able to form disulfide bonds with the nuclear import carrier is difficult as no structural data of the full-length protein are available. Furthermore, steric changes under oxidative conditions might enable different cysteines to interact with TNPO1. On the other hand, TNPO1 consists of 898 amino acids (uniprot: Q92973) with a total of 26 cysteins. Site-directed mutagenesis of all cysteins of TNPO1 would be just as laborious as of PER1. Other methods, such as NMR [154], might be more appropriate.

Peptide-based analysis of the putative M9 NLS in CRY2 246-289 showed that an exchange of the PY motif to two non-polar alanines is sufficient to inhibit nuclear

accumulation of that peptide. In addition, site-directed mutation in the coding sequence of the basic amino acids (arginines and lysines) reduced the nuclear PER1 levels. These investigations indicate the necessity of multiple amino acids within the CRY2 246-289 peptide for active nuclear import. The exchange of the PY motif (PER1 320/321) in full-length PER1 would validate those findings for a full-length clock protein. Additionally, we could use a mutated putative M9 NLS in PER1 to examine the binding site of TNPO1 and PER1 more closely. If TNPO1 would still bind to PER1 upon exchange of PER1 PY320/321AA, the interaction between the two binding partners might be promoted by disulfide-bond formation rather than non-classical NLSs.

As the mutation of cysteines in PER1 is a tedious and time-consuming approach and non-classical NLSs are difficult to identify, fragmentation of PER1 into longer peptides might give an indication on TNPO1-interacting domains of PER1 [169]. The identification of the TNPO1-binding site in PER1 would improof our understanding of the TNPO1-PER1 interaction. In addition, it would be another tool to examine the TNPO1-mediated nuclear import of PER1 in more detail.

In our study, we focused on PER1 and PER2 interaction with TNPO1 but could only obtain a TNPO1-dependent nuclear accumulation of PER1 but not of PER2. This raises questions of the purpose of a PER1-TNPO1 interaction and the difference of PER1 and PER2. In collaboration with Eva Wolf's lab, we determined distinct structural differences of PER1, PER2 and PER3, identifying a higher potential to form homodimers for PER1 and PER3 but not PER2. In contrast, PER2 showed a higher potential of interaction with other proteins, including CK2, GSK3$\beta$ or REV-ERBs, implying different functions of PER1 and PER2 as well as PER3 [279]. The TNPO1-mediated nuclear import of PER1 but not PER2 might be due to those structural differences and might be necessary for specific functions of PER1.

### 4.1.3 Altered TNPO1-mediated nuclear import of PER1 might shorten the circadian period

Within this study, we gained indications for a TNPO1-mediated alteration of PER1 nuclear accumulation as well as a short period phenotype in circadian dynamics upon depletion of *tnpo1* expression (see 3.2 and 3.6). To test whether the period shortening is due to TNPO1 mediated PER1 nuclear translocation, we performed double knockdown of *per1* and *tnpo1* expression (see 3.8). Unfortunately, the single knockdown of *per1* expression resulted in a period lengthening (mildest period lengthening:

0.2 ± 0.1 hours), whereas reduced *tnpo1* transcript levels shortened the circadian period about one hour (1.0 ± 0.1 hours). This is complicating the interpretation of the partially rescued TNPO1-dependend period shortening after RNAi-induced *tnpo1* downregulation. The double knockdown of *tnpo1* and *per1* expression, resulted in a period shortening of -0.6 ± 0.1 hours. Addition of a +0.2 hours period lengthening of single *per1* transcript depletion to the -1 hour period shortening of single *tnpo1* transcript depletion would lead to a period shortening of -0.8 hours, which still leaves a difference of 0.2 hours compared to the double knockdown, where we observed a period shortening of only -0.6 hours. This might be an indication that the short period phenotype upon knockdown of *tnpo1* expression is due to PER1 nuclear translocation, but the data is only a weak indication as the -0.2 hours period deviation could also be experimental variation.

As another possibility to test whether depletion of *tnpo1* expression has an impact on the repressive function of PER1, a co-transactivation assay could give further information. Co-transfection of *clock*, *bmal1* and an E-box-driven *luciferase* results in transcriptional activation of luciferase expression by CLOCK/BMAL1 heterodimers. Upon co-expression of *per1,* luciferase activity should be (partially) inhibited as PER and CRY repress its CLOCK/BMAL1 transcriptional activation. In line with our data, we would predict that depletion of *tnpo1* expression would result in a reduced inhibitory effect of PER1 promoting *luciferase* expression. On the other hand, a reduction of *tnpo1* transcript levels could lead to increased KPNB1-mediated nuclear import. If the classical nuclear import pathway promotes repression of CLOCK/BMAL1, a knockdown of *tnpo1* expression would lead to a decreased luciferase activity signal.

A PER1 knockout cell line might also be a useful tool to validate whether depletion of *tnpo1* expression would still lead to period shortening in homozygous *per1* knockout cells. The generation of those genome engineered cells could be accomplished using the CRISPR/Cas9 technique, which is an inexpensive and relatively fast method to generate genome modifications. An additional knockout of the *per1* gene in the generated *tnpo1* knockout cells (gRNA1_1, see 3.2.3) might verify the partial rescue of the short-period phenotype upon knockdown of *tnpo1* expression (see 3.2.2) and knockout of the *tnpo1* gene (see 3.2.3).

### 4.1.4 TNPO1 links an alternative nuclear import pathway to the circadian clock

Although most identified targets of TNPO1-mediated nuclear import are components of mRNA-processing as several heterogeneous ribonucleoproteins or the

pre-mRNA-processing proteins and PABP2 [132], cargos of TNPO1 seem to function in many pathways. TAP1 is involved in folding of the major histocompatibility complex class I in the ER [280] and FUS is a multi-functional protein which is essential for repair of double strand breaks [281]. To this end, nuclear import processes of proteins with diverse functions are mediated by TNPO1. Even though no nucleo-cytoplasmic translocation of circadian clock proteins by the alternative nuclear import carrier are known until now, it is conceivable that components of the molecular clock are targeted by TNPO1.

We showed that full-length PER1 binds to TNPO1 and normal nuclear PER1 accumulation depends on the presence of TNPO1. Our investigations indicate a specific role for PER1 as PER2 nuclear accumulation does not depend on TNPO1. Nevertheless, we cannot rule out a TNPO1 interaction with other circadian clock proteins as the peptide-based subcellular distribution assay revealed putative PY motifs in CRY1 and CRY2. Further studies will evaluate a potential nuclear import of full-length CRY proteins as well as other circadian clock proteins via TNPO1. We will validate the regulatory function of TNPO1 on circadian clock dynamics and will determine whether the carrier specifically targets the circadian clock via PER1 or if other circadian clock proteins are also transported via TNPO1.

One aspect we did not address yet is a possible time-of-day dependence of nuclear import via TNPO1. Although no evidence for TNPO1-mediated nuclear import of circadian clock protein was reported until now, indications have been found that TNPO1 (and possibly KPNB1) are expressed in a circadian manner. Sato *et al.*, 2011 reported evidence of a circadian *tnpo1* expression in the SCN. They identified an oscillation of *tnpo1* mRNA, peaking at circadian time 8 (CT 8) [282]. In line with a circadian mRNA expression of *tnpo1*, Hughes et al. (2009) could also show rhythmic mRNA levels of *tnpo1* in mouse liver (http://circadb.hogeneschlab.org/). It peaks at Zeitgeber time 8 (ZT 8), whereas the trough is at ZT 16 [283]. Comparing these rhythmic expression profiles to the transcript levels of the classical nuclear import carrier *kpnb1*, the two transporter seem to be expressed anti-phasic as *kpnb1* mRNA peaks at ZT 18 and the nadir is at ZT 6 [284]. A potential anti-phasic nuclear import of circadian clock proteins might enable specific nucleo-cytoplasmic translocation processes, which regulate different functions of circadian clock proteins. The peak of *per1* expression is at CT 9 [285], which correlates with the expression of *tnpo1*. In contrast, the protein levels of PER1 peak about six hours later at CT 15 [285]. Until now, no time series of the TNPO1 protein levels is available. Although we performed time series analyses of U-2 OS cells investigating the *tnpo1* levels,

we did not gain evidence in rhythmic *tnpo1* mRNA or protein levels (data not shown). As post transcriptional modifications and translation take place at a different pace depending on the gene of interest, we can only speculate about the peak phase of TNPO1 and KPNB1 protein levels. If *kpnb1* is translated fast, the protein level might correlate with PER1, otherwise it is more likely that the TNPO1 protein level are elevated while PER1 protein level peak.

The possibility of nuclear translocation by more than one carrier has also been discussed by Chook and Süel (2011) [132]. They conclude that several carriers can transport one cargo and the likelihood of multiple carriers is increased with fewer distinct NLSs of one carrier. However, it is unknown, why several cargos are transported by multiple carriers and the authors speculate that protein abundance or size may be the reason of multiple carriers. Furthermore, they mention that a specific regulation might be due to multiple functions of a protein but neither of these possibilities is experimentally validated. Beyond, it is not clear which cargo is transported by which carriers and why not by another. Those problems will not be solved until a systematic and comprehensive carrier-cargo interaction map will be available. However, the systematic screening for NLSs and carrier-cargo interaction is difficult. Many NLSs are less distinct than the cNLS and many cargos contain multiple recognition sites, which will only enable carrier-cargo binding in association with each other. No data on potential cooperative interaction between multiple nucleo-cytoplasmic translocation carriers, such as KPNB1 and TNPO1, are available.

## 4.2 Oxidative stress - TNPO1 - and the circadian clock

In addition, we investigated the role of TNPO1 in PER1 nuclear import under oxidative stress conditions, as it is reported that selected cargos of the non-classical carrier bind stronger or exclusively under oxidative conditions. Upon treatment with hydrogen peroxide, we detected an increased TNPO1-PER1 binding. Unexpectedly, nuclear accumulation of PER1 is decreased upon oxidative stress. Upon knockdown of *tnpo1* expression, the applied hydrogen peroxide did not further decrease nuclear localization of PER1, which might indicate a TNPO1-dependent nuclear import or cytoplasmic retention under oxidative stress conditions.

Several studies investigated the effect of oxidative stress on Ras GTPases, including the subgroup of Ran. As for the mutual regulation of the circadian clock and redox signaling, Ras GTPases seem to be regulated by intracellular redox conditions and

vice versa control redox signaling (reviewed in Ferro *et al.*, 2012 [286]). Oxidative stress inhibits the Ran-GDP to GTP exchange by the nuclear nucleotide exchange factor RCC1 [287]. Previous investigations by Kodiha et al. (2004) identified an impaired nuclear import upon stress-induced depletion of Ran-GTP. They further found indications on an altered Nup153 and KPNB1 subcellular localization under oxidative stress [288]. In line with these findings are reports about an impaired nuclear export upon oxidative stress induction due to decreased XPO1-Ran-GTP interaction. Several more NPC components undergo conformational changes upon oxidative stress, which perturb their normal nucleo-cytoplasmic translocation [289]. We did not investigate the effect of oxidative stress on KPNB1-mediated subcellular localization of PER1 and it is possible that the classical as well as the non-classical nuclear import carrier interact together or in parallel upon oxidative stress. Another possibility is an indirect effect of *tnpo1* transcript depletion, which might induce *kpnb1* expression (no indications found on mRNA levels, data not shown). Taken the published and our own data together it becomes clear that nuclear import of circadian clock proteins is complex and multiple mechanisms are reasonable.

### 4.2.1 TNPO1 as a potential PER1-mediated regulator of the circadian clock under oxidative stress conditions

As mentioned earlier, we identified a stronger TNPO1-PER1 binding under oxidative stress conditions (see 3.7.1 and 4.1.2). Application of hydrogen peroxide resulted in a more pronounced interaction between TNPO1 and PER1 but not PER2 compared to non-oxidizing conditions. Further, the induction of ROS in the examined cells reduced the PER1 nuclear levels and decelerated the PER1 nuclear import rate similar to the depletion of *tnpo1* expression. Unexpectedly, these two events (application of oxidative stress and depletion of *tnpo1* expression) both resulted in decelerated nuclear import of PER1. Decreased level of the nuclear import carrier would give reason to expect a decelerated nuclear import of PER1. However, induction of ROS could have also increased nuclear shuttling as immediate response to oxidative stress. Treatment of *tnpo1* transcript-depleted cells with hydrogen peroxide did not further reduce the single effect of the *tnpo1* knockdown, implying a TNPO1-dependent deceleration of PER1 nuclear import under oxidative stress conditions.

In conclusion, TNPO1 facilitates the regulation of oxidative stress-induced alterations of PER1 nuclear localization. The effects of either a reduced *tnpo1* transcript levels or an exogenous levels of ROS are similar and do not add up upon application of

both, sh*tnpo1* and hydrogen peroxide. However, the FRAP analyses of less than 20 cells under each condition might not be sufficient to understand the putative link between TNPO1, oxidative stress and PER1 as the intercellular variability is high even within one condition and treatment. Future analysis will validate whether an increased TNPO1 levels lead to an accelerated nuclear import of PER1 under oxidative stress conditions. Our studies propose that an increase in TNPO1 protein levels in normal redox state does not necessarily increase nuclear import of PER1, but upon oxidative stress an increase would lead to an accelerated PER1 import rate.

The mechanism of the oxidative stress-induced deceleration of PER1 nuclear entry could either be due to a reduced dissociation of the carrier-cargo complex or to a change in protein conformation leading to an altered interaction with NUPs of the NPC (see above 4.2). Another explanation could be a reduced classical nuclear import facilitated by an increased binding to TNPO1 under oxidative stress. However, the latter reasoning is unlikely as depletion of *tnpo1* expression also leads to decelerated PER1 nuclear import. One other possibility might be the lack of PER1 binding to other circadian clock proteins, such as PER3 or CRY1/2, which is promoting nuclear accumulation of PER proteins [162-164]. Future studies need to confirm the TNPO1-mediated, ROS-induced alterations of nuclear PER1 accumulation and will be essential to validate whether the TNPO1-PER1 interaction links oxidative stress to the circadian clock.

The role of a decelerated nuclear import of PER1 for circadian rhythm generation is speculative. However, we expect the same effect on circadian dynamics regardless of the inducing mechanism leading to reduced nuclear PER1 translocation. We would predict that application of oxidizing reagents result in the same alteration of circadian dynamics as knockdown of *tnpo1* expression. In regard to period alterations, we observed a period shortening upon depletion of *tnpo1* expression (see 3.2). Due to those findings, we would predict that application of oxidative reagents results in the same alteration of circadian dynamics as if oxidative stress is forwarded to the clock only by TNPO1. Preliminary investigations indicate only an acute effect upon application of hydrogen peroxide to U-2 OS reporter cells. This acute phase shift is lost within the first two days (data not shown) and therefore impedes a final solution of this question.

In fact, application of hydrogen peroxide is only suboptimal for induction of oxidative stress (or oxidative conditions) as the concentrations penetrating the cells cannot be properly determined due to neutralization of most hydrogen peroxides in the medium. Furthermore, the availability of the treatment on the cells is difficult to control.

Other oxidizing reagents as paraquat or the addition of oxidized glutathione might be more appropriate to induce ROS at specific concentrations [290, 291].

Although we identified a putative M9 motif in PER1, we could not determine the binding site of PER1 for TNPO1. In addition, we observed an increased TNPO1-PER1 binding upon induced ROS. This might be due to:

1. stronger binding at the original TNPO1 recognition site (potentially the identified putative M9 NLS) as hypothesized for DJ1 [156]

2. conformational changes in PER1 induced under oxidative conditions, which enable new binding at different PER1 sites

3. the formation of disulfide bonds as described for FOXO4 [154].

Identification of the binding sites under normal redox conditions as well as under oxidative stress will improve our understanding of the mechanism of PER1-TNPO1 interaction and might elucidate the interplay of oxidative stress, TNPO1, and the circadian clock.

### 4.2.2 Oxidative stress and its mutual regulation of the circadian clock

With this study, we are the first to report evidence for TNPO1-mediated oxidative stress regulation of circadian core clock proteins. These two mechanisms - oxidative stress and the circadian clock - control each other via multiple pathways. The discovery of rhythmic PRX oxidation even in a non-transcriptional environment, such as in red blood cells, is just one example of the extremely complex network [236, 292]. We can only assume how much impact the redox state has on the molecular clock and to what extent other mechanisms - besides the core clock - take over in oxidative stress conditions. However, PRX are not the only link between oxidative stress and the circadian clock. Sirtuins (SIRT) were shown to increase oxidative stress tolerance or even resistance in multiple tissues. Evidence was found that SRTs function at the transcriptional levels and promotes DNA repair after DSBs (reviewed in Patel et al., 2014 [293]). Furthermore, SIRT1 regulates circadian dynamics by de-acetylating BMAL1 thereby counteracting CLOCK acetylation [294, 295]. Similar to the mutual regulation of PRX and the circadian clock, sirtuins are also regulated vice versa by the molecular clock. SIRT1 enzyme activity depends on the $NAD^+$-levels, which in turn are mediated by nicotinamide phosphoribosyltransferase (NAMPT). The *nampt* promoter comprises several E-boxes,

which lead to rhythmic expression of *nampt* and downstream also to circadian rhythmicity of $NAD^+$-levels [294, 296].

Within the last decades several links of oxidative stress and the circadian clock have been identified and the mutual regulation of such fine-tuned systems turned-out to be highly complex. It seems conceivable that further connections between circadian regulation and oxidative stress control will be identified.

In this study, we gained evidence that TNPO1 binds stronger to PER1 and decelerates its nuclear translocation upon induction of oxidative stress (see 3.7). We found indications of a TNPO1-mediated nuclear import (at least) of PER1 under oxidative stress conditions. Taken our data together, TNPO1-dependent retention of cytoplasmic PER1 might possibly be another trigger affecting the molecular clock in times of oxidative stress, including the control by sirtuins [294, 295].

Despite the fact that we did not find evidence for an impaired nuclear PER2 accumulation (see 3.5 and 3.7), it is still unclear whether TNPO1 regulates nuclear import of multiple circadian clock proteins or specifically of PER1. Besides the well-established function of PER1 in near-24-hour rhythm generation, some evidence was reported for an anti-apoptotic and anti-oncogenic role of PER1 in the cellular homeostasis [297-300], which might correlate with the altered subcellular distribution of PER1 upon oxidative stress. TNPO1 might mediate stress responses of PER1 and triggers PER1 function either in circadian rhythm formation or possibly beyond.

The cooperative regulation of the circadian clock and redox homeostasis comprises a fine tuned mechanistic network and displays once more the complexity of the intracellular control of normal maintenance of cellular functions and stress responses in challenging conditions, such as oxidative stress. In fact, our understanding of ROS has changed within the last 20 years. We now appreciate the cell signaling function of ROS and differentiate between oxidative conditions crucial for cell homeostasis and oxidative stress-induced ROS leading to cellular damage on lipids, proteins and DNA (see 1.3).

### 4.2.3 Intracellular hydrogen peroxide levels

In contrast to physiological changes of the intracellular redox homeostasis, an exogenously elevated ROS level is drastically changing cellular processes. Sies (2014) summarized studies of the 1970s, in which the authors determined an intracellular hydrogen peroxide level of ~10 nM and its production rate of about 50 nmol per min per gram of tissue [301]. Interestingly, the hydrogen peroxide levels rise

about 100 nM in skeletal muscle fibers if contracted [302]. This indicates a variation of the endogenous cellular hydrogen peroxide levels of at least 10-fold. Schieber and Chandel (2014) review the differences of essential ROS levels for cell signaling and an exogenous increase leading to ROS, focusing on the subcellular compartmentalization of ROS generating enzymes. The authors conclude that the spatial separation of ROS producing pathways is necessary for a normal cellular homeostasis. Under oxidative stress conditions, an overall increased ROS production leads to broad cellular damages from DNA to protein level. Furthermore, they address evidence of an increased ROS level in cancer cells, leading to an activation of growth factor expression and therefore to increased cellular proliferation [303].

As U-2 OS cells are an osteosarcoma cell line, those cells might have an increased intracellular ROS level. With a constitutively high level, the range to investigate endogenous changes of intracellular oxidative conditions is reduced.

Another aspect might be a differential regulation depending on endo- or exogenously induction of ROS generation. Whereas ROS was reported to have essential functions as second messenger in physiological concentrations, they perturb cellular homeostasis under oxidative stress conditions. We found evidence that oxidative stress attenuates PER1 in the cytoplasm in a TNPO1-dependent manner. To do so, we applied a non-physiological concentration of hydrogen peroxide (200 μM) to the cells. The observed effects are most likely due to exogenous ROS levels, but reduced concentrations of hydrogen peroxide will potentially trigger endogenous functions of TNPO1 rather than oxidative stress-induced mechanisms. A possible scenario could be that TNPO1 binds PER1 stronger upon increased ROS levels. Therefore, the nuclear import of PER1 might be increased upon a physiological increase of ROS. If ROS levels get exogenously high, the interaction between TNPO1 and PER1 might still be strengthened, but nuclear entry through the NPC might be inhibited (see above 4.2).

## 4.3 Multiple nucleo-cytoplasmic translocation-associated components are essential for normal circadian dynamics

Until now, no systematic approach was reported to investigate the regulation of circadian dynamics via nucleo-cytoplasmic translocation. Only few components such as the nuclear import carrier KPNB1 and its adaptor protein KPNA have been identified as crucial nuclear import carriers for normal subcellular localization of circadian clock

proteins and for generation of near-24-hour rhythms [172-174]. In this study, we chose RNAi to investigate systematically the essential expression of nucleo-cytoplasmic translocation-associated components for normal circadian rhythm generation.

### 4.3.1 RNAi as the tool of choice for systematical investigation of multiple targets

To further elucidate a potential regulatory role of nucleo-cytoplasmic translocation- associated components on the circadian clock, we chose RNAi as a highly potential tool. As the nuclear pore complex is constituted of more than 30 proteins and nucleo-cytoplasmic translocation-associated proteins are numerous, the approach to test them all was performed by using shRNA constructs of our laboratory resources. Genome-wide screens have identified RNAi as a reliable tool to investigate a high number of genes and still keep experimental procedures (time and expense) reasonable [304- 306]. In addition, RNAi-screens were used to investigate questions on circadian dynamics [159, 307] and are already established in the lab.

Nevertheless, every method has its drawbacks. As for the RNAi-screen, one limiting factor is the control of knockdown efficiency. Within the performed screen, we used the knockdown of *fbxl3* expression, a well-established regulator of the circadian clock [36, 38, 39], to control for general performance of the screen. However, it is not feasible to test all targeted transcripts on their residual mRNA levels in an appropriate timeframe. To this end, we determined only the knockdown efficiencies of the sh*tnpo1* constructs when validating the phenotype (see 3.2.2). Instead, we chose up to three knockdown constructs per gene (if available) to obtain a higher confidence in the collected data (see 3.2.1).

In conclusion, it has to be kept in mind that RNAi-mediated effects in the luminescence-recorded time series could either be due to depletion of the transcript, off-target effects, or direct effects on luciferase activity. Furthermore, no alteration of circadian dynamics can either be due to an inefficient knockdown of the target, substitution, compensation, or indeed no essential participation of the targeted transcript in normal circadian rhythm generation. However, the convenience of the method as well as the experience and availability of resources in the lab convinced us to use RNAi as our method of choice to systematically investigate a potential regulatory function of nucleo-cytoplasmic translocation-associated components on circadian clock dynamics.

### 4.3.2 Nucleo-cytoplasmic translocation components of diverse functions are essential for normal circadian dynamics

We tested 62 genes transcribing components of the nucleo-cytoplasmic translocation machinery by using 167 constructs to evaluate their impact on circadian dynamics in U-2 OS reporter cells. Monitoring the bioluminescence of a *bmal1* promoter-driven *luciferase*, we determined several parameters such as period, phase and amplitude. In this study, we focused on period deviations and identified 14 targets with a significantly altered period (q value < 0.05 post Bonferroni correction) or a low correlation coefficient using at least two different RNAi constructs targeting the same transcript and thereby altering the period in the same direction. We excluded two genes, *kpna5* and *ran*, which showed significant period shortening upon knockdown using one construct and period lengthening upon another (see 3.2). Besides depletion of *tnpo1* expression, knockdown of *elys*, *gle1*, *kpnb1*, *nup85*, *nup98*, *nup153*, *nup160*, *ranbp1*, *ranbp2*, *ranbp10*, *ranbp16*, *sec13* and *xpo1* expression led to period alteration compared to the wild type. The period alterations upon knockdown of *kpnb1* and *xpo1* transcripts are in line with our investigations using pharmacological inhibitors of classical nuclear import and nuclear export (see 3.1) and support the reliability of our screen.

**Knockdown of most essential nucleo-cytoplasmic translocation components leads to long-period phenotypes**

Depletion of *kpnb1* expression prolonged the period by more than four hours using one of three constructs. In addition, transduction of a second RNAi construct, targeting the expression of the classical nuclear import carrier resulted in time series of poor oscillations, which were determined as a low CC when fitted to a sine wave using the ChronoStar 2.0 software (see 2.2.9 and 3.2). A period lengthening upon RNAi-mediated knockdown of *kpnb1* transcription was already reported by Lee *et al.* (2015) [174]. Sakakida and colleagues (2005) showed that nuclear accumulation of CRY (and PER) is mediated by KPNB1 and its adapter protein KPNA [172]. In line with these findings, Umemura et al. (2014) reported KPNA2-dependent subcellular distribution of PER. Interestingly, when overexpressing *kpna2*, PER1 and PER2 are retained in the cytoplasm [173].

Besides the *kpnb1* gene, we identified eight additional transcripts which are essential for a normal near-24-hour rhythm generation and whose resulted in severe period lengthening or poor oscillations. Interestingly, perturbation of six of those nine transcripts also resulted in reduced cell vitality (*kpnb1*, *nup98*, *nup160*, *ranbp2*, *sec13* and

*xpo1*). Only knockdown of *elys*, *nup85*, and *ranbp10* transcription lengthened the period without affecting cell vitality (table 3.2). Note: for two additional targeted transcripts (*nup153* and *ranbp1*), we obtained only low CCs upon application of different RNAi constructs.

Translated proteins of the targeted transcripts with decreased cell vitality are involved in various processes, such as RNA transport, protein translocation or spindle assembly during mitosis.

NUP160 is involved in poly(A)$^+$ RNA nucleo-cytoplasmic shuttling, but also NUP98 and NUP153 are necessary for nuclear export of RNA [308, 309]. Interestingly, NUP153 (as well as KPNA1 and Ran-GTPase) was identified as a crucial cellular component for normal expression of *per* and *tim* in *Drosophila* [310]. In our screen, we did not obtain altered period deviations upon depletion of *kpna1* expression, possibly due to compensation by one of the other six KPNAs (the same holds true for Ran-GTPase).

Besides RNA transport, nucleo-cytoplasmic protein translocation is also affected upon depletion of other RNAi targets leading to period lengthening associated with decreased cell vitality. The E3 sumo-protein ligase RANBP2 sumoylates Ran-GTP [311]. XPO1 is the major nuclear export carrier for cellular proteins, recognizes specific lysine-rich NES (see 1.2.4) and facilitates nuclear export of its cargos in a Ran-GTP-dependent manner. Proteomic studies on XPO1-mediated nuclear export identified more than 5000 proteins to be shuttled from the nucleus into the cytoplasm by this pathway [312].

The nucleo-cytoplasmic translocation protein SEC13 was already identified as an essential component for normal circadian rhythm generation by Zhang et al. (2009) [307]. However, the authors speculated that the prolonged period is rather a network effect than derived from direct interaction between SEC13 and circadian clock proteins. SEC13 plays a role in COPII vesicle coat formation and is a component of the NPC.

Interestingly, the three targeted genes, whose depletion led to period lengthening without reduced cell vitality, translate into proteins with similar functions as they are part of the NPC. NUP85 is part of the NPC sub-complex NUP107-160 and plays a role in nucleo-cytoplasmic translocation-associated to SEC13 [313]. Both proteins, SEC13 and NUP85 are part of this "fence-like coat" of the NPC and determine the faith of the passing proteins. Further, evidence was found that NUP85 is involved in spindle assembly during mitosis [314]. Another member of the mentioned sub-complex NUP107-160 is ELYS, which is one of the initiation proteins upon NPC formation after mitosis [315].

RanBP1 and RanBP10 function in Ran-GTP-mediated association and dissociation of the carrier-cargo complex. RanBP1 promotes RanGAP-induced GTP hydrolysis, thereby facilitating the dissociation of Ran and GTP [316]. RanBP10 is a guanine nucleotide exchange factor. It opposes RanBP1 effects and promotes GDP to GTP exchange on Ran [317].

Functions of the identified components leading to period lengthening upon knockdown of their expression are diverse and we are unable to propose a ranking of which pathway is more important than another. However, we found a correlation between long period phenotypes and reduced cell vitality. This has to be kept in mind for future studies, as reduced cell vitality is always an indication of broad alteration of cellular function and not only of circadian dynamics.

**Knockdown of the three targeted gene expressions leading to short-period phenotypes does not lead to decreased cell vitality**

Out of the 62 targeted genes, we identified only three genes resulting in severe period shortening upon knockdown of their expression. Besides depletion of *tnpo1* transcription, only knockdown of *ranbp16* and *gle1* transcripts led to shortened periods.

All three genes code for nucleo-cytoplasmic translocation carriers, which are involved in either nuclear protein import (TNPO1, cellular function was discussed previously; see. 1.2.4, 4.1 and 4.2), nuclear protein export (RanBP16 also known as XPO7) or nuclear RNA export (GLE1).

RanBP16 mediates nuclear export of p50RhoGAP and 14-3-3$\sigma$. The latter anchors inactivated CDK in the cytoplasm. CDK is reported to phosphorylate CLOCK, which might be an explanation for impairment of circadian dynamics upon depletion of *ranbp16* expression [274, 318, 319] Further, it interacts with the bHLH transcription factor E12 (alternative splicing product of E2A), which in turn targets the CDK inhibitor p21 [320]. Therefore, evidence for an indirect regulatory role of RanBP16 on the clock has therefore already been indicated.

In contrast, GLE1 is essential for nuclear export of poly(A)$^+$ containing RNA, similar to the function of NUP160. Mutation of this gene results in severe diseases, such as lethal congenital contracture syndrome 1 and amyotrophic lateral sclerosis [321, 322]. Although mutations in the *gle1* gene lead to severe disease, we could not validate decreased cell vitality upon depletion of *gle1* transcription. Either the expression levels were not rate limiting or compensatory mechanisms were initialized upon decrease of transcript levels, which might not be the case upon mutation in the *gle1* gene.

**Opposing effects upon decreased expression of two nuclear import carriers**

One of the most interesting findings of the RNAi-mediated depletion of nucleo-cytoplasmic translocation-associated components are the different period deviations upon knockdown of *kpnb1* and *tnpo1* expression. Although both carriers mediate nuclear protein import, which is not true for the nuclear protein export carriers XPO1 or RANBP16. The reduced transcript levels of *xpo1* and *kpnb1* result in period lengthening, whereas knockdown of *tnpo1* and *ranbp16* expression led to period shortening. We can only speculate about potential reasons as not much is known about nucleo-cytoplasmic translocation of circadian clock proteins. One explanation could be that the two different nuclear import carriers promote translocation of different proteins. A second possibility could be that circadian clock proteins with multiple functions need several carriers to translocate them into the nucleus at a specific time of the day, after specific post-translational modifications or even in different complexes.

We identified aTNPO1-dependent nuclear accumulation of PER1. However, upon depletion of *tnpo1*expression, we still detect nuclear PER1, implying another nuclear import pathway of the transcriptional repressor. Several possibilities of different import pathways are conceivable. PER1 alone might be translocated by another mechanism than in complex with CRY or other PER proteins. It is known that CRY promotes nuclear entry of PER, but PER alone is also able to translocate into the nucleus [162, 164].

Additionally, we found evidence that TNPO1-mediated nuclear import is altered under oxidative stress conditions. Different intracellular redox conditions and oxidative stress could also request different nuclear import pathways, which might facilitate different oxidative stress responses of the clock. To test whether oxidative stress is solely influencing TNPO1-mediated nuclear entry of circadian clock proteins, perturbation of the KPNB1-mediated pathway together with hydrogen peroxide treatment would indicate a correlation or exclude it.

**Concluding remarks on the identified essential components of nucleo-cytoplasmic translocation in regard to normal circadian rhythm generation**

Taken all 14 identified genes together which are necessary for near-24-hour rhythm generation, we cannot propose one specific function of the nucleo-cytoplasmic translocation machinery as essential for normal circadian dynamics. It seems that structural NPC proteins play only a minor role for normal circadian dynamics, maybe due to substitution of scaffold proteins in the NPC. We identified several components of nuclear RNA export to be of special interest for normal circadian rhythm generation. This

might be due to a more specific interaction between those proteins with RNA or due to a specific regulatory function of those proteins in RNA processing. Furthermore, knockdown of multiple genes coding for proteins involved in carrier-cargo interaction resulted in altered periods. We cannot distinguish between direct effects of potential carrier-clock protein interaction or indirect control via multiple more proteins.

However, both classical and alternative nuclear import carriers are crucial for normal circadian dynamics. Additionally, GTP exchange factors and inhibitors of the Ran-GTP-GDP exchange factors are necessary for normal rhythm generation. Surprisingly, depletion of *ran* expression itself did not result in a distinct period deviation as we obtained period lengthening upon application of one RNAi construct and period shortening upon treatment with another. This might be due to Ran-independent mechanisms as already reported for KPNB1-mediated nuclear import of cyclin B1–Cdc2 [323]. In addition, investigations with non-hydrolysable nucleotide triphosphates also indicate Ran-independent nucleo-cytoplasmic translocation for specific cargos [324].

This study presents data on 62 nucleo-cytoplasmic translocation-associated transcripts in regard to circadian rhythm generation and might be a starting point for future studies to systematically link regulatory functions of nucleo-cytoplasmic translocation to the circadian clock.

## 4.4 Limitations, achievements and perspectives

### 4.4.1 Limitations

Although frequently used in circadian clock protein investigations, one of the major constraints of this study is the application of ectopically expressed fusion proteins in order to validate subcellular localization or protein-protein interaction. We cannot assume that all results of overexpression studies hold true in endogenous systems. However, ectopically expressed proteins are a convenient and accepted tool to investigate processes which would otherwise remain unexamined mostly due to a lack of detection. One tool which is very promising for the chronobiology community but also for diverse research fields is the CRISPR/Cas9 genome engineering. It introduces specific knockouts or knockins in specific genomic loci and therefore, will help to create endogenously tagged or fused proteins (see 1.4).

Within this study, we established the CRISPR/Cas9 genome engineering technique in the laboratory [255] and generated U-2 OS cells deficient of TNPO1 protein

(see 3.2.3). This genome editing tool is an inexpensive, convenient method to create gene-specific knockouts by simple addition of an endonuclease (Cas9) and a guiding oligonucleotide (guide RNA). The Nature "method of the year 2014", CRISPR/Cas9, is an innovative and fast advancing genome editing tool. The use of bacterial defense response was first mentioned to be suitable for genome engineering in 2012 by Jinek *et al.* [325]. One year later Zhang and colleagues as well as the Church lab were the first to publish the successful use of CRISPR/Cas9 to mutate mammalian cells [250].

Although former genome editing tools as ZFNs and TALENs were successfully used to generate gene-specific knockouts and knockins, the handling and specificity of CRISPR/Cas9 seems to be much easier and highly improved as the specific DNA binding is separately introduced by a simple oligonucleotide [249]. Using the CRISPR/Cas9 method, no fusion of several enzymes or protein domains is necessary. However, the success of gene-specific knockout generation depends on the endonuclease and guide RNA as well as on the selected gene.

If the expression of the targeted gene is crucial for cell survival, one would never obtain a living homozygous knockout cell. Heterozygous gene-depleted cells with only one disrupted allele might survive but might not be sufficient for further investigations. Performing limited dilutions of the *tnpo1* (see 3.2.3) and *fbxl3* [255] gene knockout populations, we obtained several homozygous *fbxl3* knockout cell lines, introducing indels and out-of-frame shifts in multiple single clones. In contrast, by targeting the *tnpo1* gene, we only obtained one identified cell clone, with homogenous out-of-frame shifts on both alleles.

We further observed a reduced proliferation rate of these cells, which is in line with RNAi-mediated depletion of *tnpo1* expression. Another aspect are off-target effects of the CRISPR/Cas9 system, which must be carefully examined to rule out unspecific effects. Although, we did not test off-target effects in the potential *tnpo1* knockout cells, the strongly reduced TNPO1 protein levels are a promising indication that the period-shortening phenotype is due to specific out-of-frame shifts in the *tnpo1* gene.

Interestingly, TNPO1 protein levels of the gRNA1 population were reduced to 17 % compared to wild type cells. Quantification of the residual TNPO1 protein levels in gRNA1 1_1 single cells could not be determined due to the very low TNPO1 signal, which was indistinguishable from background levels (see 3.2.3).

U-2 OS cells are osteosarcoma cells and contain a highly altered genome. Referring to the American Type Culture Collection (ATCC), U-2 OS cells are a hyper-

triploid cell line. However, we sequenced the generated *tnpo1* knockout single clone (gRNA1 1_1) and identified only two different indels indicating only two alleles coding for *tnpo1*. One of the twelve sequencing results was wild type, which could either be a contamination or an indication of a third wild type allele. A careful verification will clarify successful genome editing in these cells.

Another drawback is the solely *in vitro* approach of validation of TNPO1-PER1 interaction. Within these studies, we considered the use of mouse models to translate the *in vitro* data into an *in vivo* model, but multiple constraints prevented us to do so. Neither *tnpo1* knockout mice nor mice with specific mutations in the cargo binding sites of TNPO1 are available. This might be due to an essential TNPO1 presence during embryogenesis. In line with a perturbed embryogenesis of *tnop1*-deficient mice is the observation of decreased proliferation in cells with depleted *tnpo1* expression. In addition, we experienced difficulties in the cultivation of CRISPR/Cas9-engineered putative *tnpo1* knockout cells. It seemed that upon limited dilution a reduced number of *tnpo1* targeted cells survived in single cell conditions compared to diluted wild type U-2 OS cells.

As the generation of knockout mice is expensive and time-consuming, we decided not to take the risk of possible failure due to disabled embryogenesis. Instead, we tried using murine cells of mice expressing a PER2-luciferase fusion protein. Unfortunately, we were unable to detect murine TNPO1 using two different antibodies. In contrast to human TNPO1, which is specifically detected by the Abcam antibody ab10303, we were unable to detect murine TNPO1 using ab10303 or ab67352, which were marketed to specifically detect murine TNPO1.

When summarizing the major limitations of this work, we need to address the detection of TNPO1-PER interaction: Although we were able to consequently show a TNPO1-PER1 interaction using luciferase activity as readout, we could not detect this interaction by performing western blot analyses after CoIP assays. Even upon treatment with hydrogen peroxide, we were unable to detect an interaction performing western blot assays, which might be due to a reducing lysis buffer.

Optimizing the protocol for CoIP assay, we switched the lysis buffer to a non-reducing buffer also used by Putker *et al.*, 2013 [154]. In addition, we used luciferase as a readout, which is more sensitive than immunoblotting. For future analysis, the non-reducing buffer will be used together with an optimized CoIP protocol to support the obtained data. To increase the binding strength of TNPO1 and its cargos, application

of different GDP and GTP concentrations might cause stronger binding between PER1 and the non-classical nuclear import carrier.

Furthermore, investigations in different reducing and oxidizing conditions will help to complete the obtained data on oxidative stress, TNPO1 and PER1. Additionally, blocking of the agarose beads or fixation of the protein-protein interaction prior to CoIP performance might enable the detection of a potential interaction using luciferase-free readouts, thereby supporting the data of this study (e.g. using formaldehyde).

One last aspect has to be mentioned: To link the short-period phenotype of depleted *tnpo1* expression to TNPO1-dependent nuclear import of PER1, we performed double knockdown of *tnpo1* and *per1* expression (see 3.8 and 4.1.3). Due to the period lengthening upon depletion of *per1* transcription, it is difficult to interpret the potential rescue in cells targeted with RNAi against *tnpo1* and *per1* transcripts, when compared to single perturbation of *tnpo1* expression. Future approaches will lead to the generation of *per1* knockout cells (using CRISPR/Cas9), which will enable us to investigate our hypothesis with knockdown of *tnpo1* expression only.

### 4.4.2 Achievements and perspectives - TNPO1 is an essential part of the substantial nucleo-cytoplasmic translocation machinery of molecular clock components

The aim of this study was to investigate systematically the role of nucleo-cytoplasmic translocation-involved proteins on circadian rhythm generation. Therefore, we knocked down the expression of 62 targets using RNAi, thereby identifying 14 transcripts which are crucial for normal circadian dynamics. Although it was reported that classical nuclear import is necessary for normal subcellular distribution of circadian clock proteins, this study is the first to outline the complexity of the regulatory role of nucleo-cytoplasmic translocation components on the circadian clock. We identified several RNA and protein carriers as well as associated proteins which comprise diverse functions and indicate the comprehensive regulatory function of nucleo-cytoplasmic translocation.

One of the identified genes is *tnpo1*, a non-classical nuclear import carrier. Although it is widely agreed that circadian clock proteins are translocated into the nucleus via the classical nuclear import carriers, KPNB1 and KPNA [172-174], we could show that at least for PER1 another carrier, TNPO1, is essential for normal nuclear localization. Furthermore, we determined nuclear import rates of PER1 and PER2 in wild type and

*tnpo1* transcript-depleted cells. Our findings on PER2 nuclear import rates showed a 25 % recovery of initial fluorescence intensity after 16 ± 3 minutes (see 3.6.2). This data correlates with previous studies in which we determined a recovery rate of 50 % of initial fluorescence intensity after about 30 minutes [165]. In addition, we could show that the kinetics of PER2 did not significantly change upon depletion of *tnpo1* expression (21 ± 5 minutes), whereas the PER1 nuclear import rate decreased. The mean recovery rate of 25 % of nuclear PER1-Venus fluorescence intensity was 13 ± 2 minutes and upon knockdown of *tnpo1* expression, the nuclear import rate decelerated to 24 ± 5 minutes to recover 25 % of the initial fluorescence intensity.

The nuclear import rates of PER1 and PER2 are similar in ns control cells. However, our data indicates different nuclear import mechanisms for the two transcriptional repressors.

Our data emphasize the complexity of nuclear import of circadian clock proteins as we could show that the non-classical import carrier TNPO1 interacts with circadian clock proteins, in particular PER1. The focus on classical nuclear import of the last years has to be re-fined and other components of the nucleo-cytoplasmic translocation machinery have to be included in the broad understanding of nucleo-cytoplasmic regulation of circadian rhythm generation.

Furthermore we found evidence of a TNPO1-mediated regulation of the circadian clock under oxidative stress conditions.

Future studies must carefully validate the collected data and improve our understanding of the regulatory function of nucleo-cytoplasmic translocation on the circadian clock. We are able to use this study to investigate further components of nuclear import and export in regard to their function on circadian clock dynamics.

The CRISPR/Cas9 tool might facilitate investigations of the subcellular localization in an endogenous context, which will not only validate the obtained data of overexpressed Venus-fusion proteins but will also replace ectopic expression of them.

Finally, the context of nuclear import as oxidative stress regulator of the circadian clock needs further investigations as several regulatory pathways (e.g. peroxiredoxins and sirtuins) were identified in the last years and the complexity of the mutual control becomes more and more evident.

# Bibliography

[1] Johnson, C. H. (2004). Circadian rhythms: as time glows by in bacteria. Nature 430(6995), 23-24.

[2] Cha, J., Zhou, M., and Liu, Y. (2015). Mechanism of the Neurospora circadian clock, a FREQUENCY-centric view. Biochemistry 54, 150-156.

[3] Gardner, M.J., Hubbard, K.E., Hotta, C.T., Dodd, A.N., and Webb, A.A. (2006). How plants tell the time. Biochem J 397, 15-24.

[4] Menegazzi, P., Yoshii, T., and Helfrich-Forster, C. (2012). Laboratory versus nature: the two sides of the Drosophila circadian clock. J Biol Rhythms 27, 433-442.

[5] Buhr, E.D., and Takahashi, J.S. (2013). Molecular components of the Mammalian circadian clock. Handb Exp Pharmacol, 3-27.

[6] Mohawk, J.A., Green, C.B., and Takahashi, J.S. (2012). Central and peripheral circadian clocks in mammals. Annu Rev Neurosci 35, 445-462.

[7] Gaspar, L., and Brown, S.A. (2015). Measuring circadian clock function in human cells. Methods Enzymol 552, 231-256.

[8] Peirson, S.N., Halford, S., and Foster, R.G. (2009). The evolution of irradiance detection: melanopsin and the non-visual opsins. Philos Trans R Soc Lond B Biol Sci 364, 2849-2865.

[9] Nakajima, M., Imai, K., Ito, H., Nishiwaki, T., Murayama, Y., Iwasaki, H., Oyama, T., and Kondo, T. (2005). Reconstitution of circadian oscillation of cyanobacterial KaiC phosphorylation in vitro. Science 308, 414-415.

[10] Elowitz, M.B., and Leibler, S. (2000). A synthetic oscillatory network of transcriptional regulators. Nature 403, 335-338.

[11] Wolverton, M. (2013). Living by the clock: The science of chronobiology. Penn Medicine Magazine, 17-23.

[12] Hugh, R. and von Linné, C. (1775). Elements of botany.

[13] Daan, S. (2010). The circadian clock: protein reviews 12. Springer science, 1-34

[14] Daan, S. (2000). The Colin S. Pittendrigh Lecture. Colin Pittendrigh, Jurgen Aschoff, and the natural entrainment of circadian systems. J Biol Rhythms 15, 195-207.

[15] Sollberger, A. (1962). General properties of biological rhythms. Ann N Y Acad Sci 98, 757-774.

[16] Oxford dictionary (http://www.oxforddictionaries.com/de/definition/englisch_usa/rhythm)

[17] Vitaterna, M.H., Takahashi, J.S., and Turek, F.W. (2001). Overview of circadian rhythms. Alcohol Res Health 25, 85-93.

[18] Morse, D., Cermakian, N., Brancorsini, S., Parvinen, M., and Sassone-Corsi, P. (2003). No circadian rhythms in testis: Period1 expression is clock independent and developmentally regulated in the mouse. Mol Endocrinol 17, 141-151.

[19] Stephan, F.K., and Zucker, I. (1972). Circadian rhythms in drinking behavior and locomotor activity of rats are eliminated by hypothalamic lesions. Proc Natl Acad Sci U S A 69, 1583-1586.

[20] Lucas, R.J., Douglas, R.H., and Foster, R.G. (2001). Characterization of an ocular photopigment capable of driving pupillary constriction in mice. Nat Neurosci 4, 621-626.

[21] Morin, L.P., and Cummings, L.A. (1981). Effect of surgical or photoperiodic castration, testosterone replacement or pinealectomy on male hamster running rhythmicity. Physiol Behav 26, 825-838.

[22] Moore, R.Y. (1995). Organization of the mammalian circadian system. Ciba Found Symp 183, 88-99; discussion 100-106.

[23] Ramkisoensing, A., and Meijer, J.H. (2015). Synchronization of Biological Clock Neurons by Light and Peripheral Feedback Systems Promotes Circadian Rhythms and Health. Front Neurol 6, 128.

[24] Tahara, Y., Kuroda, H., Saito, K., Nakajima, Y., Kubo, Y., Ohnishi, N., Seo, Y., Otsuka, M., Fuse, Y., Ohura, Y., *et al.* (2012). In vivo monitoring of peripheral circadian clocks in the mouse. Curr Biol 22, 1029-1034.

[25] Schibler, U., Ripperger, J., and Brown, S.A. (2003). Peripheral circadian oscillators in mammals: time and food. J Biol Rhythms 18, 250-260.

[26] Gerber, A., Saini, C., Curie, T., Emmenegger, Y., Rando, G., Gosselin, P., Gotic, I., Gos, P., Franken, P., and Schibler, U. (2015). The systemic control of circadian gene expression. Diabetes Obes Metab 17 Suppl 1, 23-32.

[27] Gekakis, N., Staknis, D., Nguyen, H.B., Davis, F.C., Wilsbacher, L.D., King, D.P., Takahashi, J.S., and Weitz, C.J. (1998). Role of the CLOCK protein in the mammalian circadian mechanism. Science 280, 1564-1569.

[28] Stratmann, M., Suter, D.M., Molina, N., Naef, F., and Schibler, U. (2012). Circadian Dbp transcription relies on highly dynamic BMAL1-CLOCK interaction with E boxes and requires the proteasome. Mol Cell 48, 277-287.

[29] Darlington, T.K., Wager-Smith, K., Ceriani, M.F., Staknis, D., Gekakis, N., Steeves, T.D., Weitz, C.J., Takahashi, J.S., and Kay, S.A. (1998). Closing the circadian loop: CLOCK-induced transcription of its own inhibitors per and tim. Science 280, 1599-1603.

[30] Kume, K., Zylka, M.J., Sriram, S., Shearman, L.P., Weaver, D.R., Jin, X., Maywood, E.S., Hastings, M.H., and Reppert, S.M. (1999). mCRY1 and mCRY2 are essential components of the negative limb of the circadian clock feedback loop. Cell 98, 193-205.

[31] Zheng, B., Larkin, D.W., Albrecht, U., Sun, Z.S., Sage, M., Eichele, G., Lee, C.C., and Bradley, A. (1999). The mPer2 gene encodes a functional component of the mammalian circadian clock. Nature 400, 169-173.

[32] Brown, S.A., Ripperger, J., Kadener, S., Fleury-Olela, F., Vilbois, F., Rosbash, M., and Schibler, U. (2005). PERIOD1-associated proteins modulate the negative limb of the mammalian circadian oscillator. Science 308, 693-696.

[33] Xing, W., Busino, L., Hinds, T.R., Marionni, S.T., Saifee, N.H., Bush, M.F., Pagano, M., and Zheng, N. (2013). SCF(FBXL3) ubiquitin ligase targets cryptochromes at their cofactor pocket. Nature 496, 64-68.

[34] Chiu, J.C., Vanselow, J.T., Kramer, A., and Edery, I. (2008). The phospho-occupancy of an atypical SLIMB-binding site on PERIOD that is phosphorylated by DOUBLETIME controls the pace of the clock. Genes Dev 22, 1758-1772.

[35] Akashi, M., Tsuchiya, Y., Yoshino, T., and Nishida, E. (2002). Control of intracellular dynamics of mammalian period proteins by casein kinase I epsilon (CKIepsilon) and CKIdelta in cultured cells. Mol Cell Biol 22, 1693-1703.

[36] Hirano, A., Yumimoto, K., Tsunematsu, R., Matsumoto, M., Oyama, M., Kozuka-Hata, H., Nakagawa, T., Lanjakornsiripan, D., Nakayama, K.I., and Fukada, Y. (2013). FBXL21 regulates oscillation of the circadian clock through ubiquitination and stabilization of cryptochromes. Cell 152, 1106-1118.

[37] Yoo, S.H., Mohawk, J.A., Siepka, S.M., Shan, Y., Huh, S.K., Hong, H.K., Kornblum, I., Kumar, V., Koike, N., Xu, M., *et al.* Ibid.Competing E3 ubiquitin ligases govern circadian periodicity by degradation of CRY in nucleus and cytoplasm. 1091-1105.

[38] Siepka, S.M., Yoo, S.H., Park, J., Song, W., Kumar, V., Hu, Y., Lee, C., and Takahashi, J.S. (2007). Circadian mutant Overtime reveals F-box protein FBXL3 regulation of cryptochrome and period gene expression. Ibid. 129, 1011-1023.

[39] Godinho, S.I., Maywood, E.S., Shaw, L., Tucci, V., Barnard, A.R., Busino, L., Pagano, M., Kendall, R., Quwailid, M.M., Romero, M.R., *et al.* (2007). The after-hours mutant reveals a role for Fbxl3 in determining mammalian circadian period. Science 316, 897-900.

[40] Yagita, K., Tamanini, F., Yasuda, M., Hoeijmakers, J.H., van der Horst, G.T., and Okamura, H. (2002). Nucleocytoplasmic shuttling and mCRY-dependent inhibition of ubiquitylation of the mPER2 clock protein. EMBO J 21, 1301-1314.

[41] Guillaumond, F., Dardente, H., Giguere, V., and Cermakian, N. (2005). Differential control of Bmal1 circadian transcription by REV-ERB and ROR nuclear receptors. J Biol Rhythms 20, 391-403.

[42] Ko, C.H., and Takahashi, J.S. (2006). Molecular components of the mammalian circadian clock. Hum Mol Genet 15 Spec No 2, R271-277.

[43] Zheng, B., Albrecht, U., Kaasik, K., Sage, M., Lu, W., Vaishnav, S., Li, Q., Sun, Z.S., Eichele, G., Bradley, A., et al. (2001). Nonredundant roles of the mPer1 and mPer2 genes in the mammalian circadian clock. Cell 105, 683-694.

[44] van der Horst, G.T., Muijtjens, M., Kobayashi, K., Takano, R., Kanno, S., Takao, M., de Wit, J., Verkerk, A., Eker, A.P., van Leenen, D., *et al.* (1999). Mammalian Cry1 and Cry2 are essential for maintenance of circadian rhythms. Nature 398, 627-630.

[45] Akashi, M., Okamoto, A., Tsuchiya, Y., Todo, T., Nishida, E., and Node, K. (2014). A positive role for PERIOD in mammalian circadian gene expression. Cell Rep 7, 1056-1064.

[46] Koike, N., Yoo, S.H., Huang, H.C., Kumar, V., Lee, C., Kim, T.K., and Takahashi, J.S. (2012). Transcriptional architecture and chromatin landscape of the core circadian clock in mammals. Science 338, 349-354.

[47] Ripperger, J.A. (2007). The rhythms of life. Genome Biol 8, 313.

[48] Allada, R., White, N.E., So, W.V., Hall, J.C., and Rosbash, M. (1998). A mutant Drosophila homolog of mammalian Clock disrupts circadian rhythms and transcription of period and timeless. Cell 93, 791-804.

[49] Price, J.L., Blau, J., Carl Rothenfluh, A., Abodeely, M., Kloss, B., and Young, M.W. Ibid.double-time is a novel Drosophila clock gene that regulates PERIOD protein accumulation. 94, 83-95.

[50] Lin, J.M., Kilman, V.L., Keegan, K., Paddock, B., Emery-Le, M., Rosbash, M., and Allada, R. (2002). A role for casein kinase 2alpha in the Drosophila circadian clock. Nature 420, 816-820.

[51] Martinek, S., Inonog, S., Manoukian, A.S., and Young, M.W. (2001). A role for the segment polarity gene shaggy/GSK-3 in the Drosophila circadian clock. Cell 105, 769-779.

[52] Fang, Y., Sathyanarayanan, S., and Sehgal, A. (2007). Post-translational regulation of the Drosophila circadian clock requires protein phosphatase 1 (PP1). Genes Dev 21, 1506-1518.

[53] Sathyanarayanan, S., Zheng, X., Xiao, R., and Sehgal, A. (2004). Posttranslational regulation of Drosophila PERIOD protein by protein phosphatase 2A. Cell 116, 603-615.

[54] Ko, H.W., Kim, E.Y., Chiu, J., Vanselow, J.T., Kramer, A., and Edery, I. (2010). A hierarchical phosphorylation cascade that regulates the timing of PERIOD nuclear entry reveals novel roles for proline-directed kinases and GSK-3beta/SGG in circadian clocks. J Neurosci 30, 12664-12675.

[55] Tyson, J.J., Hong, C.I., Thron, C.D., and Novak, B. (1999). A simple model of circadian rhythms based on dimerization and proteolysis of PER and TIM. Biophys J 77, 2411-2417.

[56] Darlington, T.K., Wager-Smith, K., Ceriani, M.F., Staknis, D., Gekakis, N., Steeves, T.D., Weitz, C.J., Takahashi, J.S., and Kay, S.A. (1998). Closing the circadian loop: CLOCK-induced transcription of its own inhibitors per and tim. Science 280, 1599-1603.

[57] Crosthwaite, S.K., Dunlap, J.C., and Loros, J.J. (1997). Neurospora wc-1 and wc-2: transcription, photoresponses, and the origins of circadian rhythmicity. Ibid. 276, 763-769.

[58] Shi, M., Collett, M., Loros, J.J., and Dunlap, J.C. (2010). FRQ-interacting RNA helicase mediates negative and positive feedback in the Neurospora circadian clock. Genetics 184, 351-361.

[59] Huang, G., Chen, S., Li, S., Cha, J., Long, C., Li, L., He, Q., and Liu, Y. (2007). Protein kinase A and casein kinases mediate sequential phosphorylation events in the circadian negative feedback loop. Genes Dev 21, 3283-3295.

[60] Yang, Y., Cheng, P., He, Q., Wang, L., and Liu, Y. (2003). Phosphorylation of FREQUENCY protein by casein kinase II is necessary for the function of the Neurospora circadian clock. Mol Cell Biol 23, 6221-6228.

[61] Denault, D.L., Loros, J.J., and Dunlap, J.C. (2001). WC-2 mediates WC-1-FRQ interaction within the PAS protein-linked circadian feedback loop of Neurospora. EMBO J 20, 109-117.

[62] He, Q., Cha, J., He, Q., Lee, H.C., Yang, Y., and Liu, Y. (2006). CKI and CKII mediate the FREQUENCY-dependent phosphorylation of the WHITE COLLAR complex to close the Neurospora circadian negative feedback loop. Genes Dev 20, 2552-2565.

[63] Merrow, M., Brunner, M., and Roenneberg, T. (1999). Assignment of circadian function for the Neurospora clock gene frequency. Nature 399, 584-586.

[64] Ishiura, M., Kutsuna, S., Aoki, S., Iwasaki, H., Andersson, C.R., Tanabe, A., Golden, S.S., Johnson, C.H., and Kondo, T. (1998). Expression of a gene cluster kaiABC as a circadian feedback process in cyanobacteria. Science 281, 1519-1523.

[65] Nishiwaki, T., Iwasaki, H., Ishiura, M., and Kondo, T. (2000). Nucleotide binding and autophosphorylation of the clock protein KaiC as a circadian timing process of cyanobacteria. Proc Natl Acad Sci U S A 97, 495-499.

[66] Iwasaki, H., Nishiwaki, T., Kitayama, Y., Nakajima, M., and Kondo, T. (2002). KaiA-stimulated KaiC phosphorylation in circadian timing loops in cyanobacteria. Ibid. 99, 15788-15793.

[67] Xu, Y., Mori, T., and Johnson, C.H. (2003). Cyanobacterial circadian clockwork: roles of KaiA, KaiB and the kaiBC promoter in regulating KaiC. EMBO J 22, 2117-2126.

[68] Kitayama, Y., Iwasaki, H., Nishiwaki, T., and Kondo, T. Ibid.KaiB functions as an attenuator of KaiC phosphorylation in the cyanobacterial circadian clock system. 2127-2134.

[69] Geiger, S.S., Fagundes, C.T., and Siegel, R.M. (2015). Chrono-immunology: progress and challenges in understanding links between the circadian and immune systems. Immunology 146, 349-358.

[70] Feillet, C., van der Horst, G.T., Levi, F., Rand, D.A., and Delaunay, F. (2015). Coupling between the Circadian Clock and Cell Cycle Oscillators: Implication for Healthy Cells and Malignant Growth. Front Neurol 6, 96.

[71] Toh, K.L., Jones, C.R., He, Y., Eide, E.J., Hinz, W.A., Virshup, D.M., Ptacek, L.J., and Fu, Y.H. (2001). An hPer2 phosphorylation site mutation in familial advanced sleep phase syndrome. Science 291, 1040-1043.

[72] Xu, Y., Padiath, Q.S., Shapiro, R.E., Jones, C.R., Wu, S.C., Saigoh, N., Saigoh, K., Ptacek, L.J., and Fu, Y.H. (2005). Functional consequences of a CKIdelta mutation causing familial advanced sleep phase syndrome. Nature 434, 640-644.

[73] Videnovic, A., Lazar, A.S., Barker, R.A., and Overeem, S. (2014). 'The clocks that time us'--circadian rhythms in neurodegenerative disorders. Nat Rev Neurol 10, 683-693.

[74] Ferrell, J.M., and Chiang, J.Y. (2015). Circadian rhythms in liver metabolism and disease. Acta Pharm Sin B 5, 113-122.

[75] Archer, S.N., Laing, E.E., Moller-Levet, C.S., van der Veen, D.R., Bucca, G., Lazar, A.S., Santhi, N., Slak, A., Kabiljo, R., von Schantz, M., *et al.* (2014). Mistimed sleep disrupts circadian regulation of the human transcriptome. Proc Natl Acad Sci U S A 111, E682-691.

[76] Truong, T., Liquet, B., Menegaux, F., Plancoulaine, S., Laurent-Puig, P., Mulot, C., Cordina-Duverger, E., Sanchez, M., Arveux, P., Kerbrat, P., *et al.* (2014). Breast cancer risk, nightwork, and circadian clock gene polymorphisms. Endocr Relat Cancer 21, 629-638.

[77] Blask, D.E., Brainard, G.C., Dauchy, R.T., Hanifin, J.P., Davidson, L.K., Krause, J.A., Sauer, L.A., Rivera-Bermudez, M.A., Dubocovich, M.L., Jasser, S.A., *et al.* (2005). Melatonin-depleted blood from premenopausal women exposed to light at night stimulates growth of human breast cancer xenografts in nude rats. Cancer Res 65, 11174-11184.

[78] Sureda, A., Hebling, U., Pons, A., and Mueller, S. (2005). Extracellular H2O2 and not superoxide determines the compartment-specific activation of transferrin receptor by iron regulatory protein 1. Free Radic Res 39, 817-824.

[79] Laviv, T., Vertkin, I., Berdichevsky, Y., Fogel, H., Riven, I., Bettler, B., Slesinger, P.A., and Slutsky, I. (2011). Compartmentalization of the GABAB receptor signaling complex is required for presynaptic inhibition at hippocampal synapses. J Neurosci 31, 12523-12532.

[80] Alberts, B., Johnson, A., Lewis, J., Raff, M., Roberts, K. and Walte, P. (2002). Molecular Biology of the Cell. 4th edition.

[81] Hertwig,R. (1876).Beitrage zu einer einheitlichen Auffassung der verschiedenen Kernformen. Morph. Jahrb. 2, 63-82.

[82] Aebi, U., Cohn, J., Buhle, L., and Gerace, L. (1986). The nuclear lamina is a meshwork of intermediate-type filaments. Nature 323, 560-564.

[83] Schirmer, E.C., Florens, L., Guan, T., Yates, J.R., 3rd, and Gerace, L. (2003). Nuclear membrane proteins with potential disease links found by subtractive proteomics. Science 301, 1380-1382.

[84] Callan, H.G., and Tomlin, S.G. (1950). Experimental studies on amphibian oocyte nuclei. I. Investigation of the structure of the nuclear membrane by means of the electron microscope. Proc R Soc Lond B Biol Sci 137, 367-378.

[85] Watson, M.L. (1959). Further observations on the nuclear envelope of the animal cell. J Biophys Biochem Cytol 6, 147-156.

[86] Wang, Y.N., Lee, H.H., Lee, H.J., Du, Y., Yamaguchi, H., and Hung, M.C. (2012). Membrane-bound trafficking regulates nuclear transport of integral epidermal growth factor receptor (EGFR) and ErbB-2. J Biol Chem 287, 16869-16879.

[87] Granzow, H., Klupp, B.G., Fuchs, W., Veits, J., Osterrieder, N., and Mettenleiter, T.C. (2001). Egress of alphaherpesviruses: comparative ultrastructural study. J Virol 75, 3675-3684.

[88] Speese, S.D., Ashley, J., Jokhi, V., Nunnari, J., Barria, R., Li, Y., Ataman, B., Koon, A., Chang, Y.T., Li, Q., *et al.* (2012). Nuclear envelope budding enables large ribonucleoprotein particle export during synaptic Wnt signaling. Cell 149, 832-846.

[89] Rose, A., and Schlieker, C. (2012). Alternative nuclear transport for cellular protein quality control. Trends Cell Biol 22, 509-514.

[90] DeGrasse, J.A., DuBois, K.N., Devos, D., Siegel, T.N., Sali, A., Field, M.C., Rout, M.P., and Chait, B.T. (2009). Evidence for a shared nuclear pore complex architecture that is conserved from the last common eukaryotic ancestor. Mol Cell Proteomics 8, 2119-2130.

[91] Reichelt, R., Holzenburg, A., Buhle, E.L., Jr., Jarnik, M., Engel, A., and Aebi, U. (1990). Correlation between structure and mass distribution of the nuclear pore complex and of distinct pore complex components. J Cell Biol 110, 883-894.

[92] Rout, M.P., and Blobel, G. (1993). Isolation of the yeast nuclear pore complex. Ibid. 123, 771-783.

[93] Cordes, V.C., Reidenbach, S., and Franke, W.W. (1995). High content of a nuclear pore complex protein in cytoplasmic annulate lamellae of Xenopus oocytes. Eur J Cell Biol 68, 240-255.

[94] Rout, M.P., Aitchison, J.D., Suprapto, A., Hjertaas, K., Zhao, Y., and Chait, B.T. (2000). The yeast nuclear pore complex: composition, architecture, and transport mechanism. J Cell Biol 148, 635-651.

[95] Cronshaw, J.M., Krutchinsky, A.N., Zhang, W., Chait, B.T., and Matunis, M.J. (2002). Proteomic analysis of the mammalian nuclear pore complex. Ibid. 158, 915-927.

[96] Jarnik, M., and Aebi, U. (1991). Toward a more complete 3-D structure of the nuclear pore complex. J Struct Biol 107, 291-308.

[97] Strambio-De-Castillia, C., Niepel, M., and Rout, M.P. (2010). The nuclear pore complex: bridging nuclear transport and gene regulation. Nat Rev Mol Cell Biol 11, 490-501.

[98] Hoelz, A., Debler, E.W., and Blobel, G. (2011). The structure of the nuclear pore complex. Annu Rev Biochem 80, 613-643.

[99] Gall, J.G. (1967). Octagonal nuclear pores. Ibid. 32, 391-399.Korge

[100] Grossman, E., Medalia, O., and Zwerger, M. (2012). Functional architecture of the nuclear pore complex. Annu Rev Biophys 41, 557-584.

[101] Bayliss, R., Littlewood, T., and Stewart, M. (2000). Structural basis for the interaction between FxFG nucleoporin repeats and importin-beta in nuclear trafficking. Cell 102, 99-108.

[102] Radu, A., Blobel, G., and Moore, M.S. (1995). Identification of a protein complex that is required for nuclear protein import and mediates docking of import substrate to distinct nucleoporins. Proc Natl Acad Sci U S A 92, 1769-1773.

[103] Hsia, K.C., Stavropoulos, P., Blobel, G., and Hoelz, A. (2007). Architecture of a coat for the nuclear pore membrane. Cell 131, 1313-1326.

[104] Hinshaw, J.E., Carragher, B.O., and Milligan, R.A. (1992). Architecture and design of the nuclear pore complex. Ibid. 69, 1133-1141.

[105] Naim, B., Brumfeld, V., Kapon, R., Kiss, V., Nevo, R., and Reich, Z. (2007). Passive and facilitated transport in nuclear pore complexes is largely uncoupled. J Biol Chem 282, 3881-3888.

[106] Paine, P.L., Moore, L.C., and Horowitz, S.B. (1975). Nuclear envelope permeability. Nature 254, 109-114.

[107] Dingwall, C., Sharnick, S.V., and Laskey, R.A. (1982). A polypeptide domain that specifies migration of nucleoplasmin into the nucleus. Cell 30, 449-458.

[108] Xu, J., Li, Y., Yang, X., Chen, Y., and Chen, M. (2013). Nuclear translocation of small G protein RhoA via active transportation in gastric cancer cells. Oncol Rep 30, 1878-1882.

[109] Ribbeck, K., and Gorlich, D. (2001). Kinetic analysis of translocation through nuclear pore complexes. EMBO J 20, 1320-1330.

[110] Dange, T., Grunwald, D., Grunwald, A., Peters, R., and Kubitscheck, U. (2008). Autonomy and robustness of translocation through the nuclear pore complex: a single-molecule study. J Cell Biol 183, 77-86.

[111] Kubitscheck, U., Grunwald, D., Hoekstra, A., Rohleder, D., Kues, T., Siebrasse, J.P., and Peters, R. (2005). Nuclear transport of single molecules: dwell times at the nuclear pore complex. Ibid. 168, 233-243.

[112] Grunwald, D., and Singer, R.H. (2010). In vivo imaging of labelled endogenous beta-actin mRNA during nucleo-cytoplasmic transport. Nature 467, 604-607.

[113] Lui, K., and Huang, Y. (2009). RanGTPase: A Key Regulator of Nucleocytoplasmic Trafficking. Mol Cell Pharmacol 1, 148-156.

[114] Powers, M.A., Forbes, D.J., Dahlberg, J.E., and Lund, E. (1997). The vertebrate GLFG nucleoporin, Nup98, is an essential component of multiple RNA export pathways. J Cell Biol 136, 241-250.

[115] Frey, S., and Gorlich, D. (2007). A saturated FG-repeat hydrogel can reproduce the permeability properties of nuclear pore complexes. Ibid. 130, 512-523.

[116] Rout, M.P., Aitchison, J.D., Magnasco, M.O., and Chait, B.T. (2003). Virtual gating and nuclear transport: the hole picture. Trends Cell Biol 13, 622-628.

[117] Yamada, J., Phillips, J.L., Patel, S., Goldfien, G., Calestagne-Morelli, A., Huang, H., Reza, R., Acheson, J., Krishnan, V.V., Newsam, S., *et al.* (2010). A bimodal distribution of two distinct categories of intrinsically disordered structures with separate functions in FG nucleoporins. Mol Cell Proteomics 9, 2205-2224.

[118] Melchior, F., Paschal, B., Evans, J., and Gerace, L. (1993). Inhibition of nuclear protein import by nonhydrolyzable analogues of GTP and identification of the small GTPase Ran/TC4 as an essential transport factor. J Cell Biol 123, 1649-1659.

[119] Pemberton, L.F., and Paschal, B.M. (2005). Mechanisms of receptor-mediated nuclear import and nuclear export. Traffic 6, 187-198.

[120] Richards, S.A., Lounsbury, K.M., and Macara, I.G. (1995). The C terminus of the nuclear RAN/TC4 GTPase stabilizes the GDP-bound state and mediates interactions with RCC1, RAN-GAP, and HTF9A/RANBP1. J Biol Chem 270, 14405-14411.

[121] Renault, L., Kuhlmann, J., Henkel, A., and Wittinghofer, A. (2001). Structural basis for guanine nucleotide exchange on Ran by the regulator of chromosome condensation (RCC1). Cell 105, 245-255.

[122] Mason, D.A., Stage, D.E., and Goldfarb, D.S. (2009). Evolution of the metazoan-specific importin alpha gene family. J Mol Evol 68, 351-365.

[123] Gorlich, D., Prehn, S., Laskey, R.A., and Hartmann, E. (1994). Isolation of a protein that is essential for the first step of nuclear protein import. Cell 79, 767-778.

[124] Gorlich, D., Henklein, P., Laskey, R.A., and Hartmann, E. (1996). A 41 amino acid motif in importin-alpha confers binding to importin-beta and hence transit into the nucleus. EMBO J 15, 1810-1817.

[125] Mingot, J.M., Kostka, S., Kraft, R., Hartmann, E., and Gorlich, D. (2001). Importin 13: a novel mediator of nuclear import and export. Ibid. 20, 3685-3694.

[126] Yoshida, K., and Blobel, G. (2001). The karyopherin Kap142p/Msn5p mediates nuclear import and nuclear export of different cargo proteins. J Cell Biol 152, 729-740.

[127] O'Reilly, A.J., Dacks, J.B., and Field, M.C. (2011). Evolution of the karyopherin-beta family of nucleocytoplasmic transport factors; ancient origins and continued specialization. PLoS One 6, e19308.

[128] Mosammaparast, N., and Pemberton, L.F. (2004). Karyopherins: from nuclear-transport mediators to nuclear-function regulators. Trends Cell Biol 14, 547-556.

[129] Quan, Y., Ji, Z.L., Wang, X., Tartakoff, A.M., and Tao, T. (2008). Evolutionary and transcriptional analysis of karyopherin beta superfamily proteins. Mol Cell Proteomics 7, 1254-1269.

[130] Andrade, M.A., and Bork, P. (1995). HEAT repeats in the Huntington's disease protein. Nat Genet 11, 115-116.

[131] Malik, H.S., Eickbush, T.H., and Goldfarb, D.S. (1997). Evolutionary specialization of the nuclear targeting apparatus. Proc Natl Acad Sci U S A 94, 13738-13742.

[132] Chook, Y.M., and Süel, K.E. (2011). Nuclear import by karyopherin-betas: recognition and inhibition. Biochim Biophys Acta 1813, 1593-1606.

[133] Forbes, D.J., Travesa, A., Nord, M.S., and Bernis, C. (2015). Reprint of "Nuclear transport factors: global regulation of mitosis". Curr Opin Cell Biol 34, 122-134.

[134] Adam, E.J., and Adam, S.A. (1994). Identification of cytosolic factors required for nuclear location sequence-mediated binding to the nuclear envelope. J Cell Biol 125, 547-555.

[135] Kalderon, D., Roberts, B.L., Richardson, W.D., and Smith, A.E. (1984). A short amino acid sequence able to specify nuclear location. Cell 39, 499-509.

[136] Robbins, J., Dilworth, S.M., Laskey, R.A., and Dingwall, C. (1991). Two interdependent basic domains in nucleoplasmin nuclear targeting sequence: identification of a class of bipartite nuclear targeting sequence. Ibid. 64, 615-623.

[137] Kosugi, S., Hasebe, M., Matsumura, N., Takashima, H., Miyamoto-Sato, E., Tomita, M., and Yanagawa, H. (2009). Six classes of nuclear localization signals specific to different binding grooves of importin alpha. J Biol Chem 284, 478-485.

[138] Lott, K., and Cingolani, G. (2011). The importin beta binding domain as a master regulator of nucleocytoplasmic transport. Biochimica et biophysica acta 1813, 1578-1592.

[139] Jakel, S., and Gorlich, D. (1998). Importin beta, transportin, RanBP5 and RanBP7 mediate nuclear import of ribosomal proteins in mammalian cells. EMBO J 17, 4491-4502.

[140] Weis, K., Ryder, U., and Lamond, A.I. (1996). The conserved amino-terminal domain of hSRP1 alpha is essential for nuclear protein import. Ibid. 15, 1818-1825.

[141] Chook, Y.M., and Blobel, G. (2001). Karyopherins and nuclear import. Current opinion in structural biology 11, 703-715.

[142] Monecke, T., Guttler, T., Neumann, P., Dickmanns, A., Gorlich, D., and Ficner, R. (2009). Crystal structure of the nuclear export receptor CRM1 in complex with Snurportin1 and RanGTP. Science 324, 1087-1091.

[143] Cingolani, G., Petosa, C., Weis, K., and Muller, C.W. (1999). Structure of importin-beta bound to the IBB domain of importin-alpha. Nature 399, 221-229.

[144] Fornerod, M., Ohno, M., Yoshida, M., and Mattaj, I.W. (1997). CRM1 is an export receptor for leucine-rich nuclear export signals. Cell 90, 1051-1060.

[145] Kosugi, S., Hasebe, M., Tomita, M., and Yanagawa, H. (2008). Nuclear export signal consensus sequences defined using a localization-based yeast selection system. Traffic 9, 2053-2062.

[146] Dong, X., Biswas, A., Süel, K.E., Jackson, L.K., Martinez, R., Gu, H., and Chook, Y.M. (2009). Structural basis for leucine-rich nuclear export signal recognition by CRM1. Nature 458, 1136-1141.

[147] Pollard, V.W., Michael, W.M., Nakielny, S., Siomi, M.C., Wang, F., and Dreyfuss, G. (1996). A novel receptor-mediated nuclear protein import pathway. Cell 86, 985-994.

[148] Cansizoglu, A.E., Lee, B.J., Zhang, Z.C., Fontoura, B.M., and Chook, Y.M. (2007). Structure-based design of a pathway-specific nuclear import inhibitor. Nat Struct Mol Biol 14, 452-454.

[149] Imasaki, T., Shimizu, T., Hashimoto, H., Hidaka, Y., Kose, S., Imamoto, N., Yamada, M., and Sato, M. (2007). Structural basis for substrate recognition and dissociation by human transportin 1. Mol Cell 28, 57-67.

[150] Rebane, A., Aab, A., and Steitz, J.A. (2004). Transportins 1 and 2 are redundant nuclear import factors for hnRNP A1 and HuR. RNA 10, 590-599.

[151] Desmond, C.R., Atwal, R.S., Xia, J., and Truant, R. (2012). Identification of a karyopherin beta1/beta2 proline-tyrosine nuclear localization signal in huntingtin protein. J Biol Chem 287, 39626-39633.

[152] Darshan, M.S., Lucchi, J., Harding, E., and Moroianu, J. (2004). The l2 minor capsid protein of human papillomavirus type 16 interacts with a network of nuclear import receptors. J Virol 78, 12179-12188.

[153] Waldmann, I., Walde, S., and Kehlenbach, R.H. (2007). Nuclear import of c-Jun is mediated by multiple transport receptors. J Biol Chem 282, 27685-27692.

[154] Putker, M., Madl, T., Vos, H.R., de Ruiter, H., Visscher, M., van den Berg, M.C., Kaplan, M., Korswagen, H.C., Boelens, R., Vermeulen, M., *et al.* (2013). Redox-dependent control of FOXO/DAF-16 by transportin-1. Mol Cell 49, 730-742.

[155] Bonifati, V., Rizzu, P., van Baren, M.J., Schaap, O., Breedveld, G.J., Krieger, E., Dekker, M.C., Squitieri, F., Ibanez, P., Joosse, M., *et al.* (2003). Mutations in the DJ1 gene associated with autosomal recessive early-onset parkinsonism. Science 299, 256-259.

[156] Bjorkblom, B., Maple-Grodem, J., Puno, M.R., Odell, M., Larsen, J.P., and Moller, S.G. (2014). Reactive oxygen species-mediated DJ1 monomerization modulates intracellular trafficking involving karyopherin beta2. Mol Cell Biol 34, 3024-3040.

[157] Takano, A., Isojima, Y., and Nagai, K. (2004). Identification of mPer1 phosphorylation sites responsible for the nuclear entry. J Biol Chem 279, 32578-32585.

[158] Lee, H., Chen, R., Lee, Y., Yoo, S., and Lee, C. (2009). Essential roles of CKIdelta and CKIepsilon in the mammalian circadian clock. Proc Natl Acad Sci U S A 106, 21359-21364.

[159] Maier, B., Wendt, S., Vanselow, J.T., Wallach, T., Reischl, S., Oehmke, S., Schlosser, A., and Kramer, A. (2009). A large-scale functional RNAi-screen reveals a role for CK2 in the mammalian circadian clock. Genes Dev 23, 708-718.

[160] Eide, E.J., Vielhaber, E.L., Hinz, W.A., and Virshup, D.M. (2002). The circadian regulatory proteins BMAL1 and cryptochromes are substrates of casein kinase Iepsilon. J Biol Chem 277, 17248-17254.

[161] Gallego, M., Kang, H., and Virshup, D.M. (2006). Protein phosphatase 1 regulates the stability of the circadian protein PER2. Biochem J 399, 169-175.

[162] Miyazaki, K., Mesaki, M., and Ishida, N. (2001). Nuclear entry mechanism of rat PER2 (rPER2): role of rPER2 in nuclear localization of CRY protein. Mol Cell Biol 21, 6651-6659.

[163] Kume, K., Zylka, M.J., Sriram, S., Shearman, L.P., Weaver, D.R., Jin, X., Maywood, E.S., Hastings, M.H., and Reppert, S.M. (1999). mCRY1 and mCRY2 are essential components of the negative limb of the circadian clock feedback loop. Cell 98, 193-205.

[164] Yagita, K., Yamaguchi, S., Tamanini, F., van Der Horst, G.T., Hoeijmakers, J.H., Yasui, A., Loros, J.J., Dunlap, J.C., and Okamura, H. (2000). Dimerization and nuclear entry of mPER proteins in mammalian cells. Genes Dev 14, 1353-1363.

[165] Öllinger, R., Korge, S., Korte, T., Koller, B., Herrmann, A., and Kramer, A. (2014). Dynamics of the circadian clock protein PERIOD2 in living cells. J Cell Sci 127, 4322-4328.

[166] Tamanini, F., Yagita, K., Okamura, H., and van der Horst, G.T. (2005). Nucleocytoplasmic shuttling of clock proteins. Methods Enzymol 393, 418-435.

[167] Kwon, I., Lee, J., Chang, S.H., Jung, N.C., Lee, B.J., Son, G.H., Kim, K., and Lee, K.H. (2006). BMAL1 shuttling controls transactivation and degradation of the CLOCK/BMAL1 heterodimer. Mol Cell Biol 26, 7318-7330.

[168] Yoshitane, H., Takao, T., Satomi, Y., Du, N.H., Okano, T., and Fukada, Y. (2009). Roles of CLOCK phosphorylation in suppression of E-box-dependent transcription. Ibid. 29, 3675-3686.

[169] Vielhaber, E., Eide, E., Rivers, A., Gao, Z.H., and Virshup, D.M. (2000). Nuclear entry of the circadian regulator mPER1 is controlled by mammalian casein kinase I epsilon. Ibid. 20, 4888-4899.

[170] Vielhaber, E.L., Duricka, D., Ullman, K.S., and Virshup, D.M. (2001). Nuclear export of mammalian PERIOD proteins. J Biol Chem 276, 45921-45927.

[171] Miyazaki, K., Nagase, T., Mesaki, M., Narukawa, J., Ohara, O., and Ishida, N. (2004). Phosphorylation of clock protein PER1 regulates its circadian degradation in normal human fibroblasts. Biochem J 380, 95-103.

[172] Sakakida, Y., Miyamoto, Y., Nagoshi, E., Akashi, M., Nakamura, T.J., Mamine, T., Kasahara, M., Minami, Y., Yoneda, Y., and Takumi, T. (2005). Importin alpha/beta mediates nuclear transport of a mammalian circadian clock component, mCRY2, together with mPER2, through a bipartite nuclear localization signal. J Biol Chem 280, 13272-13278.

[173] Umemura, Y., Koike, N., Matsumoto, T., Yoo, S.H., Chen, Z., Yasuhara, N., Takahashi, J.S., and Yagita, K. (2014). Transcriptional program of Kpna2/Importin-alpha2 regulates cellular differentiation-coupled circadian clock development in mammalian cells. Proc Natl Acad Sci U S A 111, E5039-5048.

[174] Lee, Y., Jang, A.R., Francey, L.J., Sehgal, A., and Hogenesch, J.B. (2015). KPNB1 mediates PER/CRY nuclear translocation and circadian clock function. Elife 4.

[175] Saez, L., Derasmo, M., Meyer, P., Stieglitz, J., and Young, M.W. (2011). A key temporal delay in the circadian cycle of Drosophila is mediated by a nuclear localization signal in the timeless protein. Genetics 188, 591-600.

[176] Jang, A.R., Moravcevic, K., Saez, L., Young, M.W., and Sehgal, A. (2015). Drosophila TIM binds importin alpha1, and acts as an adapter to transport PER to the nucleus. PLoS Genet 11, e1004974.

[177] Schafmeier, T., Diernfellner, A., Schafer, A., Dintsis, O., Neiss, A., and Brunner, M. (2008). Circadian activity and abundance rhythms of the Neurospora clock transcription factor WCC associated with rapid nucleo-cytoplasmic shuttling. Genes Dev 22, 3397-3402.

[178] Diernfellner, A.C., Querfurth, C., Salazar, C., Hofer, T., and Brunner, M. (2009). Phosphorylation modulates rapid nucleocytoplasmic shuttling and cytoplasmic accumulation of Neurospora clock protein FRQ on a circadian time scale. Ibid. 23, 2192-2200.

[179] Saez, L., and Young, M.W. (1996). Regulation of nuclear entry of the Drosophila clock proteins period and timeless. Neuron 17, 911-920.

[180] Meyer, P., Saez, L., and Young, M.W. (2006). PER-TIM interactions in living Drosophila cells: an interval timer for the circadian clock. Science 311, 226-229.

[181] Bhattacharya, S. (2015). Reactive oxygen species and cellular defense system. In Free radicals in human health and disease, V.Y. Rani, U., ed. (Springer), p. 430.

[182] Zulueta, J.J., Yu, F.S., Hertig, I.A., Thannickal, V.J., and Hassoun, P.M. (1995). Release of hydrogen peroxide in response to hypoxia-reoxygenation: role of an NAD(P)H oxidase-like enzyme in endothelial cell plasma membrane. Am J Respir Cell Mol Biol 12, 41-49.

[183] Bondy, S.C., and Naderi, S. (1994). Contribution of hepatic cytochrome P450 systems to the generation of reactive oxygen species. Biochem Pharmacol 48, 155-159.

[184] Werz, O., Szellas, D., and Steinhilber, D. (2000). Reactive oxygen species released from granulocytes stimulate 5-lipoxygenase activity in a B-lymphocytic cell line. Eur J Biochem 267, 1263-1269.

[185] Liu, Y., Fiskum, G., and Schubert, D. (2002). Generation of reactive oxygen species by the mitochondrial electron transport chain. J Neurochem 80, 780-787.

[186] Chen, Y.R., Chen, C.L., Zhang, L., Green-Church, K.B., and Zweier, J.L. (2005). Superoxide generation from mitochondrial NADH dehydrogenase induces self-inactivation with specific protein radical formation. J Biol Chem 280, 37339-37348.

[187] Boveris, A., Oshino, N., and Chance, B. (1972). The cellular production of hydrogen peroxide. Biochem J 128, 617-630.

[188] Schrader, M., and Yoon, Y. (2007). Mitochondria and peroxisomes: are the 'big bCarl Rother' and the 'little sister' closer than assumed? Bioessays 29, 1105-1114.

[189] Van den Branden, C., Kerckaert, I., and Roels, F. (1984). Peroxisomal beta-oxidation from endogenous substrates. Demonstration through H2O2 production in the unanaesthetized mouse. Biochem J 218, 697-702.

[190] Go, Y.M., and Jones, D.P. (2008). Redox compartmentalization in eukaryotic cells. Biochimica et biophysica acta 1780, 1273-1290.

[191] Rhee, S.G., Bae, Y.S., Lee, S.R., and Kwon, J. (2000). Hydrogen peroxide: a key messenger that modulates protein phosphorylation through cysteine oxidation. Sci STKE 2000, pe1.

[192] Shadel, G.S., and Horvath, T.L. (2015). Mitochondrial ROS signaling in organismal homeostasis. Cell 163, 560-569.

[193] Al-Gubory, K.H. (2014). Environmental pollutants and lifestyle factors induce oxidative stress and poor prenatal development. Reprod Biomed Online 29, 17-31.

[194] Yamamori, T., Yasui, H., Yamazumi, M., Wada, Y., Nakamura, Y., Nakamura, H., and Inanami, O. (2012). Ionizing radiation induces mitochondrial reactive oxygen species production accompanied by upregulation of mitochondrial electron transport chain function and mitochondrial content under control of the cell cycle checkpoint. Free Radic Biol Med 53, 260-270.

[195] Han, E.S., Muller, F.L., Perez, V.I., Qi, W., Liang, H., Xi, L., Fu, C., Doyle, E., Hickey, M., Cornell, J., *et al.* (2008). The in vivo gene expression signature of oxidative stress. Physiol Genomics 34, 112-126.

[196] Ling, J., and Soll, D. (2010). Severe oxidative stress induces protein mistranslation through impairment of an aminoacyl-tRNA synthetase editing site. Proc Natl Acad Sci U S A 107, 4028-4033.

[197] Das, A., McDonald, D.G., Dixon-Mah, Y.N., Jacqmin, D.J., Samant, V.N., Vandergrift, W.A., 3rd, Lindhorst, S.M., Cachia, D., Varma, A.K., Vanek, K.N., *et al.* (2015). RIP1 and RIP3 complex regulates radiation-induced programmed necrosis in glioblastoma. Tumour Biol.

[198] Turillazzi, E., Neri, M., Cerretani, D., Cantatore, S., Frati, P., Moltoni, L., Busardo, F.P., Pomara, C., Riezzo, I., and Fineschi, V. (2016). Lipid peroxidation and apoptotic response in rat brain areas induced by long-term administration of nandrolone: the mutual crosstalk between ROS and NF-kB. J Cell Mol Med.

[199] Sander, C.S., Hamm, F., Elsner, P., and Thiele, J.J. (2003). Oxidative stress in malignant melanoma and non-melanoma skin cancer. Br J Dermatol 148, 913-922.

[200] Rani, V., Deep, G., Singh, R.K., Palle, K., and Yadav, U.C. (2016). Oxidative stress and metabolic disorders: Pathogenesis and therapeutic strategies. Life Sci.

[201] Nagasawa, H., and Little, J.B. (1992). Induction of Sister Chromatid Exchanges by Extremely Low-Doses of Alpha-Particles. Cancer Research 52, 6394-6396.

[202] Ivanov, V.N., Zhou, H., Ghandhi, S.A., Karasic, T.B., Yaghoubian, B., Amundson, S.A., and Hei, T.K. (2010). Radiation-induced bystander signaling pathways in human fibroblasts: a role for interleukin-33 in the signal transmission. Cellular signalling 22, 1076-1087.

[203] Fu, J., Yuan, D., Xiao, L., Tu, W., Dong, C., Liu, W., and Shao, C. (2016). The crosstalk between alpha-irradiated Beas-2B cells and its bystander U937 cells through MAPK and NF-kappaB signaling pathways. Mutation research 783, 1-8.

[204] Corsini, E., Sangha, N., and Feldman, S.R. (1997). Epidermal stratification reduces the effects of UVB (but not UVA) on keratinocyte cytokine production and cytotoxicity. Photodermatol Photoimmunol Photomed 13, 147-152.

[205] Birben, E., Sahiner, U.M., Sackesen, C., Erzurum, S., and Kalayci, O. (2012). Oxidative stress and antioxidant defense. World Allergy Organ J 5, 9-19.

[206] Pannala, V.R., and Dash, R.K. (2015). Mechanistic characterization of the thioredoxin system in the removal of hydrogen peroxide. Free Radic Biol Med 78, 42-55.

[207] Preston, T.J., Muller, W.J., and Singh, G. (2001). Scavenging of extracellular H2O2 by catalase inhibits the proliferation of HER-2/Neu-transformed rat-1 fibroblasts through the induction of a stress response. J Biol Chem 276, 9558-9564.

[208] Xu, X., Leng, J.Y., Gao, F., Zhao, Z.A., Deng, W.B., Liang, X.H., Zhang, Y.J., Zhang, Z.R., Li, M., Sha, A.G., *et al.* (2014). Differential expression and anti-oxidant function of glutathione peroxidase 3 in mouse uterus during decidualization. FEBS Lett 588, 1580-1589.

[209] Kang, S.W., Chae, H.Z., Seo, M.S., Kim, K., Baines, I.C., and Rhee, S.G. (1998). Mammalian peroxiredoxin isoforms can reduce hydrogen peroxide generated in response to growth factors and tumor necrosis factor-alpha. J Biol Chem 273, 6297-6302.

[210] He, M., Nitti, M., Piras, S., Lisa Furfaro, A., Traverso, N., Pronzato, M.A., and Mann, G.E. (2015). Heme oxygenase-1-derived bilirubin protects endothelial cells against high glucose-induced damage. Free Radic Biol Med 89, 91-98.

[211] Ambrosio, G., and Flaherty, J.T. (1992). Effects of the superoxide radical scavenger superoxide dismutase, and of the hydroxyl radical scavenger mannitol, on reperfusion injury in isolated rabbit hearts. Cardiovasc Drugs Ther 6, 623-632.

[212] Stewart, R.K., Smith, G.B., Donnelly, P.J., Reid, K.R., Petsikas, D., Conlan, A.A., and Massey, T.E. (1999). Glutathione S-transferase-catalyzed conjugation of bioactivated aflatoxin B(1) in human lung: differential cellular distribution and lack of significance of the GSTM1 genetic polymorphism. Carcinogenesis 20, 1971-1977.

[213] Fletcher, M.E., Boshier, P.R., Wakabayashi, K., Keun, H.C., Smolenski, R.T., Kirkham, P.A., Adcock, I.M., Barton, P.J., Takata, M., and Marczin, N. (2015). Influence of glutathione-S-transferase (GST) inhibition on lung epithelial cell injury: role of oxidative stress and metabolism. Am J Physiol Lung Cell Mol Physiol 308, L1274-1285.

[214] Szczubial, M. (2015). Effect of supplementation with vitamins E, C and beta-carotene on antioxidative/oxidative status parameters in sows during the postpartum period. Pol J Vet Sci 18, 299-305.

[215] Galano, A., and Alvarez-Idaboy, J.R. (2011). Glutathione: mechanism and kinetics of its non-enzymatic defense action against free radicals. Rsc Advances 1, 1763-1771.

[216] Grigorescu, R., Gruia, M.I., Nacea, V., Nitu, C., Negoita, V., and Glavan, D. (2015). The evaluation of non-enzymatic antioxidants effects in limiting tumor- associated oxidative stress, in a tumor rat model. J Med Life 8, 513-516.

[217] Austin, R.C., Lentz, S.R., and Werstuck, G.H. (2004). Role of hyperhomocysteinemia in endothelial dysfunction and atheCarl Rothrombotic disease. Cell Death Differ 11 Suppl 1, S56-64.

[218] Moreno, A.A., Mukhtar, M.S., Blanco, F., Boatwright, J.L., Moreno, I., Jordan, M.R., Chen, Y., Brandizzi, F., Dong, X., Orellana, A., *et al.* (2012). IRE1/bZIP60-mediated unfolded protein response plays distinct roles in plant immunity and abiotic stress responses. PLoS One 7, e31944.

[219] Baird, T.D., Palam, L.R., Fusakio, M.E., Willy, J.A., Davis, C.M., McClintick, J.N., Anthony, T.G., and Wek, R.C. (2014). Selective mRNA translation during eIF2 phosphorylation induces expression of IBTK alpha. Molecular Biology of the Cell 25, 1686-1697.

[220] Sitte, N., Merker, K., and Grune, T. (1998). Proteasome-dependent degradation of oxidized proteins in MRC-5 fibroblasts. Febs Letters 440, 399-402.

[221] Hiramatsu, N., Messah, C., Han, J., LaVail, M.M., Kaufman, R.J., and Lin, J.H. (2014). Translational and posttranslational regulation of XIAP by eIF2alpha and ATF4 promotes ER stress-induced cell death during the unfolded protein response. Mol Biol Cell 25, 1411-1420.

[222] Maeda, T., Chua, P.P., Chong, M.T., Sim, A.B., Nikaido, O., and Tron, V.A. (2001). Nucleotide excision repair genes are upregulated by low-dose artificial ultraviolet B: evidence of a photoprotective SOS response? J Invest Dermatol 117, 1490-1497.

[223] Krokan, H.E., Standal, R., and Slupphaug, G. (1997). DNA glycosylases in the base excision repair of DNA. Biochem J 325 ( Pt 1), 1-16.

[224] Evdokimova, V., Gandhi, M., Rayapureddi, J., Stringer, J.R., and Nikiforov, Y.E. (2012). Formation of carcinogenic chromosomal rearrangements in human thyroid cells after induction of double-strand DNA breaks by restriction endonucleases. Endocr Relat Cancer 19, 271-281.

[225] Bohlander, S.K., and Kakadia, P.M. (2015). DNA Repair and Chromosomal Translocations. Recent Results Cancer Res 200, 1-37.

[226] Ranieri, D., Avitabile, D., Shiota, M., Yokomizo, A., Naito, S., Bizzarri, M., and Torrisi, M.R. (2015). Nuclear redox imbalance affects circadian oscillation in HaCaT keratinocytes. Int J Biochem Cell Biol 65, 113-124.

[227] Yoshida, Y., Maeda, T., Lee, B., and Hasunuma, K. (2008). Conidiation rhythm and light entrainment in superoxide dismutase mutant in Neurospora crassa. Molecular Genetics and Genomics 279, 193-202.

[228] Ivleva, N.B., Gao, T., LiWang, A.C., and Golden, S.S. (2006). Quinone sensing by the circadian input kinase of the cyanobacterial circadian clock. Proc Natl Acad Sci U S A 103, 17468-17473.

[229] Rutter, J., Reick, M., Wu, L.C., and McKnight, S.L. (2001). Regulation of clock and NPAS2 DNA binding by the redox state of NAD cofactors. Science 293, 510-514.

[230] Wagner, E., Deitzer, G.F., Fischer, S., Frosh, S., Kempf, O., and Stroebele, L. (1975). Endogenous oscillations in pathways of energy transduction as related to circadian rhythmicity and photoperiodic control. Biosystems 7, 68-76.

[231] Yang, G., Wright, C.J., Hinson, M.D., Fernando, A.P., Sengupta, S., Biswas, C., La, P., and Dennery, P.A. (2014). Oxidative stress and inflammation modulate Rev-erbalpha signaling in the neonatal lung and affect circadian rhythmicity. Antioxid Redox Signal 21, 17-32.

[232] Pekovic-Vaughan, V., Gibbs, J., Yoshitane, H., Yang, N., Pathiranage, D., Guo, B., Sagami, A., Taguchi, K., Bechtold, D., Loudon, A., *et al.* (2014). The circadian clock regulates rhythmic activation of the NRF2/glutathione-mediated antioxidant defense pathway to modulate pulmonary fibrosis. Genes Dev 28, 548-560.

[233] Hirayama, J., Cho, S., and Sassone-Corsi, P. (2007). Circadian control by the reduction/oxidation pathway: catalase represses light-dependent clock gene expression in the zebrafish. Proc Natl Acad Sci U S A 104, 15747-15752.

[234] Edgar, R.S., Green, E.W., Zhao, Y., van Ooijen, G., Olmedo, M., Qin, X., Xu, Y., Pan, M., Valekunja, U.K., Feeney, K.A., *et al.* (2012). Peroxiredoxins are conserved markers of circadian rhythms. Nature 485, 459-464.

[235] Kil, I.S., Ryu, K.W., Lee, S.K., Kim, J.Y., Chu, S.Y., Kim, J.H., Park, S., and Rhee, S.G. (2015). Circadian Oscillation of Sulfiredoxin in the Mitochondria. Mol Cell 59, 651-663.

[236] O'Neill, J.S., and Reddy, A.B. (2011). Circadian clocks in human red blood cells. Nature 469, 498-503.

[237] Bronson, S.K., and Smithies, O. (1994). Altering mice by homologous recombination using embryonic stem cells. The Journal of biological chemistry 269, 27155-27158.

[238] Cohen-Tannoudji, M., Robine, S., Choulika, A., Pinto, D., El Marjou, F., Babinet, C., Louvard, D., and Jaisser, F. (1998). I-SceI-induced gene replacement at a natural locus in embryonic stem cells. Mol Cell Biol 18, 1444-1448.

[239] Epinat, J.C., Arnould, S., Chames, P., Rochaix, P., Desfontaines, D., Puzin, C., Patin, A., Zanghellini, A., Paques, F., and Lacroix, E. (2003). A novel engineered meganuclease induces homologous recombination in yeast and mammalian cells. Nucleic Acids Res 31, 2952-2962.

[240] Pavletich, N.P., and Pabo, C.O. (1991). Zinc finger-DNA recognition: crystal structure of a Zif268-DNA complex at 2.1 A. Science 252, 809-817.

[241] Li, L., Wu, L.P., and Chandrasegaran, S. (1992). Functional domains in Fok I restriction endonuclease. Proc Natl Acad Sci U S A 89, 4275-4279.

[242] Bitinaite, J., Wah, D.A., Aggarwal, A.K., and Schildkraut, I. (1998). FokI dimerization is required for DNA cleavage. Ibid. 95, 10570-10575.

[243] Boch, J., Scholze, H., Schornack, S., Landgraf, A., Hahn, S., Kay, S., Lahaye, T., Nickstadt, A., and Bonas, U. (2009). Breaking the code of DNA binding specificity of TAL-type III effectors. Science 326, 1509-1512.

[244] Moscou, M.J., and Bogdanove, A.J. Ibid.A simple cipher governs DNA recognition by TAL effectors. 1501.

[245] Kim, Y., Kweon, J., Kim, A., Chon, J.K., Yoo, J.Y., Kim, H.J., Kim, S., Lee, C., Jeong, E., Chung, E., *et al.* (2013). A library of TAL effector nucleases spanning the human genome. Nat Biotechnol 31, 251-258.

[246] Bickle, T.A., and Kruger, D.H. (1993). Biology of DNA restriction. Microbiol Rev 57, 434-450.

[247] Jinek, M., Chylinski, K., Fonfara, I., Hauer, M., Doudna, J.A., and Charpentier, E. (2012). A programmable dual-RNA-guided DNA endonuclease in adaptive bacterial immunity. Science 337, 816-821.

[248] Hsu, P.D., Scott, D.A., Weinstein, J.A., Ran, F.A., Konermann, S., Agarwala, V., Li, Y., Fine, E.J., Wu, X., Shalem, O., *et al.* (2013). DNA targeting specificity of RNA-guided Cas9 nucleases. Nat Biotechnol 31, 827-832.

[249] Hwang, W.Y., Fu, Y., Reyon, D., Maeder, M.L., Tsai, S.Q., Sander, J.D., Peterson, R.T., Yeh, J.R., and Joung, J.K. Ibid.Efficient genome editing in zebrafish using a CRISPR-Cas system. 227-229.

[250] Cong, L., Ran, F.A., Cox, D., Lin, S., Barretto, R., Habib, N., Hsu, P.D., Wu, X., Jiang, W., Marraffini, L.A., *et al.* (2013). Multiplex genome engineering using CRISPR/Cas systems. Science 339, 819-823.

[251] Feng, Z., Zhang, B., Ding, W., Liu, X., Yang, D.L., Wei, P., Cao, F., Zhu, S., Zhang, F., Mao, Y., *et al.* (2013). Efficient genome editing in plants using a CRISPR/Cas system. Cell Res 23, 1229-1232.

[252] Shen, B., Zhang, W., Zhang, J., Zhou, J., Wang, J., Chen, L., Wang, L., Hodgkins, A., Iyer, V., Huang, X., *et al.* (2014). Efficient genome modification by CRISPR-Cas9 nickase with minimal off-target effects. Nat Methods 11, 399-402.

[253] Swarts, D.C., Makarova, K., Wang, Y., Nakanishi, K., Ketting, R.F., Koonin, E.V., Patel, D.J., and van der Oost, J. (2014). The evolutionary journey of Argonaute proteins. Nature structural & molecular biology 21, 743-753.

[254] Gao, F., Shen, X.Z., Jiang, F., Wu, Y., and Han, C. (2016). DNA-guided genome editing using the Natronobacterium gregoryi Argonaute. Nature biotechnology.

[255] Korge, S., Grudziecki, A., and Kramer, A. (2015). Highly Efficient Genome Editing via CRISPR/Cas9 to Create Clock Gene Knockout Cells. Journal of biological rhythms 30, 389-395.

[256] Liu, A.C., Tran, H.G., Zhang, E.E., Priest, A.A., Welsh, D.K., and Kay, S.A. (2008). Redundant function of REV-ERBalpha and beta and non-essential role for Bmal1 cycling in transcriptional regulation of intracellular circadian rhythms. PLoS genetics 4, e1000023.

[257] Strom, A.C., and Weis, K. (2001). Importin-beta-like nuclear transport receptors. Genome biology 2, REVIEWS3008, ibid.

[258] Sorokin, A.V., Kim, E.R., and Ovchinnikov, L.P. (2007). Nucleocytoplasmic transport of proteins. Biochemistry Biokhimiia 72, 1439-1457.

[259] Okada, N., Ishigami, Y., Suzuki, T., Kaneko, A., Yasui, K., Fukutomi, R., and Isemura, M. (2008). Importins and exportins in cellular differentiation. Journal of cellular and molecular medicine 12, 1863-1871.

[260] Raices, M., and D'Angelo, M.A. (2012). Nuclear pore complex composition: a new regulator of tissue-specific and developmental functions. Nature reviews Molecular cell biology 13, 687-699.

[261] Siepka, S.M., Yoo, S.H., Park, J., Song, W., Kumar, V., Hu, Y., Lee, C., and Takahashi, J.S. (2007). Circadian mutant Overtime reveals F-box protein FBXL3 regulation of cryptochrome and period gene expression. Cell 129, 1011-1023.

[262] Busino, L., Bassermann, F., Maiolica, A., Lee, C., Nolan, P.M., Godinho, S.I., Draetta, G.F., and Pagano, M. (2007). SCFFbxl3 controls the oscillation of the circadian clock by directing the degradation of cryptochrome proteins. Science 316, 900-904.

[263] Chook, Y.M., and Blobel, G. (1999). Structure of the nuclear transport complex karyopherin-beta2-Ran x GppNHp. Nature 399, 230-237.

[264] Chook, Y.M., Jung, A., Rosen, M.K., and Blobel, G. (2002). Uncoupling Kapbeta2 substrate dissociation and ran binding. Biochemistry 41, 6955-6966.

[265] Ledford, H. (2015). Epigenetics: The genome unwrapped. Nature 528, S12-13.

[266] Sung, Y.H., Kim, J.M., Kim, H.T., Lee, J., Jeon, J., Jin, Y., Choi, J.H., Ban, Y.H., Ha, S.J., Kim, C.H., *et al.* (2014). Highly efficient gene knockout in mice and zebrafish with RNA-guided endonucleases. Genome research 24, 125-131.

[267] Maruyama, T., Dougan, S.K., Truttmann, M.C., Bilate, A.M., Ingram, J.R., and Ploegh, H.L. (2015). Increasing the efficiency of precise genome editing with CRISPR-Cas9 by inhibition of nonhomologous end joining. Nature biotechnology 33, 538-542.

[268] Barrangou, R., Birmingham, A., Wiemann, S., Beijersbergen, R.L., Hornung, V., and Smith, A. (2015). Advances in CRISPR-Cas9 genome engineering: lessons learned from RNA interference. Nucleic acids research 43, 3407-3419

[269] Akashi, M., Okamoto, A., Tsuchiya, Y., Todo, T., Nishida, E., and Node, K. (2014). A positive role for PERIOD in mammalian circadian gene expression. Cell reports 7, 1056-1064.

[270] Bruice, P.Y. (2014). Organic Chemistry, 7th Edition (Pearson), 960-962.

[271] Zuckerkandl, E., and Pauling, L. (1965). Molecules as documents of evolutionary history. Journal of theoretical biology 8, 357-366.

[272] Fridell, R.A., Truant, R., Thorne, L., Benson, R.E., and Cullen, B.R. (1997). Nuclear import of hnRNP A1 is mediated by a novel cellular cofactor related to karyopherin-beta. Journal of cell science 110 ( Pt 11), 1325-1331.

[273] Tamaru, T., Hirayama, J., Isojima, Y., Nagai, K., Norioka, S., Takamatsu, K., and Sassone-Corsi, P. (2009). CK2alpha phosphorylates BMAL1 to regulate the mammalian clock. Nature structural & molecular biology 16, 446-448.

[274] Kwak, Y., Jeong, J., Lee, S., Park, Y.U., Lee, S.A., Han, D.H., Kim, J.H., Ohshima, T., Mikoshiba, K., Suh, Y.H., et al. (2013). Cyclin-dependent kinase 5 (Cdk5) regulates the function of CLOCK protein by direct phosphorylation. Ibid. 288, 36878-36889.

[275] Mehta, N., Cheng, A.H., Chiang, C.K., Mendoza-Viveros, L., Ling, H.H., Patel, A., Xu, B., Figeys, D., and Cheng, H.Y. (2015). GRK2 Fine-Tunes Circadian Clock Speed and Entrainment via Transcriptional and Post-translational Control of PERIOD Proteins. Cell reports 12, 1272-1288.

[276] Yang, Y., Duguay, D., Bedard, N., Rachalski, A., Baquiran, G., Na, C.H., Fahrenkrug, J., Storch, K.F., Peng, J., Wing, S.S., *et al.* (2012). Regulation of behavioral circadian rhythms and clock protein PER1 by the deubiquitinating enzyme USP2. Biology open 1, 789-801.

[277] Lee, K.H., Woo, K.C., Kim, D.Y., Kim, T.D., Shin, J., Park, S.M., Jang, S.K., and Kim, K.T. (2012). Rhythmic interaction between Period1 mRNA and hnRNP Q leads to circadian time-dependent translation. Molecular and cellular biology 32, 717-728.

[278] Süel, K.E., Gu, H., and Chook, Y.M. (2008). Modular organization and combinatorial energetics of proline-tyrosine nuclear localization signals. PLoS biology 6, e137.

[279] Kucera, N., Schmalen, I., Hennig, S., Öllinger, R., Strauss, H.M., Grudziecki, A., Wieczorek, C., Kramer, A., and Wolf, E. (2012). Unwinding the differences of the mammalian PERIOD clock proteins from crystal structure to cellular function. Proceedings of the National Academy of Sciences of the United States of America 109, 3311-3316.

[280] Hinz, A., Jedamzick, J., Herbring, V., Fischbach, H., Hartmann, J., Parcej, D., Koch, J., and Tampe, R. (2014). Assembly and function of the major histocompatibility complex (MHC) I peptide-loading complex are conserved across higher vertebrates. The Journal of biological chemistry 289, 33109-33117.

[281] Mastrocola, A.S., Kim, S.H., Trinh, A.T., Rodenkirch, L.A., and Tibbetts, R.S. (2013). The RNA-binding protein fused in sarcoma (FUS) functions downstream of poly(ADP-ribose) polymerase (PARP) in response to DNA damage. Ibid. 288, 24731-24741.

[282] Sato, M., Mizoro, Y., Atobe, Y., Fujimoto, Y., Yamaguchi, Y., Fustin, J.M., Doi, M., and Okamura, H. (2011). Transportin 1 in the mouse brain: appearance in regions of neurogenesis, cerebrospinal fluid production/sensing, and circadian clock. The Journal of comparative neurology 519, 1770-1780.

[283] Hughes, M.E., DiTacchio, L., Hayes, K.R., Vollmers, C., Pulivarthy, S., Baggs, J.E., Panda, S., and Hogenesch, J.B. (2009). Harmonics of circadian gene transcription in mammals. PLoS genetics 5, e1000442.

[284] Miller, B.H., McDearmon, E.L., Panda, S., Hayes, K.R., Zhang, J., Andrews, J.L., Antoch, M.P., Walker, J.R., Esser, K.A., Hogenesch, J.B., *et al.* (2007). Circadian and CLOCK-controlled regulation of the mouse transcriptome and cell proliferation. Proceedings of the National Academy of Sciences of the United States of America 104, 3342-3347.

[285] Lee, C., Etchegaray, J.P., Cagampang, F.R., Loudon, A.S., and Reppert, S.M. (2001). Posttranslational mechanisms regulate the mammalian circadian clock. Cell 107, 855-867.

[286] Ferro, E., Goitre, L., Retta, S.F., and Trabalzini, L. (2012). The Interplay between ROS and Ras GTPases: Physiological and Pathological Implications. Journal of signal transduction 2012, 365769.

[287] Chatterjee, M., and Paschal, B.M. (2015). Disruption of the ran system by cysteine oxidation of the nucleotide exchange factor RCC1. Molecular and cellular biology 35, 566-581.

[288] Kodiha, M., Chu, A., Matusiewicz, N., and Stochaj, U. (2004). Multiple mechanisms promote the inhibition of classical nuclear import upon exposure to severe oxidative stress. Cell death and differentiation 11, 862-874.

[289] Crampton, N., Kodiha, M., Shrivastava, S., Umar, R., and Stochaj, U. (2009). Oxidative stress inhibits nuclear protein export by multiple mechanisms that target FG nucleoporins and Crm1. Molecular biology of the cell 20, 5106-5116.

[290] Donati, A.J., Jeon, J.M., Sangurdekar, D., So, J.S., and Chang, W.S. (2011). Genome-wide transcriptional and physiological responses of Bradyrhizobium japonicum to paraquat-mediated oxidative stress. Applied and environmental microbiology 77, 3633-3643.

[291] Qiu, M., Chen, L., Tan, G., Ke, L., Zhang, S., Chen, H., and Liu, J. (2015). A reactive oxygen species activation mechanism contributes to JS-K-induced apoptosis in human bladder cancer cells. Scientific reports 5, 15104.

[292] Rey, G., and Reddy, A.B. (2015). Interplay between cellular redox oscillations and circadian clocks. Diabetes, obesity & metabolism 17 Suppl 1, 55-64.

[293] Patel, S.A., Velingkaar, N.S., and Kondratov, R.V. (2014). Transcriptional control of antioxidant defense by the circadian clock. Antioxidants & redox signaling 20, 2997-3006.

[294] Nakahata, Y., Kaluzova, M., Grimaldi, B., Sahar, S., Hirayama, J., Chen, D., Guarente, L.P., and Sassone-Corsi, P. (2008). The NAD+-dependent deacetylase SIRT1 modulates CLOCK-mediated chromatin remodeling and circadian control. Cell 134, 329-340.

[295] Alcendor, R.R., Gao, S., Zhai, P., Zablocki, D., Holle, E., Yu, X., Tian, B., Wagner, T., Vatner, S.F., and Sadoshima, J. (2007). Sirt1 regulates aging and resistance to oxidative stress in the heart. Circulation research 100, 1512-1521.

[296] Ramsey, K.M., Yoshino, J., Brace, C.S., Abrassart, D., Kobayashi, Y., Marcheva, B., Hong, H.K., Chong, J.L., Buhr, E.D., Lee, C., *et al.* (2009). Circadian clock feedback cycle through NAMPT-mediated NAD+ biosynthesis. Science 324, 651-654.

[297] Sugimoto, T., Morioka, N., Zhang, F.F., Sato, K., Abe, H., Hisaoka-Nakashima, K., and Nakata, Y. (2014). Clock gene Per1 regulates the production of CCL2 and interleukin-6 through p38, JNK1 and NF-kappaB activation in spinal astrocytes. Molecular and cellular neurosciences 59, 37-46.

[298] Sato, F., Wu, Y., Bhawal, U.K., Liu, Y., Imaizumi, T., Morohashi, S., Kato, Y., and Kijima, H. (2011a). PERIOD1 (PER1) has anti-apoptotic effects, and PER3 has pro-apoptotic effects during cisplatin (CDDP) treatment in human gingival cancer CA9-22 cells. European journal of cancer 47, 1747-1758.

[299] Sato, F., Nagata, C., Liu, Y., Suzuki, T., Kondo, J., Morohashi, S., Imaizumi, T., Kato, Y., and Kijima, H. (2009). PERIOD1 is an anti-apoptotic factor in human pancreatic and hepatic cancer cells. Journal of biochemistry 146, 833-838.

[300] Zhao, N., Yang, K., Yang, G., Chen, D., Tang, H., Zhao, D., and Zhao, C. (2013). Aberrant expression of clock gene period1 and its correlations with the growth, proliferation and metastasis of buccal squamous cell carcinoma. PloS one 8, e55894.

[301] Sies, H. (2014). Role of metabolic H2O2 generation: redox signaling and oxidative stress. The Journal of biological chemistry 289, 8735-8741.

[302] Palomero, J., Pye, D., Kabayo, T., Spiller, D.G., and Jackson, M.J. (2008). In situ detection and measurement of intracellular reactive oxygen species in single isolated mature skeletal muscle fibers by real time fluorescence microscopy. Antioxidants & redox signaling 10, 1463-1474.

[303] Schieber, M., and Chandel, N.S. (2014). ROS function in redox signaling and oxidative stress. Current biology : CB 24, R453-462.

[304] Boutros, M., Kiger, A.A., Armknecht, S., Kerr, K., Hild, M., Koch, B., Haas, S.A., Paro, R., Perrimon, N., and Heidelberg Fly Array, C. (2004). Genome-wide RNAi analysis of growth and viability in Drosophila cells. Science 303, 832-835.

[305] Neumann, B., Held, M., Liebel, U., Erfle, H., Rogers, P., Pepperkok, R., and Ellenberg, J. (2006). High-throughput RNAi-screening by time-lapse imaging of live human cells. Nature methods 3, 385-390.

[306] Chia, N.Y., Chan, Y.S., Feng, B., Lu, X., Orlov, Y.L., Moreau, D., Kumar, P., Yang, L., Jiang, J., Lau, M.S., *et al.* (2010). A genome-wide RNAi-screen reveals determinants of human embryonic stem cell identity. Nature 468, 316-320.

[307] Zhang, E.E., Liu, A.C., Hirota, T., Miraglia, L.J., Welch, G., Pongsawakul, P.Y., Liu, X., Atwood, A., Huss, J.W., 3rd, Janes, J., *et al.* (2009). A genome-wide RNAi-screen for modifiers of the circadian clock in human cells. Cell 139, 199-210.

[308] Vasu, S., Shah, S., Orjalo, A., Park, M., Fischer, W.H., and Forbes, D.J. (2001). Novel vertebrate nucleoporins Nup133 and Nup160 play a role in mRNA export. The Journal of cell biology 155, 339-354.

[309] Ullman, K.S., Shah, S., Powers, M.A., and Forbes, D.J. (1999). The nucleoporin nup153 plays a critical role in multiple types of nuclear export. Molecular biology of the cell 10, 649-664.

[310] Jang, A.R., Moravcevic, K., Saez, L., Young, M.W., and Sehgal, A. (2015). Drosophila TIM binds importin alpha1, and acts as an adapter to transport PER to the nucleus. PLoS genetics 11, e1004974.

[311] Sakin, V., Richter, S.M., Hsiao, H.H., Urlaub, H., and Melchior, F. (2015). Sumoylation of the GTPase Ran by the RanBP2 SUMO E3 Ligase Complex. The Journal of biological chemistry 290, 23589-23602.

[312] Kirli, K., Karaca, S., Dehne, H.J., Samwer, M., Pan, K.T., Lenz, C., Urlaub, H., and Gorlich, D. (2015). A deep proteomics perspective on CRM1-mediated nuclear export and nucleocytoplasmic partitioning. eLife 4.

[313] Debler, E.W., Ma, Y., Seo, H.S., Hsia, K.C., Noriega, T.R., Blobel, G., and Hoelz, A. (2008). A fence-like coat for the nuclear pore membrane. Molecular cell 32, 815-826.

[314] Orjalo, A.V., Arnaoutov, A., Shen, Z., Boyarchuk, Y., Zeitlin, S.G., Fontoura, B., Briggs, S., Dasso, M., and Forbes, D.J. (2006). The Nup107-160 nucleoporin complex is required for correct bipolar spindle assembly. Molecular biology of the cell 17, 3806-3818.

[315] Bilokapic, S., and Schwartz, T.U. (2013). Structural and functional studies of the 252 kDa nucleoporin ELYS reveal distinct roles for its three tethered domains. Structure 21, 572-580.

[316] Bischoff, F.R., Krebber, H., Smirnova, E., Dong, W., and Ponstingl, H. (1995). Co-activation of RanGTPase and inhibition of GTP dissociation by Ran-GTP binding protein RanBP1. The EMBO journal 14, 705-715.

[317] Schulze, H., Dose, M., Korpal, M., Meyer, I., Italiano, J.E., Jr., and Shivdasani, R.A. (2008). RanBP10 is a cytoplasmic guanine nucleotide exchange factor that modulates noncentrosomal microtubules. The Journal of biological chemistry 283, 14109-14119.

[318] Mingot, J.M., Bohnsack, M.T., Jakle, U., and Gorlich, D. (2004). Exportin 7 defines a novel general nuclear export pathway. The EMBO journal 23, 3227-3236.

[319] Laronga, C., Yang, H.Y., Neal, C., and Lee, M.H. (2000). Association of the cyclin-dependent kinases and 14-3-3 sigma negatively regulates cell cycle progression. The Journal of biological chemistry 275, 23106-23112.

[320] Lee, J.H., Zhou, S., and Smas, C.M. (2010). Identification of RANBP16 and RANBP17 as novel interaction partners for the bHLH transcription factor E12. Journal of cellular biochemistry 111, 195-206.

[321] Nousiainen, H.O., Kestila, M., Pakkasjarvi, N., Honkala, H., Kuure, S., Tallila, J., Vuopala, K., Ignatius, J., Herva, R., and Peltonen, L. (2008). Mutations in mRNA export mediator GLE1 result in a fetal motoneuron disease. Nature genetics 40, 155-157.

[322] Kaneb, H.M., Folkmann, A.W., Belzil, V.V., Jao, L.E., Leblond, C.S., Girard, S.L., Daoud, H., Noreau, A., Rochefort, D., Hince, P., *et al.* (2015). Deleterious mutations in the essential mRNA metabolism factor, hGle1, in amyotrophic lateral sclerosis. Human molecular genetics 24, 1363-1373.

[323] Takizawa, C.G., Weis, K., and Morgan, D.O. (1999). Ran-independent nuclear import of cyclin B1-Cdc2 by importin beta. Proceedings of the National Academy of Sciences of the United States of America 96, 7938-7943.

[324] Englmeier, L., Olivo, J.C., and Mattaj, I.W. (1999). Receptor-mediated substrate translocation through the nuclear pore complex without nucleotide triphosphate hydrolysis. Current biology : CB 9, 30-41.

[325] Jinek, M., Chylinski, K., Fonfara, I., Hauer, M., Doudna, J.A., and Charpentier, E. (2012). A programmable dual-RNA-guided DNA endonuclease in adaptive bacterial immunity. Science 337, 816-821.

# Appendices

## A1 Supplementary figures and tables

### A1.1 Pharmacological inhibition of classical nuclear import and nuclear export lengthens the circadian period

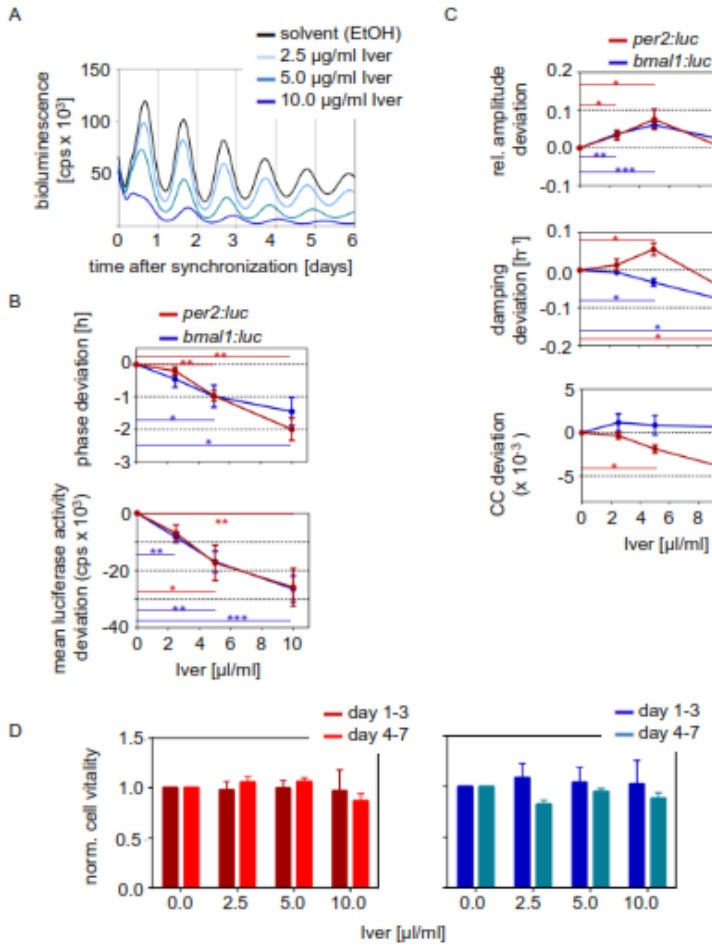


**Suppl. figure A1.1: Pharmacological inhibition of classical nuclear import lengthens the circadian period in U-2 OS reporter cells**. Cells, constitutively expressing either *bmal1*- (*bmal1:luc*, blue) or *per2*- (*per2:luc*, red) promoter-driven *luciferase* were treated with solvent (black) or the pharmacological inhibitor ivermectin (Iver) after synchronization with 1 µM dexamethasone. Treatments were applied at indicated concentrations of Iver and monitored for six days. A) Depicted are raw data of representative time series of *bmal1:luc* U-2 OS cells. B and C) Quantification of different altered parameters. Increasing concentrations of Iver lead to an earlier phase and reduced mean bioluminescence (C). Amplitude, damping of the amplitude per 24 h and CC were not consistently altered. D) Resazurin cell vitality measurements of either *per2:luc* or *bmal1:luc* U-2 OS reporter cells after pharmacological inhibition of nuclear import (error bars = SEM, $n_{B \text{ and } D}$ = 3 to 8 individual recordings; student's t test: * $p < 0.05$, ** $p < 0.01$, *** $p < 0.001$).

## A1.2 Pharmacological inhibition of nuclear export lengthens the circadian period

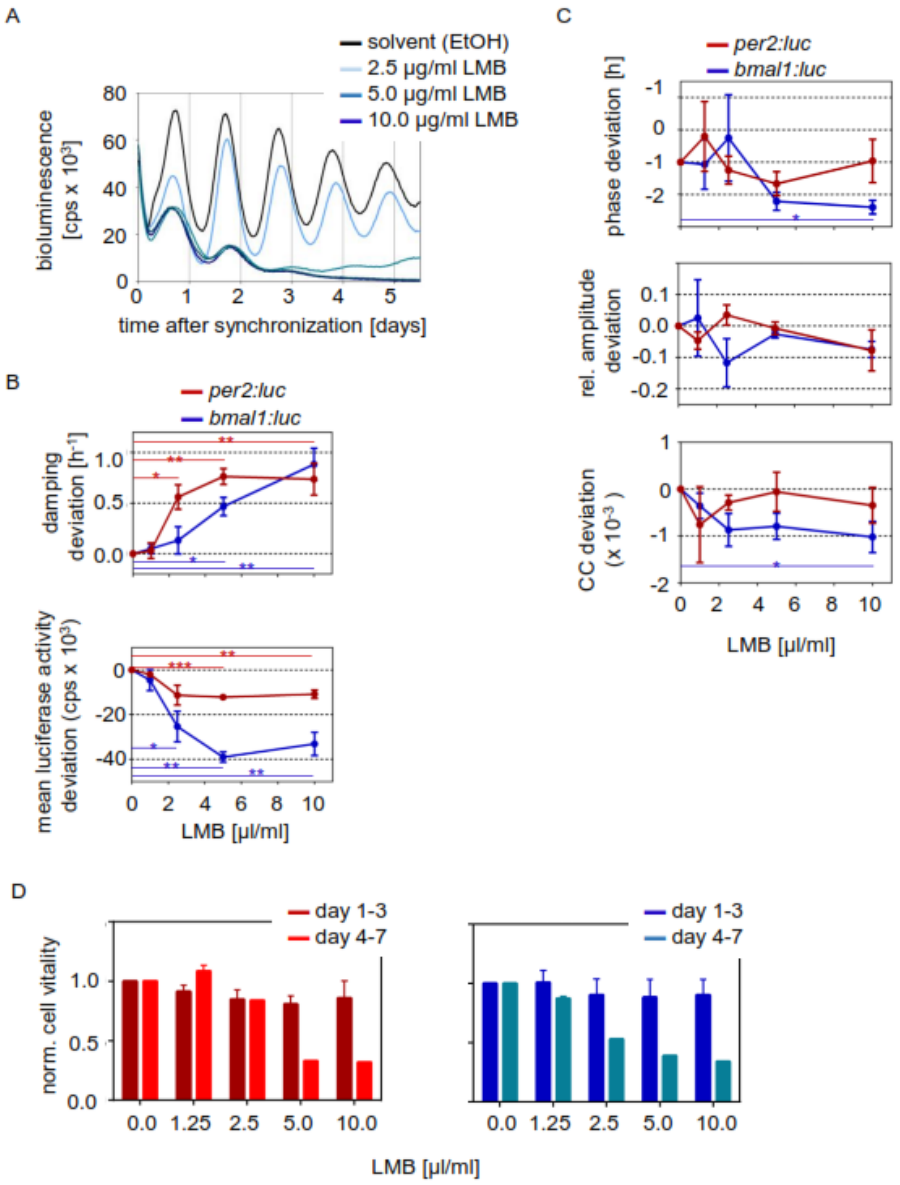


**Suppl. figure A1.2: Pharmacological inhibition of nuclear export lengthens the circadian period in U-2 OS reporter cells.** Cells, constitutively expressing either *bmal1*- (*bmal1:luc*, blue) or *per2*- (*per2:luc*, red) promoter-driven luciferase were treated with solvent (black) or the pharmacological inhibitor leptomycin B (LMB) after synchronization with 1 µM dexamethasone. Treatments were applied at indicated LMB concentrations and monitored for up to six days. A) Depicted are raw data of representative time series of *bmal1:luc* U-2 OS cells. B and C) Quantification of different altered parameters. Increasing concentrations of LMB lead to higher damping of the amplitude per 24 h and reduced mean bioluminescence (C). Phase, amplitude and CC were not consistently altered. D) Resazurin cell vitality measurements of either *per2:luc* or *bmal1:luc* U-2 OS reporter cells after pharmacological inhibition of nuclear export (error bars = SEM, $n_{B \text{ and } D}$ = 3 to 5 individual recordings; student's t-test: * $p < 0.05$, ** $p < 0.01$, *** $p < 0.001$).

## A 1.3 Alphabetical list of GE Dharmacon constructs used in the RNAi-screen

**Suppl. table A 1.1: Alphabetical list of GE Dharmacon constructs used in the RNAi-screen**. Listed are the genes as well as the ordering numbers at GE Dharmacon of each tested shRNA and controls. (The internal experimental labeling number of the construct is depicted in brackets). * sh*ranbp11* constructs were transduced twice on each plate

| targeted transcript | RNAi construct 1 | RNAi construct 2 | RNAi construct 3 |
|---|---|---|---|
| non-silencing shRNA | RHS4346 | | |
| *fbxl3* (pos. ctrl) | V2LHS_16078 (48) | V2LHS_254986 (51) | V2LHS_16077 (53) |
| *aladin* | V2LHS_266522 (74) | V3LHS_64215 (75) | V3LHS_344262 (78) |
| *cg1* | V2LHS_86275 (127) | V2LHS_86273 (143) | V2LHS_86271 (151) |
| *elys* | V2LHS_269315 (140) | V2LHS_230423 (147) | V2LHS_96564 (149) |
| *gle1* | V2LHS_235540 (129) | V2LHS_131974 (142) | V2LHS_131979 (165) |
| *kpna1* | V2LHS_133758 (104) | | |
| *kpna2* | V2LHS_238648 (92) | V2LHS_133767 (107) | V3LHS_642155 (121) |
| *kpna3* | V2LHS_133769 (85) | V2LHS_133768 (98) | V2LHS_133770 (100) |
| *kpna4* | V2LHS_133779 (111) | V2LHS_177457 (114) | V2LHS_222497 (119) |
| *kpna5* | V2LHS_7366 (88) | V2LHS_133785 (95) | V2LHS_133784 (110) |
| *kpna6* | V2LHS_50784 (105) | V2LHS_50786 (113) | V2LHS_50781 (117) |
| *kpna7* | V2LHS_61788 (102) | V2LHS_61787 (109) | V2LHS_61789 (116) |
| *kpnb1* | V2LHS_210254 (18) | V2LHS_12254 (20) | V3LHS_353241 (22) |
| *ndc1* | V2LHS_155633 (132) | V2LHS_155631 (133) | V2LHS_155635 (160) |
| *nup35* | V2LHS_42042 (144) | V2LHS_42045 (150) | V3LHS_364367 (175) |
| *nup37* | V2LHS_98824 (123) | V2LHS_98821 (131) | V2LHS_98826 (136) |
| *nup43* | V2LHS_157037 (134) | V2LHS_157038 (152) | V2LHS_157040 (161) |
| *nup50* | V2LHS_205554 (29) | V2LHS_213803 (31) | V3LHS_309548 (47) |
| *nup54* | V2LHS_154330 (5) | V3LHS_392348 (16) | |
| *nup62* | V2LHS_3885 (1) | V2LHS_244194 (2) | V3LHS_644939 (9) |
| *nup85* | V2LHS_158121 (139) | V3LHS_305916 (186) | V2LHS_158122 (156) |

| targeted transcript | RNAi construct 1 | RNAi construct 2 | RNAi construct 3 |
|---|---|---|---|
| *nup88* | V3LHS_374086 (82) | | |
| *nup93* | V2LHS_259822 (126) | V2LHS_79283 (153) | V2LHS_79281 (166) |
| *nup98* | V2LHS_191635 (3) | V2LHS_36517 (6) | V2LHS_36521 (8) |
| *nup107* | V2LHS_34273 (154) | V2LHS_34277 (167) | V3LHS_326974 (181) |
| *nup133* | V2LHS_156421 (157) | V2LHS_156420 (163) | V3LHS_325201 (178) |
| *nup153* | V2LHS_49964 (30) | V2LHS_49963 (36) | V2LHS_49962 (38) |
| *nup155* | V2LHS_27551 (67) | V3LHS_352430 (80) | V3LHS_352428 (81) |
| *nup160* | V2LHS_268280 (169) | V2LHS_101965 (172) | |
| *nup188* | V2LHS_44506 (52) | V2LHS_44504 (60) | V2LHS_44507 (70) |
| *nup205* | V2LHS_139802 (128) | V2LHS_139799 (135) | V2LHS_139800 (141) |
| *nup210* | V2LHS_175870 (130) | V2LHS_219299 (148) | V2LHS_176868 (159) |
| *nup214* | V2LHS_18093 (27) | V2LHS_18091 (35) | |
| *nupl1* | V2LHS_95333 (39) | V3LHS_349052 (42) | V3LHS_349050 (45) |
| *pom121* | V2LHS_95601 (146) | V2LHS_95600 (162) | V3LHS_305002 (179) |
| *rae1* | V2LHS_27966 (101) | V2LHS_27964 (103) | V2LHS_27965 (118) |
| *ran* | V2LHS_253868 (90) | V2LHS_5724 (93) | V2LHS_252754 (97) |
| *ranbp1* | V2LHS_171224 (71) | V3LHS_374516 (77) | V3LHS_374513 (79) |
| *ranbp2* | V3LHS_365485 (41) | V3LHS_365488 (43) | V3LHS_365484 (44) |
| *ranbp3* | V2LHS_27819 (61) | | |
| *ranbp4* | V3LHS_345191 (83) | V3LHS_345190 (84) | |
| *ranbp5* | V2LHS_237915 (65) | V2LHS_133795 (69) | V2LHS_133797 (73) |
| *ranbp6* | V2LHS_188280 (56) | V2LHS_277663 (58) | V2LHS_192540 (59) |
| *ranbp7* | V2LHS_199621 (54) | V2LHS_5807 (62) | V2LHS_198630 (68) |
| *ranbp8* | V2LHS_198260 (49) | V2LHS_5805 (55) | V2LHS_198074 (63) |
| *ranbp9* | V2LHS_68158 (137) | V2LHS_68191 (145) | V2LHS_68195 (168) |
| *ranbp10* | V2LHS_13649 (50) | V2LHS_139653 (64) | V2LHS_362782 (76) |
| *ranbp11** | V2LHS_115479 (57/94) | V2LHS_115481 (66/106) | V2LHS_115478 (72/115) |

| targeted transcript | RNAi construct 1 | RNAi construct 2 | RNAi construct 3 |
|---|---|---|---|
| *ranbp13* | V2LHS_258083 (89) | V2LHS_79451 (99) | |
| *ranbp16* | V2LHS_209206 (91) | V2LHS_215507 (96) | V3LHS_329322 (122) |
| *ranbp17* | V2LHS_116278 (86) | V2LHS_116276 (87) | V2LHS_116277 (108) |
| *rangef* | V2LHS_200037 (158) | V3LHS_308276 (184) | V3LHS_308274 (180) |
| *sec13* | V2LHS_265275 (164) | V3LHS_406089 (173) | V3LHS_406090 (174) |
| *seh1* | V2LHS_99249 (124) | V3LHS_402372 (182) | V3LHS_318551 (183) |
| *tnpo1* | V2LHS_133786 (32) | V2LHS_133788 (37) | V2LHS_133789 (40) |
| *tnpo2* | V3LHS_321424 (46) | | |
| *tnpo3* | V2LHS_42869 (25) | V2LHS_42868 (33) | |
| *tpr* | V2LHS_171500 (26) | V2LHS_171504 (34) | V2LHS_17150 (28) |
| *xpo1* | V2LHS_219111 (4) | V2LHS_172057 (17) | V2LHS_219836 (19) |
| *xpo4* | V2LHS_81441 (112) | V2LHS_81437 (120) | |
| *xpo5* | V2LHS_212431 (125) | | |
| *xpo6* | V2LHS_204891 (155) | V3LHS_386492 (177) | V3LHS_386496 (185) |
| *xpot* | V2LHS_284613 (138) | | |

## A1.4 Complete list of RNAi-screen parameter data

**Suppl. table A1.2: Complete list of RNAi-screen parameter data listed in alphabetical order of targeted transcripts**. Each of the six ($n_{sh\textit{ranbp11}} = 12$) individual time series per construct are listed. Note: ns control and positive control data are listed on top (mean = mean bioluminescence)

| targeted transcripts | period [h] | phase [h] | relative amplitude | damping [$h^{-1}$] | CC | mean [cps] | run | internal construct # |
|---|---|---|---|---|---|---|---|---|
| *ns control* | 23.8 | 18.6 | 0.3 | 1.9 | 0.98 | 38636 | 1 | |
| *ns control* | 23.2 | 19.2 | 0.3 | 2.2 | 0.98 | 48657 | 1 | |
| *ns control* | 24.5 | 20.4 | 0.2 | 2.6 | 0.94 | 31621 | 1 | |
| *ns control* | 23.3 | 19.4 | 0.3 | 2.3 | 0.98 | 39498 | 1 | |
| *ns control* | 26.2 | 18.1 | 0.1 | 1.1 | 0.68 | 36465 | 1 | |
| *ns control* | 25.7 | 21.5 | 0.1 | 0.9 | 0.77 | 32000 | 1 | |
| *ns control* | 23.4 | 18.1 | 0.3 | 1.7 | 0.98 | 40537 | 1 | |
| *ns control* | 23.5 | 17.7 | 0.3 | 1.7 | 0.98 | 38675 | 1 | |
| *ns control* | 24.2 | 18.8 | 0.2 | 1.9 | 0.97 | 41689 | 1 | |
| *ns control* | 23.3 | 18.9 | 0.3 | 2.2 | 0.98 | 44589 | 1 | |
| *ns control* | 23 | 19.1 | 0.3 | 2.3 | 0.98 | 46396 | 1 | |
| *ns control* | 25.6 | 2 | 0.1 | 0.9 | 0.73 | 32697 | 1 | |
| *ns control* | 23.8 | 18.7 | 0.2 | 2.1 | 0.97 | 33330 | 1 | |
| *ns control* | 27.7 | 16.7 | 0.1 | 0.9 | 0.83 | 33238 | 1 | |
| *ns control* | 24.5 | 18.8 | 0.2 | 1.8 | 0.97 | 41024 | 1 | |
| *ns control* | 23.2 | 19.7 | 0.3 | 2.2 | 0.98 | 44981 | 1 | |
| *ns control* | 23 | 19.7 | 0.3 | 2.1 | 0.98 | 49667 | 1 | |
| *ns control* | 24.6 | 19.3 | 0.2 | 2 | 0.97 | 47414 | 1 | |
| *ns control* | 24.1 | 18.8 | 0.2 | 2.1 | 0.98 | 34074 | 1 | |
| *ns control* | 28.3 | 15.6 | 0.1 | 1 | 0.81 | 30811 | 1 | |
| *ns control* | 24.4 | 18.9 | 0.2 | 2.1 | 0.96 | 38421 | 1 | |
| *ns control* | 23.8 | 18.7 | 0.3 | 1.8 | 0.98 | 48976 | 1 | |
| *ns control* | 38.1 | 23.2 | 0 | 0.5 | 0.76 | 36109 | 1 | |
| *ns control* | 24 | 18.2 | 0.4 | 1.8 | 0.98 | 50861 | 1 | |
| *ns control* | 23.8 | 18.4 | 0.3 | 1.7 | 0.99 | 52175 | 1 | |
| *ns control* | 23.4 | 17.6 | 0.3 | 1.6 | 0.98 | 46544 | 1 | |
| *ns control* | 23.8 | 18 | 0.4 | 1.7 | 0.98 | 55353 | 1 | |
| *ns control* | 24.3 | 19.6 | 0.2 | 1.9 | 0.98 | 42184 | 1 | |
| *ns control* | 23.6 | 18.6 | 0.3 | 2 | 0.97 | 45906 | 1 | |
| *ns control* | 24.1 | 18.6 | 0.3 | 1.8 | 0.98 | 50022 | 1 | |
| *ns control* | 24 | 18.6 | 0.3 | 2.1 | 0.97 | 43611 | 1 | |
| *ns control* | 27 | 18.2 | 0.1 | 0.9 | 0.78 | 34665 | 1 | |
| *ns control* | 27.3 | 17.7 | 0.1 | 0.9 | 0.78 | 38188 | 1 | |
| *ns control* | 24.3 | 18.6 | 0.3 | 1.9 | 0.97 | 42627 | 1 | |
| *ns control* | 23.5 | 17.7 | 0.3 | 1.8 | 0.97 | 41399 | 1 | |
| *ns control* | 24.8 | 17.8 | 0.3 | 1.6 | 0.96 | 41636 | 1 | |
| *ns control* | 23.9 | 19 | 0.3 | 2.1 | 0.98 | 44440 | 1 | |
| *ns control* | 24 | 17.9 | 0.3 | 1.9 | 0.97 | 44356 | 1 | |
| *ns control* | 26.6 | 17.8 | 0.1 | 1 | 0.8 | 40412 | 1 | |
| *ns control* | 24.3 | 18.9 | 0.3 | 1.9 | 0.98 | 47513 | 1 | |
| *ns control* | 23.5 | 17.9 | 0.3 | 1.8 | 0.98 | 48392 | 1 | |
| *ns control* | 24.1 | 18.2 | 0.3 | 1.8 | 0.98 | 55815 | 1 | |
| *ns control* | 24.1 | 19.7 | 0.2 | 2.1 | 0.97 | 35052 | 1 | |
| *ns control* | 27.6 | 22.6 | 0 | 0.9 | 0.61 | 37222 | 1 | |
| *ns control* | 23.7 | 18.4 | 0.3 | 1.7 | 0.98 | 44012 | 1 | |
| *ns control* | 24.3 | 18.7 | 0.3 | 1.8 | 0.98 | 46004 | 1 | |
| *ns control* | 23.6 | 18 | 0.3 | 1.8 | 0.98 | 44617 | 1 | |
| *ns control* | 23.9 | 18 | 0.3 | 1.8 | 0.98 | 53792 | 1 | |
| *ns control* | 24.7 | 7.7 | 0.4 | 1.4 | 0.98 | 56388 | 2 | |
| *ns control* | 24.6 | 7.2 | 0.5 | 1.4 | 0.99 | 53125 | 2 | |
| *ns control* | 24.3 | 9.8 | 0.3 | 1.4 | 0.98 | 57227 | 2 | |
| *ns control* | 24.3 | 9.3 | 0.4 | 1.4 | 0.96 | 40275 | 2 | |
| *ns control* | 24.4 | 8.7 | 0.4 | 1.4 | 0.95 | 41043 | 2 | |
| *ns control* | 24.5 | 6.5 | 0.5 | 1.4 | 0.98 | 39336 | 2 | |
| *ns control* | 24.5 | 8.2 | 0.4 | 1.5 | 0.99 | 54390 | 2 | |
| *ns control* | 24.5 | 8.9 | 0.4 | 1.5 | 0.99 | 50987 | 2 | |
| *ns control* | 24.6 | 6.7 | 0.5 | 1.4 | 0.98 | 48179 | 2 | |
| *ns control* | 24.1 | 8.4 | 0.4 | 1.4 | 0.93 | 44001 | 2 | |
| *ns control* | 24.8 | 6.6 | 0.6 | 1.4 | 0.98 | 41289 | 2 | |
| *ns control* | 24.4 | 6.9 | 0.4 | 1.4 | 0.98 | 43958 | 2 | |
| *ns control* | 24.6 | 7 | 0.5 | 1.5 | 0.98 | 47940 | 2 | |
| *ns control* | 24.5 | 8.4 | 0.4 | 1.4 | 0.99 | 49693 | 2 | |

| targeted transcripts | period [h] | phase [h] | relative amplitude | damping [h$^{-1}$] | CC | mean [cps] | run | internal construct # |
|---|---|---|---|---|---|---|---|---|
| *ns control* | 24.6 | 6.1 | 0.6 | 1.4 | 0.98 | 47666 | 2 | |
| *ns control* | 24.7 | 7.8 | 0.4 | 1.5 | 0.98 | 63179 | 2 | |
| *ns control* | 24.6 | 8.3 | 0.4 | 1.5 | 0.99 | 58225 | 2 | |
| *ns control* | 24.2 | 8.2 | 0.3 | 1.5 | 0.98 | 57703 | 2 | |
| *ns control* | 24.7 | 8.3 | 0.4 | 1.5 | 0.99 | 51160 | 2 | |
| *ns control* | 24.5 | 8.6 | 0.4 | 1.5 | 0.99 | 46993 | 2 | |
| *ns control* | 24.5 | 6.4 | 0.5 | 1.4 | 0.99 | 44117 | 2 | |
| *ns control* | 24.8 | 6.3 | 0.6 | 1.5 | 0.98 | 43220 | 2 | |
| *ns control* | 24.8 | 7.6 | 0.5 | 1.5 | 0.97 | 43810 | 2 | |
| *ns control* | 24.5 | 7.1 | 0.5 | 1.5 | 0.97 | 43584 | 2 | |
| *ns control* | 24.8 | 6.4 | 0.7 | 1.5 | 0.99 | 44576 | 2 | |
| *ns control* | 24.9 | 7 | 0.6 | 1.5 | 0.99 | 43126 | 2 | |
| *ns control* | 24.6 | 6.6 | 0.6 | 1.5 | 0.99 | 43802 | 2 | |
| *ns control* | 24.6 | 7.4 | 0.5 | 1.5 | 0.99 | 47609 | 2 | |
| *ns control* | 24.7 | 6.8 | 0.5 | 1.4 | 0.99 | 47484 | 2 | |
| *ns control* | 24 | 8.8 | 0.4 | 1.5 | 0.99 | 51302 | 2 | |
| *ns control* | 24.7 | 7.1 | 0.5 | 1.5 | 0.98 | 41757 | 2 | |
| *ns control* | 25.1 | 6.3 | 0.6 | 1.4 | 0.99 | 37003 | 2 | |
| *ns control* | 24.5 | 7.7 | 0.4 | 1.5 | 0.98 | 42196 | 2 | |
| *ns control* | 24.3 | 6.6 | 0.6 | 1.4 | 0.99 | 37082 | 2 | |
| *ns control* | 24.3 | 7.8 | 0.4 | 1.5 | 0.99 | 37715 | 2 | |
| *ns control* | 24.1 | 6.4 | 0.6 | 1.4 | 0.99 | 37585 | 2 | |
| *ns control* | 24.3 | 6.6 | 0.5 | 1.5 | 0.99 | 38454 | 2 | |
| *ns control* | 24.3 | 8.8 | 0.4 | 1.5 | 0.99 | 39108 | 2 | |
| *ns control* | 24 | 8.3 | 0.4 | 1.4 | 0.99 | 37508 | 2 | |
| *ns control* | 24.4 | 7.5 | 0.5 | 1.5 | 0.99 | 53633 | 2 | |
| *ns control* | 24.5 | 8.1 | 0.4 | 1.4 | 0.99 | 52664 | 2 | |
| *ns control* | 24.2 | 8.2 | 0.4 | 1.5 | 0.99 | 52371 | 2 | |
| *ns control* | 24.5 | 7.8 | 0.4 | 1.5 | 0.99 | 48856 | 2 | |
| *ns control* | 24.8 | 6.7 | 0.6 | 1.4 | 0.99 | 43652 | 2 | |
| *ns control* | 24.7 | 6.1 | 0.6 | 1.4 | 0.99 | 45955 | 2 | |
| *ns control* | 24.1 | 8.5 | 0.4 | 1.5 | 0.99 | 53634 | 2 | |
| *ns control* | 24.7 | 7 | 0.5 | 1.4 | 0.99 | 49420 | 2 | |
| *ns control* | 24.3 | 8.2 | 0.4 | 1.5 | 0.99 | 53196 | 2 | |
| *fbxl3* | 28.8 | 17.7 | 0.2 | 2.1 | 0.96 | 41381 | 1 | 48 |
| *fbxl3* | 26.2 | 20.1 | 0.1 | 3.5 | 0.78 | 28514 | 1 | 48 |
| *fbxl3* | 27.5 | 1.7 | 0.1 | 0.9 | 0.63 | 35127 | 1 | 48 |
| *fbxl3* | 27.3 | 8.5 | 0.4 | 1.6 | 0.99 | 55699 | 2 | 48 |
| *fbxl3* | 27.5 | 7.3 | 0.4 | 1.6 | 0.99 | 51341 | 2 | 48 |
| *fbxl3* | 26.9 | 7.9 | 0.4 | 1.5 | 0.99 | 49479 | 2 | 48 |
| *fbxl3* | 31.2 | 17.3 | 0.1 | 1.8 | 0.9 | 31012 | 1 | 51 |
| *fbxl3* | -90025 | 18 | 159.5 | 55.4 | 0.76 | 34979 | 1 | 51 |
| *fbxl3* | 30.6 | 17.9 | 0.1 | 1.6 | 0.89 | 32601 | 1 | 51 |
| *fbxl3* | 29.2 | 8.6 | 0.3 | 1.5 | 0.97 | 36048 | 2 | 51 |
| *fbxl3* | 28.8 | 8 | 0.3 | 1.6 | 0.99 | 35726 | 2 | 51 |
| *fbxl3* | 29 | 6.9 | 0.4 | 1.6 | 0.99 | 33945 | 2 | 51 |
| *fbxl3* | 27.2 | 3.3 | 0.1 | 1.7 | 0.35 | 45186 | 1 | 53 |
| *fbxl3* | 30.7 | 16.2 | 0.2 | 2.1 | 0.94 | 63874 | 1 | 53 |
| *fbxl3* | 31.1 | 16.7 | 0.1 | 1.6 | 0.93 | 68016 | 1 | 53 |
| *fbxl3* | 29.1 | 8.1 | 0.3 | 1.6 | 0.95 | 50326 | 2 | 53 |
| *fbxl3* | 29.1 | 7.1 | 0.4 | 1.7 | 0.98 | 50126 | 2 | 53 |
| *fbxl3* | 28.6 | 6.4 | 0.4 | 1.7 | 0.99 | 49443 | 2 | 53 |
| *aladin* | 23.9 | 18.4 | 0.2 | 1.9 | 0.97 | 57884 | 1 | 74 |
| *aladin* | 24 | 18.2 | 0.2 | 1.9 | 0.97 | 66459 | 1 | 74 |
| *aladin* | 24.2 | 18.4 | 0.2 | 1.8 | 0.96 | 61997 | 1 | 74 |
| *aladin* | 24.8 | 8.6 | 0.5 | 1.5 | 0.98 | 62971 | 2 | 74 |
| *aladin* | 24.7 | 8 | 0.5 | 1.5 | 0.99 | 61976 | 2 | 74 |
| *aladin* | 24.6 | 7.6 | 0.5 | 1.5 | 0.99 | 58545 | 2 | 74 |
| *aladin* | 23.9 | 18.8 | 0.2 | 1.6 | 0.97 | 53174 | 1 | 75 |
| *aladin* | 23.2 | 17.8 | 0.3 | 1.4 | 0.97 | 46287 | 1 | 75 |
| *aladin* | 23.9 | 18.6 | 0.3 | 1.6 | 0.98 | 56632 | 1 | 75 |
| *aladin* | 24.6 | 6.2 | 0.5 | 1.5 | 0.98 | 49214 | 2 | 75 |
| *aladin* | 25.1 | 7.7 | 0.4 | 1.5 | 0.98 | 50921 | 2 | 75 |
| *aladin* | 24.3 | 7.7 | 0.4 | 1.5 | 0.97 | 52883 | 2 | 75 |
| *aladin* | 30.8 | 17.5 | 0.1 | 22 | 0.85 | 36750 | 1 | 78 |
| *aladin* | 23.2 | 20 | 0.1 | 2.2 | 0.86 | 50862 | 1 | 78 |
| *aladin* | 22.9 | 20.8 | 0.1 | 3.2 | 0.89 | 66819 | 1 | 78 |
| *aladin* | 30.4 | 12.7 | 0.2 | 2.2 | 0.96 | 55013 | 2 | 78 |
| *aladin* | 25.3 | 7.3 | 0.4 | 1.6 | 0.97 | 51487 | 2 | 78 |
| *aladin* | 25.1 | 7.3 | 0.5 | 1.5 | 0.97 | 50387 | 2 | 78 |
| *cg1* | 23.8 | 18.8 | 0.4 | 2 | 0.98 | 36469 | 1 | 127 |
| *cg1* | 26.2 | 17.8 | 0.2 | 1.1 | 0.79 | 31931 | 1 | 127 |

| targeted transcripts | period [h] | phase [h] | relative amplitude | damping [h$^{-1}$] | CC | mean [cps] | run | internal construct # |
|---|---|---|---|---|---|---|---|---|
| *cg1* | 23.5 | 18.2 | 0.4 | 1.7 | 0.97 | 35874 | 1 | 127 |
| *cg1* | 24.4 | 7.2 | 0.5 | 1.5 | 0.98 | 33388 | 2 | 127 |
| *cg1* | 24.7 | 6.5 | 0.6 | 1.5 | 0.99 | 30385 | 2 | 127 |
| *cg1* | 24.5 | 6.6 | 0.5 | 1.4 | 0.99 | 32364 | 2 | 127 |
| *cg1* | 23 | 19 | 0.3 | 2 | 0.95 | 52730 | 1 | 143 |
| *cg1* | 24.8 | 17.5 | 0.2 | 1.5 | 0.75 | 41413 | 1 | 143 |
| *cg1* | 27.1 | 16.8 | 0.1 | 0.8 | 0.71 | 43584 | 1 | 143 |
| *cg1* | 23.9 | 7.2 | 0.6 | 1.6 | 0.99 | 49198 | 2 | 143 |
| *cg1* | 24 | 8.6 | 0.4 | 1.6 | 0.99 | 53368 | 2 | 143 |
| *cg1* | 23.7 | 8.9 | 0.4 | 1.5 | 0.98 | 55562 | 2 | 143 |
| *cg1* | 27 | 18.5 | 0.1 | 0.8 | 0.83 | 49943 | 1 | 151 |
| *cg1* | 27.9 | 16.2 | 0.1 | 0.8 | 0.68 | 45634 | 1 | 151 |
| *cg1* | 27.7 | 16.4 | 0.1 | 1 | 0.75 | 47230 | 1 | 151 |
| *cg1* | 23.8 | 9.1 | 0.3 | 1.3 | 0.99 | 50189 | 2 | 151 |
| *cg1* | 24.9 | 6.7 | 0.5 | 1.4 | 0.99 | 43503 | 2 | 151 |
| *cg1* | 24.3 | 8 | 0.4 | 1.4 | 0.99 | 46527 | 2 | 151 |
| *elys* | 26.7 | 20.7 | 0 | 0.7 | 0.64 | 52576 | 1 | 140 |
| *elys* | 25 | 19.2 | 0.2 | 3 | 0.94 | 77441 | 1 | 140 |
| *elys* | 23.5 | 19.8 | 0.2 | 3.1 | 0.92 | 85772 | 1 | 140 |
| *elys* | 25.6 | 7.7 | 0.4 | 1.7 | 0.99 | 59529 | 2 | 140 |
| *elys* | 25.5 | 8.7 | 0.3 | 1.7 | 0.99 | 62536 | 2 | 140 |
| *elys* | 25.5 | 8 | 0.3 | 1.8 | 0.99 | 60560 | 2 | 140 |
| *elys* | 25 | 19.3 | 0.2 | 3.6 | 0.97 | 58141 | 1 | 147 |
| *elys* | 24.3 | 18.8 | 0.2 | 2 | 0.97 | 57616 | 1 | 147 |
| *elys* | 25 | 18.8 | 0.2 | 2.2 | 0.97 | 69371 | 1 | 147 |
| *elys* | 25.4 | 7.7 | 0.4 | 1.6 | 1 | 61435 | 2 | 147 |
| *elys* | 25.4 | 8.6 | 0.4 | 1.6 | 1 | 62647 | 2 | 147 |
| *elys* | 25.3 | 9 | 0.3 | 1.6 | 0.99 | 63731 | 2 | 147 |
| *elys* | 24.9 | 18.7 | 0.2 | 2.5 | 0.96 | 68420 | 1 | 149 |
| *elys* | 27.4 | 19.6 | 0.1 | 0.8 | 0.67 | 42814 | 1 | 149 |
| *elys* | 27.2 | 20.8 | 0.1 | 0.8 | 0.69 | 51067 | 1 | 149 |
| *elys* | 25 | 9.2 | 0.3 | 1.9 | 0.96 | 59647 | 2 | 149 |
| *elys* | 25.1 | 9.8 | 0.3 | 2.1 | 0.99 | 60364 | 2 | 149 |
| *elys* | 25.2 | 8.1 | 0.3 | 1.8 | 0.99 | 54444 | 2 | 149 |
| *gle1* | 23.3 | 18.5 | 0.3 | 2.9 | 0.97 | 31290 | 1 | 129 |
| *gle1* | 22.6 | 18.5 | 0.3 | 2.3 | 0.98 | 34326 | 1 | 129 |
| *gle1* | 23.2 | 18 | 0.3 | 2.4 | 0.97 | 38043 | 1 | 129 |
| *gle1* | 24 | 7.8 | 0.4 | 1.5 | 0.99 | 32089 | 2 | 129 |
| *gle1* | 24 | 7.5 | 0.5 | 1.5 | 0.99 | 27991 | 2 | 129 |
| *gle1* | 23.8 | 7.8 | 0.4 | 1.5 | 0.99 | 28367 | 2 | 129 |
| *gle1* | 22.7 | 19.8 | 0.3 | 1.6 | 0.97 | 35667 | 1 | 142 |
| *gle1* | 27.5 | 18.7 | 0.1 | 0.9 | 0.68 | 28521 | 1 | 142 |
| *gle1* | 25.8 | 23.6 | 0.1 | 0.9 | 0.62 | 25808 | 1 | 142 |
| *gle1* | 23.9 | 7.3 | 0.5 | 1.4 | 0.99 | 39058 | 2 | 142 |
| *gle1* | 23.8 | 6.7 | 0.5 | 1.4 | 0.99 | 36958 | 2 | 142 |
| *gle1* | 23.7 | 6.9 | 0.5 | 1.4 | 0.99 | 39312 | 2 | 142 |
| *gle1* | 26.8 | 19.5 | 0.1 | 0.9 | 0.63 | 38507 | 1 | 165 |
| *gle1* | 23.2 | 18.5 | 0.3 | 1.8 | 0.98 | 46110 | 1 | 165 |
| *gle1* | 24.9 | 19.5 | 0.2 | 1.6 | 0.72 | 38453 | 1 | 165 |
| *gle1* | 24.4 | 6.8 | 0.5 | 1.5 | 0.99 | 45843 | 2 | 165 |
| *gle1* | 24.3 | 7.7 | 0.5 | 1.5 | 0.99 | 45651 | 2 | 165 |
| *gle1* | 23.7 | 8.1 | 0.4 | 1.5 | 0.99 | 47001 | 2 | 165 |
| *kpna1* | 23.2 | 19 | 0.3 | 1.7 | 0.98 | 53013 | 1 | 104 |
| *kpna1* | 23.3 | 18.7 | 0.3 | 1.7 | 0.98 | 52481 | 1 | 104 |
| *kpna1* | 23.2 | 18.7 | 0.3 | 1.6 | 0.98 | 54877 | 1 | 104 |
| *kpna1* | 24.3 | 8.1 | 0.5 | 1.4 | 0.99 | 45659 | 2 | 104 |
| *kpna1* | 24.4 | 9 | 0.5 | 1.4 | 0.99 | 48129 | 2 | 104 |
| *kpna1* | 24.2 | 8.3 | 0.4 | 1.5 | 0.99 | 49698 | 2 | 104 |
| *kpna2* | 23.2 | 19.4 | 0.3 | 1.9 | 0.98 | 65398 | 1 | 107 |
| *kpna2* | 23.1 | 19.1 | 0.4 | 1.7 | 0.98 | 62524 | 1 | 107 |
| *kpna2* | 23.4 | 18.9 | 0.4 | 1.6 | 0.98 | 68478 | 1 | 107 |
| *kpna2* | 24.4 | 7.4 | 0.5 | 1.5 | 0.98 | 51358 | 2 | 107 |
| *kpna2* | 24.4 | 7.9 | 0.5 | 1.5 | 0.99 | 51018 | 2 | 107 |
| *kpna2* | 24.1 | 7.5 | 0.4 | 1.5 | 0.99 | 52927 | 2 | 107 |
| *kpna2* | 22.5 | 19.6 | 0.3 | 1.9 | 0.97 | 52886 | 1 | 121 |
| *kpna2* | 22.8 | 18.9 | 0.3 | 1.6 | 0.98 | 44556 | 1 | 121 |
| *kpna2* | 23 | 19 | 0.3 | 1.7 | 0.98 | 55667 | 1 | 121 |
| *kpna2* | 23.8 | 8.8 | 0.5 | 1.5 | 0.99 | 47523 | 2 | 121 |
| *kpna2* | 23.8 | 8.9 | 0.4 | 1.5 | 0.99 | 45444 | 2 | 121 |
| *kpna2* | 23.6 | 9.5 | 0.4 | 1.5 | 0.99 | 51090 | 2 | 121 |
| *kpna2* | 22.1 | 18.2 | 0.3 | 1.9 | 0.98 | 45923 | 1 | 92 |
| *kpna2* | 23.2 | 18.9 | 0.2 | 1.6 | 0.85 | 45024 | 1 | 92 |

| targeted transcripts | period [h] | phase [h] | relative amplitude | damping [h$^{-1}$] | CC | mean [cps] | run | internal construct # |
|---|---|---|---|---|---|---|---|---|
| *kpna2* | 23.2 | 18.9 | 0.2 | 2.5 | 0.69 | 39757 | 1 | 92 |
| *kpna2* | 24 | 7.4 | 0.3 | 1.5 | 0.98 | 59104 | 2 | 92 |
| *kpna2* | 23.9 | 7.8 | 0.4 | 1.4 | 0.99 | 54811 | 2 | 92 |
| *kpna2* | 25 | 6.5 | 0.4 | 1.2 | 0.97 | 54439 | 2 | 92 |
| *kpna3* | 23.4 | 19.5 | 0.2 | 1.9 | 0.98 | 61694 | 1 | 100 |
| *kpna3* | 22.3 | 20.7 | 0.2 | 1.7 | 0.97 | 64846 | 1 | 100 |
| *kpna3* | 24 | 19.6 | 0.2 | 2.9 | 0.94 | 48171 | 1 | 100 |
| *kpna3* | 24.4 | 8.6 | 0.4 | 1.5 | 0.98 | 58970 | 2 | 100 |
| *kpna3* | 24.4 | 7.8 | 0.4 | 1.6 | 0.98 | 56038 | 2 | 100 |
| *kpna3* | 24.2 | 8.6 | 0.4 | 1.5 | 0.99 | 57618 | 2 | 100 |
| *kpna3* | 26 | 21.4 | 0.1 | 4.5 | 0.93 | 5152 | 1 | 85 |
| *kpna3* | 26.3 | 23.4 | 0 | 0.8 | 0.73 | 31786 | 1 | 85 |
| *kpna3* | 25.4 | 20.3 | 0.1 | 2.6 | 0.92 | 16513 | 1 | 85 |
| *kpna3* | 24.7 | 8.1 | 0.4 | 1.5 | 0.99 | 57207 | 2 | 85 |
| *kpna3* | 24.6 | 8.1 | 0.4 | 1.6 | 0.99 | 54028 | 2 | 85 |
| *kpna3* | 24.6 | 6.4 | 0.5 | 1.5 | 0.98 | 52363 | 2 | 85 |
| *kpna3* | 23.7 | 19.8 | 0.2 | 2.7 | 0.97 | 54630 | 1 | 98 |
| *kpna3* | 23.5 | 19.4 | 0.3 | 2 | 0.98 | 64566 | 1 | 98 |
| *kpna3* | 24.3 | 19.9 | 0.2 | 3 | 0.95 | 49463 | 1 | 98 |
| *kpna3* | 24.4 | 8.8 | 0.5 | 1.6 | 0.98 | 65529 | 2 | 98 |
| *kpna3* | 24.4 | 7.9 | 0.5 | 1.6 | 0.98 | 61692 | 2 | 98 |
| *kpna3* | 24.3 | 8.3 | 0.4 | 1.5 | 0.98 | 62754 | 2 | 98 |
| *kpna4* | 23.4 | 18.5 | 0.3 | 1.8 | 0.98 | 24071 | 1 | 111 |
| *kpna4* | 23.4 | 18.2 | 0.3 | 1.6 | 0.98 | 28564 | 1 | 111 |
| *kpna4* | 23.3 | 18.4 | 0.4 | 1.5 | 0.98 | 32648 | 1 | 111 |
| *kpna4* | 24.6 | 6.7 | 0.5 | 1.4 | 0.99 | 30667 | 2 | 111 |
| *kpna4* | 24.5 | 6.6 | 0.6 | 1.4 | 0.98 | 29977 | 2 | 111 |
| *kpna4* | 24.2 | 7.9 | 0.4 | 1.5 | 0.99 | 32941 | 2 | 111 |
| *kpna4* | 23.3 | 19.4 | 0.3 | 1.7 | 0.98 | 46889 | 1 | 114 |
| *kpna4* | 23 | 19.6 | 0.3 | 1.9 | 0.98 | 46103 | 1 | 114 |
| *kpna4* | 23.2 | 18.1 | 0.4 | 1.5 | 0.98 | 58677 | 1 | 114 |
| *kpna4* | 24.3 | 7.6 | 0.5 | 1.4 | 0.99 | 54180 | 2 | 114 |
| *kpna4* | 24.4 | 7.4 | 0.6 | 1.4 | 0.99 | 55593 | 2 | 114 |
| *kpna4* | 24.3 | 7.1 | 0.6 | 1.5 | 0.99 | 56158 | 2 | 114 |
| *kpna4* | 23.2 | 20.2 | 0.3 | 2 | 0.96 | 54090 | 1 | 119 |
| *kpna4* | 26.4 | 22.7 | 0 | 0.7 | 0.57 | 44447 | 1 | 119 |
| *kpna4* | 23.4 | 19.6 | 0.3 | 1.7 | 0.97 | 56699 | 1 | 119 |
| *kpna4* | 24.2 | 7.3 | 0.6 | 1.6 | 0.98 | 47492 | 2 | 119 |
| *kpna4* | 24.8 | 6.7 | 0.6 | 1.5 | 0.98 | 45240 | 2 | 119 |
| *kpna4* | 24.5 | 8.7 | 0.4 | 1.6 | 0.96 | 50045 | 2 | 119 |
| *kpna5* | 22.8 | 18.9 | 0.3 | 1.5 | 0.98 | 42745 | 1 | 110 |
| *kpna5* | 22.8 | 18.1 | 0.3 | 1.3 | 0.98 | 41740 | 1 | 110 |
| *kpna5* | 22.9 | 18.4 | 0.3 | 1.4 | 0.98 | 44914 | 1 | 110 |
| *kpna5* | 23.9 | 7.7 | 0.5 | 1.4 | 0.99 | 43171 | 2 | 110 |
| *kpna5* | 23.8 | 7.8 | 0.6 | 1.4 | 0.99 | 42072 | 2 | 110 |
| *kpna5* | 23.7 | 8.2 | 0.5 | 1.4 | 0.99 | 41773 | 2 | 110 |
| *kpna5* | 23.5 | 18.6 | 0.3 | 1.7 | 0.98 | 59131 | 1 | 88 |
| *kpna5* | 23.4 | 18.8 | 0.3 | 2 | 0.98 | 62183 | 1 | 88 |
| *kpna5* | 42.1 | 17.4 | 0 | 0.4 | 0.69 | 43827 | 1 | 88 |
| *kpna5* | 24.6 | 7.5 | 0.5 | 1.5 | 0.99 | 66521 | 2 | 88 |
| *kpna5* | 24.4 | 8.5 | 0.4 | 1.4 | 0.99 | 61218 | 2 | 88 |
| *kpna5* | 24.4 | 6.4 | 0.6 | 1.4 | 0.99 | 56273 | 2 | 88 |
| *kpna5* | 26.5 | 18.5 | 0.2 | 1.9 | 0.98 | 23724 | 1 | 95 |
| *kpna5* | 24.4 | 19.7 | 0.2 | 2.1 | 0.97 | 27738 | 1 | 95 |
| *kpna5* | 30.3 | 19 | 0.1 | 3.7 | 0.9 | 19106 | 1 | 95 |
| *kpna5* | 24.9 | 10.2 | 0.3 | 1.4 | 0.99 | 34232 | 2 | 95 |
| *kpna5* | 25 | 9.5 | 0.3 | 1.5 | 0.99 | 31949 | 2 | 95 |
| *kpna5* | 24.9 | 8.1 | 0.4 | 1.4 | 0.99 | 36136 | 2 | 95 |
| *kpna6* | 23.5 | 19.3 | 0.3 | 1.8 | 0.98 | 50485 | 1 | 105 |
| *kpna6* | 23.4 | 18.9 | 0.4 | 1.7 | 0.98 | 56315 | 1 | 105 |
| *kpna6* | 23.5 | 19 | 0.3 | 1.6 | 0.98 | 59573 | 1 | 105 |
| *kpna6* | 24.7 | 7.3 | 0.5 | 1.5 | 0.99 | 49197 | 2 | 105 |
| *kpna6* | 24.4 | 9.5 | 0.5 | 1.4 | 0.99 | 52420 | 2 | 105 |
| *kpna6* | 24.1 | 9.1 | 0.4 | 1.5 | 0.99 | 54748 | 2 | 105 |
| *kpna6* | 23.1 | 19 | 0.3 | 1.9 | 0.98 | 60565 | 1 | 113 |
| *kpna6* | 23.1 | 18.6 | 0.4 | 1.8 | 0.97 | 59060 | 1 | 113 |
| *kpna6* | 23.1 | 18.9 | 0.3 | 1.7 | 0.98 | 56618 | 1 | 113 |
| *kpna6* | 24.4 | 6.4 | 0.6 | 1.5 | 0.99 | 49768 | 2 | 113 |
| *kpna6* | 24.4 | 6.6 | 0.6 | 1.5 | 0.99 | 49766 | 2 | 113 |
| *kpna6* | 24.1 | 7.2 | 0.5 | 1.5 | 0.99 | 52149 | 2 | 113 |
| *kpna6* | 23.7 | 20 | 0.2 | 2.3 | 0.97 | 57711 | 1 | 117 |
| *kpna6* | 23.3 | 18.2 | 0.3 | 1.6 | 0.98 | 57024 | 1 | 117 |

| targeted transcripts | period [h] | phase [h] | relative amplitude | damping [h$^{-1}$] | CC | mean [cps] | run | internal construct # |
|---|---|---|---|---|---|---|---|---|
| *kpna6* | 23.6 | 18.9 | 0.3 | 1.7 | 0.98 | 66696 | 1 | 117 |
| *kpna6* | 24.3 | 8.9 | 0.4 | 1.5 | 0.99 | 57491 | 2 | 117 |
| *kpna6* | 24.6 | 7.1 | 0.5 | 1.4 | 0.99 | 54241 | 2 | 117 |
| *kpna6* | 24.6 | 6.6 | 0.5 | 1.5 | 0.99 | 53124 | 2 | 117 |
| *kpna7* | 23.8 | 19.2 | 0.3 | 1.6 | 0.98 | 64948 | 1 | 102 |
| *kpna7* | 23.7 | 19 | 0.3 | 1.6 | 0.99 | 68126 | 1 | 102 |
| *kpna7* | 24.4 | 19.8 | 0.3 | 1.7 | 0.97 | 63510 | 1 | 102 |
| *kpna7* | 24.8 | 8.8 | 0.4 | 1.4 | 0.99 | 61721 | 2 | 102 |
| *kpna7* | 24.6 | 9.3 | 0.5 | 1.4 | 0.99 | 57450 | 2 | 102 |
| *kpna7* | 24.7 | 6.6 | 0.5 | 1.4 | 0.98 | 56619 | 2 | 102 |
| *kpna7* | 23.5 | 18.8 | 0.3 | 1.9 | 0.98 | 60169 | 1 | 109 |
| *kpna7* | 23.4 | 17.7 | 0.4 | 1.5 | 0.97 | 57062 | 1 | 109 |
| *kpna7* | 23.4 | 18.6 | 0.4 | 1.8 | 0.98 | 61600 | 1 | 109 |
| *kpna7* | 24.7 | 6.4 | 0.6 | 1.5 | 0.99 | 47522 | 2 | 109 |
| *kpna7* | 24.6 | 7.6 | 0.5 | 1.5 | 0.99 | 49720 | 2 | 109 |
| *kpna7* | 24.4 | 7.2 | 0.5 | 1.5 | 0.99 | 49993 | 2 | 109 |
| *kpna7* | 23.5 | 18.9 | 0.3 | 1.6 | 0.98 | 54008 | 1 | 116 |
| *kpna7* | 23.3 | 18.7 | 0.3 | 1.5 | 0.98 | 51049 | 1 | 116 |
| *kpna7* | 23.6 | 18.4 | 0.3 | 1.5 | 0.98 | 57382 | 1 | 116 |
| *kpna7* | 23.9 | 8.3 | 0.4 | 1.3 | 0.99 | 49433 | 2 | 116 |
| *kpna7* | 24.1 | 8.9 | 0.5 | 1.3 | 0.99 | 51439 | 2 | 116 |
| *kpna7* | 23.9 | 9.1 | 0.4 | 1.3 | 0.99 | 52147 | 2 | 116 |
| *kpnb1* | 26.9 | 19.4 | 0.1 | 8.8 | 0.93 | 23990 | 1 | 18 |
| *kpnb1* | 26.4 | 19.9 | 0.1 | 10 | 0.93 | 28491 | 1 | 18 |
| *kpnb1* | 30 | 18.4 | 0.1 | 3.7 | 0.89 | 15067 | 1 | 18 |
| *kpnb1* | 26.6 | 8.7 | 0.1 | 2.5 | 0.96 | 61719 | 2 | 18 |
| *kpnb1* | 26.2 | 10.1 | 0.1 | 2.3 | 0.97 | 57842 | 2 | 18 |
| *kpnb1* | 27.2 | 7 | 0.1 | 2.6 | 0.98 | 56421 | 2 | 18 |
| *kpnb1* | 23.2 | 20.4 | 0.2 | 3.7 | 0.95 | 25791 | 1 | 20 |
| *kpnb1* | 23.3 | 19 | 0.2 | 2.9 | 0.97 | 32428 | 1 | 20 |
| *kpnb1* | 24.7 | 19.6 | 0.1 | 5.6 | 0.96 | 28841 | 1 | 20 |
| *kpnb1* | 24.4 | 9.4 | 0.3 | 1.6 | 0.94 | 38707 | 2 | 20 |
| *kpnb1* | 24.7 | 7.4 | 0.4 | 1.6 | 0.92 | 35559 | 2 | 20 |
| *kpnb1* | 24.6 | 6.5 | 0.4 | 1.6 | 0.98 | 36966 | 2 | 20 |
| *kpnb1* | 35 | 16.3 | 0.1 | 19.5 | 0.93 | 22900 | 1 | 22 |
| *kpnb1* | 136.8 | 0.6 | 0.1 | 0.9 | 0.81 | 13710 | 1 | 22 |
| *kpnb1* | 153.1 | 22.6 | 0.1 | 1.1 | 0.69 | 12674 | 1 | 22 |
| *kpnb1* | 29.5 | 8 | 0.1 | 2.7 | 0.97 | 42919 | 2 | 22 |
| *kpnb1* | 29.5 | 7.7 | 0.1 | 2.5 | 0.98 | 40473 | 2 | 22 |
| *kpnb1* | 29.4 | 9.2 | 0.1 | 3.9 | 0.97 | 32800 | 2 | 22 |
| *ndc1* | 22.8 | 18.9 | 0.2 | 1.9 | 0.97 | 64908 | 1 | 132 |
| *ndc1* | 23.5 | 19.5 | 0.2 | 2.2 | 0.97 | 66789 | 1 | 132 |
| *ndc1* | 23.2 | 18.6 | 0.3 | 1.9 | 0.97 | 68445 | 1 | 132 |
| *ndc1* | 24.4 | 7.1 | 0.5 | 1.5 | 0.98 | 51990 | 2 | 132 |
| *ndc1* | 24.5 | 7 | 0.4 | 1.5 | 0.98 | 53148 | 2 | 132 |
| *ndc1* | 24.4 | 7.5 | 0.4 | 1.5 | 0.98 | 55129 | 2 | 132 |
| *ndc1* | 24.4 | 18.2 | 0.3 | 2.2 | 0.97 | 49712 | 1 | 133 |
| *ndc1* | 27.8 | 16.4 | 0.1 | 1 | 0.74 | 36517 | 1 | 133 |
| *ndc1* | 23.9 | 18 | 0.3 | 1.9 | 0.97 | 51473 | 1 | 133 |
| *ndc1* | 25 | 6.3 | 0.7 | 1.5 | 0.99 | 40905 | 2 | 133 |
| *ndc1* | 25.2 | 6.8 | 0.5 | 1.6 | 0.99 | 40251 | 2 | 133 |
| *ndc1* | 24.5 | 8 | 0.4 | 1.6 | 0.98 | 47970 | 2 | 133 |
| *ndc1* | 24.4 | 17.9 | 0.3 | 1.9 | 0.98 | 62478 | 1 | 160 |
| *ndc1* | 23.9 | 17.9 | 0.3 | 1.7 | 0.97 | 58905 | 1 | 160 |
| *ndc1* | 24.4 | 16.9 | 0.3 | 1.7 | 0.97 | 62880 | 1 | 160 |
| *ndc1* | 24.9 | 8.7 | 0.4 | 1.6 | 0.99 | 56423 | 2 | 160 |
| *ndc1* | 25.3 | 8.3 | 0.4 | 1.5 | 0.99 | 55706 | 2 | 160 |
| *ndc1* | 24.6 | 8.4 | 0.3 | 1.6 | 0.99 | 56091 | 2 | 160 |
| *nup35* | 23.8 | 19.7 | 0.3 | 1.8 | 0.97 | 72916 | 1 | 144 |
| *nup35* | 23.9 | 19.5 | 0.3 | 1.8 | 0.98 | 71348 | 1 | 144 |
| *nup35* | 28 | 16.4 | 0.1 | 0.9 | 0.78 | 54588 | 1 | 144 |
| *nup35* | 24.4 | 9.2 | 0.4 | 1.5 | 0.99 | 60176 | 2 | 144 |
| *nup35* | 24.5 | 9.2 | 0.4 | 1.5 | 0.99 | 60423 | 2 | 144 |
| *nup35* | 24.4 | 7.3 | 0.5 | 1.5 | 0.99 | 57102 | 2 | 144 |
| *nup35* | 27.6 | 19 | 0.1 | 0.8 | 0.74 | 43663 | 1 | 150 |
| *nup35* | 23.7 | 17.8 | 0.3 | 1.6 | 0.97 | 48105 | 1 | 150 |
| *nup35* | 23.7 | 18.6 | 0.3 | 1.6 | 0.97 | 53680 | 1 | 150 |
| *nup35* | 24.5 | 7.1 | 0.6 | 1.4 | 0.99 | 36874 | 2 | 150 |
| *nup35* | 24.5 | 7.3 | 0.6 | 1.4 | 0.99 | 36987 | 2 | 150 |
| *nup35* | 24.2 | 8 | 0.5 | 1.5 | 0.99 | 37043 | 2 | 150 |
| *nup35* | 23.6 | 18.8 | 0.3 | 2.3 | 0.96 | 54228 | 1 | 175 |
| *nup35* | 23.4 | 18.2 | 0.2 | 1.9 | 0.97 | 51561 | 1 | 175 |

| targeted transcripts | period [h] | phase [h] | relative amplitude | damping [h$^{-1}$] | CC | mean [cps] | run | internal construct # |
|---|---|---|---|---|---|---|---|---|
| *nup35* | 23.7 | 18.4 | 0.2 | 2.2 | 0.97 | 46628 | 1 | 175 |
| *nup35* | 24.5 | 6.2 | 0.6 | 1.5 | 0.99 | 52411 | 2 | 175 |
| *nup35* | 24.7 | 6.3 | 0.6 | 1.5 | 0.99 | 51978 | 2 | 175 |
| *nup35* | 24.5 | 6.8 | 0.5 | 1.5 | 0.99 | 54696 | 2 | 175 |
| *nup37* | 23.6 | 19.4 | 0.3 | 1.9 | 0.98 | 56539 | 1 | 123 |
| *nup37* | 23.3 | 18.5 | 0.3 | 1.6 | 0.97 | 51633 | 1 | 123 |
| *nup37* | 23.7 | 18.6 | 0.3 | 1.7 | 0.97 | 57033 | 1 | 123 |
| *nup37* | 24.5 | 8.7 | 0.4 | 1.5 | 0.99 | 47950 | 2 | 123 |
| *nup37* | 24.7 | 8.1 | 0.4 | 1.4 | 0.99 | 45863 | 2 | 123 |
| *nup37* | 24.7 | 6.8 | 0.5 | 1.5 | 0.99 | 45335 | 2 | 123 |
| *nup37* | 24.2 | 18.5 | 0.3 | 2 | 0.97 | 71462 | 1 | 131 |
| *nup37* | 27 | 22.1 | 0 | 0.8 | 0.55 | 48755 | 1 | 131 |
| *nup37* | 27.7 | 17.7 | 0.1 | 0.7 | 0.81 | 61207 | 1 | 131 |
| *nup37* | 24.9 | 6.6 | 0.5 | 1.5 | 0.98 | 49954 | 2 | 131 |
| *nup37* | 25.3 | 6.6 | 0.5 | 1.5 | 0.98 | 49126 | 2 | 131 |
| *nup37* | 24.3 | 8.7 | 0.4 | 1.6 | 0.97 | 55656 | 2 | 131 |
| *nup37* | 23.3 | 19.9 | 0.3 | 1.9 | 0.94 | 61581 | 1 | 136 |
| *nup37* | 23.1 | 19.4 | 0.3 | 1.9 | 0.93 | 61244 | 1 | 136 |
| *nup37* | 23.2 | 19.6 | 0.3 | 1.7 | 0.96 | 67764 | 1 | 136 |
| *nup37* | 24.8 | 6.7 | 0.6 | 1.6 | 0.99 | 60566 | 2 | 136 |
| *nup37* | 24.7 | 8.5 | 0.4 | 1.6 | 0.99 | 64376 | 2 | 136 |
| *nup37* | 24.7 | 7.3 | 0.5 | 1.6 | 0.99 | 63486 | 2 | 136 |
| *nup43* | 23.3 | 19.4 | 0.2 | 2.8 | 0.93 | 62997 | 1 | 134 |
| *nup43* | 23.1 | 19.7 | 0.2 | 2.6 | 0.94 | 55692 | 1 | 134 |
| *nup43* | 23 | 19 | 0.2 | 2.3 | 0.95 | 63430 | 1 | 134 |
| *nup43* | 24.7 | 9.3 | 0.3 | 1.7 | 0.98 | 56756 | 2 | 134 |
| *nup43* | 24.6 | 9.6 | 0.2 | 1.8 | 0.97 | 57930 | 2 | 134 |
| *nup43* | 24.9 | 8.3 | 0.3 | 1.7 | 0.98 | 55847 | 2 | 134 |
| *nup43* | 22.6 | 18.5 | 0.3 | 1.4 | 0.98 | 49372 | 1 | 152 |
| *nup43* | 28.5 | 14.1 | 0.1 | 1 | 0.75 | 36039 | 1 | 152 |
| *nup43* | 22.7 | 17.9 | 0.3 | 1.4 | 0.98 | 42365 | 1 | 152 |
| *nup43* | 23.8 | 6.6 | 0.5 | 1.4 | 0.99 | 47339 | 2 | 152 |
| *nup43* | 23.7 | 8 | 0.4 | 1.4 | 0.99 | 49199 | 2 | 152 |
| *nup43* | 23.7 | 7 | 0.4 | 1.4 | 0.99 | 46200 | 2 | 152 |
| *nup43* | 24.9 | 17.9 | 0.3 | 2 | 0.97 | 61743 | 1 | 161 |
| *nup43* | 24.1 | 17.8 | 0.3 | 1.9 | 0.94 | 57828 | 1 | 161 |
| *nup43* | 24.8 | 18.1 | 0.3 | 2.2 | 0.97 | 59491 | 1 | 161 |
| *nup43* | 24.6 | 7.8 | 0.4 | 1.5 | 0.99 | 55362 | 2 | 161 |
| *nup43* | 24.7 | 8.5 | 0.4 | 1.5 | 0.99 | 53994 | 2 | 161 |
| *nup43* | 24.5 | 7.8 | 0.4 | 1.6 | 0.99 | 55163 | 2 | 161 |
| *nup50* | 24.8 | 18.8 | 0.2 | 3 | 0.97 | 32915 | 1 | 29 |
| *nup50* | 23.8 | 18.6 | 0.2 | 2.4 | 0.96 | 39562 | 1 | 29 |
| *nup50* | 26.6 | 18.1 | 0.2 | 2.4 | 0.95 | 35253 | 1 | 29 |
| *nup50* | 24.7 | 7.7 | 0.5 | 1.3 | 0.99 | 45248 | 2 | 29 |
| *nup50* | 24.7 | 7.3 | 0.5 | 1.3 | 0.99 | 42909 | 2 | 29 |
| *nup50* | 24.7 | 7.2 | 0.4 | 1.4 | 0.98 | 46400 | 2 | 29 |
| *nup50* | 22.3 | 20.5 | 0.2 | 2.9 | 0.97 | 74718 | 1 | 31 |
| *nup50* | 23.3 | 19.4 | 0.2 | 2.3 | 0.97 | 70304 | 1 | 31 |
| *nup50* | 24.3 | 19.9 | 0.2 | 3.6 | 0.93 | 74470 | 1 | 31 |
| *nup50* | 24.4 | 9 | 0.4 | 1.5 | 0.99 | 69615 | 2 | 31 |
| *nup50* | 24.4 | 8.5 | 0.4 | 1.4 | 0.99 | 64322 | 2 | 31 |
| *nup50* | 24.4 | 7.5 | 0.6 | 1.4 | 0.99 | 58785 | 2 | 31 |
| *nup50* | 23.4 | 17.8 | 0.3 | 1.7 | 0.98 | 28595 | 1 | 47 |
| *nup50* | 26.3 | 22.5 | 0.1 | 1 | 0.67 | 28750 | 1 | 47 |
| *nup50* | 24.2 | 19.4 | 0.1 | 2.7 | 0.93 | 14391 | 1 | 47 |
| *nup50* | 24.1 | 8.9 | 0.4 | 1.5 | 0.98 | 52381 | 2 | 47 |
| *nup50* | 24.6 | 7 | 0.5 | 1.4 | 0.99 | 43136 | 2 | 47 |
| *nup50* | 24.5 | 6.1 | 0.6 | 1.4 | 0.99 | 44182 | 2 | 47 |
| *nup54* | 23.1 | 20.2 | 0.2 | 2.4 | 0.97 | 26867 | 1 | 16 |
| *nup54* | 49.5 | 13 | 0.1 | 23.3 | 0.74 | 27627 | 1 | 16 |
| *nup54* | 23.3 | 20 | 0.2 | 2.2 | 0.96 | 27937 | 1 | 16 |
| *nup54* | 23.9 | 9 | 0.4 | 1.5 | 0.98 | 46994 | 2 | 16 |
| *nup54* | 24 | 7.6 | 0.5 | 1.6 | 0.99 | 41143 | 2 | 16 |
| *nup54* | 23.7 | 7.8 | 0.5 | 1.5 | 0.99 | 41314 | 2 | 16 |
| *nup54* | 24.6 | 19.4 | 0.2 | 2.5 | 0.97 | 27733 | 1 | 5 |
| *nup54* | -50.2 | 9.9 | 0.1 | 1.7 | 0.78 | 21649 | 1 | 5 |
| *nup54* | 25.1 | 19.5 | 0.2 | 2.4 | 0.97 | 29600 | 1 | 5 |
| *nup54* | 24.5 | 9.3 | 0.4 | 1.6 | 0.98 | 45839 | 2 | 5 |
| *nup54* | 24.6 | 7.5 | 0.5 | 1.7 | 0.98 | 42602 | 2 | 5 |
| *nup54* | 24.4 | 7.3 | 0.5 | 1.7 | 0.98 | 41103 | 2 | 5 |
| *nup62* | 22.3 | 20.5 | 0.2 | 3 | 0.97 | 56643 | 1 | 1 |
| *nup62* | 22.6 | 20.1 | 0.2 | 2.7 | 0.97 | 62779 | 1 | 1 |

| targeted transcripts | period [h] | phase [h] | relative amplitude | damping [h$^{-1}$] | CC | mean [cps] | run | internal construct # |
|---|---|---|---|---|---|---|---|---|
| *nup62* | 24.1 | 20.6 | 0.1 | 9.2 | 0.88 | 46124 | 1 | 1 |
| *nup62* | 24.3 | 9.2 | 0.4 | 1.5 | 0.97 | 60072 | 2 | 1 |
| *nup62* | 24.3 | 9.6 | 0.3 | 1.5 | 0.97 | 57707 | 2 | 1 |
| *nup62* | 24.2 | 8.9 | 0.3 | 1.5 | 0.97 | 55584 | 2 | 1 |
| *nup62* | 24.4 | 19.9 | 0.2 | 5.5 | 0.93 | 38312 | 1 | 2 |
| *nup62* | 23.8 | 19.2 | 0.2 | 2.8 | 0.92 | 37398 | 1 | 2 |
| *nup62* | 24.4 | 19.7 | 0.1 | 3.4 | 0.89 | 44928 | 1 | 2 |
| *nup62* | 25.1 | 6.8 | 0.5 | 1.5 | 0.99 | 42695 | 2 | 2 |
| *nup62* | 25.3 | 6.8 | 0.4 | 1.5 | 0.98 | 44464 | 2 | 2 |
| *nup62* | 24.9 | 6.2 | 0.5 | 1.6 | 0.98 | 42799 | 2 | 2 |
| *nup62* | 25.1 | 19.4 | 0.2 | 2.4 | 0.96 | 19892 | 1 | 9 |
| *nup62* | 24 | 18.3 | 0.2 | 2 | 0.96 | 28510 | 1 | 9 |
| *nup62* | 23.5 | 18.3 | 0.2 | 1.7 | 0.95 | 35743 | 1 | 9 |
| *nup62* | 24.6 | 7 | 0.5 | 1.6 | 0.99 | 39718 | 2 | 9 |
| *nup62* | 24.6 | 7.3 | 0.4 | 1.6 | 0.99 | 39581 | 2 | 9 |
| *nup62* | 24.5 | 7.2 | 0.4 | 1.6 | 0.99 | 44392 | 2 | 9 |
| *nup85* | 25.5 | 23.9 | 0 | 0.7 | 0.7 | 44546 | 1 | 139 |
| *nup85* | 25.8 | 17.3 | 0.2 | 2 | 0.95 | 54300 | 1 | 139 |
| *nup85* | 25.6 | 17.7 | 0.3 | 1.9 | 0.97 | 56163 | 1 | 139 |
| *nup85* | 24.7 | 7.7 | 0.4 | 1.6 | 0.99 | 40503 | 2 | 139 |
| *nup85* | 25.5 | 6.8 | 0.5 | 1.6 | 0.99 | 40430 | 2 | 139 |
| *nup85* | 25.3 | 6.3 | 0.6 | 1.5 | 0.99 | 38654 | 2 | 139 |
| *nup85* | 24.9 | 18.5 | 0.2 | 2.4 | 0.96 | 62711 | 1 | 156 |
| *nup85* | 29.7 | 17.5 | 0 | 0.7 | 0.71 | 49018 | 1 | 156 |
| *nup85* | 25.1 | 17.7 | 0.2 | 2.1 | 0.97 | 71510 | 1 | 156 |
| *nup85* | 25.5 | 8.4 | 0.3 | 1.6 | 0.99 | 69228 | 2 | 156 |
| *nup85* | 25.4 | 9.1 | 0.3 | 1.6 | 0.99 | 68588 | 2 | 156 |
| *nup85* | 25.5 | 8.1 | 0.3 | 1.6 | 0.99 | 68533 | 2 | 156 |
| *nup85* | 25.2 | 18.8 | 0.2 | 2.4 | 0.97 | 42846 | 1 | 186 |
| *nup85* | 23.8 | 18.1 | 0.3 | 2 | 0.97 | 49197 | 1 | 186 |
| *nup85* | 24.8 | 18.6 | 0.2 | 2.3 | 0.97 | 40335 | 1 | 186 |
| *nup85* | 25 | 7 | 0.5 | 1.6 | 0.99 | 52204 | 2 | 186 |
| *nup85* | 25.1 | 7.5 | 0.5 | 1.6 | 0.99 | 55512 | 2 | 186 |
| *nup85* | 24.9 | 7.6 | 0.5 | 1.7 | 0.99 | 55506 | 2 | 186 |
| *nup88* | 25.4 | 19.3 | 0.2 | 4.1 | 0.92 | 9529 | 1 | 82 |
| *nup88* | 23.7 | 18.9 | 0.3 | 2.6 | 0.95 | 21695 | 1 | 82 |
| *nup88* | 27.1 | 17.5 | 0.2 | 2.1 | 0.91 | 10410 | 1 | 82 |
| *nup88* | 24.4 | 8.3 | 0.4 | 1.6 | 0.99 | 34842 | 2 | 82 |
| *nup88* | 24 | 9.2 | 0.3 | 1.5 | 0.99 | 37009 | 2 | 82 |
| *nup88* | 24.2 | 6.3 | 0.5 | 1.6 | 0.99 | 35840 | 2 | 82 |
| *nup93* | 24.2 | 18.5 | 0.2 | 2.2 | 0.93 | 55151 | 1 | 126 |
| *nup93* | 28.1 | 15.8 | 0.1 | 1 | 0.58 | 42047 | 1 | 126 |
| *nup93* | 23.9 | 18.8 | 0.2 | 2.3 | 0.95 | 57916 | 1 | 126 |
| *nup93* | 24.7 | 7.8 | 0.4 | 1.7 | 0.99 | 47454 | 2 | 126 |
| *nup93* | 24.9 | 7.9 | 0.4 | 1.6 | 0.99 | 44434 | 2 | 126 |
| *nup93* | 24.3 | 8.1 | 0.3 | 1.7 | 0.99 | 46138 | 2 | 126 |
| *nup93* | 36.4 | 2.6 | 0 | 0.4 | 0.84 | 32383 | 1 | 153 |
| *nup93* | 36.1 | 3.4 | 0 | 0.5 | 0.82 | 32121 | 1 | 153 |
| *nup93* | 22.8 | 19.3 | 0.2 | 2.5 | 0.9 | 56802 | 1 | 153 |
| *nup93* | 24.4 | 6.7 | 0.5 | 1.5 | 0.99 | 46630 | 2 | 153 |
| *nup93* | 24.7 | 7.5 | 0.4 | 1.7 | 0.99 | 47640 | 2 | 153 |
| *nup93* | 24.4 | 6.9 | 0.5 | 1.5 | 0.99 | 45501 | 2 | 153 |
| *nup93* | 25.5 | 18.5 | 0.2 | 2.1 | 0.96 | 35716 | 1 | 166 |
| *nup93* | 26.6 | 17.1 | 0.1 | 1.2 | 0.8 | 31256 | 1 | 166 |
| *nup93* | 28.9 | 15.9 | 0.1 | 0.8 | 0.68 | 33127 | 1 | 166 |
| *nup93* | 24.7 | 7.9 | 0.4 | 1.7 | 0.99 | 44501 | 2 | 166 |
| *nup93* | 24.9 | 7.1 | 0.4 | 1.7 | 0.99 | 40284 | 2 | 166 |
| *nup93* | 24.4 | 8.5 | 0.3 | 1.7 | 0.99 | 42717 | 2 | 166 |
| *nup98* | 22.5 | 19.7 | 0.3 | 1.8 | 0.98 | 49940 | 1 | 3 |
| *nup98* | 22.8 | 19.5 | 0.3 | 1.8 | 0.98 | 49308 | 1 | 3 |
| *nup98* | 22.7 | 20.2 | 0.3 | 2.5 | 0.96 | 51322 | 1 | 3 |
| *nup98* | 24.3 | 7.9 | 0.5 | 1.4 | 0.99 | 46845 | 2 | 3 |
| *nup98* | 24.2 | 8.4 | 0.4 | 1.5 | 0.97 | 48976 | 2 | 3 |
| *nup98* | 24.3 | 6.6 | 0.5 | 1.5 | 0.97 | 48196 | 2 | 3 |
| *nup98* | 27 | 19.9 | 0.1 | 7.6 | 0.96 | 16743 | 1 | 6 |
| *nup98* | 26 | 19.9 | 0.1 | 4.9 | 0.91 | 19312 | 1 | 6 |
| *nup98* | 28.6 | 19.2 | 0.1 | 5.7 | 0.93 | 19433 | 1 | 6 |
| *nup98* | 25.6 | 8.3 | 0.2 | 1.7 | 0.99 | 49696 | 2 | 6 |
| *nup98* | 25.2 | 9.4 | 0.2 | 1.9 | 0.99 | 43154 | 2 | 6 |
| *nup98* | 24.8 | 8.8 | 0.2 | 1.9 | 0.99 | 51580 | 2 | 6 |
| *nup98* | 27.5 | 18.6 | 0.1 | 3.3 | 0.93 | 51476 | 1 | 8 |
| *nup98* | 26.6 | 18.8 | 0.1 | 2.5 | 0.91 | 42972 | 1 | 8 |

| targeted transcripts | period [h] | phase [h] | relative amplitude | damping [h$^{-1}$] | CC | mean [cps] | run | internal construct # |
|---|---|---|---|---|---|---|---|---|
| *nup98* | 29.4 | 18.5 | 0.1 | 3.1 | 0.88 | 26879 | 1 | 8 |
| *nup98* | 26.8 | 6.8 | 0.4 | 1.8 | 0.98 | 64919 | 2 | 8 |
| *nup98* | 26.7 | 6.6 | 0.3 | 1.8 | 0.98 | 62281 | 2 | 8 |
| *nup98* | 26.4 | 6.6 | 0.3 | 1.6 | 0.98 | 62397 | 2 | 8 |
| *nup107* | 22.9 | 20 | 0.3 | 1.8 | 0.97 | 54094 | 1 | 154 |
| *nup107* | 27.2 | 19.1 | 0.1 | 0.9 | 0.74 | 40271 | 1 | 154 |
| *nup107* | 23 | 18.8 | 0.3 | 1.7 | 0.96 | 54949 | 1 | 154 |
| *nup107* | 24.5 | 6.5 | 0.6 | 1.5 | 0.99 | 43891 | 2 | 154 |
| *nup107* | 24.6 | 6.6 | 0.5 | 1.5 | 0.99 | 43967 | 2 | 154 |
| *nup107* | 24 | 7.1 | 0.5 | 1.5 | 0.99 | 46076 | 2 | 154 |
| *nup107* | 23.3 | 19.1 | 0.2 | 1.7 | 0.97 | 82431 | 1 | 167 |
| *nup107* | 23.5 | 18.8 | 0.2 | 1.7 | 0.97 | 82054 | 1 | 167 |
| *nup107* | 23.6 | 18.2 | 0.2 | 1.6 | 0.98 | 76572 | 1 | 167 |
| *nup107* | 24.3 | 7.1 | 0.5 | 1.4 | 0.99 | 73322 | 2 | 167 |
| *nup107* | 24.2 | 7.9 | 0.3 | 1.4 | 0.99 | 79517 | 2 | 167 |
| *nup107* | 23.4 | 9.5 | 0.3 | 1.5 | 0.99 | 82548 | 2 | 167 |
| *nup107* | 24.7 | 19.2 | 0.2 | 1.9 | 0.99 | 38688 | 1 | 181 |
| *nup107* | 24.3 | 18 | 0.3 | 1.6 | 0.99 | 55552 | 1 | 181 |
| *nup107* | 24.4 | 18.2 | 0.3 | 1.7 | 0.99 | 56298 | 1 | 181 |
| *nup107* | 24.7 | 8.8 | 0.4 | 1.4 | 0.99 | 66261 | 2 | 181 |
| *nup107* | 24.7 | 9.3 | 0.4 | 1.4 | 0.99 | 68085 | 2 | 181 |
| *nup107* | 24.9 | 7.3 | 0.5 | 1.5 | 0.99 | 64512 | 2 | 181 |
| *nup133* | 25.4 | 19.4 | 0.2 | 2.3 | 0.95 | 59592 | 1 | 157 |
| *nup133* | 25.4 | 19.2 | 0.2 | 1.9 | 0.96 | 54726 | 1 | 157 |
| *nup133* | 25.3 | 18.7 | 0.2 | 1.9 | 0.95 | 63414 | 1 | 157 |
| *nup133* | 25.8 | 8.2 | 0.4 | 1.4 | 1 | 71639 | 2 | 157 |
| *nup133* | 25.7 | 9.4 | 0.3 | 1.5 | 0.99 | 77371 | 2 | 157 |
| *nup133* | 25.5 | 9.3 | 0.3 | 1.5 | 0.99 | 71696 | 2 | 157 |
| *nup133* | 27.7 | 20 | 0.1 | 0.8 | 0.54 | 30674 | 1 | 163 |
| *nup133* | 26.4 | 15.2 | 0.1 | 1.2 | 0.78 | 35107 | 1 | 163 |
| *nup133* | 39 | 21.8 | 0 | 0.4 | 0.69 | 33462 | 1 | 163 |
| *nup133* | 24.3 | 7.1 | 0.5 | 1.6 | 0.99 | 46745 | 2 | 163 |
| *nup133* | 24.8 | 6.5 | 0.6 | 1.6 | 0.99 | 40972 | 2 | 163 |
| *nup133* | 24.4 | 7.5 | 0.4 | 1.6 | 0.99 | 43258 | 2 | 163 |
| *nup133* | 23.6 | 19.6 | 0.2 | 1.9 | 0.98 | 45608 | 1 | 178 |
| *nup133* | 23.3 | 19.7 | 0.2 | 1.8 | 0.98 | 53082 | 1 | 178 |
| *nup133* | 23.3 | 18.3 | 0.3 | 1.5 | 0.99 | 46767 | 1 | 178 |
| *nup133* | 24.4 | 7.3 | 0.6 | 1.4 | 0.99 | 59151 | 2 | 178 |
| *nup133* | 24.4 | 8 | 0.5 | 1.5 | 0.99 | 55574 | 2 | 178 |
| *nup133* | 24.3 | 7.9 | 0.5 | 1.5 | 0.99 | 61816 | 2 | 178 |
| *nup153* | 23.3 | 20.5 | 0.2 | 2.9 | 0.97 | 65730 | 1 | 30 |
| *nup153* | 23.8 | 19.9 | 0.2 | 2.2 | 0.97 | 64220 | 1 | 30 |
| *nup153* | 24.4 | 21 | 0.1 | 2.9 | 0.94 | 63922 | 1 | 30 |
| *nup153* | 25.1 | 10.1 | 0.3 | 1.5 | 1 | 90164 | 2 | 30 |
| *nup153* | 25 | 10.1 | 0.3 | 1.5 | 0.99 | 86830 | 2 | 30 |
| *nup153* | 25 | 8.9 | 0.3 | 1.5 | 0.99 | 77591 | 2 | 30 |
| *nup153* | 25.6 | 18.4 | 0.1 | 2.4 | 0.89 | 58246 | 1 | 36 |
| *nup153* | 26.2 | 18.3 | 0.1 | 2.1 | 0.88 | 56861 | 1 | 36 |
| *nup153* | 34.7 | 16.3 | 0.1 | 7.6 | 0.75 | 33761 | 1 | 36 |
| *nup153* | 26.3 | 8.6 | 0.3 | 1.7 | 0.96 | 85191 | 2 | 36 |
| *nup153* | 26 | 8.6 | 0.2 | 1.6 | 0.99 | 81647 | 2 | 36 |
| *nup153* | 25.8 | 8.6 | 0.2 | 1.8 | 0.99 | 80074 | 2 | 36 |
| *nup153* | 25.6 | 19.1 | 0.1 | 2.7 | 0.93 | 38099 | 1 | 38 |
| *nup153* | 25.4 | 19 | 0.1 | 3.5 | 0.94 | 42233 | 1 | 38 |
| *nup153* | -59.9 | 12.3 | 0.1 | 7.2 | 0.75 | 33682 | 1 | 38 |
| *nup153* | 25.2 | 8.9 | 0.2 | 1.9 | 0.91 | 74286 | 2 | 38 |
| *nup153* | 25.7 | 7.6 | 0.3 | 1.8 | 0.97 | 70577 | 2 | 38 |
| *nup153* | 25.6 | 7.3 | 0.3 | 1.6 | 0.98 | 71231 | 2 | 38 |
| *nup155* | 25 | 19.6 | 0.2 | 2.8 | 0.97 | 38426 | 1 | 67 |
| *nup155* | 23.4 | 19.1 | 0.2 | 2.2 | 0.98 | 64075 | 1 | 67 |
| *nup155* | 26.4 | 18.8 | 0.2 | 3.3 | 0.95 | 56319 | 1 | 67 |
| *nup155* | 24.6 | 8.8 | 0.4 | 1.5 | 0.98 | 58356 | 2 | 67 |
| *nup155* | 24.5 | 9.4 | 0.4 | 1.5 | 0.98 | 58039 | 2 | 67 |
| *nup155* | 24.5 | 7.2 | 0.4 | 1.5 | 0.98 | 53891 | 2 | 67 |
| *nup155* | 22.6 | 21.4 | 0.1 | 3.1 | 0.89 | 15503 | 1 | 80 |
| *nup155* | 42.3 | 18.6 | 0 | 0.4 | 0.79 | 18110 | 1 | 80 |
| *nup155* | 22.2 | 22.2 | 0.1 | 3 | 0.88 | 22974 | 1 | 80 |
| *nup155* | 24.6 | 7.4 | 0.4 | 1.7 | 0.98 | 35259 | 2 | 80 |
| *nup155* | 24.5 | 6.9 | 0.4 | 1.7 | 0.99 | 33724 | 2 | 80 |
| *nup155* | 24.2 | 6.7 | 0.5 | 1.6 | 0.99 | 33276 | 2 | 80 |
| *nup155* | 24.8 | 18.5 | 0.2 | 2.6 | 0.96 | 41352 | 1 | 81 |
| *nup155* | 27.1 | 3.5 | 0 | 0.8 | 0.63 | 37878 | 1 | 81 |

| targeted transcripts | period [h] | phase [h] | relative amplitude | damping [h$^{-1}$] | CC | mean [cps] | run | internal construct # |
|---|---|---|---|---|---|---|---|---|
| *nup155* | 24.6 | 18 | 0.2 | 2.2 | 0.94 | 50402 | 1 | 81 |
| *nup155* | 25.3 | 7.3 | 0.4 | 1.5 | 0.99 | 75965 | 2 | 81 |
| *nup155* | 25.3 | 7 | 0.4 | 1.5 | 0.99 | 72948 | 2 | 81 |
| *nup155* | 25.1 | 6.4 | 0.4 | 1.5 | 0.98 | 69874 | 2 | 81 |
| *nup160* | 26.4 | 17.8 | 0.2 | 2 | 0.99 | 48019 | 1 | 169 |
| *nup160* | 25.7 | 17.1 | 0.2 | 1.8 | 0.96 | 53590 | 1 | 169 |
| *nup160* | 26.3 | 17.7 | 0.2 | 2 | 0.98 | 50295 | 1 | 169 |
| *nup160* | 26.5 | 7.1 | 0.4 | 1.9 | 0.99 | 72898 | 2 | 169 |
| *nup160* | 26.6 | 9 | 0.3 | 1.9 | 0.99 | 75032 | 2 | 169 |
| *nup160* | 26.4 | 8.7 | 0.2 | 1.9 | 0.99 | 72415 | 2 | 169 |
| *nup160* | 29.3 | 17.7 | 0.1 | 2.3 | 0.94 | 60671 | 1 | 172 |
| *nup160* | 28.6 | 17.8 | 0.1 | 2.4 | 0.93 | 57488 | 1 | 172 |
| *nup160* | 27.2 | 18 | 0.2 | 2.3 | 0.92 | 73908 | 1 | 172 |
| *nup160* | 27.8 | 7.9 | 0.2 | 2.1 | 0.99 | 81262 | 2 | 172 |
| *nup160* | 27.8 | 8.6 | 0.2 | 2 | 0.98 | 78537 | 2 | 172 |
| *nup160* | 27.6 | 8.4 | 0.2 | 2.4 | 0.99 | 78589 | 2 | 172 |
| *nup188* | 24.2 | 18.4 | 0.2 | 2.4 | 0.96 | 37266 | 1 | 52 |
| *nup188* | 23.4 | 18.1 | 0.3 | 2.4 | 0.98 | 49698 | 1 | 52 |
| *nup188* | 24.8 | 19.5 | 0.2 | 3 | 0.92 | 30746 | 1 | 52 |
| *nup188* | 24.8 | 8.4 | 0.4 | 1.6 | 0.99 | 56420 | 2 | 52 |
| *nup188* | 24.8 | 7.3 | 0.5 | 1.5 | 0.99 | 52422 | 2 | 52 |
| *nup188* | 24.8 | 7.4 | 0.4 | 1.5 | 0.98 | 51401 | 2 | 52 |
| *nup188* | 23.3 | 19.7 | 0.3 | 2.2 | 0.99 | 40478 | 1 | 60 |
| *nup188* | 23 | 19.3 | 0.3 | 2.1 | 0.99 | 44266 | 1 | 60 |
| *nup188* | 24.4 | 18.7 | 0.2 | 2.1 | 0.97 | 48259 | 1 | 60 |
| *nup188* | 24.6 | 8 | 0.5 | 1.5 | 0.98 | 62194 | 2 | 60 |
| *nup188* | 24.6 | 7.5 | 0.5 | 1.5 | 0.98 | 57840 | 2 | 60 |
| *nup188* | 24.6 | 7 | 0.5 | 1.5 | 0.99 | 59192 | 2 | 60 |
| *nup188* | 22.8 | 20 | 0.2 | 2.6 | 0.95 | 87636 | 1 | 70 |
| *nup188* | 23.2 | 19.8 | 0.2 | 2.5 | 0.96 | 91391 | 1 | 70 |
| *nup188* | 23.6 | 19 | 0.2 | 2.2 | 0.95 | 96591 | 1 | 70 |
| *nup188* | 24.5 | 8.9 | 0.4 | 1.5 | 0.98 | 66357 | 2 | 70 |
| *nup188* | 24.4 | 8.5 | 0.4 | 1.4 | 0.97 | 66076 | 2 | 70 |
| *nup188* | 24.2 | 8.6 | 0.3 | 1.5 | 0.97 | 62918 | 2 | 70 |
| *nup205* | 22.9 | 19.2 | 0.2 | 2.7 | 0.92 | 28338 | 1 | 128 |
| *nup205* | 22.6 | 18.5 | 0.2 | 2.2 | 0.96 | 29572 | 1 | 128 |
| *nup205* | 22.9 | 20 | 0.2 | 2.3 | 0.75 | 26504 | 1 | 128 |
| *nup205* | 24.3 | 6.7 | 0.4 | 1.6 | 0.99 | 28998 | 2 | 128 |
| *nup205* | 24.7 | 6.4 | 0.4 | 1.6 | 0.99 | 26236 | 2 | 128 |
| *nup205* | 24.1 | 7.3 | 0.3 | 1.5 | 0.98 | 29313 | 2 | 128 |
| *nup205* | 24.1 | 20.4 | 0.2 | 2.4 | 0.95 | 41216 | 1 | 135 |
| *nup205* | 23.7 | 19.5 | 0.2 | 2 | 0.95 | 47929 | 1 | 135 |
| *nup205* | 26.6 | 0.5 | 0 | 0.7 | 0.71 | 33878 | 1 | 135 |
| *nup205* | 25 | 6.9 | 0.5 | 1.5 | 0.99 | 54308 | 2 | 135 |
| *nup205* | 25 | 8.6 | 0.4 | 1.5 | 0.99 | 56086 | 2 | 135 |
| *nup205* | 24.7 | 8 | 0.4 | 1.5 | 0.99 | 60432 | 2 | 135 |
| *nup205* | 31.4 | 6.8 | 0.1 | 3.2 | 0.97 | 13328 | 2 | 141 |
| *nup205* | 31.7 | 7.3 | 0.1 | 3 | 0.96 | 13582 | 2 | 141 |
| *nup205* | 32.3 | 6.5 | 0.1 | 4.5 | 0.93 | 10154 | 2 | 141 |
| *nup210* | 25.5 | 19 | 0.2 | 2 | 0.96 | 57696 | 1 | 130 |
| *nup210* | 28 | 18.6 | 0.1 | 1 | 0.83 | 40235 | 1 | 130 |
| *nup210* | 26.8 | 22.1 | 0.1 | 0.7 | 0.78 | 45289 | 1 | 130 |
| *nup210* | 25.1 | 6.7 | 0.5 | 1.5 | 0.98 | 43863 | 2 | 130 |
| *nup210* | 25.3 | 6.7 | 0.5 | 1.5 | 0.99 | 40706 | 2 | 130 |
| *nup210* | 24.6 | 8.6 | 0.4 | 1.5 | 0.98 | 44765 | 2 | 130 |
| *nup210* | 24.1 | 19 | 0.3 | 2.1 | 0.98 | 49011 | 1 | 148 |
| *nup210* | 23.5 | 17.4 | 0.3 | 1.5 | 0.96 | 44134 | 1 | 148 |
| *nup210* | 24.2 | 18.1 | 0.3 | 1.9 | 0.98 | 53880 | 1 | 148 |
| *nup210* | 24.8 | 6.6 | 0.5 | 1.5 | 0.99 | 47686 | 2 | 148 |
| *nup210* | 24.9 | 8 | 0.4 | 1.5 | 0.99 | 49179 | 2 | 148 |
| *nup210* | 24.1 | 8.8 | 0.4 | 1.5 | 0.99 | 50643 | 2 | 148 |
| *nup210* | 23.1 | 19.6 | 0.4 | 2 | 0.99 | 52313 | 1 | 159 |
| *nup210* | 23.1 | 18 | 0.3 | 1.6 | 0.98 | 45773 | 1 | 159 |
| *nup210* | 23.2 | 19.1 | 0.4 | 1.7 | 0.99 | 46031 | 1 | 159 |
| *nup210* | 24.3 | 7.2 | 0.5 | 1.6 | 0.99 | 52486 | 2 | 159 |
| *nup210* | 24.5 | 7.1 | 0.6 | 1.6 | 0.99 | 50784 | 2 | 159 |
| *nup210* | 24.3 | 7.7 | 0.5 | 1.5 | 0.99 | 55177 | 2 | 159 |
| *nup214* | 23.7 | 19.1 | 0.3 | 2.5 | 0.97 | 35809 | 1 | 27 |
| *nup214* | 28.9 | 17.6 | 0 | 0.6 | 0.78 | 23983 | 1 | 27 |
| *nup214* | 26.4 | 18.7 | 0.1 | 2.2 | 0.92 | 23868 | 1 | 27 |
| *nup214* | 24.8 | 7.2 | 0.5 | 1.4 | 0.98 | 44372 | 2 | 27 |
| *nup214* | 25.1 | 7.1 | 0.5 | 1.5 | 0.98 | 42780 | 2 | 27 |

| targeted transcripts | period [h] | phase [h] | relative amplitude | damping [$h^{-1}$] | CC | mean [cps] | run | internal construct # |
|---|---|---|---|---|---|---|---|---|
| *nup214* | 24.6 | 6.1 | 0.5 | 1.5 | 0.98 | 42676 | 2 | 27 |
| *nup214* | 22.8 | 21.3 | 0.2 | 3 | 0.94 | 71687 | 1 | 35 |
| *nup214* | 23 | 20.5 | 0.2 | 2.2 | 0.93 | 68083 | 1 | 35 |
| *nup214* | 27.3 | 17.9 | 0.1 | 3.6 | 0.86 | 58829 | 1 | 35 |
| *nup214* | 25.2 | 7.8 | 0.4 | 1.8 | 0.98 | 55828 | 2 | 35 |
| *nup214* | 25.3 | 7.8 | 0.4 | 1.9 | 0.96 | 53340 | 2 | 35 |
| *nup214* | 25.3 | 6.6 | 0.5 | 1.7 | 0.99 | 49348 | 2 | 35 |
| *nupl1* | 24 | 21.5 | 0.1 | 9.2 | 0.84 | 21533 | 1 | 39 |
| *nupl1* | 21.3 | 23.5 | 0.1 | 6.4 | 0.74 | 23643 | 1 | 39 |
| *nupl1* | 34.3 | 17.8 | 0.1 | 6.5 | 0.88 | 14833 | 1 | 39 |
| *nupl1* | 24.8 | 7.8 | 0.4 | 1.5 | 0.99 | 47002 | 2 | 39 |
| *nupl1* | 24.8 | 7 | 0.5 | 1.5 | 0.99 | 43991 | 2 | 39 |
| *nupl1* | 24.5 | 6.8 | 0.5 | 1.6 | 0.99 | 44205 | 2 | 39 |
| *nupl1* | 24.4 | 19.9 | 0.1 | 4.2 | 0.96 | 18132 | 1 | 42 |
| *nupl1* | 704.2 | 6.5 | 1 | 55.5 | 0.81 | 19585 | 1 | 42 |
| *nupl1* | 24.6 | 20 | 0.1 | 5.1 | 0.95 | 14598 | 1 | 42 |
| *nupl1* | 24.6 | 7.9 | 0.3 | 1.7 | 0.97 | 26249 | 2 | 42 |
| *nupl1* | 24.6 | 8 | 0.3 | 1.7 | 0.98 | 25882 | 2 | 42 |
| *nupl1* | 24.2 | 7.3 | 0.4 | 1.6 | 0.99 | 25792 | 2 | 42 |
| *nupl1* | 26.3 | 18.9 | 0.1 | 3.8 | 0.97 | 29258 | 1 | 45 |
| *nupl1* | 24.1 | 19.1 | 0.1 | 2.6 | 0.97 | 28609 | 1 | 45 |
| *nupl1* | 29.2 | 18.7 | 0.1 | 4.9 | 0.94 | 21172 | 1 | 45 |
| *nupl1* | 25.1 | 7 | 0.4 | 1.7 | 0.97 | 41999 | 2 | 45 |
| *nupl1* | 25.1 | 7.4 | 0.3 | 1.7 | 0.98 | 42263 | 2 | 45 |
| *nupl1* | 25 | 6.7 | 0.4 | 1.6 | 0.99 | 39070 | 2 | 45 |
| *pom121* | 22.6 | 19.5 | 0.3 | 1.6 | 0.99 | 42596 | 1 | 146 |
| *pom121* | 22.8 | 18.9 | 0.4 | 1.5 | 0.98 | 48208 | 1 | 146 |
| *pom121* | 22.9 | 19.1 | 0.4 | 1.6 | 0.99 | 50461 | 1 | 146 |
| *pom121* | 23.8 | 8.5 | 0.4 | 1.3 | 0.99 | 49580 | 2 | 146 |
| *pom121* | 23.8 | 8.7 | 0.5 | 1.3 | 0.99 | 49866 | 2 | 146 |
| *pom121* | 23.9 | 7.4 | 0.5 | 1.3 | 0.99 | 49564 | 2 | 146 |
| *pom121* | 21.4 | 21 | 0.1 | 1.2 | 0.42 | 33528 | 1 | 162 |
| *pom121* | 23.2 | 17.6 | 0.2 | 1.5 | 0.85 | 32249 | 1 | 162 |
| *pom121* | 23.2 | 17.8 | 0.3 | 2 | 0.97 | 32177 | 1 | 162 |
| *pom121* | 24.3 | 6.4 | 0.6 | 1.6 | 0.99 | 32476 | 2 | 162 |
| *pom121* | 24.6 | 6.4 | 0.6 | 1.6 | 0.99 | 30204 | 2 | 162 |
| *pom121* | 23.7 | 8 | 0.4 | 1.6 | 0.99 | 34260 | 2 | 162 |
| *pom121* | 24.8 | 18.2 | 0.4 | 1.7 | 0.99 | 65646 | 1 | 179 |
| *pom121* | 24.6 | 18.8 | 0.3 | 2 | 0.98 | 61699 | 1 | 179 |
| *pom121* | 24.3 | 17 | 0.4 | 1.5 | 0.98 | 61856 | 1 | 179 |
| *pom121* | 25 | 8.1 | 0.5 | 1.5 | 0.99 | 59707 | 2 | 179 |
| *pom121* | 25.2 | 8.4 | 0.5 | 1.5 | 0.99 | 59516 | 2 | 179 |
| *pom121* | 24.9 | 8.1 | 0.5 | 1.5 | 0.99 | 62612 | 2 | 179 |
| *rae1* | 22.9 | 19.7 | 0.2 | 1.9 | 0.98 | 39823 | 1 | 101 |
| *rae1* | 22.6 | 19.5 | 0.3 | 1.8 | 0.98 | 48401 | 1 | 101 |
| *rae1* | 22.2 | 21.4 | 0.2 | 2.2 | 0.95 | 29354 | 1 | 101 |
| *rae1* | 24.4 | 7.6 | 0.5 | 1.5 | 0.99 | 60142 | 2 | 101 |
| *rae1* | 24.3 | 7 | 0.6 | 1.5 | 0.99 | 54924 | 2 | 101 |
| *rae1* | 24.1 | 7.6 | 0.4 | 1.5 | 0.99 | 55060 | 2 | 101 |
| *rae1* | 22.8 | 19.8 | 0.2 | 2 | 0.98 | 58723 | 1 | 103 |
| *rae1* | 22.7 | 19.4 | 0.2 | 1.9 | 0.97 | 64629 | 1 | 103 |
| *rae1* | 23.2 | 20.1 | 0.2 | 1.9 | 0.96 | 58353 | 1 | 103 |
| *rae1* | 24.4 | 8.8 | 0.4 | 1.5 | 0.98 | 62228 | 2 | 103 |
| *rae1* | 24.2 | 8.8 | 0.4 | 1.5 | 0.98 | 57698 | 2 | 103 |
| *rae1* | 24.2 | 8.3 | 0.3 | 1.5 | 0.98 | 56963 | 2 | 103 |
| *rae1* | 23.6 | 18.6 | 0.3 | 2.1 | 0.98 | 64170 | 1 | 118 |
| *rae1* | 23.4 | 18.7 | 0.3 | 1.7 | 0.97 | 61349 | 1 | 118 |
| *rae1* | 23.6 | 18.3 | 0.4 | 1.7 | 0.98 | 65049 | 1 | 118 |
| *rae1* | 24.2 | 7.3 | 0.5 | 1.6 | 0.99 | 54202 | 2 | 118 |
| *rae1* | 24.5 | 6.4 | 0.6 | 1.5 | 0.99 | 52095 | 2 | 118 |
| *rae1* | 24.3 | 7.5 | 0.5 | 1.5 | 0.99 | 52944 | 2 | 118 |
| *ran* | 23.7 | 18.1 | 0.3 | 2 | 0.99 | 50510 | 1 | 90 |
| *ran* | 25.4 | 20 | 0.1 | 1.2 | 0.65 | 38826 | 1 | 90 |
| *ran* | 25.5 | 17.8 | 0.2 | 1.7 | 0.97 | 31299 | 1 | 90 |
| *ran* | 24.8 | 9.1 | 0.3 | 1.4 | 0.99 | 63016 | 2 | 90 |
| *ran* | 24.9 | 6.7 | 0.5 | 1.5 | 0.99 | 54243 | 2 | 90 |
| *ran* | 24.8 | 6 | 0.5 | 1.4 | 0.99 | 51944 | 2 | 90 |
| *ran* | 22.6 | 19 | 0.3 | 2 | 0.99 | 46460 | 1 | 93 |
| *ran* | 22.9 | 19 | 0.3 | 1.8 | 0.99 | 47160 | 1 | 93 |
| *ran* | 22.7 | 18.8 | 0.3 | 1.9 | 0.98 | 51766 | 1 | 93 |
| *ran* | 24.1 | 8 | 0.4 | 1.4 | 0.97 | 45845 | 2 | 93 |
| *ran* | 24.1 | 7.2 | 0.5 | 1.5 | 0.99 | 46179 | 2 | 93 |

| targeted transcripts | period [h] | phase [h] | relative amplitude | damping [h$^{-1}$] | CC | mean [cps] | run | internal construct # |
|---|---|---|---|---|---|---|---|---|
| *ran* | 24.1 | 6.2 | 0.6 | 1.5 | 0.99 | 42928 | 2 | 93 |
| *ran* | 26.5 | 18.2 | 0.2 | 2.9 | 0.96 | 23834 | 1 | 97 |
| *ran* | 24.4 | 18.9 | 0.2 | 2.7 | 0.97 | 38968 | 1 | 97 |
| *ran* | 27.1 | 18 | 0.2 | 3.4 | 0.94 | 21050 | 1 | 97 |
| *ran* | 25.3 | 9 | 0.4 | 1.9 | 0.93 | 53036 | 2 | 97 |
| *ran* | 24.9 | 8.5 | 0.4 | 1.7 | 0.98 | 46541 | 2 | 97 |
| *ran* | 24.5 | 7.7 | 0.5 | 1.6 | 0.99 | 52045 | 2 | 97 |
| *ranbp1* | 23.9 | 19.7 | 0.2 | 2.6 | 0.97 | 52203 | 1 | 71 |
| *ranbp1* | 23.2 | 19.8 | 0.2 | 2.3 | 0.97 | 55182 | 1 | 71 |
| *ranbp1* | 24.6 | 20.2 | 0.2 | 2.9 | 0.93 | 56406 | 1 | 71 |
| *ranbp1* | 25 | 8.6 | 0.3 | 1.5 | 0.97 | 51179 | 2 | 71 |
| *ranbp1* | 24.9 | 9.3 | 0.4 | 1.5 | 0.97 | 50539 | 2 | 71 |
| *ranbp1* | 24.7 | 7.5 | 0.3 | 1.5 | 0.96 | 48643 | 2 | 71 |
| *ranbp1* | 23.1 | 18.9 | 0.3 | 1.8 | 0.98 | 39224 | 1 | 77 |
| *ranbp1* | 22.9 | 18.5 | 0.3 | 1.7 | 0.99 | 53120 | 1 | 77 |
| *ranbp1* | 22.8 | 18.9 | 0.2 | 1.7 | 0.98 | 41165 | 1 | 77 |
| *ranbp1* | 24.2 | 9.8 | 0.4 | 1.4 | 0.99 | 63098 | 2 | 77 |
| *ranbp1* | 24.5 | 7.3 | 0.5 | 1.4 | 0.99 | 57468 | 2 | 77 |
| *ranbp1* | 24.5 | 6.3 | 0.5 | 1.4 | 0.98 | 54970 | 2 | 77 |
| *ranbp1* | 25.4 | 20.7 | 0.1 | 3.1 | 0.93 | 55355 | 1 | 79 |
| *ranbp1* | 27 | 0.2 | 0.1 | 1 | 0.48 | 45073 | 1 | 79 |
| *ranbp1* | 24.5 | 20.5 | 0.1 | 2.5 | 0.91 | 58680 | 1 | 79 |
| *ranbp1* | 27.3 | 16.2 | 0.2 | 0.9 | 0.68 | 56632 | 2 | 79 |
| *ranbp1* | 25.6 | 8.5 | 0.3 | 1.5 | 0.96 | 50349 | 2 | 79 |
| *ranbp1* | 25.3 | 7.1 | 0.5 | 1.5 | 0.98 | 48292 | 2 | 79 |
| *ranbp2* | 23.5 | 19.7 | 0.3 | 2 | 0.99 | 47652 | 1 | 41 |
| *ranbp2* | 28 | 20.2 | 0.1 | 0.9 | 0.72 | 36239 | 1 | 41 |
| *ranbp2* | 27.5 | 18.4 | 0.2 | 2.4 | 0.97 | 29835 | 1 | 41 |
| *ranbp2* | 23.8 | 9.6 | 0.4 | 1.5 | 0.95 | 57913 | 2 | 41 |
| *ranbp2* | 24.2 | 8.7 | 0.5 | 1.5 | 0.98 | 57511 | 2 | 41 |
| *ranbp2* | 23.8 | 7.6 | 0.5 | 1.6 | 0.99 | 53537 | 2 | 41 |
| *ranbp2* | 25.2 | 19 | 0.2 | 2.5 | 0.95 | 31219 | 1 | 43 |
| *ranbp2* | 24.6 | 18.2 | 0.2 | 2.1 | 0.95 | 32076 | 1 | 43 |
| *ranbp2* | 29.7 | 18.9 | 0.1 | 3.2 | 0.85 | 12083 | 1 | 43 |
| *ranbp2* | 25 | 7.5 | 0.5 | 1.6 | 0.97 | 38223 | 2 | 43 |
| *ranbp2* | 25.4 | 8.3 | 0.4 | 1.6 | 0.97 | 38208 | 2 | 43 |
| *ranbp2* | 25.4 | 6.5 | 0.5 | 1.5 | 0.98 | 36155 | 2 | 43 |
| *ranbp2* | 26.5 | 17.9 | 0.2 | 2 | 0.93 | 41640 | 1 | 44 |
| *ranbp2* | 24.9 | 18.4 | 0.2 | 2.3 | 0.97 | 47368 | 1 | 44 |
| *ranbp2* | 27.6 | 18.7 | 0.2 | 3.1 | 0.94 | 23436 | 1 | 44 |
| *ranbp2* | 24.7 | 8.9 | 0.4 | 1.5 | 0.92 | 52367 | 2 | 44 |
| *ranbp2* | 25.2 | 8.8 | 0.3 | 1.6 | 0.92 | 54175 | 2 | 44 |
| *ranbp2* | 25 | 7.2 | 0.5 | 1.4 | 0.98 | 51372 | 2 | 44 |
| *ranbp3* | 24.2 | 18.2 | 0.3 | 1.9 | 0.99 | 32894 | 1 | 61 |
| *ranbp3* | 24.1 | 17.5 | 0.3 | 1.8 | 0.98 | 40154 | 1 | 61 |
| *ranbp3* | 25.4 | 17.8 | 0.3 | 1.7 | 0.98 | 31675 | 1 | 61 |
| *ranbp3* | 24.9 | 7.5 | 0.4 | 1.4 | 0.98 | 66697 | 2 | 61 |
| *ranbp3* | 24.8 | 8.1 | 0.4 | 1.4 | 0.98 | 63820 | 2 | 61 |
| *ranbp3* | 25 | 6.2 | 0.5 | 1.4 | 0.99 | 60222 | 2 | 61 |
| *ranbp4* | 24.8 | 20.1 | 0.2 | 1.9 | 0.94 | 21613 | 1 | 83 |
| *ranbp4* | 23.6 | 17.7 | 0.3 | 1.4 | 0.98 | 45319 | 1 | 83 |
| *ranbp4* | 24.1 | 19.6 | 0.2 | 1.7 | 0.98 | 40774 | 1 | 83 |
| *ranbp4* | 24.5 | 7.7 | 0.5 | 1.5 | 0.99 | 58075 | 2 | 83 |
| *ranbp4* | 24.4 | 7.7 | 0.5 | 1.4 | 0.99 | 55935 | 2 | 83 |
| *ranbp4* | 24.4 | 6.8 | 0.5 | 1.4 | 0.98 | 52564 | 2 | 83 |
| *ranbp4* | 23 | 20.5 | 0.2 | 2.8 | 0.96 | 19114 | 1 | 84 |
| *ranbp4* | 23.1 | 17.6 | 0.3 | 1.6 | 0.98 | 34261 | 1 | 84 |
| *ranbp4* | 23.8 | 18.4 | 0.2 | 1.4 | 0.95 | 39496 | 1 | 84 |
| *ranbp4* | 24.3 | 7.3 | 0.5 | 1.5 | 0.98 | 53813 | 2 | 84 |
| *ranbp4* | 24.2 | 7 | 0.6 | 1.5 | 0.98 | 51568 | 2 | 84 |
| *ranbp4* | 24.3 | 6.4 | 0.6 | 1.5 | 0.98 | 53817 | 2 | 84 |
| *ranbp5* | 23.3 | 20.2 | 0.2 | 2.5 | 0.97 | 43426 | 1 | 65 |
| *ranbp5* | 22.9 | 18.8 | 0.3 | 1.9 | 0.98 | 53780 | 1 | 65 |
| *ranbp5* | 23.4 | 19.3 | 0.2 | 2.1 | 0.97 | 56343 | 1 | 65 |
| *ranbp5* | 24.6 | 7.1 | 0.5 | 1.5 | 0.99 | 60185 | 2 | 65 |
| *ranbp5* | 24.6 | 6.8 | 0.5 | 1.5 | 0.98 | 56122 | 2 | 65 |
| *ranbp5* | 24.3 | 7.3 | 0.4 | 1.5 | 0.98 | 59640 | 2 | 65 |
| *ranbp5* | 23.3 | 18.4 | 0.3 | 2.5 | 0.97 | 48264 | 1 | 69 |
| *ranbp5* | 23.8 | 18.3 | 0.3 | 2 | 0.98 | 47071 | 1 | 69 |
| *ranbp5* | 25 | 17.4 | 0.2 | 2.3 | 0.96 | 51619 | 1 | 69 |
| *ranbp5* | 24.5 | 8.2 | 0.5 | 1.5 | 0.98 | 50265 | 2 | 69 |
| *ranbp5* | 24.7 | 7.7 | 0.5 | 1.4 | 0.99 | 49941 | 2 | 69 |

| targeted transcripts | period [h] | phase [h] | relative amplitude | damping [h$^{-1}$] | CC | mean [cps] | run | internal construct # |
|---|---|---|---|---|---|---|---|---|
| *ranbp5* | 24.5 | 7.1 | 0.6 | 1.5 | 0.98 | 47618 | 2 | 69 |
| *ranbp5* | 25.2 | 18.5 | 0.2 | 2.1 | 0.94 | 79794 | 1 | 73 |
| *ranbp5* | 25.8 | 17 | 0.2 | 1.8 | 0.92 | 81991 | 1 | 73 |
| *ranbp5* | 26.4 | 18.4 | 0.2 | 1.8 | 0.93 | 85426 | 1 | 73 |
| *ranbp5* | 25.8 | 7.8 | 0.4 | 1.5 | 0.99 | 70331 | 2 | 73 |
| *ranbp5* | 25.8 | 6.9 | 0.5 | 1.5 | 0.99 | 70750 | 2 | 73 |
| *ranbp5* | 25.1 | 6.9 | 0.6 | 1.6 | 0.99 | 64824 | 2 | 73 |
| *ranbp6* | 23.7 | 20.1 | 0.2 | 2 | 0.98 | 51254 | 1 | 56 |
| *ranbp6* | 23.4 | 18.8 | 0.3 | 1.7 | 0.98 | 55600 | 1 | 56 |
| *ranbp6* | 23.4 | 19.7 | 0.3 | 1.6 | 0.97 | 61987 | 1 | 56 |
| *ranbp6* | 24.4 | 8.1 | 0.5 | 1.5 | 0.99 | 64731 | 2 | 56 |
| *ranbp6* | 24.4 | 7.8 | 0.5 | 1.5 | 0.99 | 59356 | 2 | 56 |
| *ranbp6* | 24.3 | 7.3 | 0.5 | 1.5 | 0.98 | 61813 | 2 | 56 |
| *ranbp6* | 24.6 | 20.3 | 0.2 | 2 | 0.95 | 63554 | 1 | 58 |
| *ranbp6* | 23.6 | 19.8 | 0.3 | 1.8 | 0.98 | 79108 | 1 | 58 |
| *ranbp6* | 23.8 | 18.9 | 0.3 | 1.6 | 0.97 | 81988 | 1 | 58 |
| *ranbp6* | 24.8 | 7.3 | 0.5 | 1.6 | 0.99 | 73178 | 2 | 58 |
| *ranbp6* | 24.7 | 8.5 | 0.4 | 1.6 | 0.99 | 81307 | 2 | 58 |
| *ranbp6* | 24.5 | 8 | 0.4 | 1.6 | 0.99 | 80659 | 2 | 58 |
| *ranbp6* | 23.7 | 20 | 0.2 | 2.7 | 0.97 | 65591 | 1 | 59 |
| *ranbp6* | 23.3 | 19.8 | 0.2 | 2.7 | 0.98 | 72398 | 1 | 59 |
| *ranbp6* | 24.3 | 19.3 | 0.2 | 2.2 | 0.96 | 70321 | 1 | 59 |
| *ranbp6* | 24.7 | 8.5 | 0.4 | 1.5 | 0.98 | 72154 | 2 | 59 |
| *ranbp6* | 24.6 | 8.1 | 0.5 | 1.5 | 0.98 | 68863 | 2 | 59 |
| *ranbp6* | 25.6 | 7 | 0.5 | 1.4 | 0.99 | 67427 | 2 | 59 |
| *ranbp7* | 24.4 | 17.7 | 0.3 | 1.8 | 0.99 | 35678 | 1 | 54 |
| *ranbp7* | 23.7 | 8.7 | 0 | 0.7 | 0.34 | 31518 | 1 | 54 |
| *ranbp7* | 25.7 | 19 | 0.2 | 2 | 0.98 | 25065 | 1 | 54 |
| *ranbp7* | 24.5 | 7.7 | 0.6 | 1.4 | 0.99 | 50027 | 2 | 54 |
| *ranbp7* | 24.3 | 7.4 | 0.7 | 1.4 | 0.99 | 48735 | 2 | 54 |
| *ranbp7* | 24.2 | 6.9 | 0.6 | 1.4 | 0.99 | 50289 | 2 | 54 |
| *ranbp7* | 23.7 | 19.3 | 0.3 | 2.4 | 0.98 | 51046 | 1 | 62 |
| *ranbp7* | 27.3 | 19.5 | 0.1 | 1 | 0.74 | 44717 | 1 | 62 |
| *ranbp7* | 26 | 23.9 | 0.1 | 0.8 | 0.9 | 49392 | 1 | 62 |
| *ranbp7* | 24.7 | 8.2 | 0.4 | 1.5 | 0.99 | 60312 | 2 | 62 |
| *ranbp7* | 24.5 | 9.3 | 0.4 | 1.5 | 0.99 | 59506 | 2 | 62 |
| *ranbp7* | 25.6 | 5.9 | 0.4 | 1.3 | 0.98 | 61157 | 2 | 62 |
| *ranbp7* | 24.3 | 21 | 0.2 | 4 | 0.95 | 31806 | 1 | 68 |
| *ranbp7* | 23.2 | 19.8 | 0.2 | 3 | 0.97 | 46939 | 1 | 68 |
| *ranbp7* | 26 | 20.2 | 0.2 | 2.3 | 0.96 | 27382 | 1 | 68 |
| *ranbp7* | 24.7 | 9.1 | 0.4 | 1.6 | 0.98 | 51861 | 2 | 68 |
| *ranbp7* | 24.7 | 8.7 | 0.4 | 1.6 | 0.98 | 48213 | 2 | 68 |
| *ranbp7* | 24.6 | 7.1 | 0.4 | 1.5 | 0.98 | 45552 | 2 | 68 |
| *ranbp8* | 24.7 | 18.8 | 0.2 | 3 | 0.96 | 70853 | 1 | 49 |
| *ranbp8* | 23.4 | 19.7 | 0.2 | 2.7 | 0.96 | 75973 | 1 | 49 |
| *ranbp8* | 26.7 | 19 | 0.1 | 4.2 | 0.93 | 78345 | 1 | 49 |
| *ranbp8* | 25.1 | 8.7 | 0.4 | 1.5 | 0.99 | 62934 | 2 | 49 |
| *ranbp8* | 25.1 | 8 | 0.5 | 1.5 | 0.99 | 61559 | 2 | 49 |
| *ranbp8* | 24.8 | 8.2 | 0.4 | 1.5 | 0.99 | 60001 | 2 | 49 |
| *ranbp8* | 24.1 | 18.3 | 0.3 | 2.2 | 0.98 | 53698 | 1 | 55 |
| *ranbp8* | 23.7 | 18 | 0.3 | 1.9 | 0.99 | 54279 | 1 | 55 |
| *ranbp8* | 24.7 | 18.5 | 0.3 | 2 | 0.98 | 55234 | 1 | 55 |
| *ranbp8* | 24.8 | 8.1 | 0.5 | 1.5 | 0.97 | 51029 | 2 | 55 |
| *ranbp8* | 24.7 | 8.4 | 0.4 | 1.5 | 0.99 | 54979 | 2 | 55 |
| *ranbp8* | 24.5 | 6.8 | 0.5 | 1.5 | 0.99 | 50163 | 2 | 55 |
| *ranbp8* | 23.3 | 18.7 | 0.3 | 2.1 | 0.98 | 37735 | 1 | 63 |
| *ranbp8* | 23.7 | 18.4 | 0.3 | 2 | 0.98 | 47308 | 1 | 63 |
| *ranbp8* | 24 | 18.7 | 0.3 | 2.1 | 0.97 | 46630 | 1 | 63 |
| *ranbp8* | 25 | 7.8 | 0.5 | 1.4 | 0.99 | 55483 | 2 | 63 |
| *ranbp8* | 24.9 | 6.6 | 0.5 | 1.5 | 0.99 | 51581 | 2 | 63 |
| *ranbp8* | 24.5 | 7.6 | 0.4 | 1.5 | 0.99 | 53606 | 2 | 63 |
| *ranbp9* | 24.2 | 20.2 | 0.2 | 3 | 0.94 | 34020 | 1 | 137 |
| *ranbp9* | 24 | 18.5 | 0.3 | 2.2 | 0.96 | 43206 | 1 | 137 |
| *ranbp9* | 24.8 | 18.3 | 0.3 | 2.1 | 0.97 | 44143 | 1 | 137 |
| *ranbp9* | 24.6 | 7.9 | 0.4 | 1.6 | 0.99 | 47623 | 2 | 137 |
| *ranbp9* | 24.7 | 7.2 | 0.5 | 1.5 | 0.99 | 46189 | 2 | 137 |
| *ranbp9* | 24.6 | 6.7 | 0.5 | 1.5 | 0.99 | 44021 | 2 | 137 |
| *ranbp9* | 23.6 | 18.7 | 0.3 | 1.7 | 0.98 | 39853 | 1 | 145 |
| *ranbp9* | 23.6 | 16.6 | 0.3 | 1.3 | 0.97 | 40366 | 1 | 145 |
| *ranbp9* | 23.4 | 18.8 | 0.3 | 1.6 | 0.97 | 36715 | 1 | 145 |
| *ranbp9* | 24.6 | 8.2 | 0.5 | 1.4 | 0.99 | 44025 | 2 | 145 |
| *ranbp9* | 24.7 | 7.7 | 0.5 | 1.4 | 0.99 | 41336 | 2 | 145 |

| targeted transcripts | period [h] | phase [h] | relative amplitude | damping [h$^{-1}$] | CC | mean [cps] | run | internal construct # |
|---|---|---|---|---|---|---|---|---|
| *ranbp9* | 24.6 | 6.6 | 0.6 | 1.4 | 0.99 | 44904 | 2 | 145 |
| *ranbp9* | 25 | 19.5 | 0.2 | 2.7 | 0.95 | 67209 | 1 | 168 |
| *ranbp9* | 24 | 19 | 0.2 | 2 | 0.98 | 72660 | 1 | 168 |
| *ranbp9* | 24.5 | 18.4 | 0.2 | 2 | 0.98 | 63494 | 1 | 168 |
| *ranbp9* | 24.9 | 7.6 | 0.6 | 1.5 | 0.99 | 58271 | 2 | 168 |
| *ranbp9* | 25 | 7.5 | 0.6 | 1.5 | 0.99 | 59607 | 2 | 168 |
| *ranbp9* | 24.6 | 8.9 | 0.4 | 1.6 | 0.99 | 64377 | 2 | 168 |
| *ranbp10* | 23.7 | 19.6 | 0.1 | 5.9 | 0.93 | 60044 | 1 | 50 |
| *ranbp10* | 23.6 | 18.7 | 0.2 | 2.7 | 0.95 | 56657 | 1 | 50 |
| *ranbp10* | 19.5 | 1.2 | 0.1 | 21.2 | 0.69 | 43961 | 1 | 50 |
| *ranbp10* | 24.6 | 9.5 | 0.2 | 2 | 0.95 | 67566 | 2 | 50 |
| *ranbp10* | 24.6 | 8 | 0.3 | 1.8 | 0.99 | 64771 | 2 | 50 |
| *ranbp10* | 23.9 | 9.4 | 0.2 | 1.8 | 0.98 | 62981 | 2 | 50 |
| *ranbp10* | 24.2 | 20.1 | 0.2 | 3.5 | 0.95 | 58955 | 1 | 64 |
| *ranbp10* | 46.3 | 17.3 | 0.1 | 0.8 | 0.69 | 43482 | 1 | 64 |
| *ranbp10* | 59.7 | 1.4 | 0 | 0.1 | 0.81 | 48229 | 1 | 64 |
| *ranbp10* | 24.3 | 8.5 | 0.4 | 1.5 | 0.98 | 73559 | 2 | 64 |
| *ranbp10* | 24.4 | 9.1 | 0.4 | 1.5 | 0.99 | 66472 | 2 | 64 |
| *ranbp10* | 24.1 | 8.3 | 0.4 | 1.4 | 0.98 | 63376 | 2 | 64 |
| *ranbp10* | 26.4 | 20.1 | 0.2 | 2.2 | 0.94 | 29366 | 1 | 76 |
| *ranbp10* | 23.5 | 19.9 | 0.2 | 2.1 | 0.97 | 65362 | 1 | 76 |
| *ranbp10* | 26 | 19.8 | 0.2 | 2.3 | 0.95 | 48043 | 1 | 76 |
| *ranbp10* | 25.6 | 9.2 | 0.3 | 1.5 | 0.98 | 72083 | 2 | 76 |
| *ranbp10* | 25.7 | 7 | 0.4 | 1.5 | 0.98 | 64343 | 2 | 76 |
| *ranbp10* | 25.5 | 6.1 | 0.5 | 1.5 | 0.98 | 58034 | 2 | 76 |
| *ranbp11* | 23.6 | 20 | 0.2 | 3.4 | 0.96 | 32621 | 1 | 57/94 |
| *ranbp11* | 23.4 | 19.8 | 0.2 | 2.4 | 0.96 | 31961 | 1 | 57/94 |
| *ranbp11* | 24.6 | 20.5 | 0.2 | 3.9 | 0.91 | 29216 | 1 | 57/94 |
| *ranbp11* | 24.4 | 19.6 | 0.2 | 3.4 | 0.96 | 31718 | 1 | 57/94 |
| *ranbp11* | 23.1 | 19.6 | 0.2 | 2.4 | 0.97 | 36189 | 1 | 57/94 |
| *ranbp11* | 23.3 | 21 | 0.2 | 3.2 | 0.91 | 29373 | 1 | 57/94 |
| *ranbp11* | 24.3 | 8.6 | 0.4 | 1.6 | 0.98 | 50764 | 2 | 57/94 |
| *ranbp11* | 24.1 | 7.7 | 0.5 | 1.6 | 0.99 | 46150 | 2 | 57/94 |
| *ranbp11* | 24.1 | 7 | 0.5 | 1.6 | 0.98 | 46057 | 2 | 57/94 |
| *ranbp11* | 24 | 8.7 | 0.4 | 1.6 | 0.99 | 48895 | 2 | 57/94 |
| *ranbp11* | 23.9 | 8.3 | 0.5 | 1.5 | 0.99 | 44920 | 2 | 57/94 |
| *ranbp11* | 23.9 | 7.2 | 0.6 | 1.5 | 0.99 | 44201 | 2 | 57/94 |
| *ranbp11* | 23 | 20.8 | 0.2 | 2.2 | 0.96 | 21796 | 1 | 66/106 |
| *ranbp11* | 23.2 | 18.6 | 0.3 | 1.6 | 0.99 | 33561 | 1 | 66/106 |
| *ranbp11* | 23.3 | 19.7 | 0.2 | 1.8 | 0.98 | 33706 | 1 | 66/106 |
| *ranbp11* | 23.2 | 19.7 | 0.3 | 1.8 | 0.98 | 40487 | 1 | 66/106 |
| *ranbp11* | 23.1 | 18 | 0.4 | 1.4 | 0.98 | 49861 | 1 | 66/106 |
| *ranbp11* | 23.2 | 19.5 | 0.3 | 1.7 | 0.98 | 43917 | 1 | 66/106 |
| *ranbp11* | 24.1 | 7.9 | 0.5 | 1.5 | 0.99 | 59661 | 2 | 66/106 |
| *ranbp11* | 24 | 8.4 | 0.5 | 1.5 | 0.99 | 54344 | 2 | 66/106 |
| *ranbp11* | 24 | 7.3 | 0.6 | 1.5 | 0.99 | 53053 | 2 | 66/106 |
| *ranbp11* | 24.1 | 7.4 | 0.5 | 1.5 | 0.99 | 47422 | 2 | 66/106 |
| *ranbp11* | 24 | 8.7 | 0.5 | 1.4 | 0.99 | 51658 | 2 | 66/106 |
| *ranbp11* | 24 | 7.6 | 0.5 | 1.5 | 0.99 | 49899 | 2 | 66/106 |
| *ranbp11* | 25.3 | 20 | 0.2 | 2 | 0.95 | 31434 | 1 | 72/115 |
| *ranbp11* | 24.2 | 19.2 | 0.2 | 1.7 | 0.97 | 41293 | 1 | 72/115 |
| *ranbp11* | 24.8 | 21 | 0.1 | 3.2 | 0.93 | 23889 | 1 | 72/115 |
| *ranbp11* | 23.3 | 20.9 | 0.2 | 2.4 | 0.96 | 41281 | 1 | 72/115 |
| *ranbp11* | 22.9 | 19.6 | 0.3 | 1.8 | 0.98 | 57365 | 1 | 72/115 |
| *ranbp11* | 22.8 | 20.4 | 0.2 | 2.2 | 0.97 | 47909 | 1 | 72/115 |
| *ranbp11* | 24.9 | 7 | 0.4 | 1.5 | 0.99 | 54839 | 2 | 72/115 |
| *ranbp11* | 24.9 | 6.9 | 0.4 | 1.5 | 0.98 | 54400 | 2 | 72/115 |
| *ranbp11* | 24.7 | 6.3 | 0.4 | 1.4 | 0.98 | 53185 | 2 | 72/115 |
| *ranbp11* | 24.1 | 7.2 | 0.6 | 1.5 | 0.99 | 51864 | 2 | 72/115 |
| *ranbp11* | 24.2 | 6.8 | 0.6 | 1.4 | 0.99 | 51706 | 2 | 72/115 |
| *ranbp11* | 24.1 | 7.2 | 0.5 | 1.4 | 0.99 | 52330 | 2 | 72/115 |
| *ranbp13* | 25 | 20.6 | 0.1 | 4.5 | 0.94 | 18253 | 1 | 89 |
| *ranbp13* | 23.3 | 19.3 | 0.2 | 2.1 | 0.98 | 34633 | 1 | 89 |
| *ranbp13* | 23.7 | 19.8 | 0.2 | 2.1 | 0.96 | 31600 | 1 | 89 |
| *ranbp13* | 24.7 | 8.6 | 0.4 | 1.5 | 0.99 | 48200 | 2 | 89 |
| *ranbp13* | 24.6 | 7.4 | 0.5 | 1.5 | 0.99 | 43303 | 2 | 89 |
| *ranbp13* | 24.5 | 7 | 0.4 | 1.4 | 0.99 | 46489 | 2 | 89 |
| *ranbp13* | 21.9 | 20.4 | 0.2 | 2.9 | 0.97 | 29986 | 1 | 99 |
| *ranbp13* | 215616405.4 | 6 | 290929.8 | 50.6 | 0.68 | 30332 | 1 | 99 |
| *ranbp13* | 23.9 | 20.3 | 0.1 | 4.8 | 0.92 | 17403 | 1 | 99 |
| *ranbp13* | 24.1 | 8.4 | 0.4 | 1.6 | 0.98 | 57958 | 2 | 99 |
| *ranbp13* | 23.9 | 8 | 0.4 | 1.6 | 0.99 | 53021 | 2 | 99 |

| targeted transcripts | period [h] | phase [h] | relative amplitude | damping [h$^{-1}$] | CC | mean [cps] | run | internal construct # |
|---|---|---|---|---|---|---|---|---|
| *ranbp13* | 23.9 | 7.7 | 0.4 | 1.5 | 0.99 | 55379 | 2 | 99 |
| *ranbp16* | 23.8 | 19 | 0.3 | 1.8 | 0.98 | 54742 | 1 | 122 |
| *ranbp16* | 23.6 | 18.8 | 0.3 | 1.7 | 0.97 | 54263 | 1 | 122 |
| *ranbp16* | 28.8 | 15.3 | 0.1 | 0.7 | 0.81 | 47099 | 1 | 122 |
| *ranbp16* | 24.6 | 7.1 | 0.5 | 1.5 | 0.98 | 45661 | 2 | 122 |
| *ranbp16* | 24.9 | 7 | 0.6 | 1.5 | 0.99 | 43512 | 2 | 122 |
| *ranbp16* | 24.5 | 7.4 | 0.4 | 1.5 | 0.98 | 46075 | 2 | 122 |
| *ranbp16* | 22.5 | 19.7 | 0.3 | 2.1 | 0.98 | 57368 | 1 | 91 |
| *ranbp16* | 26.3 | 15.9 | 0.1 | 1.1 | 0.8 | 52266 | 1 | 91 |
| *ranbp16* | 23.3 | 19.9 | 0.2 | 2.1 | 0.96 | 55311 | 1 | 91 |
| *ranbp16* | 24.1 | 7.6 | 0.4 | 1.5 | 0.97 | 53690 | 2 | 91 |
| *ranbp16* | 24.1 | 8 | 0.4 | 1.5 | 0.98 | 56644 | 2 | 91 |
| *ranbp16* | 23.9 | 7.5 | 0.4 | 1.5 | 0.99 | 55491 | 2 | 91 |
| *ranbp16* | 23 | 19.7 | 0.3 | 1.9 | 0.98 | 33775 | 1 | 96 |
| *ranbp16* | 22.8 | 19.1 | 0.3 | 1.6 | 0.99 | 39058 | 1 | 96 |
| *ranbp16* | 23.1 | 18.9 | 0.3 | 1.5 | 0.98 | 36113 | 1 | 96 |
| *ranbp16* | 23.7 | 8 | 0.4 | 1.4 | 0.99 | 63249 | 2 | 96 |
| *ranbp16* | 23.8 | 7.6 | 0.4 | 1.5 | 0.99 | 58762 | 2 | 96 |
| *ranbp16* | 23.6 | 7.2 | 0.5 | 1.4 | 0.99 | 59669 | 2 | 96 |
| *ranbp17* | 22.9 | 19.1 | 0.2 | 1.6 | 0.97 | 50713 | 1 | 108 |
| *ranbp17* | 22.7 | 18.8 | 0.2 | 1.5 | 0.97 | 49083 | 1 | 108 |
| *ranbp17* | 22.8 | 18.9 | 0.3 | 1.6 | 0.98 | 55532 | 1 | 108 |
| *ranbp17* | 23.9 | 7.3 | 0.5 | 1.5 | 0.99 | 43808 | 2 | 108 |
| *ranbp17* | 24.2 | 6.5 | 0.5 | 1.4 | 0.99 | 43051 | 2 | 108 |
| *ranbp17* | 23.8 | 8 | 0.3 | 1.5 | 0.99 | 47016 | 2 | 108 |
| *ranbp17* | 24.2 | 19.6 | 0.2 | 2.2 | 0.97 | 37675 | 1 | 86 |
| *ranbp17* | 26.6 | 0 | 0.1 | 0.9 | 0.54 | 33043 | 1 | 86 |
| *ranbp17* | 25.3 | 19.5 | 0.2 | 2.3 | 0.94 | 34026 | 1 | 86 |
| *ranbp17* | 24.8 | 8.8 | 0.4 | 1.5 | 0.98 | 59990 | 2 | 86 |
| *ranbp17* | 24.9 | 7.5 | 0.5 | 1.5 | 0.98 | 53507 | 2 | 86 |
| *ranbp17* | 24.7 | 8 | 0.4 | 1.5 | 0.98 | 54127 | 2 | 86 |
| *ranbp17* | 23.4 | 18.4 | 0.2 | 1.7 | 0.97 | 48759 | 1 | 87 |
| *ranbp17* | 23 | 18.8 | 0.2 | 1.9 | 0.96 | 55048 | 1 | 87 |
| *ranbp17* | 25.9 | 2.2 | 0 | 0.8 | 0.57 | 48147 | 1 | 87 |
| *ranbp17* | 24.7 | 8.2 | 0.4 | 1.4 | 0.98 | 56815 | 2 | 87 |
| *ranbp17* | 25 | 7.5 | 0.4 | 1.4 | 0.99 | 53108 | 2 | 87 |
| *ranbp17* | 24.8 | 6.6 | 0.5 | 1.4 | 0.98 | 52348 | 2 | 87 |
| *rangrf* | 23.9 | 18.8 | 0.3 | 1.8 | 0.98 | 60754 | 1 | 158 |
| *rangrf* | 23.2 | 18.6 | 0.3 | 1.8 | 0.97 | 60312 | 1 | 158 |
| *rangrf* | 23.9 | 18.4 | 0.3 | 1.8 | 0.98 | 65402 | 1 | 158 |
| *rangrf* | 24.5 | 7.2 | 0.6 | 1.5 | 0.99 | 56842 | 2 | 158 |
| *rangrf* | 24.7 | 7.3 | 0.5 | 1.5 | 0.99 | 58896 | 2 | 158 |
| *rangrf* | 24.4 | 8.3 | 0.4 | 1.5 | 0.99 | 60197 | 2 | 158 |
| *rangrf* | 24.2 | 20.5 | 0.2 | 2.6 | 0.96 | 60835 | 1 | 180 |
| *rangrf* | 23.3 | 20.3 | 0.2 | 2.2 | 0.97 | 63751 | 1 | 180 |
| *rangrf* | 23.3 | 18.8 | 0.3 | 1.8 | 0.97 | 64757 | 1 | 180 |
| *rangrf* | 24.5 | 7.6 | 0.5 | 1.6 | 0.99 | 60206 | 2 | 180 |
| *rangrf* | 24.4 | 8.8 | 0.4 | 1.6 | 0.99 | 66334 | 2 | 180 |
| *rangrf* | 24.5 | 7.4 | 0.5 | 1.6 | 0.99 | 64918 | 2 | 180 |
| *rangrf* | 23.6 | 18.4 | 0.3 | 1.7 | 0.99 | 53586 | 1 | 184 |
| *rangrf* | 23.4 | 17.6 | 0.3 | 1.6 | 0.97 | 55305 | 1 | 184 |
| *rangrf* | 23.5 | 18.7 | 0.3 | 1.8 | 0.98 | 51843 | 1 | 184 |
| *rangrf* | 24.5 | 7.1 | 0.4 | 1.5 | 0.99 | 56668 | 2 | 184 |
| *rangrf* | 24.6 | 7.8 | 0.5 | 1.4 | 0.99 | 56350 | 2 | 184 |
| *rangrf* | 24.5 | 8 | 0.4 | 1.5 | 0.99 | 59150 | 2 | 184 |
| *sec13* | 31.3 | 19.1 | 0 | 0.7 | 0.68 | 47349 | 1 | 164 |
| *sec13* | 29.4 | 18.1 | 0.1 | 21.3 | 0.73 | 49724 | 1 | 164 |
| *sec13* | 29.5 | 18.4 | 0.1 | 13.7 | 0.77 | 48797 | 1 | 164 |
| *sec13* | 26.6 | 8.1 | 0.2 | 2.2 | 0.99 | 84267 | 2 | 164 |
| *sec13* | 27 | 8.1 | 0.2 | 2.1 | 0.99 | 78808 | 2 | 164 |
| *sec13* | 26.5 | 7.6 | 0.2 | 2.3 | 1 | 79597 | 2 | 164 |
| *sec13* | 29.4 | 17.1 | 0.2 | 2.4 | 0.97 | 45316 | 1 | 173 |
| *sec13* | 28.3 | 16.8 | 0.1 | 2.1 | 0.93 | 47776 | 1 | 173 |
| *sec13* | 28.2 | 16.6 | 0.2 | 2.2 | 0.97 | 60566 | 1 | 173 |
| *sec13* | 27.6 | 6.6 | 0.3 | 2 | 0.99 | 67281 | 2 | 173 |
| *sec13* | 27.8 | 8.1 | 0.2 | 1.9 | 0.98 | 67874 | 2 | 173 |
| *sec13* | 28.1 | 6.6 | 0.3 | 2.2 | 0.99 | 68814 | 2 | 173 |
| *sec13* | 28 | 17.5 | 0.2 | 2.3 | 0.95 | 70710 | 1 | 174 |
| *sec13* | 28.4 | 17.3 | 0.1 | 2.2 | 0.91 | 61893 | 1 | 174 |
| *sec13* | 27.4 | 17.3 | 0.2 | 2.1 | 0.92 | 87500 | 1 | 174 |
| *sec13* | 28.1 | 7.9 | 0.2 | 2.1 | 0.99 | 88734 | 2 | 174 |
| *sec13* | 28 | 8 | 0.2 | 2.1 | 0.98 | 79120 | 2 | 174 |

| targeted transcripts | period [h] | phase [h] | relative amplitude | damping [h$^{-1}$] | CC | mean [cps] | run | internal construct # |
|---|---|---|---|---|---|---|---|---|
| *sec13* | 28.2 | 8.4 | 0.2 | 2.1 | 0.98 | 80920 | 2 | 174 |
| *seh1* | 26.4 | 18.5 | 0.3 | 1.6 | 0.98 | 29265 | 1 | 124 |
| *seh1* | 25.2 | 19 | 0.3 | 2 | 0.98 | 31277 | 1 | 124 |
| *seh1* | 25.8 | 17.9 | 0.3 | 1.6 | 0.98 | 39313 | 1 | 124 |
| *seh1* | 26.1 | 7 | 0.5 | 1.5 | 0.99 | 43102 | 2 | 124 |
| *seh1* | 26.4 | 6.9 | 0.5 | 1.6 | 0.99 | 39073 | 2 | 124 |
| *seh1* | 25.9 | 7.6 | 0.4 | 1.6 | 0.99 | 44745 | 2 | 124 |
| *seh1* | 22.8 | 19.1 | 0.3 | 2.2 | 0.97 | 65418 | 1 | 182 |
| *seh1* | 23.1 | 19.4 | 0.2 | 2.1 | 0.97 | 59558 | 1 | 182 |
| *seh1* | 23.6 | 18.6 | 0.3 | 2 | 0.98 | 68595 | 1 | 182 |
| *seh1* | 24.9 | 7.5 | 0.5 | 1.4 | 0.99 | 57881 | 2 | 182 |
| *seh1* | 25.1 | 7.3 | 0.5 | 1.4 | 0.99 | 57963 | 2 | 182 |
| *seh1* | 24.8 | 8.2 | 0.4 | 1.4 | 0.99 | 62241 | 2 | 182 |
| *seh1* | 24.5 | 18.6 | 0.3 | 1.7 | 0.99 | 38497 | 1 | 183 |
| *seh1* | 23.8 | 18.3 | 0.3 | 1.6 | 0.98 | 47172 | 1 | 183 |
| *seh1* | 24.3 | 18.6 | 0.3 | 1.7 | 0.99 | 51238 | 1 | 183 |
| *seh1* | 24.9 | 7.6 | 0.5 | 1.5 | 0.99 | 52970 | 2 | 183 |
| *seh1* | 25 | 8.2 | 0.5 | 1.5 | 0.99 | 54450 | 2 | 183 |
| *seh1* | 25.1 | 6.9 | 0.6 | 1.4 | 0.99 | 52513 | 2 | 183 |
| *tnpo1* | 22.3 | 19.3 | 0.3 | 2 | 0.98 | 56900 | 1 | 32 |
| *tnpo1* | 25.6 | 18.7 | 0.1 | 1 | 0.51 | 54896 | 1 | 32 |
| *tnpo1* | 21.4 | 22.8 | 0.1 | 2.5 | 0.61 | 55352 | 1 | 32 |
| *tnpo1* | 23.1 | 9.9 | 0.3 | 1.5 | 0.94 | 60659 | 2 | 32 |
| *tnpo1* | 23.5 | 7.9 | 0.5 | 1.6 | 0.98 | 56013 | 2 | 32 |
| *tnpo1* | 23.6 | 7.2 | 0.6 | 1.6 | 0.98 | 54834 | 2 | 32 |
| *tnpo1* | 22.1 | 20.4 | 0.2 | 1.9 | 0.97 | 45441 | 1 | 37 |
| *tnpo1* | 22.2 | 19.4 | 0.2 | 1.8 | 0.98 | 38957 | 1 | 37 |
| *tnpo1* | 23.7 | 20.7 | 0.1 | 4 | 0.95 | 34933 | 1 | 37 |
| *tnpo1* | 22.9 | 10.2 | 0.4 | 1.7 | 0.98 | 49718 | 2 | 37 |
| *tnpo1* | 22.9 | 9 | 0.5 | 1.6 | 0.97 | 53523 | 2 | 37 |
| *tnpo1* | 23 | 7.9 | 0.5 | 1.6 | 0.99 | 47283 | 2 | 37 |
| *tnpo1* | 22.9 | 18.8 | 0.3 | 1.7 | 0.99 | 69614 | 1 | 40 |
| *tnpo1* | 22.7 | 19.5 | 0.3 | 1.8 | 0.98 | 71169 | 1 | 40 |
| *tnpo1* | 22.7 | 20.5 | 0.2 | 1.9 | 0.98 | 66229 | 1 | 40 |
| *tnpo1* | 23.9 | 7.6 | 0.5 | 1.5 | 0.99 | 72614 | 2 | 40 |
| *tnpo1* | 23.9 | 7.4 | 0.6 | 1.5 | 0.99 | 67138 | 2 | 40 |
| *tnpo1* | 23.7 | 7 | 0.6 | 1.5 | 0.99 | 62297 | 2 | 40 |
| *tnpo2* | 23.1 | 19 | 0.2 | 2.1 | 0.98 | 38043 | 1 | 46 |
| *tnpo2* | 23.4 | 17.2 | 0.3 | 1.7 | 0.97 | 39903 | 1 | 46 |
| *tnpo2* | 21.7 | 21 | 0.1 | 1.8 | 0.93 | 32607 | 1 | 46 |
| *tnpo2* | 23.6 | 9.5 | 0.3 | 1.5 | 0.97 | 43161 | 2 | 46 |
| *tnpo2* | 23.9 | 7.3 | 0.6 | 1.5 | 0.98 | 44114 | 2 | 46 |
| *tnpo2* | 23.8 | 7.1 | 0.6 | 1.5 | 0.98 | 45112 | 2 | 46 |
| *tnpo3* | 23.7 | 19.1 | 0.2 | 2.3 | 0.98 | 58325 | 1 | 25 |
| *tnpo3* | 23.7 | 18.9 | 0.2 | 2.4 | 0.98 | 50117 | 1 | 25 |
| *tnpo3* | 24.6 | 19.3 | 0.2 | 2.7 | 0.96 | 49062 | 1 | 25 |
| *tnpo3* | 24.9 | 8.2 | 0.4 | 1.5 | 0.99 | 64836 | 2 | 25 |
| *tnpo3* | 25 | 8 | 0.4 | 1.6 | 0.99 | 62922 | 2 | 25 |
| *tnpo3* | 24.8 | 6.8 | 0.5 | 1.5 | 0.99 | 57420 | 2 | 25 |
| *tnpo3* | 23.9 | 19.5 | 0.2 | 2.3 | 0.96 | 63004 | 1 | 33 |
| *tnpo3* | 26.5 | 20.6 | 0.1 | 0.9 | 0.72 | 52120 | 1 | 33 |
| *tnpo3* | 24.9 | 20.6 | 0.1 | 4 | 0.94 | 44046 | 1 | 33 |
| *tnpo3* | 24.3 | 10.2 | 0.3 | 1.5 | 0.91 | 45501 | 2 | 33 |
| *tnpo3* | 24.3 | 8.8 | 0.4 | 1.5 | 0.94 | 46851 | 2 | 33 |
| *tnpo3* | 24.1 | 8.3 | 0.4 | 1.5 | 0.99 | 47067 | 2 | 33 |
| *tpr* | 23.8 | 19.6 | 0.3 | 2.1 | 0.98 | 19592 | 1 | 26 |
| *tpr* | 298711.7 | 6 | 347.1 | 336.3 | 0.68 | 19495 | 1 | 26 |
| *tpr* | 24.4 | 18.7 | 0.3 | 2.1 | 0.98 | 22382 | 1 | 26 |
| *tpr* | 24.8 | 9.6 | 0.3 | 1.5 | 0.99 | 35429 | 2 | 26 |
| *tpr* | 25 | 8 | 0.4 | 1.5 | 0.99 | 32451 | 2 | 26 |
| *tpr* | 24.8 | 6.8 | 0.3 | 1.5 | 0.98 | 32901 | 2 | 26 |
| *tpr* | 23.3 | 17.5 | 0.4 | 1.5 | 0.96 | 58123 | 1 | 28 |
| *tpr* | 22.9 | 19 | 0.2 | 1.6 | 0.97 | 43874 | 1 | 28 |
| *tpr* | 23.3 | 19 | 0.3 | 1.6 | 0.97 | 59487 | 1 | 28 |
| *tpr* | 24 | 7.9 | 0.5 | 1.6 | 0.99 | 55574 | 2 | 28 |
| *tpr* | 24 | 9.7 | 0.4 | 1.5 | 0.99 | 58253 | 2 | 28 |
| *tpr* | 24.1 | 8.3 | 0.4 | 1.6 | 0.99 | 57563 | 2 | 28 |
| *tpr* | 23.3 | 19.6 | 0.2 | 1.9 | 0.97 | 43035 | 1 | 34 |
| *tpr* | 23.3 | 19 | 0.2 | 2 | 0.98 | 41309 | 1 | 34 |
| *tpr* | 23.2 | 20.9 | 0.2 | 2.3 | 0.95 | 33577 | 1 | 34 |
| *tpr* | 24.4 | 7.3 | 0.5 | 1.4 | 0.98 | 37634 | 2 | 34 |
| *tpr* | 24.5 | 9 | 0.4 | 1.4 | 0.98 | 39404 | 2 | 34 |

| targeted transcripts | period [h] | phase [h] | relative amplitude | damping [$h^{-1}$] | CC | mean [cps] | run | internal construct # |
|---|---|---|---|---|---|---|---|---|
| *tpr* | 24.3 | 6.6 | 0.6 | 1.3 | 0.99 | 35305 | 2 | 34 |
| *xpo1* | 25.6 | 19.2 | 0.2 | 4.6 | 0.95 | 7034 | 1 | 17 |
| *xpo1* | 45.2 | 14 | 0.1 | 37.3 | 0.91 | 13178 | 1 | 17 |
| *xpo1* | 64 | 11.9 | 0.1 | 82.1 | 0.78 | 1690 | 1 | 17 |
| *xpo1* | 25.5 | 8.4 | 0.2 | 1.7 | 0.99 | 24417 | 2 | 17 |
| *xpo1* | 25 | 8.7 | 0.2 | 1.8 | 0.99 | 22005 | 2 | 17 |
| *xpo1* | 25.5 | 5.8 | 0.4 | 1.7 | 0.99 | 23560 | 2 | 17 |
| *xpo1* | 26.9 | 18.6 | 0.2 | 6.4 | 0.93 | 3706 | 1 | 19 |
| *xpo1* | 147.2 | 8.1 | 0.2 | 569.6 | 0.8 | 5066 | 1 | 19 |
| *xpo1* | 41.8 | 14.1 | 0.1 | 30.7 | 0.76 | 1895 | 1 | 19 |
| *xpo1* | 25 | 7 | 0.3 | 1.9 | 0.99 | 25182 | 2 | 19 |
| *xpo1* | 25.2 | 6.6 | 0.3 | 1.9 | 0.99 | 23494 | 2 | 19 |
| *xpo1* | 25.2 | 5.2 | 0.4 | 1.8 | 0.99 | 24042 | 2 | 19 |
| *xpo1* | 28.2 | 18.4 | 0.2 | 9.9 | 0.95 | 8679 | 1 | 4 |
| *xpo1* | 39.1 | 14.1 | 0.1 | 25.8 | 0.86 | 6425 | 1 | 4 |
| *xpo1* | 51.8 | 12.3 | 0.1 | 139.6 | 0.88 | 12177 | 1 | 4 |
| *xpo1* | 25.6 | 6.8 | 0.2 | 2 | 0.99 | 23111 | 2 | 4 |
| *xpo1* | 25.1 | 6.9 | 0.3 | 2 | 0.99 | 19458 | 2 | 4 |
| *xpo1* | 25.3 | 6.5 | 0.2 | 1.9 | 0.99 | 23638 | 2 | 4 |
| *xpo4* | 23.3 | 19.2 | 0.3 | 1.6 | 0.98 | 50372 | 1 | 112 |
| *xpo4* | 23.2 | 17.8 | 0.4 | 1.4 | 0.98 | 48626 | 1 | 112 |
| *xpo4* | 23.2 | 18.6 | 0.4 | 1.5 | 0.98 | 52877 | 1 | 112 |
| *xpo4* | 24.4 | 7.1 | 0.5 | 1.4 | 0.99 | 48814 | 2 | 112 |
| *xpo4* | 24.3 | 8.9 | 0.5 | 1.4 | 0.99 | 51816 | 2 | 112 |
| *xpo4* | 24.1 | 9.2 | 0.5 | 1.5 | 0.99 | 51670 | 2 | 112 |
| *xpo4* | 23.5 | 18.6 | 0.3 | 2 | 0.97 | 43916 | 1 | 120 |
| *xpo4* | 23.4 | 18.2 | 0.3 | 2 | 0.96 | 45109 | 1 | 120 |
| *xpo4* | 23.5 | 18.2 | 0.4 | 1.7 | 0.97 | 46945 | 1 | 120 |
| *xpo4* | 24.2 | 7.9 | 0.5 | 1.6 | 0.97 | 41698 | 2 | 120 |
| *xpo4* | 24.7 | 7.3 | 0.5 | 1.5 | 0.98 | 36694 | 2 | 120 |
| *xpo4* | 24.3 | 6.6 | 0.5 | 1.6 | 0.97 | 39983 | 2 | 120 |
| *xpo5* | 22.8 | 20.7 | 0.2 | 1.9 | 0.92 | 35777 | 1 | 125 |
| *xpo5* | 23.2 | 19 | 0.2 | 1.7 | 0.92 | 35607 | 1 | 125 |
| *xpo5* | 22.8 | 21.2 | 0.2 | 1.9 | 0.93 | 27802 | 1 | 125 |
| *xpo5* | 24.8 | 7.6 | 0.4 | 1.4 | 0.98 | 38640 | 2 | 125 |
| *xpo5* | 25.1 | 7.3 | 0.4 | 1.4 | 0.99 | 36341 | 2 | 125 |
| *xpo5* | 24.8 | 7.8 | 0.3 | 1.4 | 0.98 | 38372 | 2 | 125 |
| *xpo6* | 22.2 | 20 | 0.2 | 2.5 | 0.96 | 65508 | 1 | 155 |
| *xpo6* | 22.4 | 19.7 | 0.2 | 2.1 | 0.97 | 64393 | 1 | 155 |
| *xpo6* | 22.8 | 19.1 | 0.3 | 2 | 0.97 | 66083 | 1 | 155 |
| *xpo6* | 24.2 | 8.1 | 0.4 | 1.6 | 0.99 | 60766 | 2 | 155 |
| *xpo6* | 24.8 | 6.2 | 0.6 | 1.5 | 0.99 | 57646 | 2 | 155 |
| *xpo6* | 24.6 | 6.6 | 0.5 | 1.5 | 0.99 | 58195 | 2 | 155 |
| *xpo6* | 24.2 | 20 | 0.2 | 2.2 | 0.97 | 32204 | 1 | 177 |
| *xpo6* | 23.8 | 20.1 | 0.2 | 1.9 | 0.96 | 38980 | 1 | 177 |
| *xpo6* | 23.6 | 18.2 | 0.3 | 1.5 | 0.97 | 48086 | 1 | 177 |
| *xpo6* | 24.7 | 8.7 | 0.5 | 1.6 | 0.98 | 62701 | 2 | 177 |
| *xpo6* | 24.8 | 9.5 | 0.4 | 1.5 | 0.99 | 60234 | 2 | 177 |
| *xpo6* | 24.9 | 8.5 | 0.4 | 1.6 | 0.99 | 69196 | 2 | 177 |
| *xpo6* | 23.3 | 18.6 | 0.3 | 1.8 | 0.98 | 39928 | 1 | 185 |
| *xpo6* | 23.2 | 18.9 | 0.3 | 1.9 | 0.97 | 43702 | 1 | 185 |
| *xpo6* | 23.5 | 18.2 | 0.3 | 1.7 | 0.97 | 36148 | 1 | 185 |
| *xpo6* | 24.8 | 6.5 | 0.6 | 1.5 | 0.99 | 44937 | 2 | 185 |
| *xpo6* | 24.9 | 6.3 | 0.6 | 1.5 | 0.99 | 43964 | 2 | 185 |
| *xpo6* | 24.7 | 7.6 | 0.4 | 1.6 | 0.99 | 45554 | 2 | 185 |
| *xpot* | 28.5 | 18.1 | 0.2 | 2.3 | 0.92 | 33903 | 1 | 138 |
| *xpot* | 27.4 | 19.6 | 0.1 | 1 | 0.58 | 35754 | 1 | 138 |
| *xpot* | 26.5 | 17.5 | 0.2 | 2.4 | 0.96 | 42324 | 1 | 138 |
| *xpot* | 24.6 | 8.6 | 0.3 | 1.7 | 0.98 | 39870 | 2 | 138 |
| *xpot* | 25.4 | 6.7 | 0.5 | 1.6 | 0.99 | 36054 | 2 | 138 |
| *xpot* | 24.3 | 8.6 | 0.3 | 1.6 | 0.98 | 39647 | 2 | 138 |

## A1.5 Residual *tnpo1* levels do not correlate with parameter alterations of circadian rhythms upon knockdown of *tnpo1* expression.

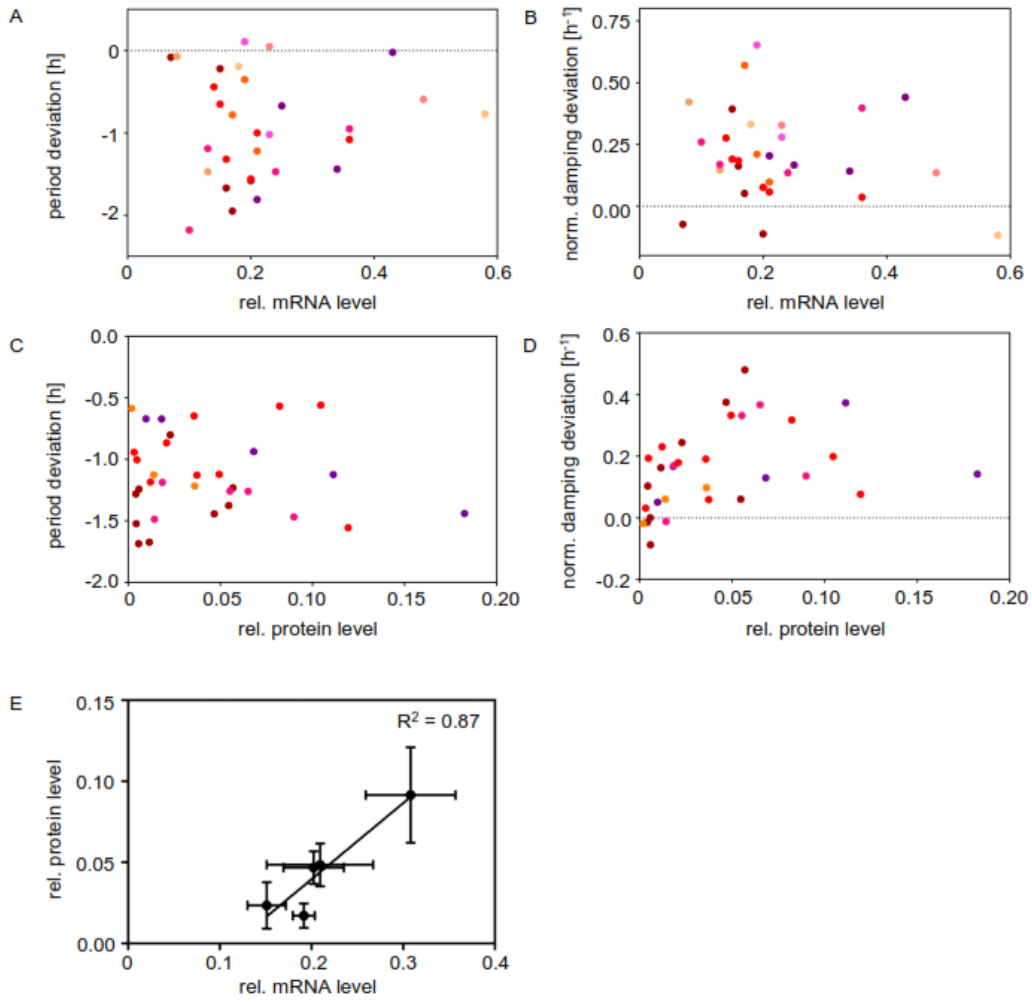


**Suppl. figure A1.3: Residual *tnpo1* levels do not correlate with parameter alterations of circadian rhythms upon knockdown of *tnpo1* expression.** U-2 OS cells harboring a *bmal1* promoter-driven *luciferase* were lentivirally transduced with one of nine different RNAi constructs (red color coded) targeting *tnpo1* expression. After bioluminescence recordings of up to seven days, relative *tnpo1* mRNA levels were correlated to the corresponding period shortening (A) or damping of the amplitude per 24 h (B; damping). Protein levels of five of the nine RNAi constructs were determined and correlated to period deviation (C) and damping (D). E) Correlation and linear regression ($R^2$) of *tnpo1* mRNA and protein levels of five different RNAi constructs targeting *tnpo1* expression in U-2 OS reporter cells (error bars = SD; n = 2 to 10 individual recordings).

## A1.6 Validation of CRISPR/Cas9 genome edited cells

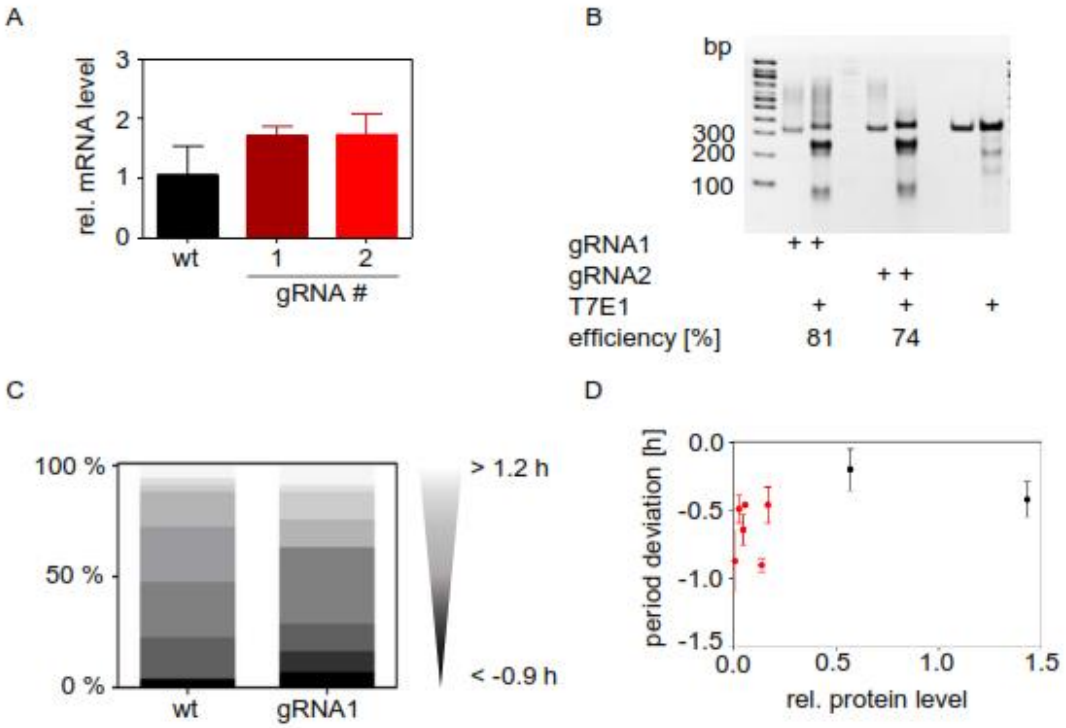


**Suppl. figure A1.4: Validation of CRISPR/Cas9 genome edited cells**. U-2 OS cells expressing a *bmal1* promoter-driven *luciferase* were lentivirally transduced with CRISPR/Cas9 and one of two different guide RNAs directed to the *tnpo1* open reading frame (gRNA1, red or gRNA2, dark red). A) Relative *tnpo1* mRNA levels of the genome edited (red) and wild type (wt, black) cell populations were determined (error bars = SD, n = 3 dishes within one recording). B) T7 endonuclease test of CRISPR/Cas9 edited cells. Depicted are the PCR-products of gRNA1 and gRNA2 as well as of wild type cells either with or without T7 endonuclease (T7E1) treatment. The PCR-products of the 316 bp wild type is partially fragmented to 227 and 89 bp in gRNA1 edited cells. In gRNA2 genome edited cells the fragments of effective indel insertion are of 236 and 80 bp length. C) Quantification of single cell period shortening after limited dilution of gRNA1 edited or wild type reporter cells (n = 32 to 34 cells). D) TNPO1 protein levels vs period deviation of gRNA1 CRISPR/Cas9 genome edited (red) or wild type (black) single cells (error bars = SEM, n = 3 to 6 independent experiments).

## A1.7 M9 NLSs of TNPO1 cargos

**Suppl. table A1.3: Alphabetically listed M9 NLSs of TNPO1 cargos** [132].

| | |
|---|---|
| CLK3 | --RSPSFGEDYYGP--SRSRHRR-RSRERG---PY |
| CPSF6 | --PPTNSGMPTSDS--RGPPPTDPYGRPP----PY |
| CYCLIN T1 | ----VNMLHSLLSA--QGVQPTQPTAFEFVR--PY |
| ETLE | ----GQEEWTNSR--HKAPSARTAKGVYRDQ--PY |
| EWS | ----G-GRRGGRGGPGKMD-KGEHRQERRDR--PY |
| FUS | ----G-GDRGGFGP-GKMDSRGEHRQDRRER--PY |
| HCC1 | --RSRSK-ERRRSR--SRSRDRRFRGRYRS---PY |
| HEXIM1 | ---WG-QQQRQLGK--KKHRRRPSKKKRHWK--PY |
| hnRNP A0 | --SYGPMKSGGGGG-GGGSSWGG-RSNSG----PY |
| hnRNP A1 | FGNYN-NQSSNFGP-MKGGNFGG-RSSG-----PY |
| hnRNP A2 | --NYN-QQPSNYGP-MKSGNFGGSRNMGG----PY |
| hnRNP A3 | --NYSGQQQSNYGP-MKGGSFGG-RSSGS----PY |
| hnRNP D | YGDYS-NQQSGYG---KVSRRGG-HQNSYK---PY |
| hnRNP F | -FKSSQEEVRSYSD--PPLKFMSVQRPG-----PY |
| hnRNP H1 | ----GEGERPAQNE--KRKEKNIKRGGNRFE--PY |
| hnRNP M | ---HHQAQRFRFSP-MGVDHMSGLSGVNV----PG |
| HuR | -ADYS-GQQSTYG---KASRGGGNHQNNYQ---PY |
| JKTBP-1 | ----RDRGYDKADR--EEGKERRHHRREELA--PY |
| PABP-2 | ------DDWNGTRPSLKAPPARPVKGAYREH--PY |
| SAM68 | ------HPDYKYRP--RRKPKNLLKKDRYVFPLPY |
| SOX14 | ---YG-GDRGGYG--GKMGGRNDYRNDQRNR--PY |
| TAFII68 | ----SSRLEEDDGDVAMSDAQDGPRVRYN----PY |
| WBS16 | ----PSFVVPSSGP--GPRAGARPRRRIQPV--PY |

## A1.8 Conservation of clock-derived putative M9 NLSs containing a PY motif

**Suppl. table A1.4: Conservation of clock-derived putative M9 NLSs containing a PY motif.**

| | |
|---|---|
| BMAL1(110-132) | |
| human | ...KLTVLRMAVQHMKTLRGATNPY... |
| mouse | ...********************... |
| rat | ...********************... |
| chicken | ...********************... |
| frog | ...********R*************... |
| BMAL1 (544-566) | |
| human | ...TPDIPSSGLLSGQAQENPGYPY... |
| mouse | ...******T***P*****T*****... |
| rat | ...******A***P*****T*****... |
| chicken | ...****S*A******I*DSS****... |
| frog | ...GI*PV*T-*VP*--MDSS*F**... |
| PER1 (299-321) | |
| human | ...RIRGGPDRDPGPRYQPFRLTPY... |
| mouse | ...********************... |
| rat | ...********************... |
| PER1 (862-884) | |
| human | ...PPSTPWPTPPATTPFPAVVQPY... |
| mouse | ...*S*G***P*********M****... |
| rat | ...*S*G***P**************... |
| PER1 (914-936) | |
| human | ...VTPMVALVLPNYLFPTPSSYPY... |
| mouse | ...****************P****... |
| rat | ...***************S*T****... |

| | |
|---|---|
| CRY1 (232-254) | |
| human | ...NFERPRMNANSLLASPTGLSPY... |
| mouse | ...********************... |
| rat | ...********************... |
| monkey | ...********************... |
| cow | ...********************... |
| CRY2 (251-273) | |
| human | ...NYERPRMNANSLLASPTGLSPY... |
| mouse | ...********************... |
| rat | ...********************... |
| monkey | ...********************... |
| cowe | ...********************... |
| PER2 (224-246) | |
| human | ...AKFVEFLAPHDVGVFHSFTSPY... |
| mouse | ...***********S****Y*T**... |
| rat | ...***********S****Y*T**... |
| PER2 (272-294) | |
| human | ...RVSVRKSHENEIRYHPFRMTPY... |
| mouse | ...****G*H*******Q*******... |
| rat | ...****G*H*******Q*******... |
| PER2 (1201-1223) | |
| human | ...AIDVAECVYCENKEKGNICIPY... |
| mouse | ...****TG*****SE******L**... |
| rat | ...****TG*****SE****L*L**... |

## A1.9 Putative M9 clock peptide sequences and hnRNP A1 M9 NLS

**Suppl. table A1.5: Putative M9 clock peptide sequences and hnRNP A1 M9 NLS, which are C-terminally fused to ECFP.** Amino acid positions are indicated in brackets.

| | |
|---|---|
| hnRNP A1 (M9; 268-305) | GNYNNQNQSSNFGPMKGGNFGGRSSGPYGGGGQYFAKPRNQGGYGGS |
| BMAL1 (95-150) | LASLVPTCNAMSRKLDKLTVLRMAVQHMKTLRGATNPYTEANYKPTFLSDDE LKHL |
| BMAL1 (522-590) | LNITSTPPPDASSPGGKKILNGGTPDIPSSGLLSGQAQENPGYPYSDSSSIL GENPHIGIDMIDNDQGS |
| CRY1 (227-269) | ERKAWVANFERPRMNANSLLASPTGLSPYLRFGCLSCRLFYFKL |
| CRY2 (246-289) | RKAWVANYERPRMNANSLLASPTGLSPYLRFGCLSCRLFYYRLW |
| PER1 (294-337) | EKSVFCRIRGGPDRDPGPRYQPFRLTPYVTKIRVSDGAPAQPCC |
| PER1 (857-900) | SHPSPVPPSTPWPTPPATTPFPAVVQPYPLPVFSPRGGPQPLPP |
| PER1 (909-952) | AFPAPLVTPMVALVLPNYLFPTPSSYPYGALQTPAEGPPTPASH |
| PER2 (219-262) | RDAFSDAKFVEFLAPHDVGVFHSFTSPYKLPLWSMCSGADSFT |
| PER2 (250-315) | LWSMCSGADSFTQECMEEKSFFCRVSVRKSHENEIRYHPFRMTPYLVKVRDQ QGAESQLCCLLLAE |
| PER2 (1196 1239) | TGGLPAAIDVAECVYCENKEKGNICIPYEEDIPSLGLSEVSDTK |

## A1.10 Putative M9 clock peptides show nuclear accumulation

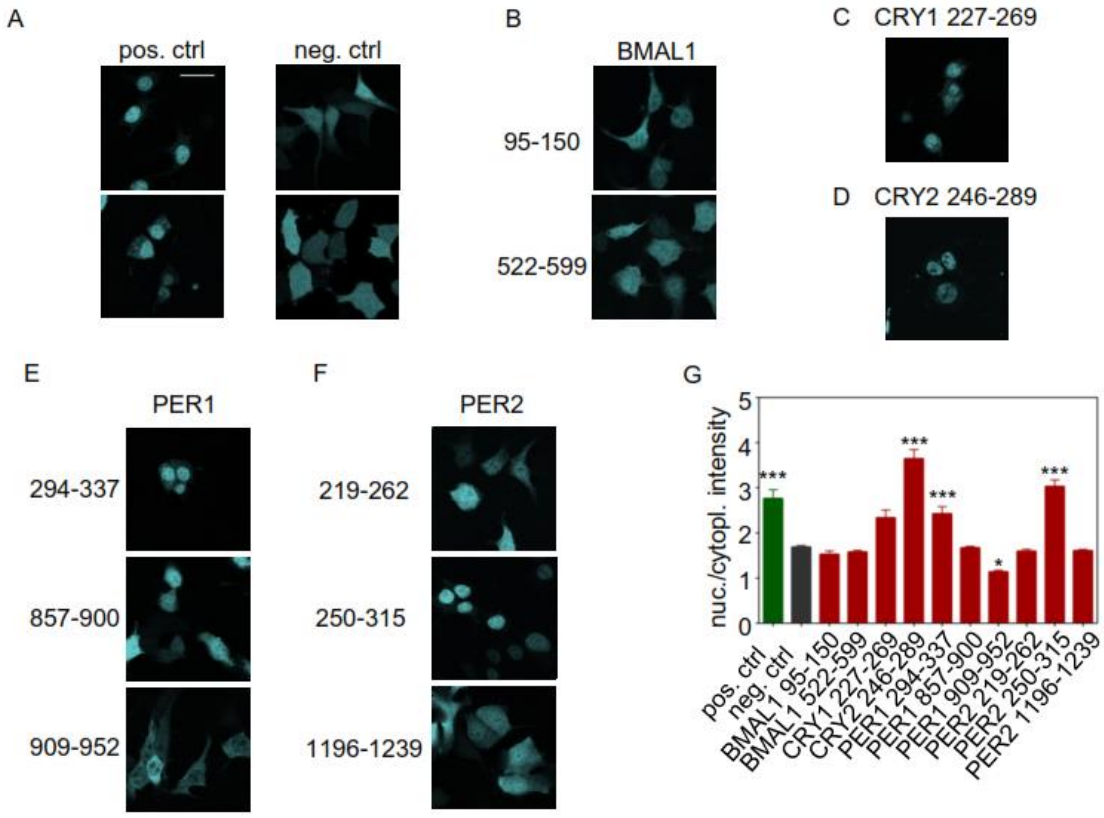


**Suppl. figure A1.5: Putative M9 clock peptides show nuclear accumulation**. Putative M9 clock peptides were C-terminally fused to ECFP prior to transient transfection of HEK293 cells. Depicted are representative images of HEK293 cells expressing ECFP alone (neg. ctrl; A) or fused to peptides of either the M9 NLS of hnRNP A1 (pos. ctrl; A) or putative M9 NLSs of BMAL1 (B), CRY1 (C), CRY2 (D), PER1 (E) or PER2 (F). Images show ECFP fluorescence; scale bar = 50 μm. G) Quantification of all analyzed. Determined is the ratio of nuclear to cytoplasmic fluorescence intensity (error bars = SEM, n = 62 to 262, One-way-ANOVA, post-test Dunnett's multiple comparison test: ** $p < 0.05$, *** $p < 0.001$; all other peptides are non-significantly different from the neg. ctrl).

## A1.11 Site-directed mutagenesis in the *gfp* open-reading frame (orf) of pGiPZ plasmids does not reduce RNAi efficiency

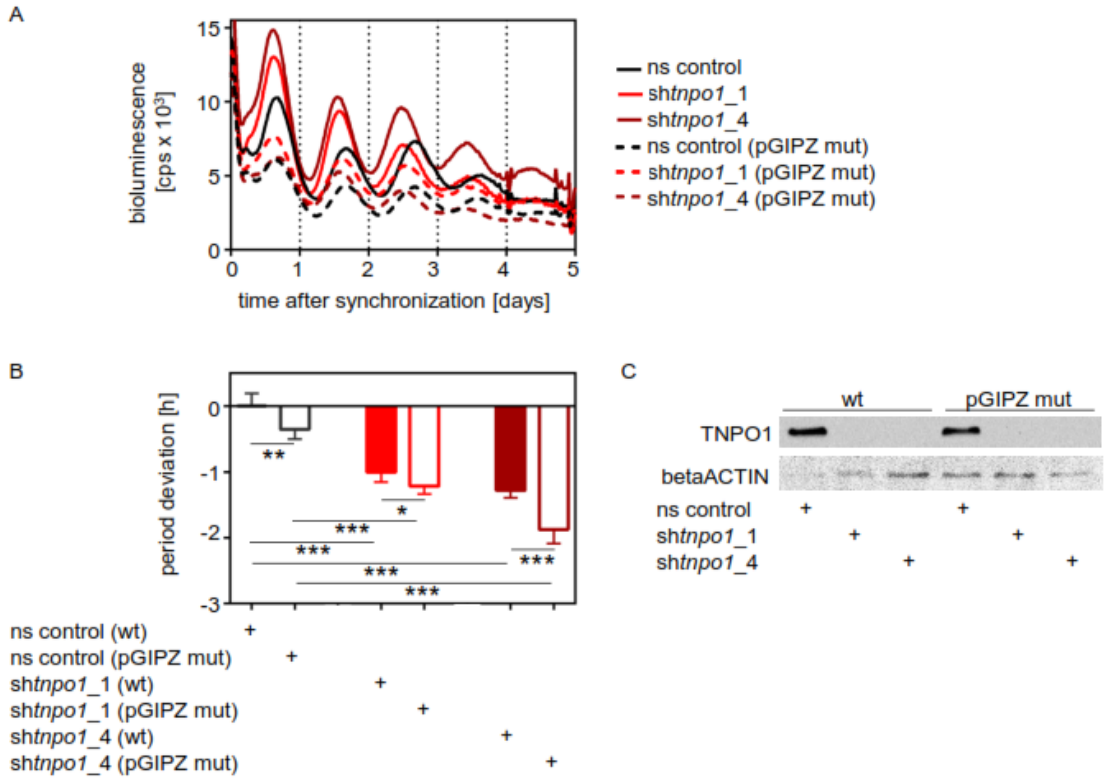


**Suppl. figure A1.6: Site-directed mutagenesis in the *gfp* open-reading frame (orf) of pGiPZ plasmids does not reduce RNAi efficiency**. The mutated pGIPZ plasmids coding either ns control RNAi or shRNA constructs targeting *tnpo1* expression (sh*tnpo1*_1 or _sh*tnpo1*_4) were lentivirally transduced into U-2 OS cells harboring a *bmal1* promoter-driven *luciferase* prior to synchronization with 1 µM dexamethasone. A) Representative time series of U-2 OS reporter cells either transduced with wild type (wt, connected curves) or mutated (mut, dashed curves) pGIPZ plasmids. B) Period deviation upon knockdown of *tnpo1* expression (red) using sh*tnpo1*_1 and sh*tnpo1*_4 as well as ns control RNAi encoded on either wild type (filled bars) or mutant (empty bars) pGIPZ vectors (error bars = SD, n = 6 to 8, student's t-test: * $p < 0.05$, ** $p < 0.01$, *** $p < 0.001$). C) Detection of TNPO1 protein levels of U-2 OS cells either transduced with wild type (wt) or mutated (mut) pGIPZ plasmids coding for ns control or shRNA targeting *tnpo1* expression.

## A1.12 Decreased nuclear localization of circadian clock protein-derived putative M9 NLSs upon depletion of *tnpo1* expression

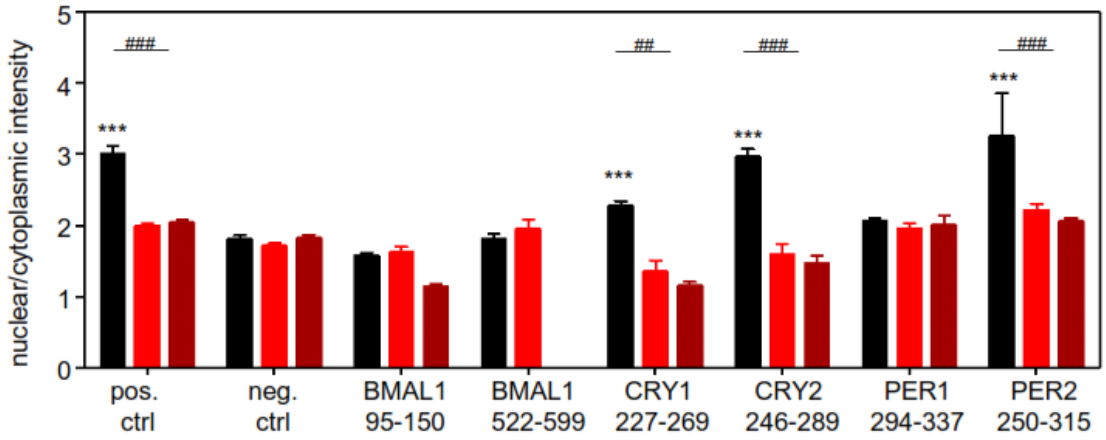


**Suppl. figure A1.7: Decreased nuclear localization of circadian clock protein-derived putative M9 NLSs upon depletion of *tnpo1* expression**. HEK293 cells were lentivirally transduced with mutated pGIPZ coding either the ns control shRNA or shRNA targeting *tnpo1* transcription (sh*tnpo1*_1 and sh*tnpo1*_4). Additionally, ECFP fused to putative M9 clock peptides was transiently transfected into the RNAi transduced U-2 OS cells. M9 of hnRNP A1 was used as positive control (pos. ctrl), whereas ECFP alone was transfected as negative control (neg. ctrl) for the subcellular distribution assay. The subcellular localization upon knockdown of *tnpo1* transcript levels was analyzed for putative M9 peptides of BMAL1, CRY1, CRY2, PER1 or PER2. A) Representative images of fluorescent cells. The wild type subcellular distribution is depicted in the upper row, transducing the ns control construct. The middle (sh*tnpo1*_1) and lower (sh*tnpo1*_4) rows show fluorescent images upon depletion of *tnpo1* expression B) Mean ratio of nuclear to cytoplasmic ECFP-putative M9 fluorescence intensity upon knockdown of *tnpo1* transcripts (ns control: black, sh*tnpo1*_1: red and sh*tnpo1*_4: dark red; error bars = SEM, n = 6 to 185 cells, statistics: * indicates a significant difference of nuclear to cytoplasmic intensity ratios, when compared to the ratios of neg. ctrl (ECFP alone) in ns control cells; # indicates significant difference of nuclear to cytoplasmic intensity ratios of *tnpo1* expression-depleted cells compared to the ratios of ns control cells of the same ECFP fusion protein. Note: for statistical analysis, the ratios of both sh*tnpo1* targeted cell populations were combined prior to comparison to ratios of ns control cells. One-way-ANOVA, post-test: Tukey's multiple comparison test: *** $p < 0.001$, ### $p < 0.001$).

## A1.13 Single amino acid exchange in the PY motif does not alter subcellular distribution of putative M9 clock peptides

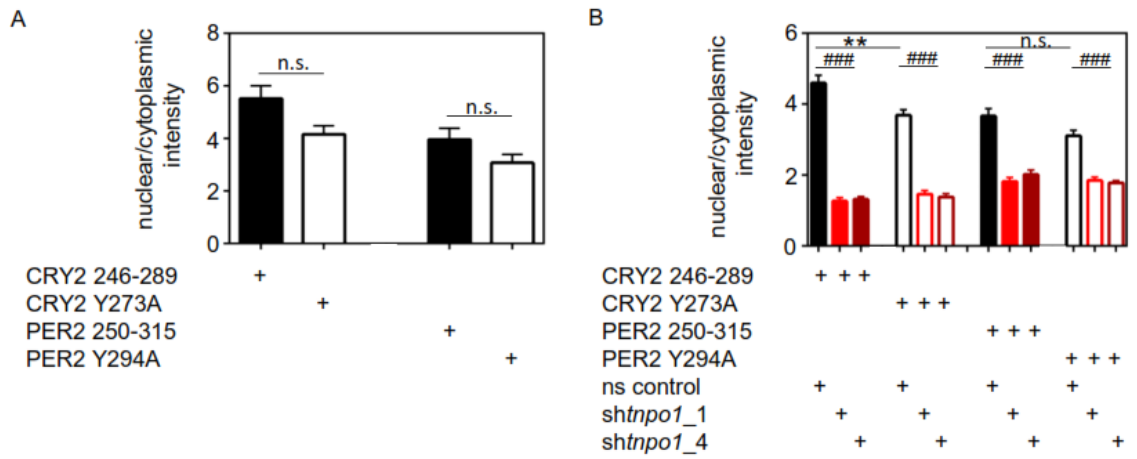


**Suppl. figure A1.8: Single amino acid exchange in the PY motif does not alter subcellular distribution of putative M9 clock peptides**. A) Subcellular distribution assay of U-2 OS cells expressing either the wild type peptides CRY2 246-289, PER2 250-315 (filled bars) or the mutant peptides CRY2 Y273A and PER2 Y294A (empty bars). B) The ECFP-M9 clock peptide (filled bars) or -mutant peptide fusion proteins (empty bars) were either transfected in U-2 OS cells ectopically expressing mutant pGIPZ coding the ns control (black) or sh*tnpo1* (sh*tnpo1*_1, red; sh*tnpo1*_4, dark red) shRNA constructs. * indicates statistical significance of nucleo-cytoplasmic fluorescence intensity ratios of ns control upon comparison of wild type and mutant peptide cells. Furthermore, ratios of ns control cells were compared to the ratios of *tnpo1* transcript-depleted cells of the same transfected fusion protein (statistics indicated as $^{\#}$). Note: Ratios of both knockdown constructs targeting *tnpo1* expression were combined for statistical analysis (error bars = SEM, n = 9 to 118 cells, One-way-ANOVA, post-test: Sidak's multiple comparison test: n.s. = non-significant, ** $p < 0.01$, $^{\#\#\#}$ $p < 0.001$).

## A1.14 Establishment of CoIPs of TNPO1 and circadian clock proteins

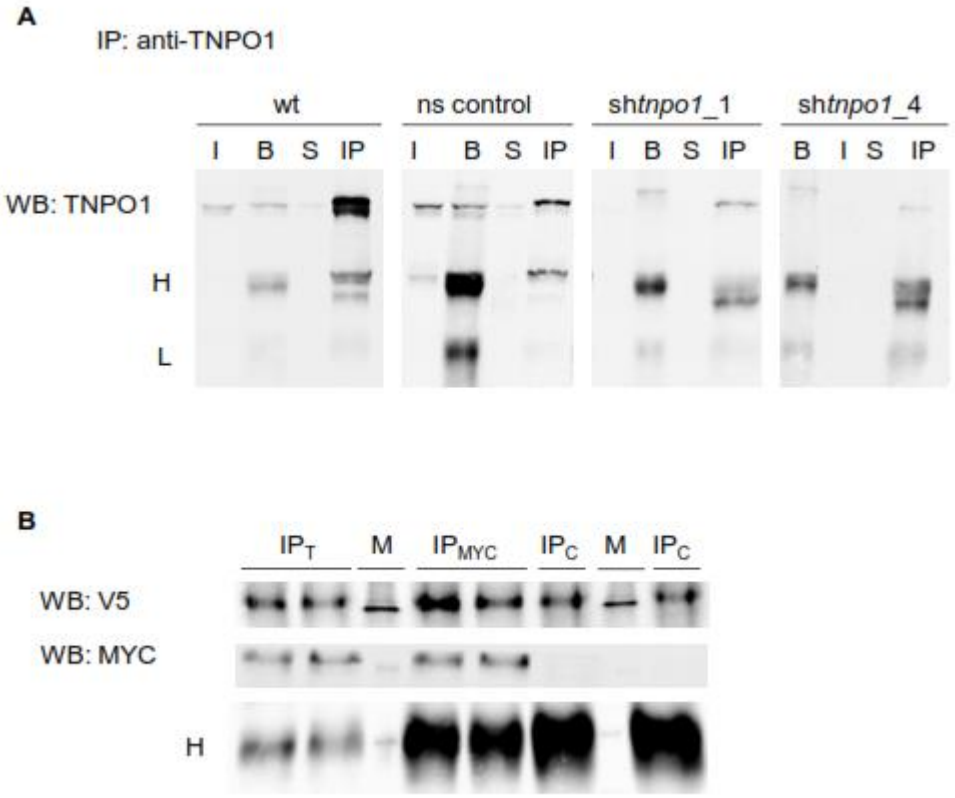


**Suppl. figure A1.9: Establishment of CoIPs of TNPO1 and circadian clock proteins**. A) Immunoprecipitation (IP) of endogenous TNPO1 using lysates of wild type (wt) U-2 OS cells or cells, lentivirally transduced with RNAi targeting *tnpo1* expression or ns control. Lysates (I; input) were incubated with agarose beads only (B) prior to IP with a monoclonal antibody against endogenous TNPO1 (IP). After IP, beads were pelleted (IP) and separated from supernatants (S). Heavy (H) and light (L) antibody chains of the immunoprecipitated antibody are labeled. B) Co-immunoprecipitation (CoIP) of TNPO1 and PER1. Whole cell lysates of HEK293 cells transiently transfected with MYC-TNPO1 and PER1-V5 were set up as input (I) and incubated with anti-TNPO1 (T), anti-MYC or control IgG (C, specificity control) antibody. IPs ($IP_T$, $IP_{MYC}$ or $IP_C$) were run on a denaturing SDS prior to detection of PER1-V5 (anti-V5) or MYC-TNPO1 (anti-MYC). Heavy chains of antibodies used in the IP (H) as well as marker lanes in the SDS-PAGE (M) are indicated.

## A1.15 Enriched firefly luciferase activity upon co-expression of TNPO1 and PER proteins

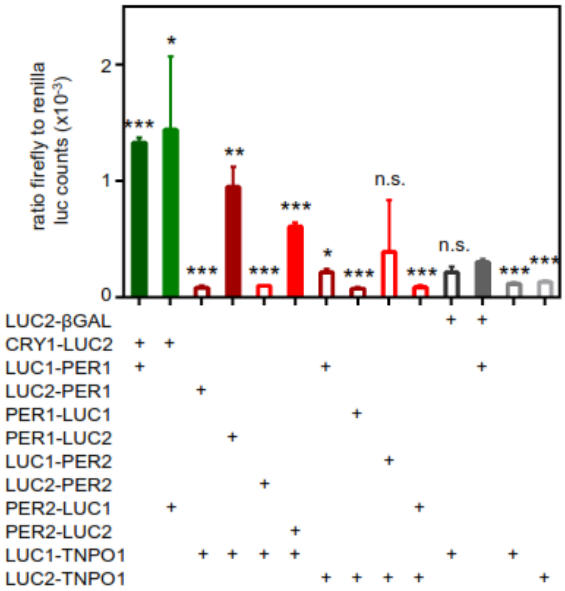


**Suppl. figure A1.10: Enriched firefly luciferase activity upon co-expression of TNPO1 and PER proteins**. HEK293 cells were transfected with renilla luciferase as well as split firefly luciferase (LUC1 or LUC2) fusion proteins. LUC1 and 2 were fused to either PER1 or PER2 and TNPO1 (red). LUC fusion proteins of PER1 or PER2 and CRY1 (green) serve as positive controls, whereas TNPO1 or PER1 co-transfected with $\beta$ Galactosidase ($\beta$GAL) function as negative controls (grey). Additionally, either LUC1- or LUC2-TNPO1 were transfected with renilla luciferase solely (grey). Firefly luciferase activity was normalized to full-length renilla luciferase activity. Combinations which emit a significantly stronger signal than LUC1-PER and LUC2-$\beta$GAL (negative control, grey filled bar) are depicted in filled bars, whereas non-significant and significantly reduced signals are displayed as empty bars (error bars = SD, n = 3, student's t-test: n.s. = non-significant, * $p < 0.05$, ** $p < 0.01$, *** $p < 0.001$).

## A1.16 Efficient knockdown of *tnpo1* expression using RNAi

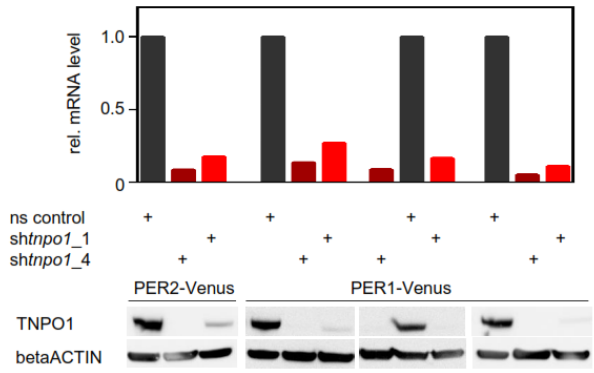


**Suppl. figure A1.11: Efficient knockdown of *tnpo1* expression using RNAi.** U-2 OS cells, ectopically expressing either PER1- or PER2-Venus were lentivirally transduced with ns control RNAi (grey) or constructs, targeting *tnpo1* expression (sh*tnpo1*_1 or sh*tnpo1*_4; red). Depicted are *tnpo1* mRNA (top) and protein (bottom) levels of the transduced cells. betaACTIN was used as loading control for western blot.

## A1.17 TNPO1-PER2 interaction is not consistently increased under oxidative stress.

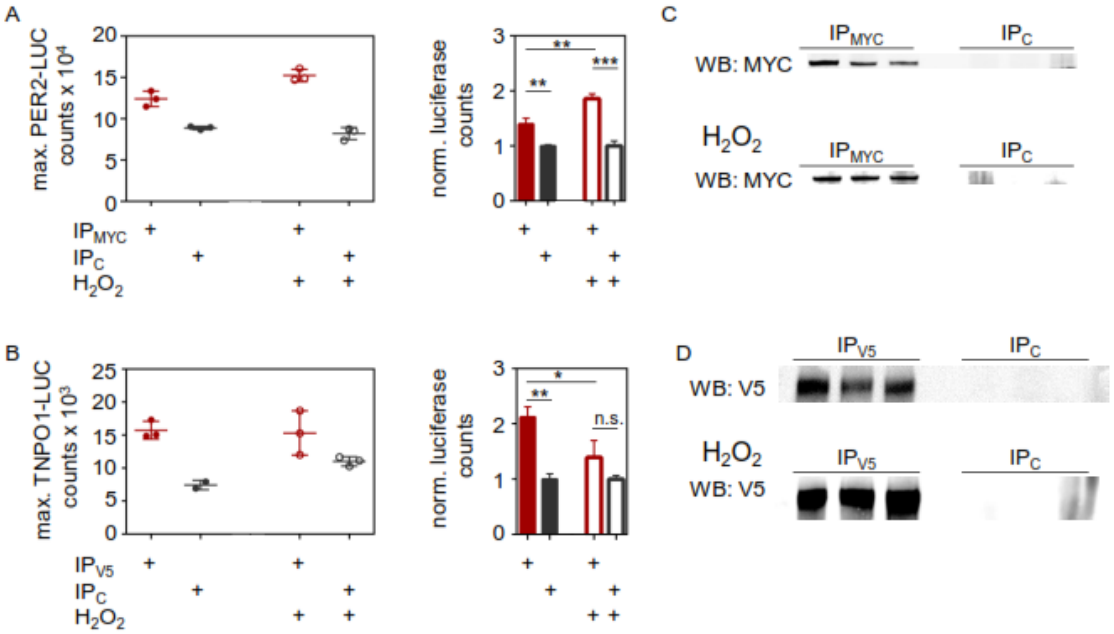


**Suppl. figure A1.12: TNPO1-PER2 interaction is not increased under oxidative stress.** Representative experiments of CoIPs using whole cell lysates of HEK293 ectopically expressing TNPO1 and PER2 in normal (filled columns) and oxidative stress (empty columns) conditions. Oxidative stress was induced upon application of 200 µM hydrogen peroxide. MYC-TNPO1 was immunoprecipitated using anti-MYC antibody ($IP_{MYC}$; red; A) prior to measurement of luciferase activity of PER1-LUC. Vice-versa anti-V5 CoIPs were performed in PER1-V5 and TNPO1-LUC assays ($IP_{V5}$; red; C) prior to detection of TNPO1-LUC activity. All assays were controlled by the IP of an unspecific control IgG ($IP_C$; grey). Left: representative single luciferase measurements. Right: Mean ratios of luminescence signals determined in specific to control CoIPs (error bars = SD, n = 2 to 3, student's t-test: n.s. = non-significant, * $p < 0.05$; ** $< 0.01$; *** $< 0.001$). B and D) Western blot detection of the immunoprecipitated proteins; either MYC-TNPO1 (B) or PER2-V5 (D).

## A1.18 Nuclear accumulation of PER2 is not decreased upon depletion of *tnpo1* expression or oxidative stress

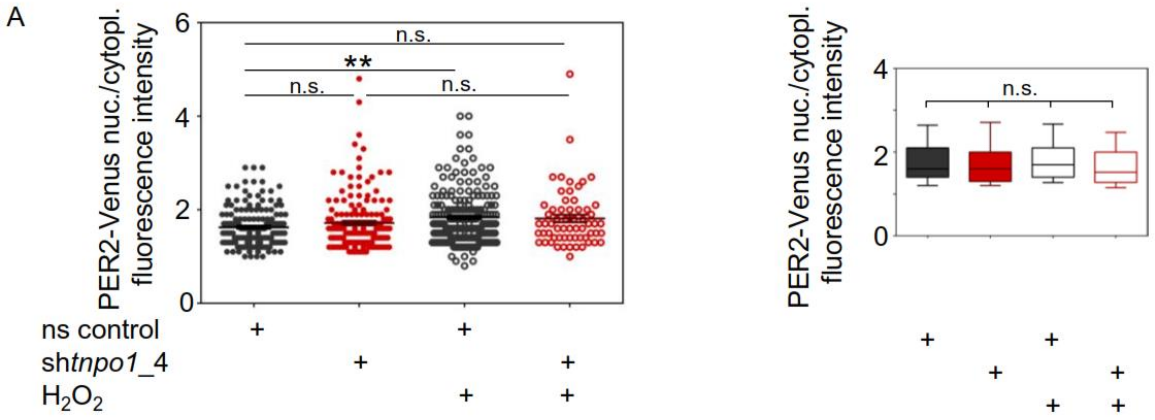


**Suppl. figure A1.13: Nuclear accumulation of PER2 is not decreased upon depletion of *tnpo1* expression or oxidative stress.** U-2 OS cells were lentivirally transduced with either ns control RNAi (grey) or a construct targeting *tnpo1* expression (sh*tnpo1*_4, red). Subcellular localization of ectopically expressed PER2-Venus was imaged before (filled circles) and 30 min after treatment with 200 µM hydrogen peroxide (empty circles). A) Representative experiment of PER2-Venus subcellular localization. Ratios of nuclear to cytoplasmic fluorescence intensities of individual cells are depicted (error bars = SEM, n = 61 to 192, One-way-ANOVA, post-test: Tukey's multiple comparison test: n.s. = non-significant, ** $p < 0.01$). B) Summary of all performed experiments. Quantified ratios of PER2-Venus fluorescence intensities of ns control treated cells under non-oxidizing conditions (grey, filled box plot) were non-significantly different to cells with depleted *tnpo1* expression (red, filled box plot) as well as to cells under oxidizing conditions (empty box plots) (whiskers indicate the 10th to 90th percentile and boxes indicate the 25th to 75th percentile; n = 185 to 352 , One-way-ANOVA, post-test: Tukey's multiple comparison test: n.s. = non-significant, ** $p < 0.001$).

## A1.19 Reduced nuclear import rate of PER1 under oxidative stress conditions

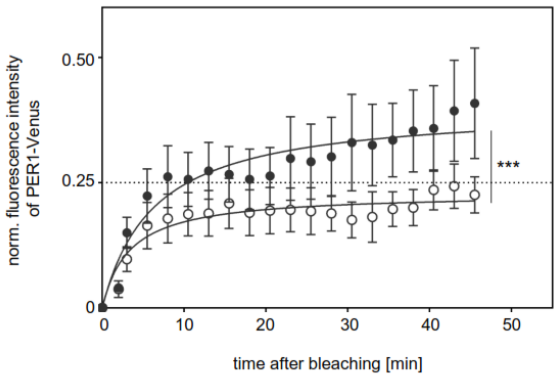


**Suppl. figure A1.14: Reduced nuclear import rate of PER1 under oxidative stress conditions**. U-2 OS cells ectopically expressing PER1-Venus were either incubated for 30 min with 200 µM hydrogen peroxide (empty circles) or solvent (water, filled circles). An image of the initial fluorescence intensity was taken prior to bleaching the nuclei with a 100 % laser power. Afterwards images were taken every 2.5 min for up to 45 min (error bars = SEM; n = 6 to 7 cells; Two-way-ANOVA: *** $p < 0.001$, post-test: Sidak's multiple comparison test: non-significant)

## A1.20 Similar mean recovery curves of sh*tnpo1*_4 and ns control RNAi transduced cells under oxidizing conditions

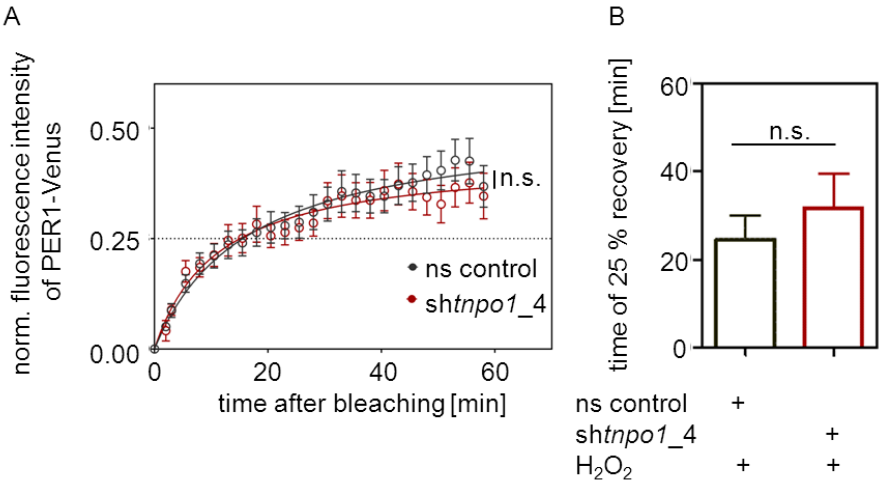


**Suppl. figure A1.15: Oxidative stress does not alter the TNPO1-mediated nuclear import rate of PER1**. U-2 OS cells, ectopically expressing PER1-Venus, were lentivirally transduced with RNAi targeting *tnpo1* expression (sh*tnpo1*_4, red) or ns control RNAi (ns control, grey). A) Cells were imaged 30 min after treatment with 200 µM hydrogen peroxide (empty circles). An image of pre-beaching fluorescence was taken prior to bleaching the nuclei with 100 % laser intensity. Afterwards images were taken every 2.5 min for up to ~1 h. Depicted is the mean of 15 single cell recovery curves. B) Mean recovery time needed to regain 25 % of initial fluorescence intensity after treatment with hydrogen peroxide (error bars = SEM, n = 15 cells for each RNAi treatment, left: Two-way-ANOVA, post-test: Sidak's multiple comparison test: n.s. = non-significant; right: student's t-test: n.s. = non-significant).

## A1.21 Single cell FRAP analysis of PER1 nuclear import

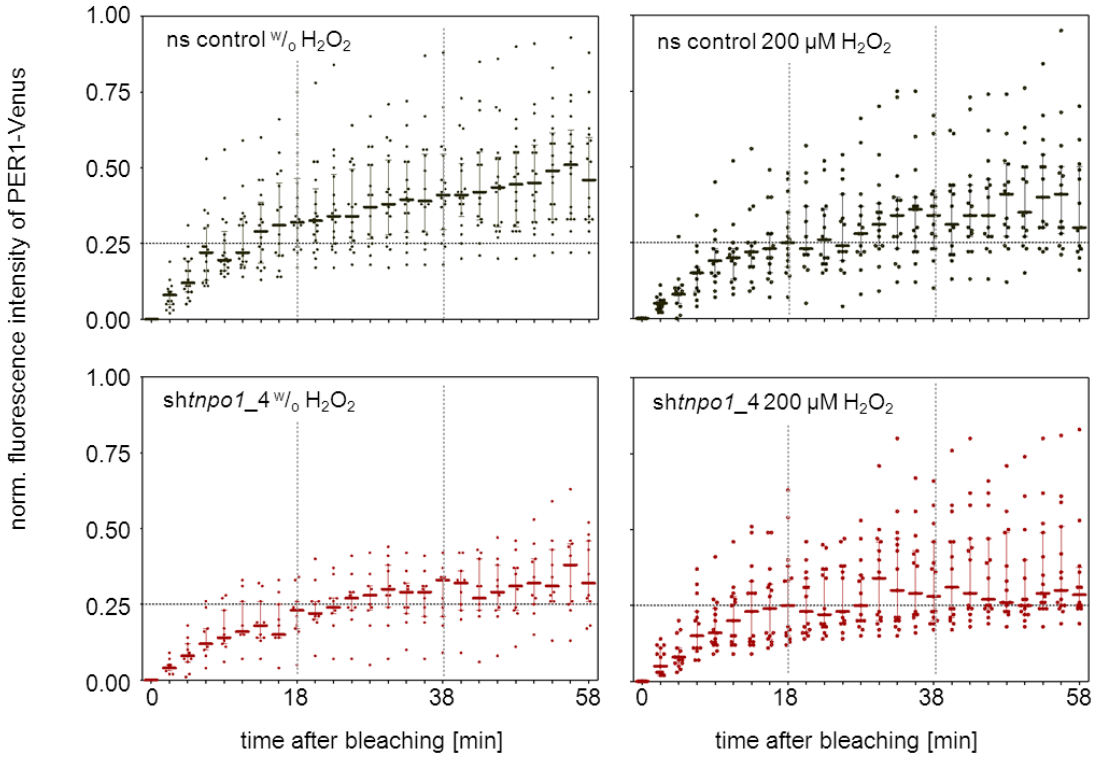


**Suppl. figure A1.16: Recovery curves of single cell FRAP analyses of PER1-Venus upon impairment of *tnpo1* expression under oxidative stress**. U-2 OS cells, ectopically expressing PER1-Venus, were lentivirally transduced with RNAi targeting *tnpo1* expression (sh*tnpo1*_4, red) or ns control RNAi (ns control, grey). A) Cells were imaged 30 min after treatment with 200 µM hydrogen peroxide (right) or solvent (water, left). An image was taken prior to bleaching the nuclei with 100 % laser intensity. Afterwards images were taken every 2.5 min for up to ~1 h. Depicted are the single cell recovery data points as well as the median (horizontal bars; error bars = interquartile range, representing the range between 25-75 % of all values, n = 11-18 cells for each condition).

## A1.22 Indications on *per1*-mediated period shortening upon perturbation of *tnpo1* expression

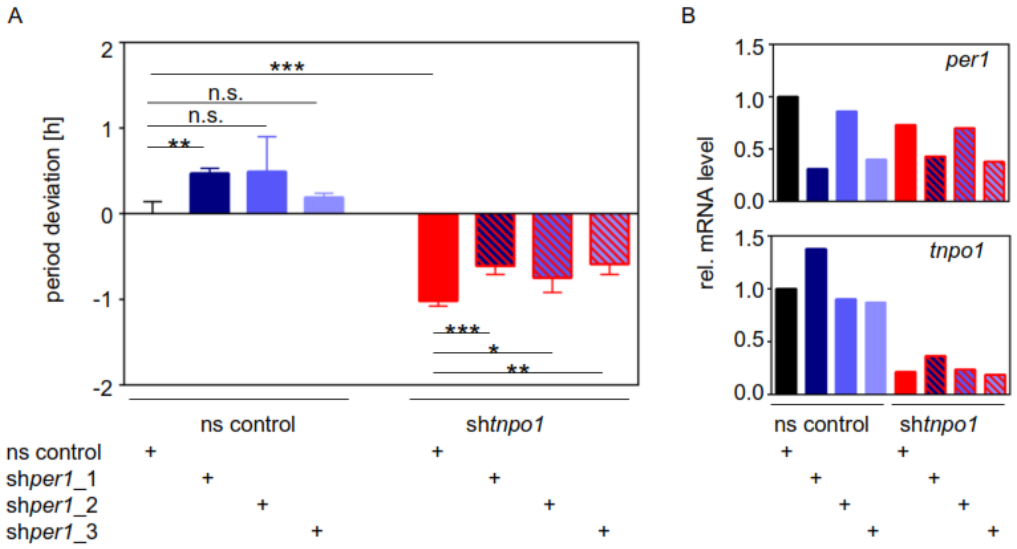


**Suppl. figure A1.17: Indications on per1-mediated period shortening upon perturbation of *tnpo1* expression**. RNAi constructs directed against *tnpo1* (red, sh*tnpo1*) and *per1* (blue, sh*per1*_1-3) were either individually (single color bars) or simultaneously (two-colored bars) transduced in U-2 OS cells harboring a *bmal1* promoter-driven *luciferase*. Periods deviations to time series of ns control cells (black). To apply the same amount of virus, the single knockdowns were substituted with ns control virus. A) Period deviation upon knockdown of *tnpo1* and *per1* expression (error bars = SD, n = 2 to 6 wells, student's t-test: n.s. = non-significant, * $p < 0.05$, *** $p < 0.001$). B) Relative mRNA levels of per1 (upper panel) or tnpo1 (lower panel)).

# A2 Supplementary material and methods

## A2.1 SOP - lentivirus production

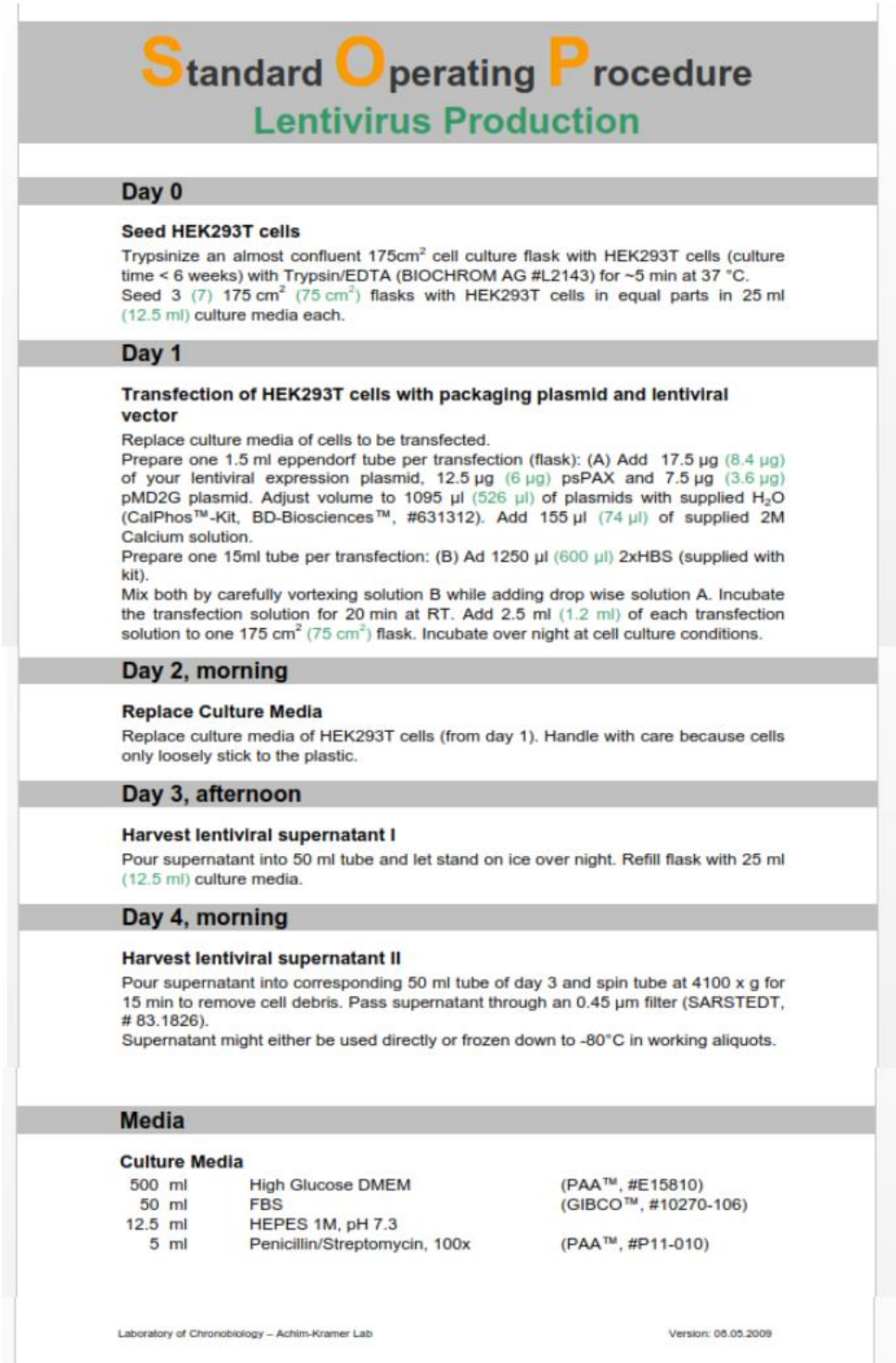

**Standard Operating Procedure**

**Lentivirus Production**

### Day 0

**Seed HEK293T cells**

Trypsinize an almost confluent 175cm² cell culture flask with HEK293T cells (culture time < 6 weeks) with Trypsin/EDTA (BIOCHROM AG #L2143) for ~5 min at 37 °C.
Seed 3 (7) 175 cm² (75 cm²) flasks with HEK293T cells in equal parts in 25 ml (12.5 ml) culture media each.

### Day 1

**Transfection of HEK293T cells with packaging plasmid and lentiviral vector**

Replace culture media of cells to be transfected.
Prepare one 1.5 ml eppendorf tube per transfection (flask): (A) Add 17.5 µg (8.4 µg) of your lentiviral expression plasmid, 12.5 µg (6 µg) psPAX and 7.5 µg (3.6 µg) pMD2G plasmid. Adjust volume to 1095 µl (526 µl) of plasmids with supplied $H_2O$ (CalPhos™-Kit, BD-Biosciences™, #631312). Add 155 µl (74 µl) of supplied 2M Calcium solution.
Prepare one 15ml tube per transfection: (B) Ad 1250 µl (600 µl) 2xHBS (supplied with kit).
Mix both by carefully vortexing solution B while adding drop wise solution A. Incubate the transfection solution for 20 min at RT. Add 2.5 ml (1.2 ml) of each transfection solution to one 175 cm² (75 cm²) flask. Incubate over night at cell culture conditions.

### Day 2, morning

**Replace Culture Media**

Replace culture media of HEK293T cells (from day 1). Handle with care because cells only loosely stick to the plastic.

### Day 3, afternoon

**Harvest lentiviral supernatant I**

Pour supernatant into 50 ml tube and let stand on ice over night. Refill flask with 25 ml (12.5 ml) culture media.

### Day 4, morning

**Harvest lentiviral supernatant II**

Pour supernatant into corresponding 50 ml tube of day 3 and spin tube at 4100 x g for 15 min to remove cell debris. Pass supernatant through an 0.45 µm filter (SARSTEDT, # 83.1826).
Supernatant might either be used directly or frozen down to -80°C in working aliquots.

### Media

**Culture Media**

| | | |
|---|---|---|
| 500 ml | High Glucose DMEM | (PAA™, #E15810) |
| 50 ml | FBS | (GIBCO™, #10270-106) |
| 12.5 ml | HEPES 1M, pH 7.3 | |
| 5 ml | Penicillin/Streptomycin, 100x | (PAA™, #P11-010) |

Laboratory of Chronobiology – Achim-Kramer Lab Version: 06.05.2009

## A2.2 RNAi-screen: plate design

plate 1

| | 1 | 2 | 3 | 4 | 5 | 6 | 7 | 8 | 9 | 10 | 11 | 12 |
|---|---|---|---|---|---|---|---|---|---|---|---|---|
| A | 67 | 68 | 1 | 70 | 71 | 72 | 73 | 74 | 76 | 77 | 78 | 79 |
| B | 103 | ns1 | 69 | 2 | 3 | 4 | 5 | 26 | 8 | 25 | 16 | 80 |
| C | 102 | 17 | 18 | ns1 | 19 | 20 | 22 | 6 | 27 | 29 | 30 | 82 |
| D | 101 | 31 | 32 | 33 | 34 | 35 | 36 | 37 | 38 | 39 | ns1 | 81 |
| E | 100 | 40 | 41 | 42 | 43 | 44 | ns1 | 45 | 46 | 47 | 48 | 83 |
| F | 49 | 99 | 50 | 51 | 93 | 53 | 91 | 55 | ns1 | 87 | 57 | 86 |
| G | 98 | ns1 | 95 | 94 | ns1 | 92 | 62 | 90 | 64 | 88 | 66 | 85 |
| H | 97 | 96 | 59 | 60 | 52 | 61 | 54 | 63 | 89 | 65 | 56 | 84 |

plate 2

| | 1 | 2 | 3 | 4 | 5 | 6 | 7 | 8 | 9 | 10 | 11 | 12 |
|---|---|---|---|---|---|---|---|---|---|---|---|---|
| A | 104 | 105 | 106 | 107 | 108 | 109 | 110 | 111 | 112 | 113 | 28 | 115 |
| B | 116 | 117 | 118 | 119 | 120 | ns1 | 75 | 122 | 132 | 123 | ns1 | 124 |
| C | 125 | ns1 | 126 | 127 | 128 | 129 | 130 | 131 | ns1 | 133 | 134 | 135 |
| D | 136 | 137 | 138 | ns1 | 139 | 140 | ns1 | 141 | 142 | 143 | 144 | 145 |
| E | 146 | 147 | 148 | 149 | 150 | 151 | 152 | 153 | 154 | 155 | 156 | 157 |
| F | 158 | ns1 | 171 | 161 | 162 | 163 | 164 | 165 | 166 | ns1 | 167 | 168 |
| G | 169 | 182 | 160 | 172 | 173 | ns1 | 174 | 175 | 176 | 178 | 121 | 180 |
| H | 181 | 170 | 183 | 184 | 185 | 186 | 9 | 159 | 114 | 58 | 179 | 177 |

## A2.3 Vector maps

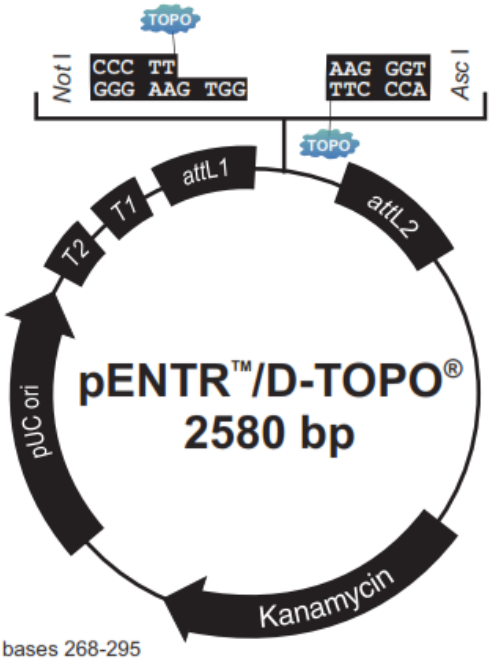


**Comments for pENTR™/D-TOPO®**
**2580 nucleotides**

*rrn*B T2 transcription termination sequence: bases 268-295
*rrn*B T1 transcription termination sequence: bases 427-470
M13 forward (-20) priming site: bases 537-552
*att*L1: bases 569-668 (c)
TOPO® recognition site 1: bases 680-684
Overhang: bases 685-688
TOPO® recognition site 2: bases 689-693
*att*L2: bases 705-804
T7 Promoter/priming site: bases 821-840 (c)
M13 reverse priming site: bases 845-861
Kanamycin resistance gene: bases 974-1783
pUC origin: bases 1904-2577

(c) = complementary sequence

invitrogen™

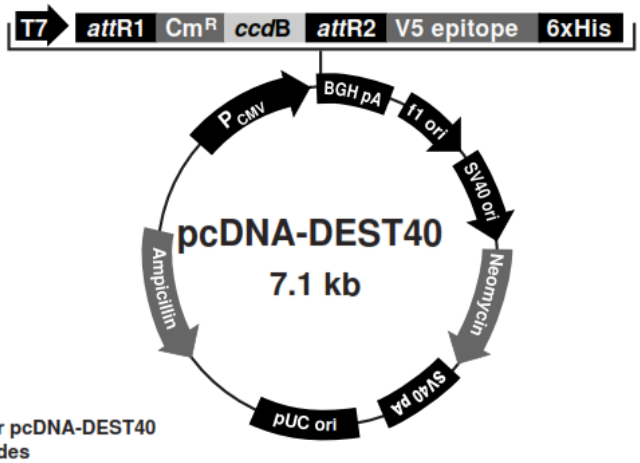


**Comments for pcDNA-DEST40**
**7143 nucleotides**

CMV promoter: bases 232-819
T7 promoter: bases 863-882
*attR1* recombination site: bases 911-1035
Chloramphenicol resistance gene: bases 1144-1803
*ccdB* gene: bases 2145-2450
*attR2* recombination site: bases 2491-2615
V5 epitope: bases 2641-2682
6xHis tag: bases 2692-2709
BGH polyadenylation region: bases 2735-2962
f1 origin: bases 3008-3436
SV40 early promoter and origin: bases 3463-3771
Neomycin resistance ORF: bases 3846-4640
SV40 early polyadenylation region: bases 4816-4946
pUC origin: bases 5329-6002
Ampicillin (*bla*) resistance ORF: bases 6147-7007 (complementary strand)
*bla* promoter: bases 7008-7106 (complementary strand)

Invitrogen™
life technologies

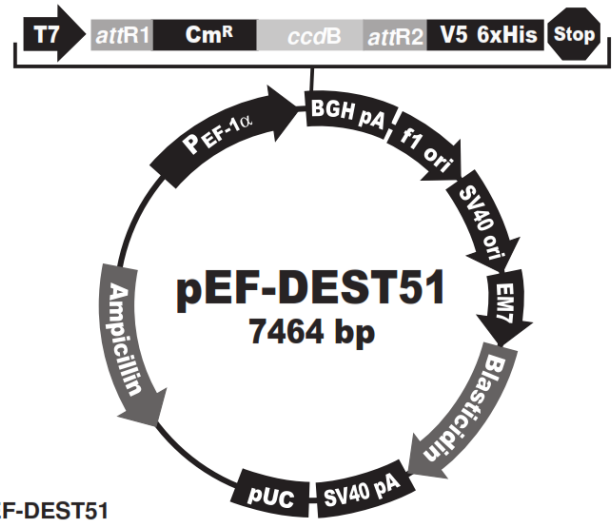


**Features of pEF-DEST51**
**7464 nucleotides**

EF-1α promoter: bases 470-1653
T7 promoter: bases 1670-1689
*att*R1 recombination site: bases 1720-1844
Chloramphenicol resistance gene: bases 1953-2612
*ccd*B gene: bases 2954-3259
*att*R2 recombination site: bases 3300-3424
V5 epitope: bases 3450-3491
6xHis tag: bases 3501-3518
BGH polyadenylation region: 3544-3771
f1 origin: bases 3817-4245
SV40 early promoter and origin: bases 4250-4594
EM7 promoter: bases 4629-4684
Blasticidin resistance gene: bases 4703-5101
SV40 early polyadenylation region: bases 5259-5389
pUC origin: bases 5772-6445
Ampicillin resistance gene (*bla*): bases 6590-7450 (c)
*bla* promoter: bases 7451-85 (c)
(c) = complementary strand

Invitrogen
life technologies

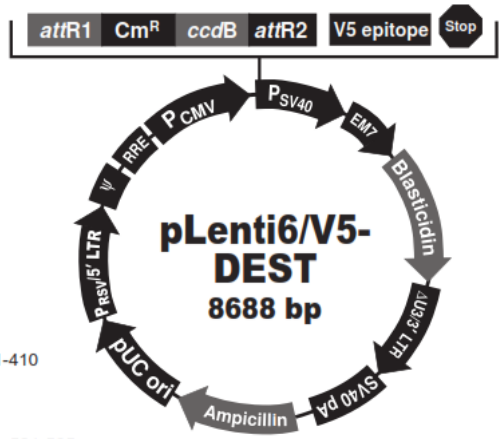


**Comments for pLenti6/V5-DEST**
**8688 nucleotides**

RSV/5′ LTR hybrid promoter: bases 1-410
  RSV promoter: bases 1-229
  HIV-1 5′ LTR: bases 230-410
5′ splice donor: base 520
HIV-1 psi (ψ) packaging signal: bases 521-565
HIV-1 Rev response element (RRE): bases 1075-1308
3′ splice acceptor: base 1656
3′ splice acceptor: base 1684
CMV promoter: bases 1809-2392
*attR1* site: bases 2440-2564
Chloramphenicol resistance gene ($Cm^R$): bases 2673-3332
*ccdB* gene: bases 3674-3979
*attR2* site: bases 4020-4144
V5 epitope: bases 4197-4238
SV40 early promoter and origin: bases 4293-4602
EM7 promoter: bases 4657-4723
Blasticidin resistance gene: bases 4724-5122
ΔU3/3′ LTR: bases 5208-5442
  ΔU3: bases 5208-5261
  3′ LTR: bases 5262-5442
SV40 polyadenylation signal: bases 5514-5645
*bla* promoter: bases 6504-6602
Ampicillin (*bla*) resistance gene: bases 6603-7463
pUC origin: bases 7608-8281

Invitrogen™
life technologies

## lentiCRISPR v2 (Addgene)

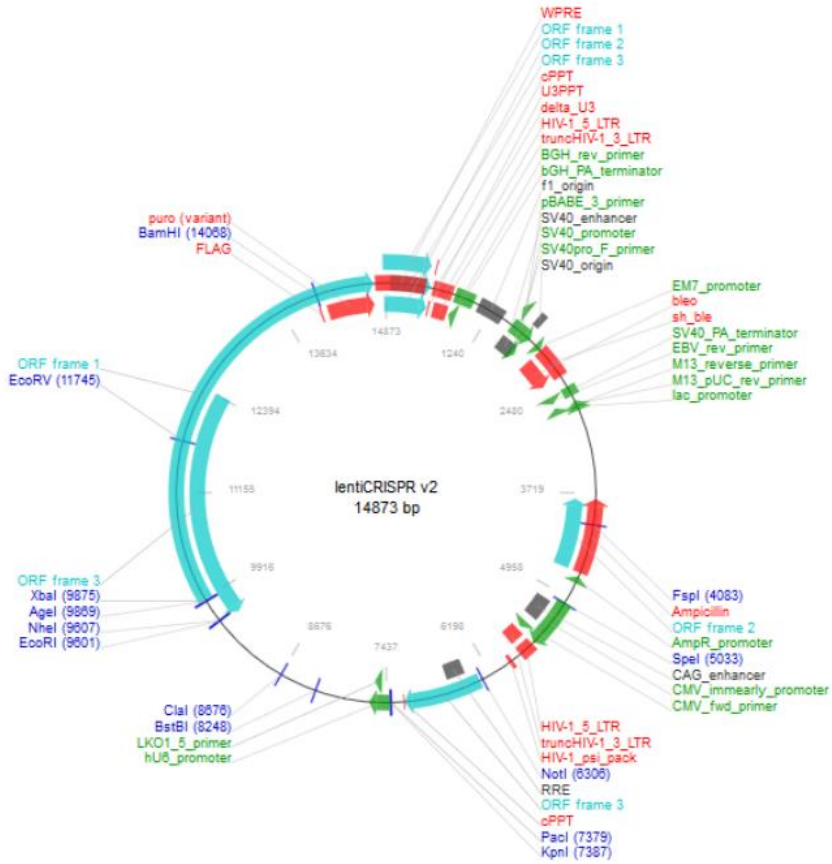

**pc-MYC-CMV-D12 (AG Wanker)**

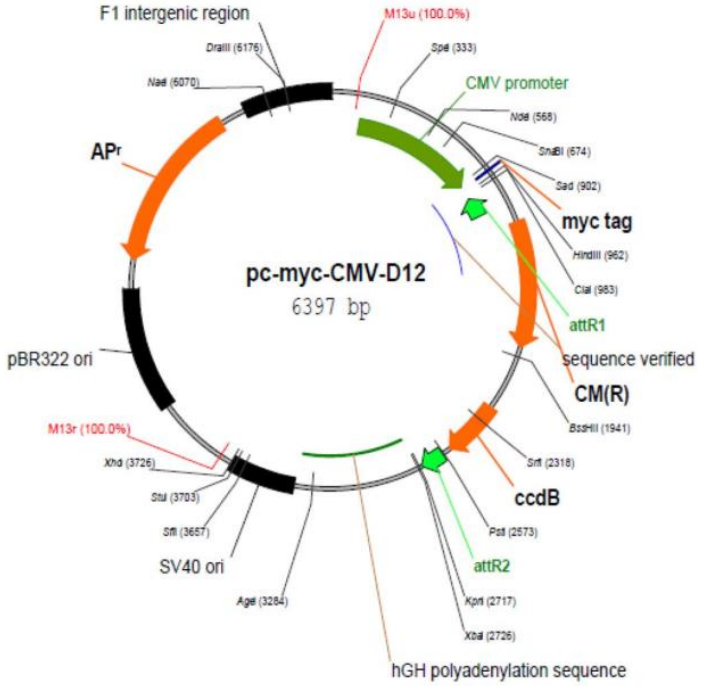


**pGIPZ (Dharmacon/Open biosystems)**

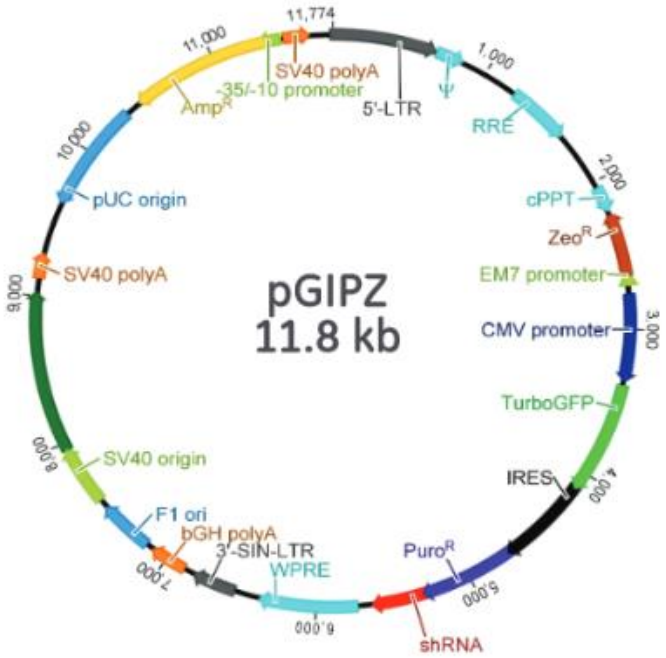

## pECFP-C1 (Clontech; not available anymore)

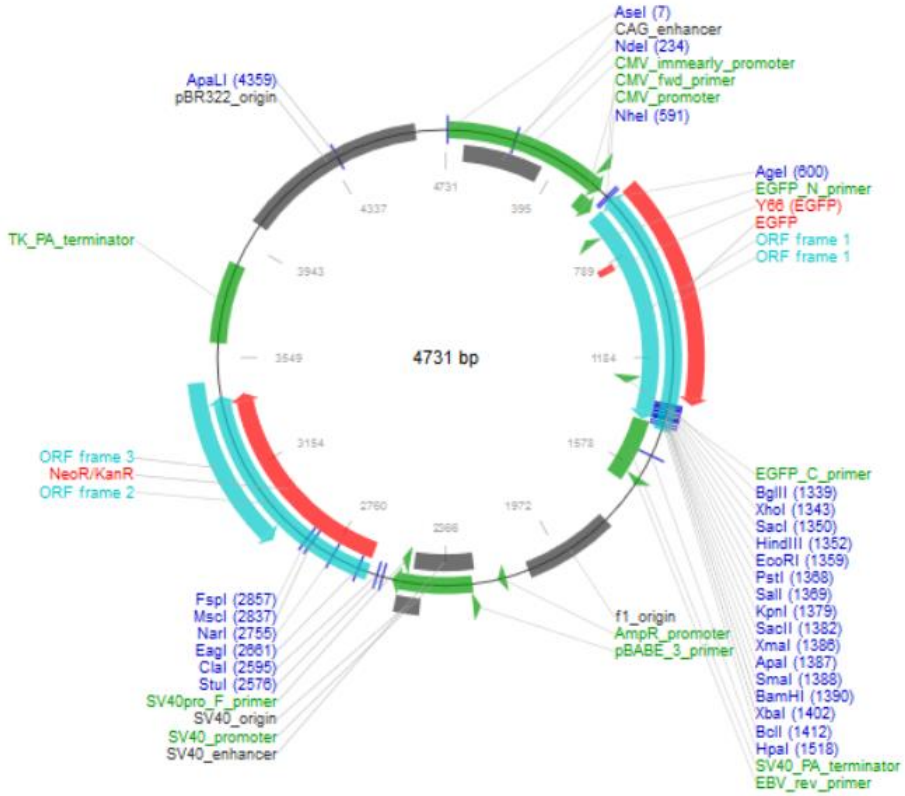


## pUC19 vector (New England Biolabs)

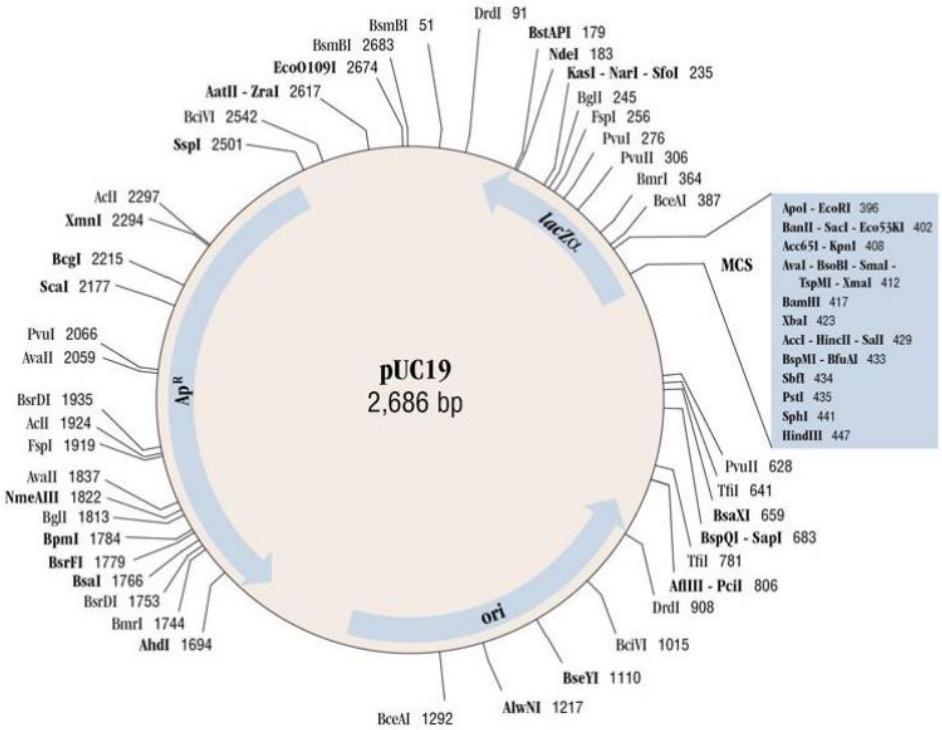

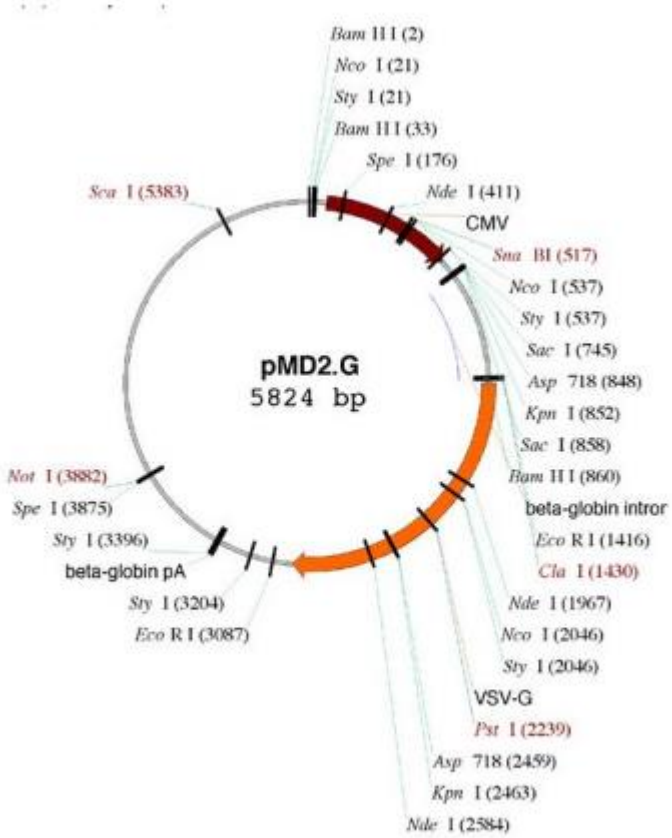
pMD2.G
5824 bp
Bam H I (2)
Nco I (21)
Sty I (21)
Bam H I (33)
Spe I (176)
Nde I (411)
CMV
Sna BI (517)
Nco I (537)
Sty I (537)
Sac I (745)
Asp 718 (848)
Kpn I (852)
Sac I (858)
Bam H I (860)
beta-globin intror
Eco R I (1416)
Cla I (1430)
Nde I (1967)
Nco I (2046)
Sty I (2046)
VSV-G
Pst I (2239)
Asp 718 (2459)
Kpn I (2463)
Nde I (2584)
Sca I (5383)
Not I (3882)
Spe I (3875)
Sty I (3396)
beta-globin pA
Sty I (3204)
Eco R I (3087)

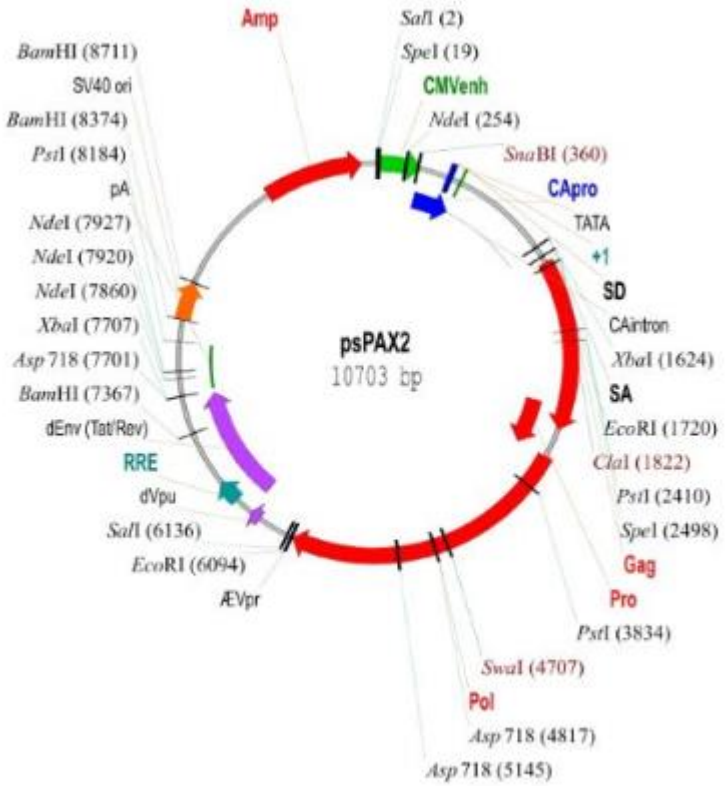
psPAX2
10703 bp
Amp
SalI (2)
SpeI (19)
CMVenh
NdeI (254)
SnaBI (360)
CApro
TATA
+1
SD
CAintron
XbaI (1624)
SA
EcoRI (1720)
ClaI (1822)
PstI (2410)
SpeI (2498)
Gag
Pro
PstI (3834)
SwaI (4707)
Pol
Asp 718 (4817)
Asp 718 (5145)
BamHI (8711)
SV40 ori
BamHI (8374)
PstI (8184)
pA
NdeI (7927)
NdeI (7920)
NdeI (7860)
XbaI (7707)
Asp 718 (7701)
BamHI (7367)
dEnv (Tat/Rev)
RRE
dVpu
SalI (6136)
EcoRI (6094)
ÆVpr

## pEX-A (Eurofins MWG Operon)

eurofins mwg|operon

**pEX-A vector map, multiple cloning site and full sequence**

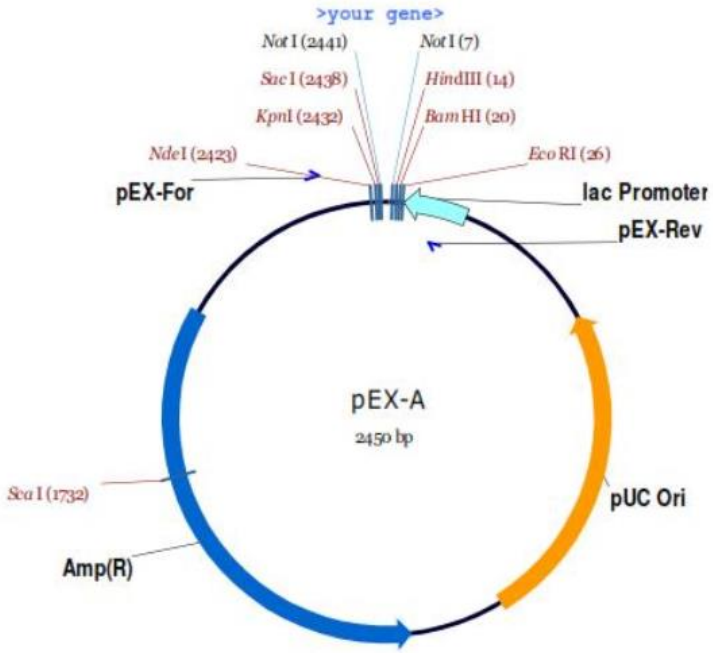

# List of Publications

**Korge, S.**, Grudziecki, A., and Kramer, A. (2015). Highly Efficient Genome Editing via CRISPR/Cas9 to Create Clock Gene Knockout Cells. Journal of biological rhythms 30, 389-395.

Ollinger, R., **Korge, S.**, Korte, T., Koller, B., Herrmann, A., and Kramer, A. (2014). Dynamics of the circadian clock protein PERIOD2 in living cells. Journal of cell science 127, 4322-4328.

Hildebrand, J., Spörl, F., **Korge, S.**, Gallinat, S., Wenck, H., Deppert, W., Knott, A., and Blatt, T. (2012). Cell cycle regulator Cdkn1c (p57/KIP2) shows distinct expression in epidermal differentiation. European journal of dermatology : EJD 22, 694-696.

Spörl, F., **Korge, S.**, Jurchott, K., Wunderskirchner, M., Schellenberg, K., Heins, S., Specht, A., Stoll, C., Klemz, R., Maier, B., Wenck H, Schrader A, Kunz D, Blatt T, Kramer A. (2012). Kruppel-like factor 9 is a circadian transcription factor in human epidermis that controls proliferation of keratinocytes. Proceedings of the National Academy of Sciences of the United States of America 109, 10903-10908.

# Abbreviations

| | |
|---|---|
| ® | registered |
| ™ | trade mark |
| ∞ | infinity |
| α | alpha |
| β | beta |
| γ | gamma |
| δ/Δ | delta |
| ε | epsilon |
| μ | micro |
| ϰ | kappa |
| π | pi |
| aa. | amino acid |
| ad | fill up to a final volume of... |
| ALADIN | adracalin |
| aq. dest. | distilled water |
| amp | amplitude |
| ARM | repeats armadillo repeats |
| arnt | aryl hydrocarbon receptor nuclear translocator |
| ATCC | American Type Culture Collection |
| ATP | adenosin triphosphate β GAL beta-galactosidase |
| BER | base excision repair |
| bHLH | basic helix-loop-helix |
| BMAL1 | **B**rain and **M**uscle **A**ryl hydrocarbon receptor nuclear translocator-**L**ike protein **1**, transcriptional activator in mammals |
| *bmal1:luc* | *luciferase* gene driven by a 0.9 kb *bmal1* promoter |
| bp | base pairs |
| c-box | clock elements, WCC binding site |
| CC | correlation coefficient |
| CDC | cell division control protein 2 homolog, Cyclin-dependent kinase |
| CDK | cyclin-dependent kinase |
| cDNA | complementary DNA |
| CDS | coding sequence |
| CG1 | kinase binding protein CGI-121 |
| CIP | intestinal alkaline phosphatase |
| CK | casein kinase |
| CLOCK | **C**ircadian **L**ocomotor **O**utput **C**ycles **K**aput, transcriptional activator in mammals |
| CLK3 | CDC-like kinase 3, TNPO1 cargo |
| CM | complete medium |
| cNLS | classical nuclear localization signal |

| | |
|---|---|
| cps | counts per second |
| CPSF6 | Cleavage And Polyadenylation Specific Factor 6, TNPO1 cargo |
| CRISPR | **C**lustered **R**egulatory **I**nterspaced **S**hort **P**alindromic **R**epeats |
| crispRNA | CRISPR RNA, target recognition site of guide RNA |
| CoIP | Co-immunoprecipitation |
| COPII | coat protein complex II |
| cos | cosine |
| CRM1 | exportin 1 |
| CRY | cryptochrome, transcriptional repressor in multiple species |
| CSE1L, CAS | exportin 2 |
| CT | circadian time |
| crtl | control |
| CYCLE | circadian, transcriptional activator in Drosophila melanogaster |
| CYCLIN T1 | Human Immunodeficiency Virus Type 1 (HIV-1) Expression (Elevated) 1, TNPO1 cargo |
| *D. melanogaster* | *Drosophila melanogaster* |
| Da | dalton |
| Damping, damp. | decrease in amplitude per 24 hours |
| DBD | domain DNA-binding domain |
| DBT | doubletime, kinase in Drosophila melanogaster |
| DJ1 | protein deglycase DJ1 |
| DNA | deoxyribonucleic acid |
| dNTP | desoxynucleoside triphosphate |
| DSB | double strand breaks |
| dsDNA | double-stranded DNA |
| e | exponential |
| *E.coli* | *Escherichia coli* |
| E-box | enhancer element, CLOCK/BMAL1-binding site |
| ECFP | enhanced cyan fluorescent protein |
| EGFR | epidermal growth factor receptor |
| EGFP | enhanced green fluorescent protein |
| ELYS | embryonic large molecule derived from yolk sac |
| ER | endoplasmic reticulum |
| *et al.* | and others |
| ETLE | étoile protein, TNPO1 cargo |
| ETOH | ethanol |
| EWS | ewing sarcoma breakpoint region 1, TNPO1 cargo |
| EYFP, Venus | enhanced yellow fluorescent protein |
| FASPS | familial advanced sleep phase syndrome |
| FBXL | F-box and leucine-rich repeat protein |
| FG-repeat | phenylalanine-glycine-rich repeat |
| FRAP | fluorescence recovery after photobleaching |
| FRQ | frequency, molecular clock protein in *Neurospora crassa* |

| | |
|---|---|
| FOK 1 | restriction endonuclease of Flavobacterium okeanokoites |
| FOXO4 | forkhead box O 4, TNPO1 cargo |
| FRH | FRQ interacting RNA helicase |
| FUS | fused in sarcoma protein, TNPO1 cargo |
| fwd | forward |
| g | gramm |
| *gapdh* | gene encoding glyceraldehyde 3-phosphate dehydrogenase |
| GDP | guanosine diphosphate |
| GFP | green fluorescent protein |
| GLE1 | nucleoporin GLE1 |
| GP210 | nuclear pore membrane glycoprotein 210 |
| GRK2 | beta-adrenergic receptor kinase |
| gRNA | guide RNA |
| GSK | glycogen synthase kinase |
| GTP | guanosine triphosphate |
| h | hour |
| H8 loop | HEAT repeat 8 loop |
| HCC1 | Ran-binding protein 39, TNPO1 cargo |
| HEAT repeat | **H**untingtin, **E**longation factor 3, protein phosphatase 2**A** and **T**OR1 repeat |
| HEK293 | human embryonic kidney cell line |
| HEK293T | human embryonic kidney cell line, high transfectability |
| HEXIM1 | hexamethylene bis-bcetamide Inducible protein, TNPO1 cargo1 |
| HR | homologous recombination |
| HRP | horseradish peroxidase |
| HuR | ELAV (Embryonic Lethal, Abnormal Vision, *D. melanogaster*)-Like 1 (Hu Antigen R), TNPO1 cargo |
| IBB | importin β-binding domain |
| IgG | immunoglobulin G |
| indel | insertions or deletions |
| INM | inner nuclear membrane |
| IP | immunoprecipitation |
| $IP_C$ | control IP |
| IPO | importin |
| Iver | ivermectin |
| JKTBP | heterogeneous nuclear ribonucleoprotein D-like, TNPO1 cargo |
| k | kilo |
| $K_m$ | Michaelis-Menten constant |
| *kap* | gene family karyopherin |
| KPNA | karyopherin alpha |
| KPNB | importin beta |
| l | litre |
| LAR | luciferase activity reagent |
| lat. | latin |

| | |
|---|---|
| LMB | leptomycin B |
| LOS1 | loss of suppression protein 1 |
| LUC | firefly luciferase |
| m | milli or meter |
| M | mega or molar |
| M9 | non-classical, hydrophobic nuclear localization signal, TNPO1-binding site |
| MAPK | mitogen-activated protein kinases max maximum |
| Min | minute |
| MLP | muscle LIM protein |
| mRNA | mature RNA |
| MSN | multicopy suppressor of SNf1 mutation |
| MTR q | 5-methyltetrahydrofolate-homocysteine methyltransferase |
| mut | mutated |
| MYC | Myc proto-oncogene protein |
| n | nano or number of... |
| *N. crassa* | *Neurospora crassa* |
| n.d. | not determined |
| n.s. | non-significant |
| $NAD^+$/NADH | nicotinamide adenine dinucleotide |
| NADPH | nicotinamide adenine dinucleotide phosphate |
| NAMPT | nicotinamide phosphoribosyltransferase |
| NDC1 | nuclear division cycle 1 homolog |
| NE | nuclear envelope neg. negative |
| NES | nuclear export signal |
| NER | nucleotide excision repair |
| NF-$\varkappa$B | nuclear factor-kappa B |
| NHEJ | non-homologous end-joining |
| NLS | nuclear localization signal |
| NMD5 | Nmd5p |
| NMR | nuclear magnetic resonance |
| norm. | normalized |
| NPAS | neuronal PAS domain-containing protein, transcriptional activator |
| NPC | nuclear pore complex |
| NRF2 | nuclear factor, erythroid 2 like 2 |
| ns control, ns | non-silencing control |
| NSP1 | FG-nucleoporin NSP1 |
| nup | nucleoporin |
| ONM | outer nuclear membrane |
| p53 | tumor suppressor gene p53 |
| PABP | poly $A^+$ binding protein, TNPO1 cargo |
| PAGE | poly-acrylamide gel electrophoresis |
| PAM motif | protospacer adjacent motif |
| PAS | domain Period-Arnt-Sim domain |

| | |
|---|---|
| PCR | polymerase chain reaction |
| PDR6 | ABC transporter G family member 34 |
| PER | Period, transcrptional repressor in diverse species |
| *per2:luc* | *luciferase* gene driven by a 0.5 kb *per2* promoter |
| PKA | protein kinase A |
| PNS | perinuclear space |
| polyA$^+$ | poly adenylation |
| POM121 | POM121 transmembrane nucleoporin |
| pos. | positive |
| PP | protein phosphatase |
| PRX | peroxiredoxin |
| PSE1 | protein secretion enhancer 1 |
| PY motif | proline-tyrosine motif |
| qRT-PCR | quantitative real-time PCR |
| $R^2$ | statistical measure of the goodness of a fitted regression line |
| RAE1 | ribonucleic acid export 1 |
| Ran | RAS-related nuclear protein |
| RanBP | Ran binding protein |
| RanGAP | Ran GTPase activating protein |
| RanGEF | Ran guanine nucleotide exchange factor |
| RanGRF | Ran guanine nucleotide release factor |
| RCC | nuclear nucleotide exchange factor |
| rel. | relative |
| rev | reverse |
| REVERB | nuclear receptor subfamily 1 group D member 1, repressor of RORE element-driven genes |
| RHT | retinohypathalamic tract |
| RNA | ribonucleic acid |
| RNAi | RNA-interference |
| RNP | ribonucleoprotein |
| ROR | RAR-related orphan receptor, activator of RORE element-driven genes |
| RORE | RAR-related orphan receptors elements, binding sites for RORs and |
| REVERBs | nuclear receptor subfamily 1 group D member 1 |
| ROS | reactive oxygen species |
| RT | reverse transcriptase |
| SAM68 | Src-Associated substrate in Mitosis of 68 kDa, TNPO1 cargo |
| SCN | suprachiasmatic nucleus |
| SD | standard deviation |
| Sec | second |
| SEH1 | SEC13 Homolog |
| SEC61/SEC13 | SECretory protein 61/13 |
| SEM | standard error of the mean |
| shRNA | short hairpin RNA |

| | |
|---|---|
| SIRT | sirtuin |
| SNP | snurprotein1 |
| SOD | superoxide dismutase |
| SOP | standard operating procedure |
| SOX14 | Sex Determining Region Y-Box 14, TNPO1 cargo |
| SRX | sulforedoxin |
| ssDNA | single-stranded DNA |
| suppl. | supplementary |
| SXM1 | suppressor of mRNA export mutant 1 |
| t | time |
| T | temperature |
| $T_M$ | melting temperature |
| T7E1 | T7 endonuclease I |
| TAFII68 | TAF15 RNA polymerase II, TATA box binding protein (TBP)-associated factor, 68kDa, TNPO1 cargo |
| TALEN | Transcription activator-like effector nucleases |
| TAP | Transporter-associated with antigen processing |
| TIM | timeless, transcriptional repressor in Drosophila melnogaster |
| TNPO1 | Transportin 1 |
| TPR | Translocated Promoter Region, component of NPC |
| tracrRNA | trans-activating crispRNA |
| tRNA | transfer RNA |
| TTFL | transcriptional-translational feedback loop |
| U-2-OS | human osteosarcoma cell line |
| UPR | unfolded protein response |
| UV | ultraviolet |
| V | volume |
| v/v | volume per volume |
| w/v | weight per volume |
| w | with |
| WB | western blot |
| WBS16 | Williams-Beuren Syndrome Chromosome Region 16/RCC1-Like G Exchanging Factor-Like Protein,TNPO1 cargo |
| WC White Collar, | transcriptional activator of *Neurospora crassa* molecular clock |
| WCC | White Collar Complex |
| WGRF | wingless receptor fragments |
| wo | without |
| wt | wild type |
| x g | times gravity |
| XPO | Exportin |
| ZNF | Zinc-finger nucleases |
| ZT | Zeitgeber time |

# Danksagung

An dieser Stelle möchte ich den Menschen danken, die mich während meiner Doktorarbeit auf wissenschaftlich und persönlicher Ebene gefördert, vielleicht manchmal auch gefordert, aber vor allem immer unterstützt haben.

Zuerst möchte ich Prof. Dr. Achim Kramer für die Möglichkeit danken, dass ich meine Doktorarbeit in seinem Labor durchführen konnte. Das Gebiet der Chronobiologie hat mich seit meinem Hiwi-Job in seiner Arbeitsgruppe begeistert und interessiert und bis heute nicht los gelassen. Vielen Dank für die gute Betreuung, die stets offene Tür, die konstruktiven Anregungen und das durchgängige Interesse an meiner Arbeit.

Prof. Dr. Florian Heyd möchte ich für die freundliche Übernahme der Begutachtung und dem Interesse an dieser Arbeit herzlich danken.

Ich danke der Arbeitsgruppe von Prof. Herrmann, am Institut für Biologie Humboldt Universität zu Berlin, insbesondere Dr. Thomas Korte, für die stets freundliche Unterstützung.

Der gesamten Arbeitsgruppe ‚Chronobiologie', sowie den ehemaligen Mitgliedern, die mich während meiner Zeit als Doktorand begleitet haben, möchte ich ebenfalls meinen Dank aussprechen. Dank euch, habe ich unser Labor immer als zweites zu Hause empfunden, wo ich Menschen treffe, die sich gegenseitig schätzen und unterstützen. Insbesondere möchte ich Annette Hayungs für ihre administrative, oft sehr spontan-eingeforderte Unterstützung danken. Spontan trifft es auch bei vielen anderen Labormitgliedern, die ich stets um Hilfe und Anregungen auf dem Flur anhalten konnte. Vielen Dank Silke Reischl, Thomas Wallach, Ute Abraham, Bharath Ananthasubramaniam und Elyzana Putrianti. Bert Maier danke ich darüber hinaus auch für die sportliche Motivation. Den Mädels aus „unserem Büro", Neta Tuvia, Veronika Lang und Katja Schellenberg möchte ich neben der fachlichen Kompetenz auch für die Freundschaft danken, die sich innerhalb unserer vier Wände aufgebaut hat.

Astrid Grudziecki und Sebastian Jäschke gilt ein ganz besonderer Dank, da sie mich nicht nur während meines Laboralltags, sondern auch in privaten Achterbahnfahrten begleitet haben.

Rupert Öllinger möchte ich für die Unterstützung und Integration in sein Thema danken und auch dafür, dass ich mich auch nach unserer Zusammenarbeit stets an ihn wenden kann.

Vielen Dank auch an die Studenten, die meine Arbeit unterstützt haben, Almut Eisele, Shpetime Jonuzi, Aila Kattner und Lea Ehrhardt. Letzterer gilt ebenfalls ein besonderer Dank. Die

Zusammenarbeit während Leas Masterarbeit war überaus konstruktiv und hat mir sehr viel Freude bereitet.

All jene, die mir während des Verfassens meiner Dissertation mit Rat und Tat zur Seite gestanden haben, möchte ich ebenfalls danken, besonders Silke Reischl, Sarah Erdmann, Constanze Haufe, Daniela Hombach, Sebastian Jäschke und Carsten Wloka.

Nun bleibt mir noch all denen zu danken, die außerhalb des Laboralltags mein Leben bereichern. Vielen Dank an meine Freunde, die - ob nah oder fern - mit mir gelitten und gelacht haben und immer für mich da sind.

Ich danke auch Daniel Leipold, der während der Schreibphase viel Geduld, Verständnis und motivierende Worte für mich fand, der lieber stumm am anderen Ende meines Skypes saß, anstatt mit seinen Freunden Fußball zu schauen. Zum Schluss möchte ich meinem Bruder Marcel, seiner Frau Rebekka und ganz besonders meinen Eltern danken. Ihr Lieben, die ihr mich immer bedingungslos und uneingeschränkt mit all meinen Ideen und Problemen unterstützt, ich danke euch aus tiefstem Herzen.

# Statement of Authorship

I declare on oath that I completed this work under the title "A non-conventional nuclear import pathway for circadian clock proteins" on my own and that information which has been directly or indirectly taken from other sources has been noted as such. Neither this, nor a similar work, has been published or presented to an examination committee.

Sandra Korge
Berlin, 05th of December 2016